Design, Synthese und Evaluation selektiver Inhibitoren in Modellen der akuten myeloischen Leukämie sowie in der Parkinson-Krankheit

TECHNISCHE UNIVERSITÄT DARMSTADT

Vom Fachbereich Chemie
der Technischen Universität Darmstadt

zur Erlangung des akademischen Grades eines
Doctor rerum naturalium (Dr. rer. nat.)

genemigte
kumulative Dissertation

vorgelegt von
Stefan Göring, Master of Science
aus Gera

Referent: Prof. Dr. Boris Schmidt
Korreferentin: Prof. Dr. Katja Schmitz
Tag der Einreichung: 09. Oktober 2014
Tag der mündlichen Prüfung: 15. Dezember 2014

Darmstadt 2015
D17

Meiner Familie

Die vorliegende Arbeit wurde unter der Leitung von Prof. Dr. Boris Schmidt am Clemens Schöpf-Institut für Organische Chemie und Biochemie der Technischen Universität Darmstadt vom Januar 2012 bis Dezember 2014 angefertigt.

Danksagung

Meinem Doktorvater *Prof. Dr. B. Schmidt* danke ich für die Betreuung dieser Arbeit, der regelmäßigen Bereitschaft zur Diskussion, den Anregungen jeglicher Art sowie für das mir entgegengebrachte Vertrauen.

Ein weiterer Dank gilt meinen ehemaligen Kollegen *Binia*, *Constantin*, *Eva*, *Andrea*, *Alexander*, *Marlyse*, *Jiamin*, *Upendra*, *Thomas* und *Fabio* für das freundliche Arbeitsklima und der netten Zusammenarbeit.

Thomas und *Fabio* danke ich für ihre Unterstützung in den ersten Monaten meiner Promotion.

Allen aktiven Mitgliedern des Arbeitskreises – *Christoph*, *Theresa*, *Dennis* und *Johannes* – danke ich für die gute Teamarbeit, der steten Hilfsbereitschaft und den zahlreichen gemeinsamen Stunden, auch neben der Arbeit im Labor.

Binia, *Theresa*, *Christoph* und *Dennis* danke ich für die lustige Zeit auch außerhalb des Labors.

Ich danke *Theresa* und *Dennis* für die gewissenhafte Korrektur dieser Arbeit.

Frau Rudolf danke ich für die netten Unterhaltungen, das Anfertigen meiner Massenspektren und vor allem bei der Unterstützung jeglicher HPLC-Probleme.

Jean-Marc und *Veerle* danke ich für die gute Zusammenarbeit sowie für die stete Diskussionsbereitschaft.

Meinen Eltern und meiner ganzen Familie gilt ein großer Dank für die bedingungslose Unterstützung während meines gesamten Studiums und der Promotion.

Meiner Frau *Christine* danke ich einfach für alles!

Teile dieser Arbeit wurden bereits veröffentlicht oder zur Veröffentlichung eingereicht

1. Ghislaine Marlyse Okala Amombo, Thomas Kramer, Fabio Lo Monte, Stefan Göring, Matthias Fach, Steven Smith, Stephanie Kolb, Robert Schubenel, Karlheinz Baumann, Boris Schmidt, „*Modification of a promiscuous inhibitor shifts the inhibition from γ-secretase to FLT-3*", *Bioorganic & Medicinal Chemistry Letters***2012**, *22*, 7634-7640.

2. Thomas Kramer, Fabio Lo Monte, Stefan Göring, Ghislaine Marlyse Okala Amombo, Boris Schmidt, „*Small molecule kinase inhibitors for LRRK2 and their application to Parkinson´s disease models*", *ACS Chemical Neuroscience* **2012**, *3*, 151-160.

3. Sandra Schulz*, Stefan Göring*, Boris Schmidt, Carsten Hopf, „*LRRK2 Kinase Inhibitors as New Drugs for Parkinson's Disease?*", *RSC Drug Discovery Series*, **2013**, *34* (Emerging Drugs and Targets for Parkinson's Disease), 266-293.

4. Eva Christine Naumann*, Stefan Göring*, Isabella Ogorek, Sascha Weggen, Boris Schmidt, „*Membrane anchoring γ-secretase modulators with terpene-derived moieties*",*Bioorganic & Medicinal Chemistry Letters* **2013**, *23*, 3852-3856.

5. Stefan Göring, Jean-Marc Taymans, Veerle Baekelandt, Boris Schmidt, „*Indolinone based LRRK2 kinase inhibitors with a key hydrogen bond*", *Bioorganic & Medicinal Chemistry Letters***2014**, *24*, 4630-4637.

6. Stefan Göring*, Dennis Bensinger*, Eva Christine Naumann, Boris Schmidt, „*Computer-guided design, synthesis and biological evaluation of quinoxalinebisarylureas as FLT3 inhibitors*" wird zeitnah zur Veröffentlichung eingereicht.

* Erstautor.

Inhaltsverzeichnis

Abkürzungsverzeichnis **x**

Aminosäurenverzeichnis xiii

Einleitung **1**

1Leukämie **2**

1.1 Krebs in Deutschland 2

1.1.1 Leukämie – Entstehung, Arten und Symptome 4

1.1.2 Diagnostik und Therapiemöglichkeiten der AML 6

1.1.3 Zytogenetische und molekulargenetische Merkmale der AML 9

1.1.4 Das „2-Klassen-Modell“ über die Entwicklung der Leukämie 10

1.2 FLT3 als molekulares Target in der Tumortherapie 12

1.2.1 Struktur und Funktion von Proteinkinasen 12

1.2.2 Rezeptor-Tyrosinkinasen 14

1.2.3 FLT3 – Eine-Klasse-III Rezeptor-Tyrosinkinase 15

1.2.4 Signalwege des FLT3-Rezeptors 17

1.2.5 FLT3 und seine Rolle in der akuten myeloischen Leukämie 19

1.2.6 Inhibitionsarten von Proteinkinase-Inhibitoren 20

1.2.7 Molekulare Interaktionen in biologischen Systemen 23

1.2.8 *Small molecules* zur Behandlung der AML – Stand der Forschung 25

2Die Parkinson-Erkrankung **31**

2.1 Einführung und Geschichte 31

2.2 Die Ätiologie von Morbus Parkinson 32

2.2.1 Neuropathologie der Parkinson-Erkrankung 33

2.2.2 Gegenwärtige Behandlung der Parkinson-Krankheit 34

2.2.3 Genetisch bedingtes Parkinson-Syndrom 37

2.3 α-Synuclein und dessen Rolle in der Parkinson-Krankheit 38

2.4 LRRK2 als therapeutisches Target zur Behandlung der Parkinson-Krankheit 40

2.4.1 Nomenklatur, Struktur und Mutationen von LRRK2 40

2.4.2 LRRK2 und dessen Rolle in der Parkinson-Krankheit 41

2.4.3 Inhibitoren zur Behandlung der Parkinson-Krankheit – Stand der Forschung 42

3Aufgabenstellung und Zielsetzung der Arbeit 46

4Kumulativer Teil der Arbeit 47

4.1 Modifikation einer Inhibitorleitstruktur weg von der γ-Sekretase und hin zu der FLT3 Inhibition 47

4.2 Computer unterstütztes Design, Synthese und biologische Evaluation von Chinoxalinbisarylharnstoffen als FLT3 Inhibitoren 76

4.3 *Small molecule* Kinase-Inhibitoren für LRRK2 und ihre Anwendung in Modellen der Parkinson-Krankheit 111

4.4 LRRK2 Kinase-Inhibitoren als neue Medikamente für die Parkinson-Krankheit? 122

4.5 Indolinon-basierende LRRK2-Kinase-Inhibitoren mit einer wichtigen Wasserstoffbrücke 151

4.6 Zusätzlich bearbeitete Themen neben dem Schwerpunkt der FLT3- und LRRK2-Inhibition 181

4.6.1 Membran-verankerte γ-Sekretase Modulatoren mit Terpen abgeleiteten Resten 181

5Zusammenfassung und Ausblick 208

5.1 Zusammenfassung 208

5.2 Ausblick 210

6Literaturverzeichnis 213

7Anhang 221

7.1 Abbildungsverzeichnis 221

7.2 Erklärungen 224

7.3 Lebenslauf 226

Abkürzungsverzeichnis

Aβ	Amyloid-β-Peptid
ABL1	*Abelson Murine Leukemia Viral Oncogene Homolog 1*
ADME	*Absorption, Distribution, Metabolisms, Excretion*
AGC	*protein kinases A, G and C group*
ALL	akute lymphatische Leukämie
AML	akute myeloische Leukämie
ATP	Adenosintriphosphat
ATRA	*all-trans-retinoic acid*
BCR	*breakpoint cluster region*
BSc	Boris Schmidt-Substanzdatenbankeintragsnummer
bzw.	beziehungsweise
c-KIT	*v-kit Hardy-Zuckerman 4 feline sarcoma viral oncogene homolog*
cal	Kalorien
CEAMK	*calcium/calmodulin-dependent protein kinase*
CBPA	*CCAAT/enhancer binding protein*
CK1	*casein kinase 1*
ClogD	berechneter Verteilungskoeffizient bei pH 7,4
CMCG	beinhaltet CDK, MAPK, GSK3, CLK Familien
CNS MPO	*Central Nervous System Multiparameter Optimization*
COMT	Catechol-O-Methyltransferase
COR	*C-terminal of Ras*
CLL	chronisch lymphatische Leukämie
CML	chronisch myeloische Leukämie
CSF-1	*colony stimulating factor 1 (macrophage)*
CT	Computertomografie
Da	Dalton
DFG	D: Asparaginsäure, F: Phenylalanin, G: Glycin
DNA	*deoxyribonucleic acid*
ERK	*extracellular-signal regulated kinase*
FAB	*French-American-British*
FDA	*Food and Drug Administration*
FGFR	*fibroblast growth factor receptor*
FL	FLT3-Ligand

FLT2	*fetal liver tyrosine kinase 2*
FLT3	*FMS-like tyrosine kinase 3*
FMS	*formerly McDonough feline sarcoma viral oncogene homolog*
GEKID	Gesellschaft der epidemiologischen Krebsregister e.V.
GPCR	*G-protein-coupled receptor*
GRB2	*growth factor receptor-bound protein 2*
GTP	Guanosintriphosphat
IC_{50}	mittlere inhibitorische Konzentration
IDH1	*cytoplasmatic isocitrate dehydrogenase 1*
IDH2	*mitochondrial isocitrate dehydrogenase 2*
ITD	*internal tandem duplication*
JM	Juxtamembran
JM-B	*JM binding motif*
JM-S	*JM switch motif*
JM-Z	*JM zipper motif*
K-RAS	*Kirsten rat sarcoma viral oncogene homolog*
KI	Kinase-Insert
L-DOPA	Levodopa
LB	*Lewy bodies*
LN	*Lewy neurites*
logP	Verteilungskoeffizient zwischen Oktanol und Wasser
LRR	*leucine-rich repeat*
LRRK2	*leucine-rich repeat kinase 2*
LT-HSC	*long term hematopoietic stem cells*
µM	Mikromolar
MAO-B	Monoaminooxidase-B
MPTP	1-Methyl-4-phenyl-1,2,3,6-tetrahydropyridin
MRT	Magnetresonanztomografie
mTOR	*mammilian target of rapamycin*
N-RAS	*neuroblastoma RAS viral (v-ras) oncogene homolog*
NAC	*non-amyloid component*
nM	Nanomolar
NMP	*nucleophosphim*
PDB	*protein data base*

PDGFR	*platelet-derived growth factor receptor*
PI3K	*phosphatidylinositol 3-kinase*
PINK1	*phosphatase and tensin homolog (PTEN)-induced putative kinase 1*
PKB	*protein kinase B*
PTK	Proteintyrosinkinase
RNA	*ribonucleic acid*
ROC	*Ras of complex*
RTK	Rezeptor-Tyrosinkinase
SHC	*SH2-containing sequence proteins*
SHIP	*SH2-domain-containing inositol phosphatase*
SNCA	α-Synuclein
SNpc	*Substantia nigra pars compacta*
ST-HSC	*short term hematopoietic stem cells*
STAT5	*signal transducter and activator of transcription 5*
STE	*homologs of yeast sterile 7, sterile 11, sterile 20 kinases*
STK-1	*stem cell tyrosine kinase-1*
TET2	*ten-eleven translocation 2*
TK	*tyrosine kinase*
TKI	Tyrosinkinase-Inhibitor
TKL	*tyrosine kinase-like*
TM	Transmembran
TPSA	*topological polar surface area*
VEGFR	*vascular endothelial growth factor receptor*
WHO	*World Health Organization*
ZfKD	Zentrum für Krebsregisterdaten

Aminosäurenverzeichnis

Aminosäure	Dreibuchstabencode	Einbuchstabencode
Alanin	Ala	A
Arginin	Arg	R
Asparagin	Asn	N
Asparaginsäure	Asp	D
Cystein	Cys	C
Glutamin	Gln	Q
Glutaminsäure	Glu	E
Glycin	Gly	G
Histidin	His	H
Isoleucin	Ile	I
Leucin	Leu	L
Lysin	Lys	K
Methionin	Met	M
Phenylalanin	Phe	F
Prolin	Pro	P
Serin	Ser	S
Threonin	Thr	T
Tryptophan	Trp	W
Tyrosin	Tyr	Y
Valin	Val	V

Einleitung

Bereits vor hunderten von Jahren forschten die Alchimisten, um ein geeignetes Elixier für die Heilung aller Krankheiten zu finden. Gefunden wurde es jedoch bis heute noch nicht. Im Gegenteil, durch zunehmende Forschung und das somit verstärkte Verständnis über Krankheiten und deren Ursachen steigt die Komplexibilität der Entwicklung von Medikamenten und somit auch die Therapie von Krankheiten.[1]

Heutzutage stellen Enzym-Inhibitoren ein wichtiges Gebiet, mit rund ein Drittel aller weltweit verkauften Medikamenten, dar.[2] Die Klassifizierung der Enzyme erfolgt dabei in sechs Klassen: Oxidoreduktasen, Transferasen, Hydrolasen, Isomerasen, Lyasen und Ligasen. Eine Untergruppe der Transferasen bilden dabei die sogenannten Kinasen. Wie sich aus dem Namen der Untergruppe ableiten lässt, katalysieren Kinasen die Übertragung eines Phosphatrestes von Adenosintriphosphat (ATP) auf ein Substrat, dort speziell auf Hydroxylgruppen. Aufgrund dessen werden sie auch Phosphoryltransferasen genannt. Hierbei können unterschiedliche biologische Moleküle wie Proteine, Lipide oder auch Nukleotide phosphoryliert werden.[3] Die größte Gruppe der Kinasen umfasst die Klasse der Proteinkinasen. Je nach Art der phosphorylierten Gruppe kann zwischen Serin-, Threonin und Tyrosin-Kinasen unterschieden werden. Proteinkinasen spielen eine wesentliche Rolle in vielen biologischen Prozessen wie Metabolismus, Transkription, Apoptose, Differenzierung von Zellen und nehmen eine wichtige Rolle in der Funktionsweise des Nerven- und Immunsystems sowie der Homöostase ein.[4]

Das menschliche Kinom umfasst 518 Proteinkinasen. Es ist unterteilt in 10 Gruppen, 143 Familien und 212 Subfamilien (Abbildung 1).[4] Fehlregulationen und Mutationen von Proteinkinasen spielen eine zentrale Rolle bei humanen Krankheiten. Demnach sind die Proteinkinasen nach den GPCRs (*G-protein-coupled receptors*) die zweitwichtigsten Targets in der Arzneimittelforschung.[5] Im Fokus dieser Arbeit stehen zwei interessante Enzyme, die *FMS-like tyrosine kinase 3* (FLT3) und die *leucine-rich repeat kinase 2* (LRRK2). Während Mutationen von FLT3 in Verbindung mit der akuten myeloischen Leukämie gebracht werden, sind Mutationen von LRRK2 mitverantwortlich für das Parkinson-Syndrom. Die Entwicklung potenter und selektiver Inhibitoren ist daher ein wertvoller Ansatzpunkt zur Behandlung dieser Krankheiten. Die Inhibition von FLT3, einer Tyrosinkinase, und LRRK2, ein Vertreter der Serin/Threoninkinasen, stellen somit aussichtsreiche Targets in der Krebstherapie bzw. zur Behandlung der Parkinson-Krankheit dar.

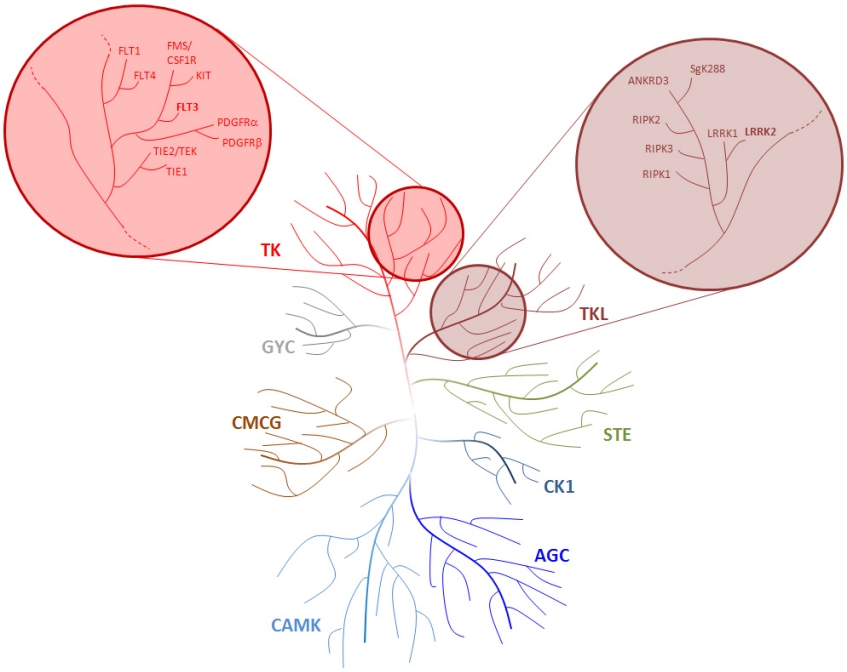

Abbildung 1: Schematische Darstellung des menschlichen Kinoms, sowie deren wichtige Hauptgruppen. AGC: *protein kinases A, G and C group* (beinhaltet PKA, PKG und PKC Familien); CAMK: *calcium/calmodulin-dependent protein kinase*; CK1: *casein kinase 1*; CMCG: beinhaltet CDK, MAPK, GSK3, CLK Familien; STE: *homologs of yeast sterile 7, sterile 11, sterile 20 kinases*; TK: *tyrosine kinase*; TKL: *tyrosine kinase-like*. In Anlehnung an Manning *et al.*[4]

1 Leukämie

1.1 Krebs in Deutschland

Jeder zweite Mann (51 %) und fast jede zweite Frau (43 %) müssen derzeit davon ausgehen, im Laufe ihres Lebens an Krebs zu erkranken.[6] Dies sind die alarmierenden Zahlen, die gemeinsam von der Gesellschaft der epidemiologischen Krebsregister e.V. (GEKID) und dem Zentrum für Krebsregisterdaten (ZfKD) im Robert Koch-Institut erstmal für das Jahr 2010 ermittelt worden sind. Demnach sind ZfKD-Schätzungen zufolge erstmalig 477 300 Krebserkrankungen registriert worden, wobei jeder vierte Mann und jede fünfte Frau an der Krebserkrankung verstirbt. Mit ca. 252 400 Krebserkrankungen erkranken Männer häufiger als Frauen (224 900), wobei mehr als die Hälfte der Krebsneuerkrankungen auf Lungen-, Brustdrüsen-, Darm- und Prostatakrebs zurückzuführen ist (Abbildung 2). Das mittlere Erkrankungsalter liegt bei Männer und Frauen gleichermaßen bei 69 Jahren, wobei bei den

über 65-jährigen Männern die Erkrankungsraten fast doppelt so hoch sind wie die der Frauen.[6]

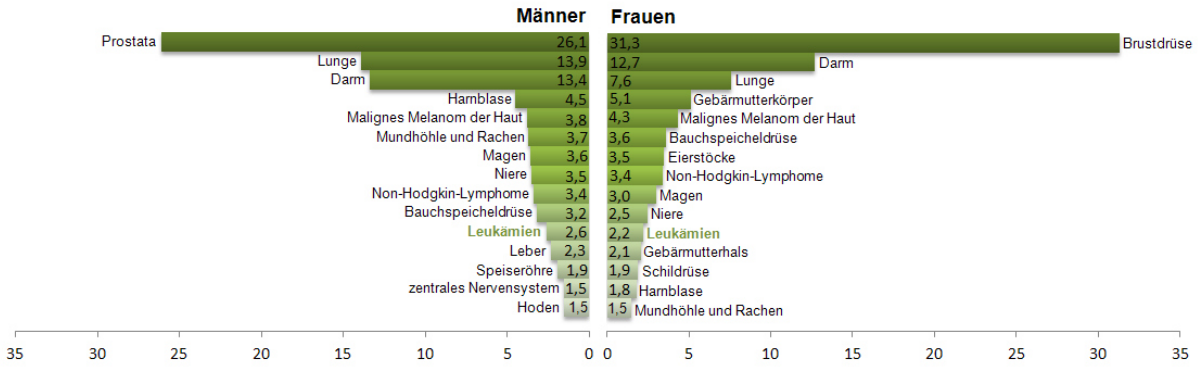

Abbildung 2: Prozentualer Anteil der Tumorlokalisationen bei Krebsneuerkrankungen in Deutschland 2010.[6]

Mit 2,6 % bei den Männern und 2,2 % bei den Frauen sind 2010 etwa 11 500 Menschen in Deutschland an Leukämie erkrankt. Das Leukämierisiko liegt bei Kindern unter 15 Jahren bei hohen 6 %, wobei es mit zunehmendem Alter unabhängig vom Geschlecht bei Jugendlichen und jüngeren Erwachsenen sinkt. Erst ab dem 30. Lebensjahr erhöht sich die Wahrscheinlichkeit an Leukämie zu erkranken kontinuierlich, jedoch tragen Männer ein höheres Risiko als Frauen.[6] Rund ein Drittel aller Krebserkrankungen bei Kindern unter 15 Jahren sind auf Leukämien zurückzuführen (Abbildung 3). Die akute lymphatische Leukämie (ALL) stellt mit 26,3 % den größten Anteil dar, gefolgt von der akuten myeloischen Leukämie (AML) (4,4 %). Warum die Leukämien im Kindesalter so oft auftreten ist noch unbekannt. Umwelteinflüsse und ein unzureichendes ausgeprägtes Immunsystem im Säuglingsalter sind Basis einiger Hypothesen.[6]

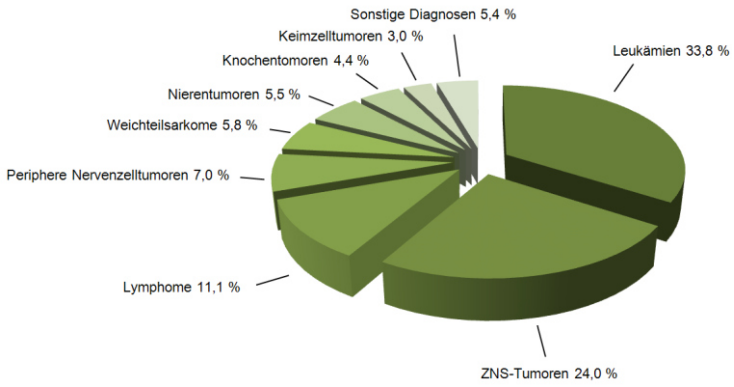

Abbildung 3: Prozentualer Anteil der Krebsneuerkrankungen bei Kinder in Deutschland aus den Jahren 2003-2012.[6]

1.1.1 Leukämie – Entstehung, Arten und Symptome

Blut ist für uns Menschen lebenswichtig. Es übernimmt verschiedene wertvolle Funktionen von der Sauerstoffversorgung der Gewebe, den Abtransport von Kohlenstoffdioxid, den Transport von Nährstoffen, die Wärmeregulation bis hin zur Immunabwehr durch Antikörper und weiße Blutkörperchen. Je nach Körpergewicht liegt die Gesamtblutmenge bei einem Menschen zwischen fünf und sechs Litern.[7] Das Blut besteht aus flüssigen sowie aus festen Bestandteilen. Letztere machen etwa 42 % aus und beinhalten die Blutkörperchen, welche aus den roten (Erythrozyten) und den weißen Blutkörperchen (Leukozyten), sowie den Blutplättchen (Thrombozyten) zusammengesetzt sind. Den restlichen Anteil mit etwa 58 % macht das Blutplasma aus. Die Hämatopoese findet überwiegend im Knochenmark statt.[7] Täglich werden mehrere Milliarden Zellen neu gebildet, welche aus einer Gruppe von hämatopoetischen Stammzellen ausgehen. Es konnten zwei verschiedene Typen an hämatopoetischen Stammzellen in Mausmodellen gefunden und charakterisiert werden: die Langzeit-Stammzellen (LT-HSC: *long term hematopoietic stem cells*) und die Kurzzeit-Stammzellen (ST-HSC: *short term hematopoietic stem cells*). Während LT-HSC in der Lage sind sich stetig zu erneuern, ist diese Eigenschaft bei ST-HSC nur begrenzt möglich.[8, 9] Letztere differenzieren weiter zu den sogenannten multipotenten Vorläuferzellen. Die multipotenten Vorläuferzellen teilen sich und bilden zwei weitere Gruppen an Vorläuferzellen: die myeloische Vorläuferzelle und die lymphatische Vorläuferzelle (Abbildung 4).[10] Aus diesen Vorläuferzellen wird durch weitere Teilung und Differenzierung über verschiedene Zwischenstufen die unterschiedlichen Blutkörperchen erzeugt. Während sich aus den myeloischen Vorläuferzellen die Erythrozyten, Thrombozyten und Granulozyten (bestimmte Art der Leukozyten) bilden, gehen aus den lymphatischen Vorläuferzellen die natürlichen Killerzellen, sowie die B- und T-Lymphozyten hervor. Anschließend werden diese aus dem Knochenmark freigesetzt und können ihrer entsprechenden Funktion nachgehen.

Von einer Leukämie wird gesprochen, wenn die Blutzusammensetzung gestört ist und die Zellen ihre Funktionen nicht mehr erfüllen können. Die Zellen teilen sich unkontrolliert und ungehemmt (Abbildung 4). Es kann keine Differenzierung mehr stattfinden, folglich können die Zellen ihrer eigentlichen Aufgabe nicht mehr nachgehen. 1845 beschrieb der deutsche Arzt Rudolph Ludwig Karl Virchow erstmals das Krankheitsbild der Leukämie an einer Patientin.[11] Er beobachtete die stark vermehrten weißen Blutzellen, diagnostizierte „weißes Blut“ und führte letztlich den Begriff „Leukämie“ ein. Heutzutage wird unter Leukämie

(altgr. *leukós* „weiß“ und *αἷμα haima* „das Blut“) eine bösartige Erkrankung des blutbildenden Systems verstanden, wobei es zu einer starken Vermehrung der weißen Blutkörperchen (Leukozyten) kommt.

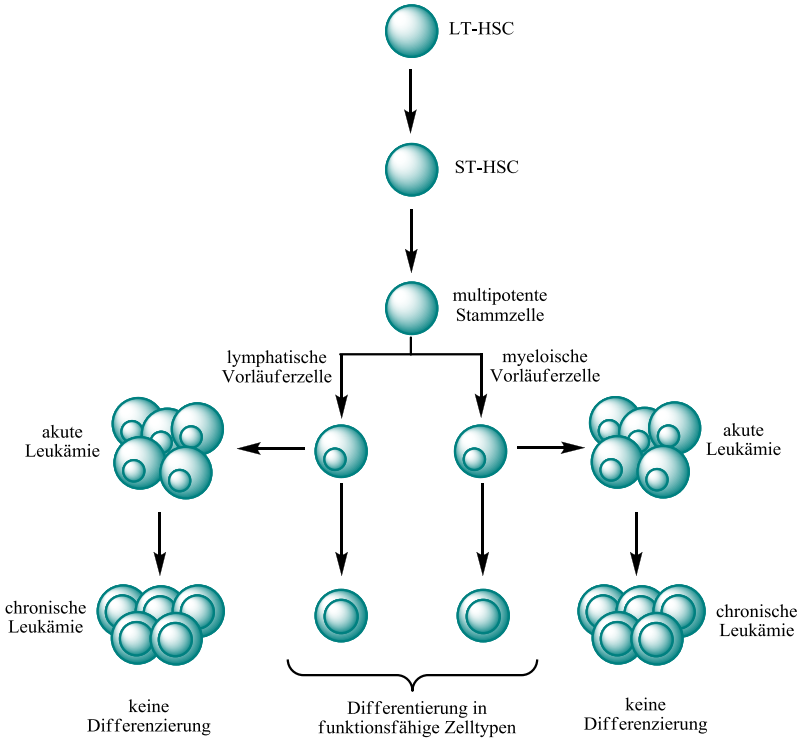

Abbildung 4: Entstehung der Leukämien ausgehend von den LT-HSC (*long term hematopoietic stem cells*) über den myeloischen und lymphatischen Differenzierungsweges. In Anlehnung an E. Elert.[10]

Je nach Art der veränderten Vorläuferzelle und dem Krankheitsverlauf wird die Leukämie in unterschiedliche Klassen aufgeteilt (Abbildung 4, Tabelle 1). Während die akuten Leukämien bereits von Beginn an lebensbedrohlich sind und innerhalb weniger Wochen bzw. Monaten zum Tode führen können, verlaufen die chronischen Leukämien schleichend über mehrere Jahre. Akute Leukämien entstehen in der Blastenphase und unterliegen einer schnellen Selbsterneuerung der Zellen, welche durch weitere Entwicklung der entarteten Vorläuferzellen zu chronischen Leukämien führen.[10, 12-14] Diese verdrängen die normale Blutbildung, wodurch entsprechende Krankheitssymptome auftreten. Die Infektionsabwehr ist gesenkt und durch die Abnahme der roten Blutkörperchen tritt bei den betroffenen Patienten eine Blutarmut (Anämie) auf.[7]

Mit 28 % weltweit bzw. mit 27 % in Deutschland (im Jahr 2010) ist die akute myeloische Leukämie die zweithäufigste auftretende Form (Tabelle 1).[10] Die Symptome fallen je nach Art der Leukämien unterschiedlich aus. Bei den chronischen Leukämien verlaufen die

Krankheitssymptome meist schleichend, sodass die betroffenen Patienten die Krankheit lange nicht bemerken. Meist wird diese Art erst nach Blutuntersuchungen diagnostiziert. Anders hingegen sieht es bei den akuten Leukämien aus. Hier sind vielfältige Krankheitssymptome erkennbar. Die häufigsten Kennzeichen sind neben Anämie, Atemnot, Nasenbluten sowie Zahnfleischbluten, vor allem eine vergrößerte Milz und Leber, sowie Fieber und schwer verlaufende Infekte.[7] Die Ursachen für die Entstehung akuter Leukämien sind unterschiedlichster Art. Die bekanntesten sind ionisierende Strahlung, Tabakkonsum, Insektizide sowie Herbizide und auch toxische Chemikalien wie Benzol.[6, 7, 15-17] Aber auch genetische Ursachen scheinen eine entscheidende Rolle einzunehmen. So tritt bei Patienten die an dem Down-Syndrom (Trisomie 21) erkrankt sind, die akute myeloische Leukämie besonders häufig auf (Tabelle 2).

Tabelle 1: Prozentuale Verteilung der unterschiedlichen Leukämieformen in Deutschland (2010) sowie weltweit.

Typ	Anteil [%]	
	Deutschland (2010)[6]	**weltweit[10]**
chronisch myeloische Leukämie (CML)	10	13
akute myeloische Leukämie (AML)	27	28
chronisch lymphatische Leukämie (CLL)	37	30
akute lymphatische Leukämie (ALL)	8	13
Sonstige (ungenau bezeichnete Leukämieformen)	18	17

1.1.2 Diagnostik und Therapiemöglichkeiten der AML

Ist der Verdacht einer akuten Leukämie aufgekommen, wird der Arzt zunächst Milz, Leber und Lymphknoten abtasten, da eine Vergrößerung dieser kennzeichnend für akute Leukämien sind. Anschließend werden Blutuntersuchungen durchgeführt, bei der eine Anämie oder auch ein Mangel an Blutplättchen festgestellt werden. Im Falle der akuten Leukämie wird ebenso eine abnormal hohe Anzahl an weißen Blutkörperchen gefunden. Mittels lichtmikroskopischer Untersuchungen lassen sich anschließend die charakteristischen leukämischen Zellen bzw. Blasten erkennen. Rötlich-violette Einschlüsse in den Zellen, die sogenannten Auer-Stäbchen, sind typisch für eine akute myeloische Leukämie.[18] Um eine 100%ige Gewissheit zu haben, muss zusätzlich zu den Blutuntersuchungen eine Knochenmarkpunktion durchgeführt werden. Durch die Entnahme des Knochenmarks wird bei positiv erkrankten Patienten eine erhöhte Anzahl an entarteten Vorläuferzellen gefunden,

wohingegen gesunde Leukozyten bei der akuten Leukämie kaum noch zu finden sind. Bildgebende Verfahren wie Röntgenuntersuchungen mittels Magnetresonanztomografie (MRT) und Computertomografie (CT) sowie der Sonografie könne zudem zeigen, ob die entarteten leukämischen Zellen bereits innere Organe befallen haben.

Ist die Diagnose der akuten myeloischen Leukämie gefallen, muss eine schnelle Behandlung erfolgen, da diese sonst binnen weniger Wochen bzw. Monaten zum Tode führt. Ziel der Behandlung ist es, eine gesunde Blutbildung wieder zu gewährleisten und die leukämischen Zellen zu beseitigen. Ausgangspunkt hierfür ist die Behandlung mittels Chemotherapie durch Verabreichung von Zytostatika (grie. *cyto* „Zelle“ und *statik* „anhalten“). Grundlage der Chemotherapie ist die Zerstörung aller Zellen, die sich schnell teilen können, wobei entartete Zellen besonders anfällig sind. Die verwendeten Medikamente können als Monotherapie oder als Kombinationstherapie eingesetzt werden, sind meist sehr giftig und werden nach Verabreichung über den Blutkreislauf im gesamten Körper verteilt. Nachteil hierbei ist, dass nicht nur leukämische Zellen zerstört werden, sondern auch gesunde, sich schnell teilende Zellen wie Schleimhaut- und Haarwurzelzellen.[7] Zytostatika können je nach Krankheitsbild durch weitere Therapiemöglichkeiten, wie Signalübertragungshemmern (Tyrosinkinaseinhibitoren), therapeutische Antikörper oder Strahlenbehandlung ergänzt oder gänzlich ersetzt werden. Die Behandlung mittels Zytostatika wird in unterschiedliche Phasen aufgeteilt. In der ersten Phase, der Induktionschemotherapie, soll eine komplette Remission erlangt werden. Hier sollen keine leukämischen Zellen im Blut mehr nachweisbar sein. Die zweite Phase, Konsolidierungstherapie genannt, hat das übergeordnete Ziel die Remission zu erhalten und gegebenenfalls ausstehende Leukämiezellen zu beseitigen. In der mehrjährigen dritten Phase, Erhaltungstherapie, werden intensivere Behandlungsmethoden eingebaut.[18]

Um die größtmögliche und schnellste Wirkung zu erreichen, werden bei der Behandlung der AML Zytostatika in Kombination eingesetzt. Das Cytosin-Arabinosid (Cytarabin **1**, kurz: araC, Abbildung 5) ist eines der effektivsten Medikamente in der Chemotherapie zur Behandlung der AML. Es ist ein Nukleosid-Analogon des Cytosins und wird nach der Phosphorylierung an der Stelle des natürlichen Analoges in die DNA der Zellen eingebaut und verursacht den Zelltod. In Kombination mit einem Anthracyclin (Daunorubicin **2,** Abbildung 5) wurde diese Therapie schon vor über 40 Jahren entwickelt und hat sich bis heute etabliert.[19, 20] Daunorubicin **2** ist aufgrund seiner planaren Struktur ein DNA-Interkalator. Die Transkription der DNA zur RNA und demzufolge auch die Zellteilung werden blockiert. *In vitro* Versuche zeigten, dass die Effizienz solch eines Kombinationstherapeutikum abhängig von der Formulierung bzw. des molaren Verhältnisses

ist. CPX-351 ist eine liposomale Formulierung von Cytarabin **1** und Daunorubicin **2** in einem molarem Verhältnis von 5:1, konnte die klinische Phase II erfolgreich abschließen und befindet sich nun in Phase III.[21]

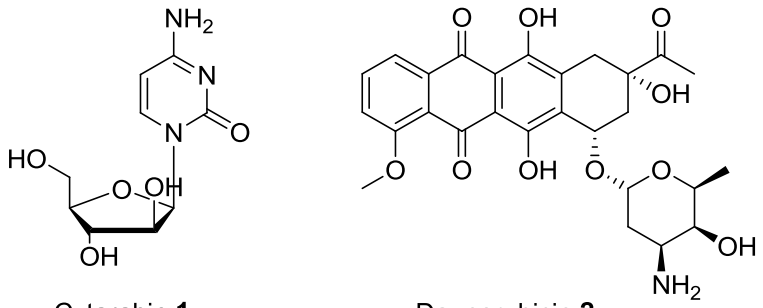

Cytarabin **1** Daunorubicin **2**

Abbildung 5: Strukturen der Zytostatika von Cytarabin **1** und Daunorubicin **2** für die Behandlung der AML.[19, 20]

1.1.3 Zytogenetische und molekulargenetische Merkmale der AML

Die Abgrenzung der AML von der akuten lymphatischen Leukämie (ALL) ist für die Prognose und vor allem für den weiteren Verlauf der Behandlung von entscheidender Bedeutung. Für die Klassifizierung der AML können zwei verschiedene Systeme betrachtet werden. In der Vergangenheit wurde die AML anhand der FAB-Klassifikation (*French-American-British*) vorgenommen. Hierbei erfolgte die Klassifizierung vor allem nach mikroskopisch auffälligen Gesichtspunkten (zytomorphologisch). Das FAB-System wird jedoch vermehrt durch die modernere WHO-Klassifikation (*World Health Organization*) ersetzt, die neben zytomorphologischen Kriterien auch zytogenetische und molekulargenetische Veränderungen mit einbezieht.[22] Die AML ist eine sehr heterogene Erkrankung, wobei in den letzten Jahren eine Vielzahl an molekulargenetischen Veränderungen gefunden wurde.[12, 23] Hierbei werden besonders Genmutationen oder Fehlregulation des NPM1-Gens (*nucleophosphim*) in 30 %, des CEBPA-Gens (*CCAAT/enhancer binding protein*) in 30 %, intern duplizierte Sequenzen (*internal tandem duplications*, ITDs) (20 %) sowie Tyrosinkinase-Mutationen (11-14 %) des FLT3-Gens, Mutationen des TET2-Gens (*ten-eleven translocation 2*) in 7 % und Mutationen des IDH1/IDH2-Gen (*cytoplasmatic isocitrate dehydrogenase 1 and mitochondrial isocitrate dehydrogenase 2*) in 15-33 % der Fälle gefunden.[12, 24] Dies war ausschlaggebend für eine

Revision des WHO-Systems im Jahr 2008, mit Einbezug der gewonnenen prognostischen Faktoren und Genmutationen (Tabelle 2).[25-27]

Tabelle 2: WHO-Klassifikation (2008) der akuten myeloischen Leukämie.[25-27]

AML mit wiederkehrenden zytogenetischen Anomalien	AML mit t(8;21)(q22;q22); RUNX1-RUNX1T1 AML mit inv(16)(p13.1q22) oder (16;16)(p13.1;q22); CBFB-MYH11 APL mit t(15;17)(q22;q12); PML-RARA1 AML mit t(9;11)(p22;q23); MLLT3-MLL AML mit t(6;9)(p23;q34); DEK-NUP214 AML mit inv(3)(q21q26.2) oder t(3;3)(q21;q26.2); RPN1-EVI1 AML (megakaryoblastisch) mit t(1;22)(p13;q13); RBM15-MKL1 AML mit mutiertem NPM1 AML mit mutiertem CEBPA
AML mit Myelodysplasie-assoziierten Veränderungen	
Therapieassoziierte myeloide Neoplasien	
AML ohne weitere Kategorie	AML mit minimaler Differenzierung AML ohne Ausreifung AML mit Ausreifung Akute myelomonozytäre Leukämie Akute monoblastäre/monozytäre Leukämie Akute erythroide Leukämie Akute megakaryoblastische Leukämie Akute basophile Leukämie Akute Panmyelosis mit Myelofibrose
Myeloisches Sarkom	
Myeloische Proliferationen bei Down-Syndrom	Transient abnormale Down Syndrom assoziierte myeloische Leukämie
Blastische plasmazytoide dendritische Zell-Neoplasien	
Akute Leukämien mit unklarer Linienzugehörigkeit	Akute undifferenzierte Leukämie Akute Leukämie mit gemischtem Phänotyp und t(9;22)(q34;q11.2); BCR-ABL1 Akute Leukämie mit gemischtem Phänotyp und (v;11q23); MLL-Umgruppierung Akute Leukämie mit gemischtem Phänotyp, B/myeloid Akute Leukämie mit gemischtem Phänotyp, T/myeloid Natürliche-Killer-Zell lymphoblastische Leukämie/Lymphom

1.1.4 Das „2-Klassen-Modell“ über die Entwicklung der Leukämie

Die Charakterisierung leukämischer Zellen bei AML-Patienten zeigte, dass diese Krankheit auf der einen Seite kennzeichnend für die Dysregulation von Transkriptionsfaktoren in der normalen hämatopoetischen Differenzierung sowie auf der anderen Seite an genetischen Veränderung von Genen beteiligt ist, welche die Signalwege von Zellwachstum und Apoptose beeinflussen. Basierend auf diesen Erkenntnissen, stellten Gilliland und Griffin im Jahr 2002 das „2-Klassen-Modell“ für die Erklärung und das Verständnis bezüglich der Entstehung der Leukämie auf.[28] Demnach ist erst durch das simultane Auftreten zweier unterschiedlicher

Mutationen, Klasse-I- und Klasse-II-Mutationen, die Entwicklung einer Leukämie insbesondere der AML wahrscheinlich (Abbildung 6). Zusammen führen diese beiden Gruppen zur Entwicklung neoplastischer Transformationen blutbildender Zellen. Klasse-I-Mutationen sind *gain-of-function* Mutationen und umfassen Gene, die für die Aktivierung der Signaltransduktion wie Zellwachstum, Zellüberleben und Apoptosehemmung verantwortlich sind. Neben N-RAS, K-RAS und c-KIT, zählt vor allem das FLT3-Gen, welches das meist mutierte Gen in der AML ist, zu dieser Gruppe.[28] Klasse-II-Mutationen, *loss-of-function* Mutationen, betreffen die Transkriptionsfaktoren, wodurch es zu einer gestörten Differenzierung der Zellen kommt. Hierzu zählen besonders die Gene CEBPA, NMP1, MLL und PML/RARA.

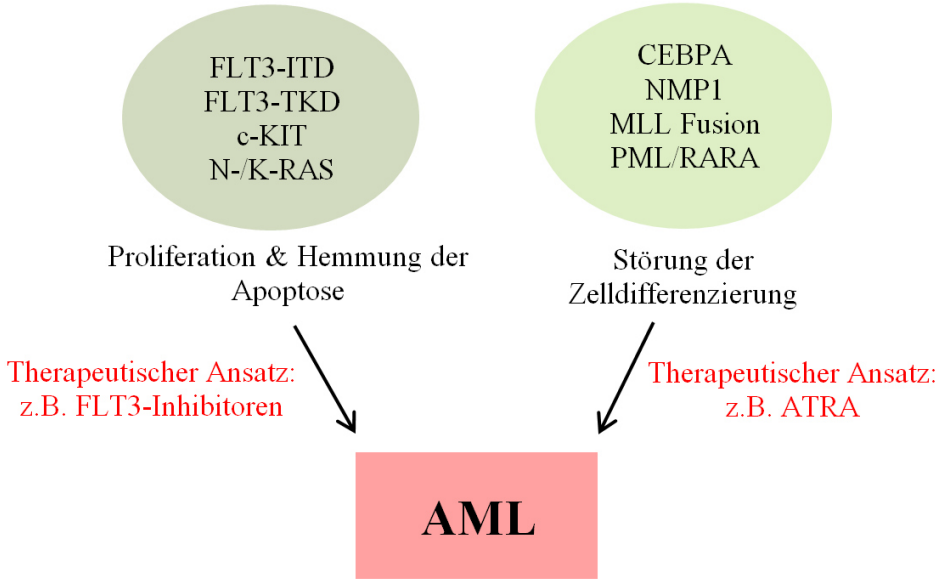

Abbildung 6: Das „2-Klassen-Modell“ der akuten myeloischen Leukämie. Nach diesem Modell fördert das Auftreten zweier Mutationen aus den Klasse-I und Klasse-II die Entwicklung der AML. ATRA (Vitamin-A-Säure bzw. all-*tans*-Retinsäure, *all-trans-retinoic acid*).[28, 29]

1.2 FLT3 als molekulares Target in der Tumortherapie

1.2.1 Struktur und Funktion von Proteinkinasen

Proteinkinasen regulieren eine Zahl von zellulären Prozessen wie Gentranskription, Zellwachstum, Proliferation, Metabolismus und Zelldifferenzierung.[30, 31] Sie katalysieren die reversible Übertragung eines γ-Phosphatrests des Adenosintriphosphats (ATPs) auf bestimmte Aminosäuren des Proteins (Abbildung 7). Demnach werden zwischen Serin-, Threonin- und Tyrosinkinasen unterschieden, wobei mit ca. 80 % die Serin/Threonin-spezifischen Kinasen die größte Gruppe bilden. ATP bindet an das aktive Zentrum der Kinase, worauf nach Bindung des Substrats der γ-Phosphatrest des ATPs auf ein Serin-, Threonin- oder Tyrosinrest des Substrates übertragen wird.[32] In Eukaryoten sind ungefähr 30 % aller Proteine reversibel phosphoryliert.[1]

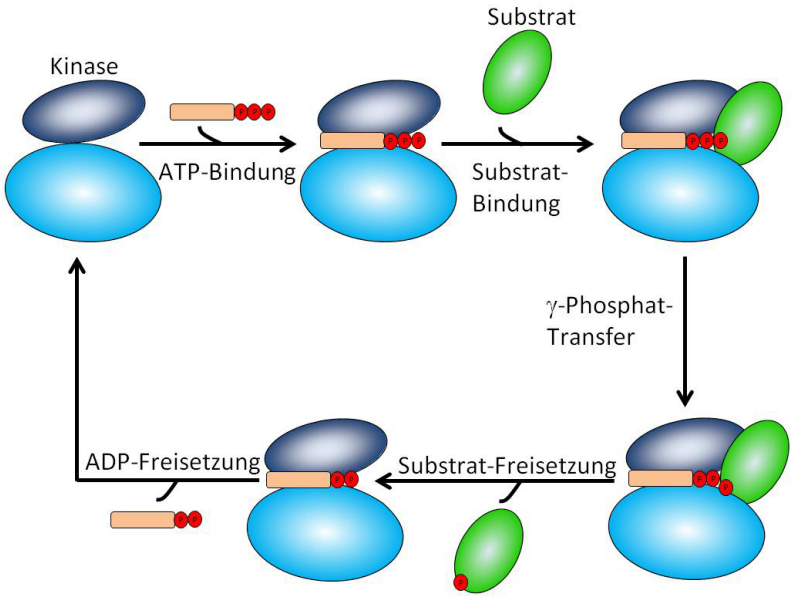

Abbildung 7: Schematische Darstellung der Übertragung einer γ-Phosphatgruppe des ATPs auf ein Substrat. In Anlehnung an Ubersax *et al.*[32]

Proteinkinasen sind hochflexible Enzyme mit hoher konformativer Beweglichkeit ihrer einzelnen Elemente.[30] Durch die Übertragung einer Phosphatgruppe ändern sich die elektrostatischen Eigenschaften des Proteins, wodurch konformative Umlagerungen induziert und so neue Bindungsstellen freigegeben werden können. Klassische Proteinkinasen besitzen eine katalytische Domäne mit ungefähr 250 Aminosäuren, welche in zwei Untereinheiten aufgeteilt ist. Die N-terminale Untereinheit besteht überwiegend aus β-Faltblättern, wohingegen der größere C-terminale Teil durch α-Helices geprägt ist (Abbildung 8).[32] Das

katalytisch aktive Zentrum, die ATP-Bindungstasche, liegt zwischen diesen beiden Untereinheiten und wird auch als *hinge-region* (Gelenk-Region) bezeichnet. Gewöhnlich besitzt die *hinge-region* eine Aminosäure mit einem Wasserstoff-Akzeptor, welcher von zwei Aminosäuren mit Wasserstoff-Donoren flankiert ist.[33] Der *activation loop* (Aktivierungsschleife) beinhaltet die Aminosäurereste Serin, Threonin oder Tyrosin, welche alle phosphoryliert werden können. Sind diese Reste nicht phophoryliert, besetzt die Aktivierungsschleife Teile der ATP-Bindungstasche. Im phosphoryliertem Zustand kommt es zu einer Konformationsänderung, wobei die Aktivierungsschleife sich der Oberfläche zuneigt und so die ATP-Bindungsstelle freigibt.[33] ATP kann jetzt binden und die Phosphatübertragung auf ein Substrat katalysieren. Die N-terminale Seite der Aktivierungsschleife enthält das hochkonservierte DFG-Motiv (D: Asparaginsäure, F: Phenylalanin, G: Glycin). Die Asparaginsäure ist katalytisch an der Phosphatübertragung beteiligt und bildet zusätzlich mit Lysin eine Salzbrücke. Das DFG-Motiv kann in zwei Konformationen vorliegen: DFG-*in* und DFG-*out*. In der DFG-*out* Konformation dreht sich die katalytisch wichtige Asparaginsäure aus der ATP-Bindungstasche, worauf die beiden angrenzenden Aminosäuren, Phenylalanin und Glycin, sich ebenfalls mitdrehen.

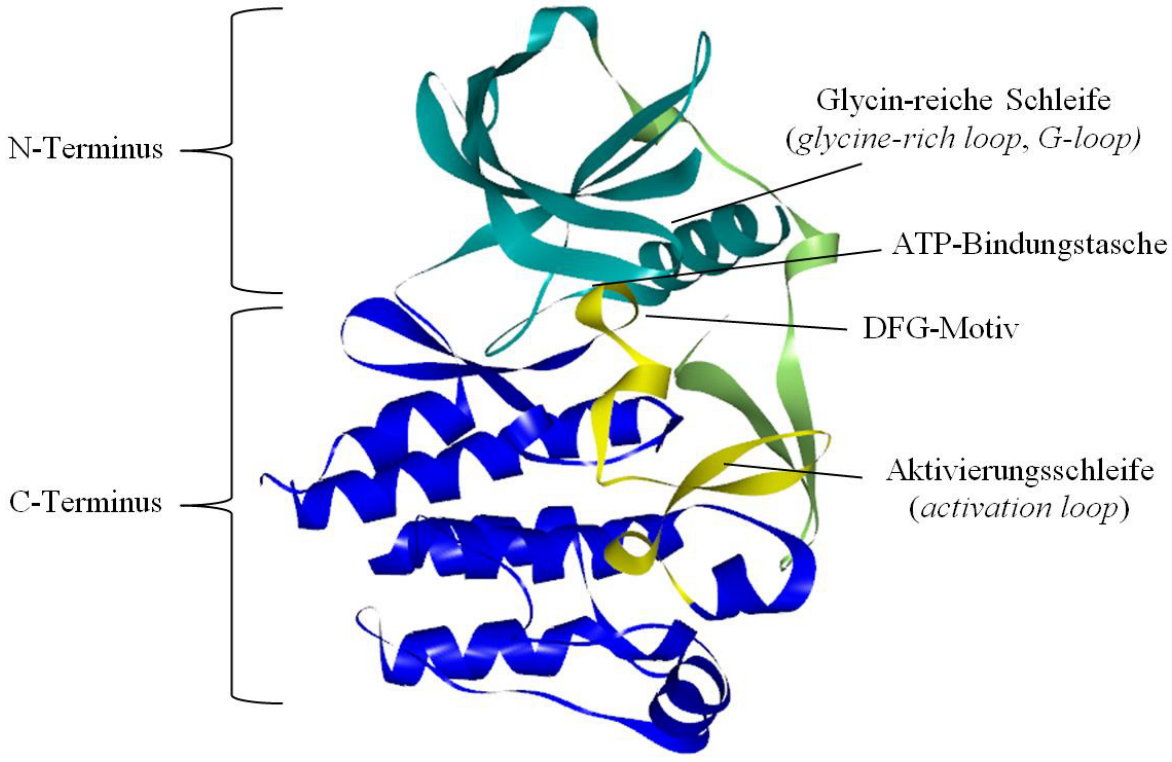

Abbildung 8: Allgemeine Struktur einer Kinase dargestellt anhand von FLT3 (PDB: 1RJB). Dargestellt mit *Discovery Studio 4 Visualizer*.

Durch die Rotation des Phenylalanins wird eine große hydrophobe Bindungsregion freigegeben, welche von zentraler Bedeutung für die Kinasefunktion und Entwicklung von Inhibitoren ist.[33] Innerhalb der ATP-Bindungstasche befindet sich weiterhin eine Glycin-reiche Schleife (*glycine-rich loop*) mit dem stark konservierten GXGXXG-Motiv. Alternativ wird dieses Motiv auch als *G-loop* bzw. *P-loop* bezeichnet.[30] Der sogenannte *Gatekeeper* ist eine der wichtigsten und relevantesten Aminosäuren in der ATP-Bindungstasche und ist für die Kinasefunktion essentiell. Er ist für die richtige Positionierung des ATP-Moleküls, welches das Substrat phophoryliert, verantwortlich. Die Größe und das Volumen dieser Aminosäure bestimmen den Zugang zur hydrophoben Region hinter ihr und kann somit zur Selektivität eines Inhibitors beitragen.[33]

1.2.2 Rezeptor-Tyrosinkinasen

Die Hämatopoese ist ein streng regulierter Prozess. Ausgehend von einer kleinen, sich stetig selbsterneuerten Zellpopulation entwickeln sich hochdifferenzierte Zellen mit spezifischen Funktionen. Dieser Prozess wird von einer Zahl von Wachstumsfaktoren sowie Zytokinen kontrolliert. Einige von ihnen binden an Rezeptoren, die sich in der Zellmembran befinden, wodurch die Signalweitergabe in die Zelle erfolgen kann.[34]

Proteintyrosinkinasen (PTKs) katalysieren die Übertragung eines γ-Phosphatrests des ATPs auf einen Tyrosinrest des Polypeptids. Zurzeit sind mehr als 90 humane PTKs bekannt, welche sich in zwei große Klassen unterteilen: Nicht-Rezeptor-Tyrosinkinasen und Rezeptor-Tyrosinkinasen (RTKs). 58 davon codieren für die transmembranen RTKs, welche sich wiederum in 20 Subfamilien unterteilen, wobei die Unterteilung anhand ihrer extrazellulären, Liganden-bindende Domäne vorgenommen wird (Abbildung 9).[35, 36] Während Klasse I und Klasse II RTKs überwiegend über eine cysteinreiche extrazelluläre Domäne verfügen, besitzen Mitglieder der FGFR (*fibroblast growth factor receptor*), PDGFR (*platelet-derived growth factor receptor*) und VEGFR (*vascular endothelial growth factor receptor*) zwischen drei und sieben Immunglobulin-ähnliche Domänen. Die RTKs der Klassen II-V, VII, XI und XIV werden im blutbildenden Gewebe exprimiert und deshalb werden die meisten von ihnen in Verbindung mit der Entstehung der Leukämie gebracht.[36, 37]

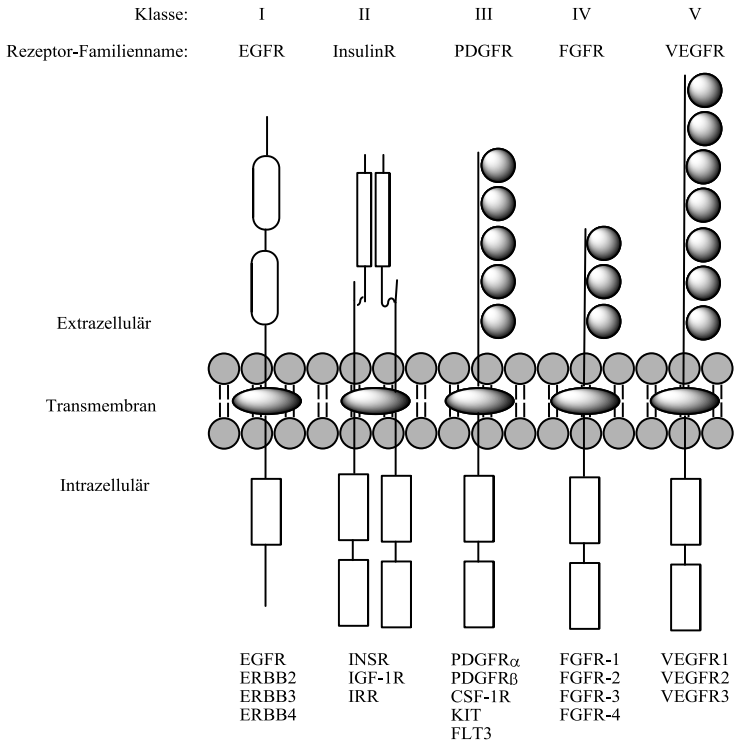

Abbildung 9: Schematische Darstellung der RTKs aus den Klassen I-V. In Anlehnung an Blume-Jensen *et al*.[35]

1.2.3 FLT3 – Eine Klasse-III-Rezeptor-Tyrosinkinase

Klasse III RTKs spielen eine entscheidende Rolle in der normalen, aber auch in der abnormalen Blutbildung. Neben c-KIT, PDGFRα, PDGFRβ, CSF-1 gehört ebenso FLT3 zu dieser Gruppe. FLT3 (*FMS-like tyrosine kinase 3*), auch bekannt als *stem cell tyrosine kinase-1* (STK-1) oder *fetal liver tyrosine kinase 2* (FLT2), ist auf dem Chromosom 13q12 lokalisiert und wurde erstmals 1991 unabhängig von zwei Gruppen beschrieben.[38-40] Wie alle RTKs der Klasse III besitzt FLT3 eine glykosylierte extrazelluläre Liganden-binde Domäne mit fünf Immunglobulin-ähnlichen Motiven. Eine Transmembran-Domäne (TM), eine Juxtamembran-Domäne (JM) und zwei intrazelluläre Tyrosinkinase-Domänen (TK1 und TK2), welche durch ein Kinase-Insert (KI) getrennt sind, vervollständigen die Struktur von FLT3 (Abbildung 10).[41-43] Humanes FLT3 besteht aus 993 Aminosäuren und tritt mit 134 kDa als unglykosyliertes, mit 140 kDa als schwach glykosyliertes und mit 160 kDa als stark glykosyliertes Protein auf.[44] FLT3 wird vorzugsweise in unreifen hämatopoetischen Stammzellen ($CD34^+$) exprimiert und ist entscheidend für die normale Funktion der Stammzellen und das Immunsystem. Außerdem ist es in der Placenta, der Keimdrüse und

dem Gehirn zu finden, jedoch ist hier die Funktion des FLT3-Rezeptors noch unbekannt.[42, 45] In abnormal hohen Konzentrationen wird FLT3 in den meisten humanen Leukämien gefunden, vor allem in mehr als 90 % der Fälle in AML.[42]

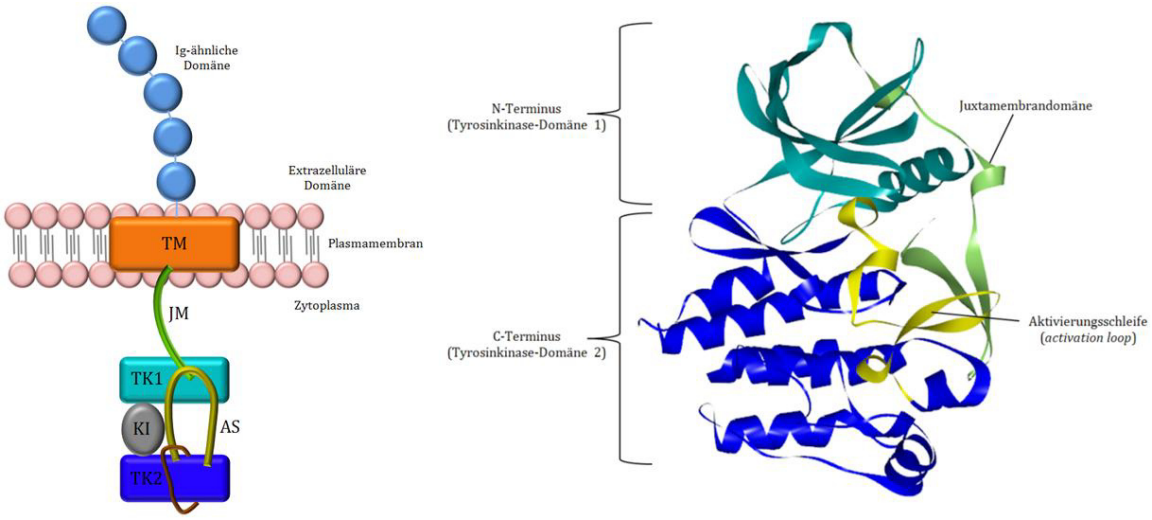

Abbildung 10: Links: Schematische Darstellung des FLT3-Rezeptors. TM: Transmembran-Domäne; JM: Juxtamembran-Domäne; TK1 und TK2: Tyrosinkinase-Domäne 1 und 2; KI: Kinase-Insert, AS: Aktivierungsschleife. Rechts: Kristallstruktur von FLT3 (PDB: 1RJB). Dargestellt mit *Discovery Studio 4 Visualizer*.

2004 wurde erstmals die Kristallstruktur der autoinhibierten, unphosphorylierten Form der TK-Domäne sowie der JM-Domäne von FLT3 gelöst (Abbildung 10).[45] Die Kinasedomäne, die Aktivierungsschleife und die JM-Domäne bilden dabei die grundsätzlichen Merkmale der autoinhibierten FLT3-Struktur. Die Kinasestruktur von FLT3 entspricht den typischen Faltungsmustern, bestehend aus N- und C-terminaler Einheit, welche in den meisten Proteinkinasen zu finden sind. Die N-terminale Domäne ist geprägt aus 5 verdrehten antiparallelen β-Faltblättern, wohingegen die C-terminale Domäne überwiegend aus α-Helices aufgebaut ist. Beide Domänen sind typischerweise durch ein flexibles Polypeptid (Kinase-Insert) miteinander verbunden, wodurch eine freie Rotationsbewegung zwischen den beiden Einheiten zustande kommen kann. Sobald die N-terminale Einheit sich von der C-terminalen wegdreht, befindet sich die Kinase im katalytischen inaktiven Zustand, und umgekehrt.[45] Das DFG-Motiv der Aktivierungsschleife (AS) wird von den Aminosäuren D829, F830 und G831 gebildet. Die JM-Domäne kann in drei unterschiedliche, topologische Bereiche unterteilt werden: *JM binding motif* (JM-B), *JM switch motif* (JM-S) und *JM zipper* oder *linker peptide* (JM-Z). JM-B (Y572-M578) wird Bindungsmotiv genannt, da es fast vollständig in die FLT3-Struktur eingebettet ist. Auch wenn JM-B aus lediglich sieben

Aminosäuren besteht, steht es in Kontakt mit nahezu allen strukturell wertvollen Komponenten, die an den Aktivierungs- und Inaktivierungszyklus der zytoplasmatischen Domäne von FLT3 beteiligt sind.[45] JM-S (Val579-Val592) bildet ein antiparalleles β-Faltblatt und erhält seinen Namen dadurch, dass es zwei wichtige Tyrosinreste, Tyr589 und Tyr591, enthält. Deren Phosphorylierungsgrad ist in der Aktivierung und Regulation der enzymatischen Aktivität des Rezeptors involviert. JM-Z (Asp593-Trp603) ist am C-Terminus der JM-Domäne lokalisiert und ist hauptsächlich mit der N-terminalen Einheit assoziiert, an der es sich außen entlang faltet.[45] Die Glycin-reiche Schleife GXGXXG wird von den Aminosäureresten 617-622 gebildet.

1.2.4 Signalwege des FLT3-Rezeptors

Der FLT3-Signalweg scheint eine entscheidende Funktion für die Entwicklung hämatopoetischer Stammzellen zu übernehmen. Die Rezeptoren der Tyrosinkinasen werden durch die extrazelluläre Bindung eines spezifischen Liganden aktiviert und übermitteln extrazelluläre Signale in den zytoplasmatischen Bereich. Der Ligand für FLT3 (FLT3-Ligand, FL) ist ein Typ-I-Membranprotein, das zu einer kleinen Gruppe der Wachstumsfaktoren gehört und die Proliferation sowie Differenzierung blutbildender Zellen anregt.[13, 46] Drei Isoformen des FL sind bislang bekannt. Der FL wird in den meisten Geweben wie Prostata, Lunge, Niere, Eierstöcke, Hoden und Herz, einschließlich den blutbildenden Organen (Milz, Thymusdrüse, Knochenmark) exprimiert.[13]

Die Bindung des FL löst zunächst eine schnelle Konformationsänderung aus, wobei es zu einer Homodimerisierung des membrangebundenen FLT3-Rezeptors kommt. Diese Homodimerisierung bewirkt, dass verschiedene Tyrosinreste der zytoplasmatischen Tyrosinkinase-Domäne freigelegt werden. Die anschließende Auto- bzw. Transphosphorylierung spezifischer Tyrosinreste erfolgt innerhalb von 5-15 Minuten nach Bindung des FL (Abbildung 11).[46-48] Obwohl der Signalweg nach Bindung des FL an den FLT3-Rezeptor noch nicht vollkommen entschlüsselt worden ist, ist jedoch bewiesen, dass wenn die Kinase einmal aktiviert wurde, sie ein regelrechtes Netzwerk von Proteinen beeinflusst. Die Bindung des Liganden aktiviert vor allem PI3K (*phosphatidylinositol 3-kinase*) und RAS, was zu einer steigenden Zellproliferation sowie zu einer Apoptosehemmung führt.[48] Die PI3K-Aktivität wird vermutlich durch Interaktionen zwischen FLT3 und SHC-Proteinen (*SH2-containing sequence proteins*), sowie

wahrscheinlich durch SHIP (*SH2-domain-containing inositol phosphatase*) reguliert. Aktivierte PI3K stimuliert weiterhin nachgeschaltete Proteine, hier besonders AKT/PKB (*protein kinase B*) und mTOR (*mammilian target of rapamycin*), welche die Transkription und Translation wichtiger regulatorischer Gene initiieren.[13, 48]

Einmal aktivierte FLT3 interagiert mit GRB2 (*growth factor receptor-bound protein 2*) über SHC und aktiviert so RAS. Die Aktivierung von RAS beeinflusst über verschiedene Zwischenproteine die Aktivierung von ERK (*extracellular-signal regulated kinase*) und STAT5 (*signal transducter and activator of transcription 5*). All diese Signalwege sind in der Zellproliferation, Differenzierung und der Apoptose involviert.[42, 48]

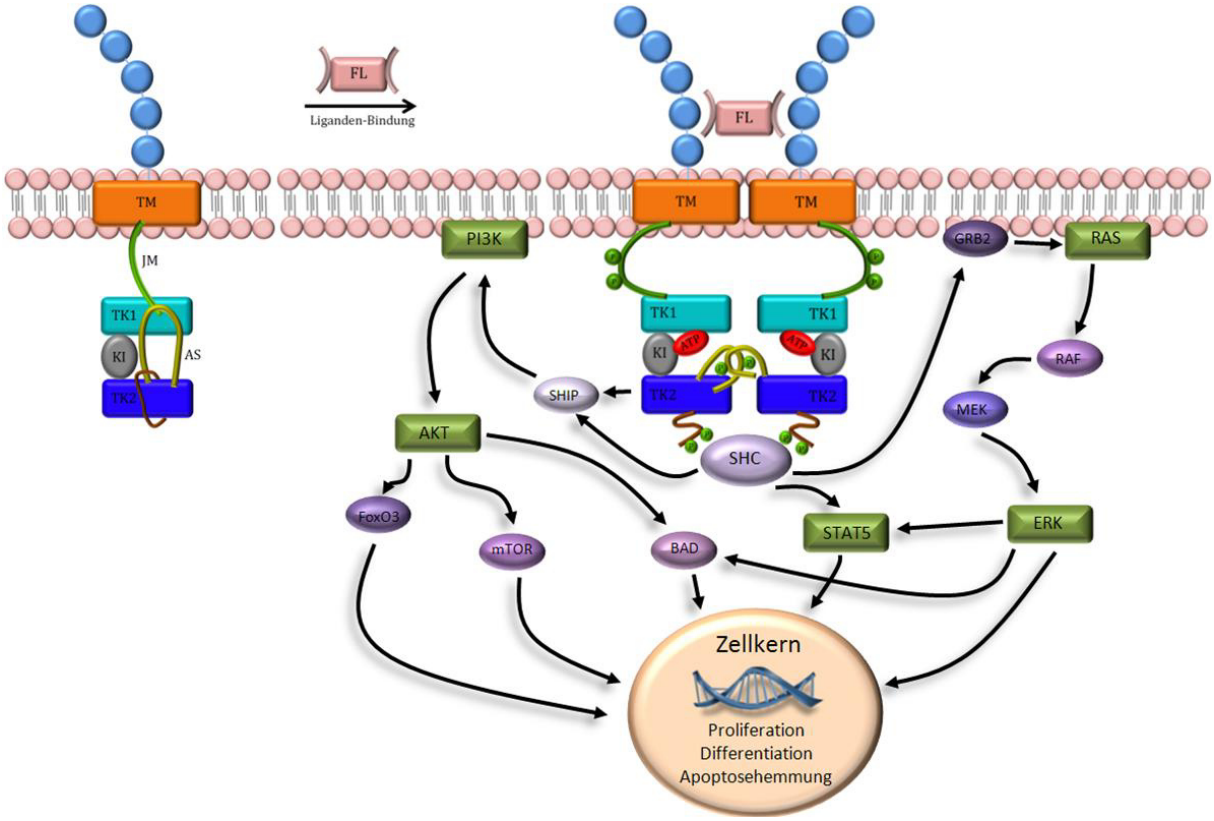

Abbildung 11: Bindung des FLT3-Liganden (FL) mit anschließender Homodimerisierung des Rezeptors. Durch die Aktivierung von FLT3 wird ein intrazelluläres Signalnetzwerk gestartet.[13, 46]

1.2.5 FLT3 und seine Rolle in der akuten myeloischen Leukämie

Die molekulare Pathogenese der AML ist bislang noch nicht komplett entschlüsselt.[49] Fest steht jedoch, dass in größer 90 % der auftretenden AML-Fälle FLT3 und sein Ligand in abnormal hohen Konzentration exprimiert wird.[42, 43, 50, 51] Dies ist ein Indiz dafür, dass die Aktivierung von FLT3 durch seinen Liganden eine wichtige Rolle in humanen Leukämien, besonders in der AML einnimmt.

Des Weiteren handelt es sich bei der AML, wie bereits in Kapitel 1.1.3 erwähnt, um eine sehr heterogene Erkrankung.[12, 49] Vor allem Genmutationen des FLT3-Rezeptors sind in den letzten Jahren vermehrt in den Vordergrund gerückt, da diese die meist bekannten und am häufigsten auftretenden Gen-Abnormitäten in der AML darstellen. Ungefähr 30 % aller AML diagnostizierten Fälle weisen Mutationen des FLT3-Gens auf, wobei die Häufigkeit der *de novo* AML mit 26 % höher ist, als in der sekundären AML (9 %).[13] Rund ein Drittel aller AML-Patienten weisen drei unterschiedliche Klassen aktivierender Mutationen auf. Die erste Klasse an Mutationen wurde erstmals 1996 von Nakao *et al*. beschrieben.[52] Hierbei handelt es sich um interne Tandem-Duplikationen (*internal tandem duplications*, ITDs) in der JM-Domäne und sind in den leukämischen Blasten von ungefähr 20-23 % zu finden.[46, 50, 53, 54] Darauffolgend haben im Jahr 2001 zwei weitere Gruppen, unabhängig voneinander, aktivierende Punkt-Mutationen in der TK-Domäne des Asp835- bzw. des Ile836-Restes identifiziert.[55, 56] Diese treten weniger häufig auf und sind in rund 6-12 % der AML-Patienten nachweisbar.[46, 53] Die dritte Klasse aktivierender Mutationen wurde 2004 entschlüsselt.[57, 58] Hierbei handelt es sich ebenfalls um Punktmutationen, jedoch in der JM-Domäne lokalisiert, welche mit 2 % sehr selten auftreten.[53] Erst vergangenes Jahr, 2013, wurde ein neuer Typ von FLT3-Mutationen in der ATP-Bindungstasche gefunden. Die Gruppe um Opatz *et al*. identifizierte die Punktmutation Asn676Lys in der TK-Domäne 1 von FLT3 und wurde in 6 % der AML-Fälle nachgewiesen.[46, 59]

ITDs bestehen aus variablen Duplikationen von Basenpaaren, welche auf den Exons 14 und 15 der JM-Domäne lokalisiert sind.[54] Die Länge variiert im Allgemeinen zwischen 3 und mehr als 400 Basenpaaren.[13, 46] Die JM-Domäne der RTKs übernimmt meistens autoinhibitorische Funktionen, indem sie die Aktivierung der Kinase blockt und somit die Selbst-Dimerisierung verhindert. Durch das Auftreten von ITD-Mutationen kommt es zu einer Zerstörung der Sekundärstruktur, was zu einer konstitutiven, Liganden-unabhängigen Aktivierung der Kinase führt.[13, 60] Dieser Konformationswechsel der JM begünstigt die Liganden-unabhängige Homodimerisierung und demzufolge auch die Autophosphorylierung

und Aktivierung des FLT3-Rezeptors. Folglich kommt es zu einer Zytokin-unabhängigen Proliferation durch auslösen des Signalwegs. ITDs treten nicht nur im FLT3-Rezeptor auf, sondern kommen ebenfalls im verwandten KIT-Rezeptor sowie in nicht-humanen Genen vor.[51]

Bei der zweiten, größeren Klasse an FLT3-Mutationen handelt es sich um Punktmutationen in der TK-Domäne des FLT3-Rezeptors, welche auf dem Exon 20 lokalisiert sind.[53] Hierbei handelt es sich um Mutationen der Aktivierungsschleife. Neben Ile836 treten vor allem Mutationen des Asp835-Restes auf. Bislang sind unterschiedliche Mutationen von Asp835 bekannt: D835Y, D835H, D835V und D835N. Anstelle der Aminosäure Ile836 werden die Mutationen mit Methionin (I836M) und mit Asparagin (I836N) gefunden.[13, 54] Die Punktmutationen beeinflussen die Stabilisierung der Aktivierungsschleife der geöffneten ATP-Bindungstasche, wodurch es ebenfalls zu einer Liganden-unabhängigen Aktivierung des FLT3-Rezeptors kommt.[53] Punktmutationen sind weniger häufig als ITDs, jedoch sind sie von entscheidender therapeutischer Bedeutung im Hinblick auf die Behandlung mit Tyrosinkinase-Inhibitoren (TKIs). Einige dieser weisen Resistenzen auf und zeigen keine, oder nur geringe Aktivität gegenüber den D835-Mutanten.[60]

In den seltensten Fällen (2 %) weisen AML-Patienten beide Mutationen, ITDs und Punktmutationen, gleichzeitig auf, welche mit einer sehr schlechten Prognose assoziiert sind. Bei 40 % ist diese Doppel-Mutation auf demselben Allel lokalisiert.[13, 46]

1.2.6 Inhibitionsarten von Proteinkinase-Inhibitoren

Eine der größten Targetfamilien sind die Proteinkinasen. Verschiedene Signalwege werden von ihnen gesteuert und versetzen Proteine vom inaktiven in den aktiven Zustand. Das Design von Inhibitoren richtet sich zum größten Teil auf eine kompetitive Inhibition, bei der das ATP aus seiner Bindungstasche verdrängt wird. ATP ist eines der wichtigsten Energieübertragungsmoleküle im zellulären Stoffwechsel und wird nicht nur von den Kinasen, sondern auch von weiteren zahlreichen Cofaktoren verwendet.

Je nach Inhibition lassen sich Proteinkinaseinhibitoren in unterschiedliche Gruppen einteilen. Die meisten der entwickelten Inhibitoren sind ATP-kompetitiv und zählen zu den Typ-I-Inhibitoren. Diese imitieren die Interaktionen der Adenineinheit und binden an dessen Stelle. Typischerweise werden dabei ein bis drei Wasserstoffbrückenbindungen mit der *hinge-region* ausgebildet.[61, 62] Die Kinase befindet sich bei der Typ-I-Inhibition im aktiven Zustand, wobei

sich das DFG-Motiv in der DFG-*in*-Konformation befindet und die regulatorische Tasche besetzt. Der *Gatekeeper* kontrolliert den Zugang zu einer weiteren, zweiten hydrophoben Bindungstasche. Da sich die Kinasen innerhalb der ATP-Bindungstasche sequenziell und strukturell sehr ähnlich sind, ist es oft schwierig selektive Kinaseinhibitoren herzustellen. Demnach ist ein Ansatzpunkt Inhibitoren zu entwickeln, welche Zugang zu dieser zweiten hydrophoben Bindungstasche haben, da diese ein Zugewinn an Aktivität und Selektivität darstellt.[63, 64] Jedoch können klinisch relevante Resistenzmutationen an dieser *Gatekepper*-Position auftreten und die Bindung der Inhibitoren verhindern.[64]

Im Gegensatz zu der Typ-I-Inhibition binden und stabilisieren Moleküle des Typs II die inaktive DFG-*out* Konformation der Proteinkinase. Durch die unterschiedlichen Positionierungen der DFG-Aminosäurenreste in der *out*-Konformation wird eine zusätzliche Tasche, die allosterische Bindungstasche, freigegeben. Diese allosterische Bindungstasche ist meist hydrophober Natur und Inhibitoren des Typ-II binden sowohl in der ATP als auch in der allosterischen Tasche.[62, 65] Typ-II-Inhibitoren weisen typischerweise eine höhere zelluläre Aktivität auf, vermutlich da sie an die DFG-*out*-Konformation binden und diese eine geringere Affinität für ATP aufweist.[61]

Allosterische Inhibitoren, welche die dritte Klasse bilden, binden ausschließlich in eine allosterische Bindungstasche der inaktiven Proteinkinase. Inhibitoren, die zu dieser Klasse zählen, weisen einen hohen Grad an Kinaseselektivität auf, da sie mit einzigartigen Bereichen außerhalb der ATP-Bindungstasche der Kinase wechselwirken können.[63, 65-67] Jedoch ist es manchmal kompliziert eine genaue Unterscheidung zwischen Typ-II und Typ-III Inhibitoren zu treffen, da aufgrund der Tatsache, dass Inhibitoren, welche außerhalb der ATP-Bindungstasche binden in kinetischen Experimenten ATP-kompetitive Inhibitoren darstellen können.[63]

Typ-IV-Inhibitoren sind Moleküle, welche an einige Ångström entfernten allosterischen Taschen, außerhalb der ATP-Bindungstasche binden und imstande sind die inaktive Konformation zu stabilisieren.[66, 67]

Neben der bisher erwähnten reversiblen gibt es außerdem irreversible Inhibition. Diese Klasse an Inhibitoren ist imstande irreversible, kovalente Bindungen mit einem Cysteinrest der ATP-Bindungstasche einzugehen. Der Inhibitor wird hierbei mit einem elektrophilen Rest versehen (Michael-Akzeptor), welcher schließlich in einer Michael-Addition eine kovalente Bindung mit dem elektronenreichen Schwefel des Cysteins ausbilden kann. In Folge dessen blockiert der Inhibitor irreversibel die Bindung von ATP an die Kinase, wodurch diese in einer inaktiven Form vorliegt.[63-65]

Trotz der zahlreichen Entwicklungen von Medikamenten gegenüber bestimmte Kinasen und den dazugehörigen hohen aufgebrachten Investitionen haben es nur eine Handvoll von Substanzen auf den Markt geschafft. Gegenwärtig sind lediglich 16 niedermolekulare Kinaseinhibitoren von der FDA (*Food and Drug Administration*) für die Krebsbehandlung zugelassen worden (eine Auswahl ist in Abbildung 12 dargestellt).[68-70] Alle diese Verbindungen sind ATP-kompetitiv und gehören entweder zu den Typ-I oder den Typ-II-Inhibitoren. Ein repräsentatives Beispiel für die Typ-I-Inhibition ist Sunitinib **3**. Dieses wurde 2006 von der FDA für die Behandlung von gastrointestinalen Stromatumoren sowie zur Behandlung des Nierenzellkarzinom zugelassen.[62, 71] Es zeigte sich jedoch, dass Sunitinib **3** eines der prominentesten Profile für einen Multikinaseinhibitor aufwies. Das Risiko solcher, meist unbeabsichtigt hergestellten Multikinaseinhibitoren ist, dass sie mehrere, auch unbekannte Kinasen inhibieren, wodurch es zu einer Wirkstofftoxizität kommen kann.[63] Erlotinib **4**, Gefitinib **5**, Dasatinib **6**, und Lapatinib **7** sind ebenfalls Inhibitoren des Typs I.[62, 63]

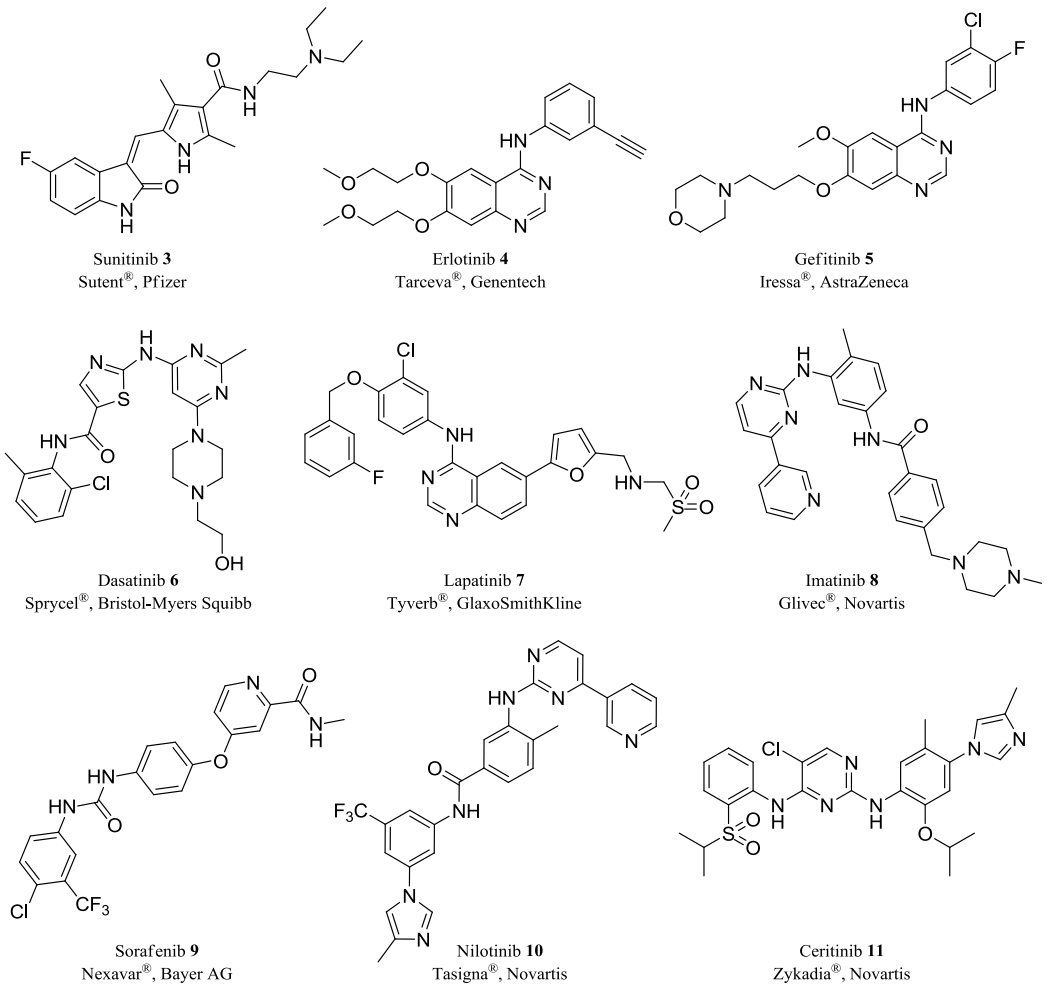

Abbildung 12: Auswahl der von der FDA zugelassenen Medikamente für die Krebsbehandlung.[68-70]

Eine Erfolgsgeschichte war die Entdeckung von Imatinib **8**, ein Medikament, welches neben Sorafenib **9** und Nilotinib **10**, zu den Typ-II-Inhibitoren zählt.[62] Imatinib **8** wurde als erster BCR-ABL (BCR: *breakpoint cluster region*, ABL oder ABL1: *Abelson Murine Leukemia Viral Oncogene Homolog* 1) Tyrosinkinaseinhibitor im Jahre 2001 für die Behandlung der chronischen myeloischen Leukämie (CML) zugelassen und bestand alle Stufen der klinischen Phasen. Die Entwicklung solch eines Inhibitors revolutionierte die Behandlung von Krebs. Erstmalig konnte so ein Krankheitsbild selektiv behandelt werden. Imatinib **8** wies geringe Nebenwirkungen auf, jedoch war die Therapie nicht günstig, sodass dieser in kürzester Zeit zu einem „*Blockbuster*" der Firma Novartis wurde.[1, 63] Neue, weiterentwickelte BCR-ABL-Inhibitoren, wie Erlotinib **4** und Nilotinib **10**, sind nicht nur potenter, sondern inhibieren zudem Mutationen innerhalb der Kinasedomäne.
Für die Behandlung von Lungenkrebs wurde kürzlich im April 2014 Ceritinib **11** von der FDA zugelassen.[69]

1.2.7 Molekulare Interaktionen in biologischen Systemen

Wie wirkt überhaupt ein Arzneistoff? Für die Entwicklung eines Medikamentes steht diese Frage im Vordergrund und gilt es zu beantworten. Um seine Wirkung richtig zu entfalten, muss der Wirkstoff im Körper an ein ganz bestimmtes Zielmolekül binden. Hauptangriffspunkt sind dabei meist Proteine, wie Enzyme oder Rezeptoren. Aber auch Nucleinsäuren (DNA, RNA) stellen Zielmoleküle für Wirkstoffe dar.[1] Zwischenmolekulare Interaktionen sind Schlüsselvorgänge und nehmen in chemischen als auch in biologischen Erkennungsprozessen eine entscheidende Rolle ein. Um in die Bindungstasche des Proteins zu gelangen, ist es wichtig, dass der Wirkstoff die richtige Größe und Gestalt aufweist. Damit sich spezifische Wechselwirkungen zwischen dem Protein und Liganden ausbilden können, ist es von Bedeutung, dass die Oberflächeneigenschaften beider zueinander passen. Dieses Verständnis ist für das rationale Wirkstoffdesign und für die Leitstrukturoptimierung in der medizinischen Chemie von zentraler Bedeutung. Organische Moleküle können mit ihrem Target-Protein kovalente als auch nicht kovalente Bindungen eingehen. Im Folgenden wird ein Überblick über die nichtkovalenten Wechselwirkungen gegeben.
Wichtige Hinweise auf molekulare Interaktionen kann eine Kristallstruktur des Liganden im Komplex mit dem Target-Protein geben. Da alle biochemischen Prozesse in Wasser stattfinden, erfolgt demnach auch die Bindung des Liganden an sein Zielprotein in wässriger

Umgebung. Durch Diffusion eines Liganden in die Bindungstasche des Proteins werden einige Wassermoleküle aus dieser verdrängt. Die meisten der Wassermoleküle sind austauschbar, einige jedoch stehen in unmittelbarem Kontakt zum Protein und können ein Wasserstoffbrückennetzwerk ausbilden.[1, 72] Somit werden gleichzeitig neue, direkte Wasserstoffbrücken zwischen dem Liganden und dem Protein ausgebildet und andererseits diverse Wasserstoffbrücke gebrochen. Wasserstoffbrücken zählen zu den elektrostatischen Wechselwirkungen und sind zugleich die wichtigsten Interaktionen mit Bindungsenergien von -0,2 bis -40 kcal/mol in biologischen Prozessen.[73, 74] Vor allem Interaktionen zwischen der NH- und Carbonylgruppen, sowie Interaktionen zwischen Hydroxygruppen und Ether-, Carbonyl- und Estergruppen gehören mit einem Abstand zwischen 2,6-3,2 Å dazu.[72] Wasserstoffbrücken zu aromatischen π-Systemen sind ebenfalls literaturbekannt und sind schwächer als die klassischen Wasserstoffbrücken (Abbildung 13).[72, 73, 75] Hierzu gehören N-H···π und O-H···π Interaktionen, wobei der Abstand leicht größer zwischen 3,2-3,8 Å ist. In den stabilsten Geometrien der N-H···π und O-H···π Interaktionen befindet sich das Wasser bzw. Stickstoff Molekül über den Zentren des aromatischen Rings. Außerdem wurde belegt, dass die einzähnige Bindungsgeometrie gegenüber der zwei- und dreizähnigen bevorzugt wird. Aufgrund der geringeren Elektronegativität des Stickstoffs wechselwirkt dieser schwächer mit π-Systemen als der H-Brücken Donor des Wassers.[73, 75]

Neben den Wasserstoffbrückenbindungen nehmen Interaktionen mit Halogenen ebenfalls eine wichtige Rolle ein. Die Stärke der Halogenbrücken nimmt mit zunehmender Molmasse von Chlor über Brom zu Iod hin zu. Organofluorverbindun-gen bilden jedoch selten Halogenbrücken aus.[76] Im Gegensatz zu Fluor besitzen die schwereren Halogene einmalige elektronische Eigenschaften, wenn sie an eine Aryl- oder elektronenziehende Gruppe gebunden sind.[72] Aufgrund der Anisotropie der Elektronendichteverteilung können die nichtbindenden Elektronen im äußeren Ring eine negative Ladung ausbilden. Folge dessen entsteht ein positiver Bereich, auch *σ-hole* genannt, welcher in der Lage ist, mit den freien Elektronenpaaren der Carbonylgruppe zu wechselwirken.[72]

Hydrophobe Wechselwirkungen, hier besonders hervorzuheben die Aren-Aren Interaktionen, sind allgegenwärtig in Proteinen. Obwohl die π-π-Wechselwirkungen relativ schwach von Natur aus sind, nehmen sie dennoch eine essentielle Rolle bei der Faltung und thermischen Stabilität von Proteinen ein.[75, 77, 78] Drei unterschiedliche Geometrien des Benzendimers sind bekannt: die parallel verschobene, die *Face-to-Face* Anordnung sowie die T-förmige *Edge-to-Face* Geometrie (Abbildung 13). In Studien wurde gezeigt, dass 60 % der aromatischen Seitenketten von Tryptophan, Tyrosin und Phenylalanin π-π-Wechselwirkungen eingehen, mit

einer Präferenz für die parallel verschobene und die T-förmige Anordnung.[73, 75] Die Wechselwirkungsenergie der *Edge-to-Face* Anordnung ist beeinflussbar durch Substituenten. So erhöhen elektronenziehende Substituenten (CN, NO_2) die Stabilität, wohingegen Elektronendonor Substituenten, wie OH und NH_2, das Dimer destabilisieren können. Die C···C Bindungsabstände bei Arenen liegen zwischen 3,4 und 3,8 Å.[73]

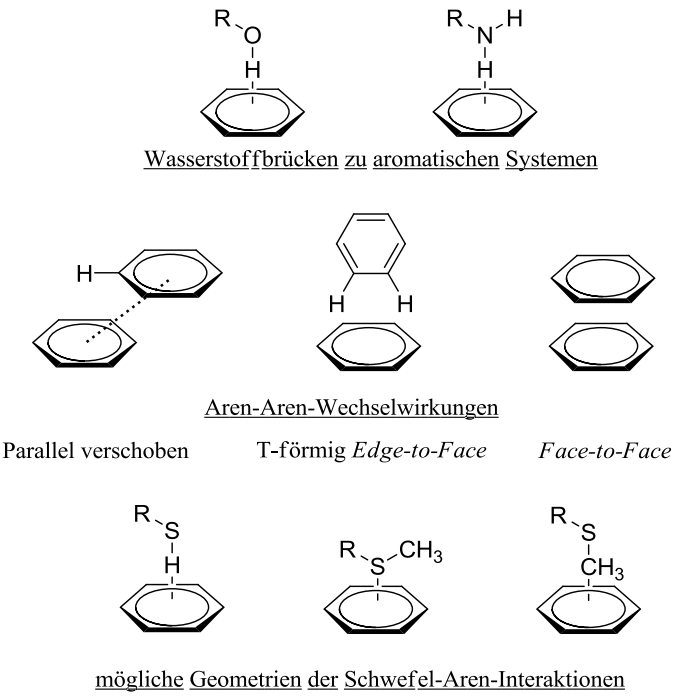

Abbildung 13: Häufig auftretende molekulare Interaktionen in biologischen Systemen.[73, 75]

Eine weitere interessante Wechselwirkung in biologischen Prozessen ist die Interaktion zwischen dem Schwefel, vor allem den Cystein- und Methionin-Seitenketten, und dem Aren. Jedoch sollte der Ausdruck der Schwefel-Aren-Interaktion als Vereinfachung angesehen werden, da sie in unterschiedlichen Wechselwirkungsgeometrien, wie S···π, S-H···π, S-C···π soweie C-H···S vorliegen können (Abbildung 13). Die Schwefel-Aren-Interaktionen treten mit Abständen von 3,6-4,3 Å auf.[72, 73]

1.2.8 *Small molecules* zur Behandlung der AML – Stand der Forschung

Die Erkenntnis, dass die Aktivierung des FLT3-Signalwegs durch Mutationen eine zentrale Rolle in der Pathogenese der AML einnimmt, hat die Pharmaindustrie und einige

Forschungsgruppen dazu angetrieben potentielle Wirkstoffe für die Behandlung der AML zu entwickeln. Eine Option dabei ist, die Kinase und somit ihre Aktivität mittels *small molecules* (niedermolekulare Moleküle) zu inhibieren. Bei den derzeit zugelassenen Wirkstoffen bzw. Arzneimitteln handelt es sich überwiegend um *small molecules*. Aufgrund der hohen Kosten der Wirkstoffentwicklung und der hohen Durchfallquote potentieller Wirkstoffe in klinischen Studien, liegt es im Interesse der Medizinalchemiker bereits vorab die Eigenschaften solcher Wirkstoffkandidaten abzuschätzen und gegebenenfalls auch zu verbessern. Mit der von Lipinski aufgestellten Regel „*Rule of Five*“ kann von denkbaren Wirkstoffen die Löslichkeit und orale Bioverfügbarkeit beurteilt werden.[79] Hierzu sollten folgende Parameter erfüllt sein. Die Verbindung sollte nicht mehr als fünf Wasserstoffdonatoren und nicht mehr als 10 Wasserstoffakzeptoren enthalten. Des Weiteren sollte die molekulare Masse weniger als 500 g/mol betragen und der Verteilungskoeffizient (logP) zwischen Oktanol und Wasser geringer als 5 sein. Bei einer Vielzahl von Wirkstoffen ist die Durchdringung der Blut-Hirn-Schranke von entscheidender Bedeutung. Im Jahre 2010 haben Forscher deshalb eine Multiparameter-Optimierung für das zentrale Nervensystem (*Central Nervous System Multiparameter Optimization*, CNS MPO) durchgeführt, wobei 119 CNS-Wirkstoffe und 108 Pfizer CNS-Kandidaten untersucht worden sind.[80] Hierbei wurden sechs fundamentale physikochemische Parameter ermittelt und begutachtet, welche spezifisch der ADME-Problematik (*Absorption*, *Distribution*, *Metabolisms*, *Excretion*) angepasst sind. Die anschließende Gewichtung von Lipophilie (ClogP), berechnetem Verteilungskoeffizient bei pH 7,4 (ClogD), der molekularen Masse, dem *topological polar surface area*-Wert (TPSA) sowie der Anzahl an Wasserstoffdonatoren und dem basischen Zentrum (pK_a) ermöglicht eine Abschätzung der Hirngängigkeit angehender Wirkstoffe.[80]

Derzeit gibt es eine Reihe von Inhibitoren für FLT3, welche in unterschiedlichen Übersichtsartikeln beschrieben werden.[13, 43, 46, 47, 50, 53, 54, 60, 81-83] Die erste Generation an *small molecules* mit FLT3-Aktivität wurden nicht speziell als FLT3-Inhibitoren entwickelt, sondern anfänglich gegen andere Kinasen (PDGFR, c-KIT) oder als Breitbandinhibitor. Einige befinden sich derzeit in klinischen Studien und werden in AML-Patienten als einzelnes Agens oder in Kombination mit der Chemotherapie bewertet.

Die ersten FLT3-Inhibitoren wurden ursprünglich für den PDGFR-Rezeptor entwickelt und werden durch drei Chinoxaline (AG1295 **12**, AG1296 **13** und AGL2043 **14**) vertreten (Abbildung 14). Sie weisen einen IC_{50}-Wert von ungefähr 300 nM auf und erzeugten *in vitro* Apoptose FLT3-mutierter leukämischer Zellen.[84-87] Jedoch haben sie aufgrund ihrer

schlechten Löslichkeit und geringen Effizienz nie den Schritt in die klinischen Studien geschafft.[46]

Darauffolgend wurden einige weitere Verbindungen entdeckt, welche *in vitro* und *in vivo* evaluiert worden sind. Hierzu zählen besonders der Polyzyklus Midostaurin **15**, der Breitbandinhibitor Sunitinib **3**, Lestaurtinib **16**, Tandutinib **17** und Sorafenib **9**

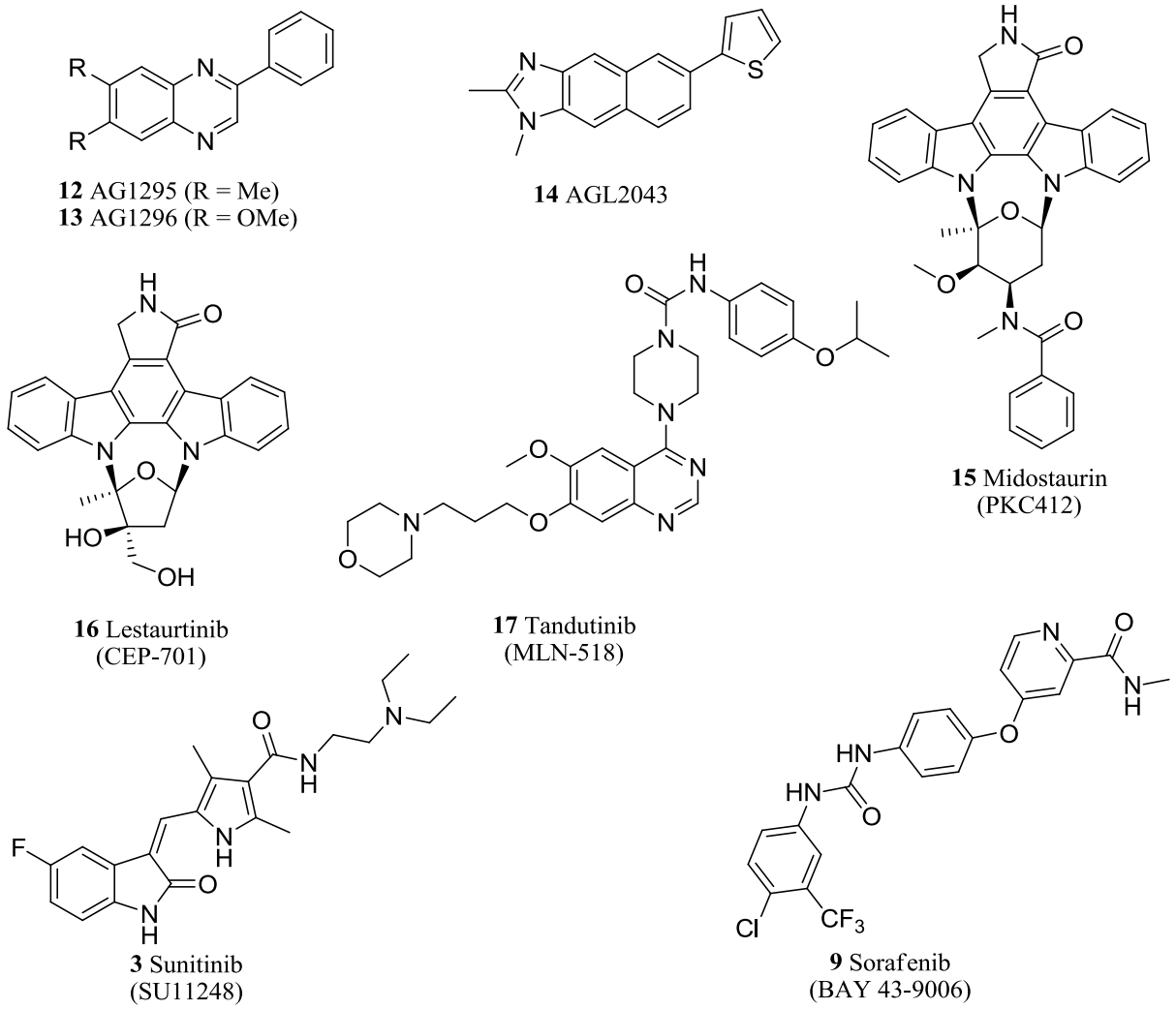

Abbildung 14: FLT3-Inhibitoren der ersten Generation. Diese wurden nicht speziell für FLT3 entwickelt, sondern gegenüber anderen Kinasen.[46, 53]

(Abbildung 14). Der Multikinaseinhibitor Midostaurin **15** ist einer der effektivsten FLT3-Inhibitoren mit einem IC_{50}-Wert von 10 nM und ist für FLT3-positive Leukämiezellen toxisch. Jedoch inhibiert er ebenso PDGFR und c-Kit im nanomolarem Bereich.[88] In klinischen Studien wird **15** als Einzelpräparat und auch in Kombination mit klassischer

Chemotherapie untersucht. In einer klinischen Phase IIb Studie wurden 60 Patienten mit wild-Typ FLT3 AML und 35 Patienten mit mutierter FLT3 AML zufällig ausgewählt und erhielten Midostaturin **15** in Dosen von 50-100 mg zweimal wöchentlich.[89] Es konnte bei 71 % der AML-Patienten mit mutierter FLT3 eine Blastenreduktion von größer 50 % erhalten werden, verglichen zu 42 % der wild-Typ AML-Patienten.

Die kombinierte Therapie von Midostaurin **15** mit Cytarabin **1** und Daunorubicin **2** (siehe Kapitel 1.1.2 Abbildung 5) erbrachte in der klinischen Phase Ib sehr gute Ergebnisse.[90] Basierend auf diesen Ergebnissen wird zurzeit der Einfluss von Midostaurin **15** bei ITD-positiver AML in einer internationalen Phase III Studie an über 700 Patienten untersucht.

Die pharmakodynamischen und pharmakokinetischen Effekte des Multikinaseinhibitors Sunitinib **3** wurden ebenfalls in zwei Phase I Studien untersucht und evaluiert. Es war der erste Wirkstoff, bei dem eine anti-FLT3-Wirkung nachgewiesen werden konnte. Nach ansteigender oraler Verabreichung von Sunitinib **3** wies ein Drittel der 29 Patienten eine klare Abnahme der FLT3-Phosphorylierung auf.[91]

Sorafenib **9**, ebenfalls ein Multikinaseinhibitor, weist eine höhere Aktivität gegenüber FLT3-ITD Mutationen ($IC_{50} = 5$ nM) als zu der FLT3-D835Y Mutation ($IC_{50} = 500$ nM) auf.[92] Dies zeigte sich auch in einer Phase I Studie mit 15 Patienten.[93] Es konnte eine signifikante Reduktion der Blasen in allen sechs ITD-positiven AML-Patienten nachgewiesen werden. Dem gegenüber zeigte Sorafenib **9** nur moderate Aktivität bei AML-Patienten mit wild-Typ FLT3 (43 %) und keine bei AML-Patienten mit FLT3-TKD-Mutationen. Vielversprechender verläuft dabei die kombinierte Therapie mit Zytostatika.[94] In einer kombinierten Phase I/II Studie erreichten nach einem Jahr 74 % der 51 AML-Patienten komplette Remission. Zurzeit wird Sorafenib **9** in weiteren Studien untersucht.

Ebenso Lestaurtinib **16** und Tandutinib **17**, Inhibitoren der PDGFR-Familie, wurden in klinischen Studien untersucht.[95-97] Vor allem bei Lestaurtinib **16** zeigten vorklinische Studien eine starke FLT3-Inhibition im tiefen nanomolarem Bereich. Deshalb wird Lestaurtinib **16** derzeit in zwei klinischen Phase III Studien untersucht.[53]

Inhibitoren der zweiten Generation wurden speziell gegen FLT3 synthetisiert. Hierzu zählen beispielsweise das Indazolderivat KW-2449 **18**, das Bisindolylmethanon **19**, der Makrozyklus SB1518 **20**, Quizartinib **21** und der erst im April diesen Jahres veröffentlichte Wirkstoff G-749 **22** (Abbildung 15).

Während KW-2449 **18** und Mahboobi 98 **19** weniger selektiv sind, weisen die drei weiteren Inhibitoren eine sehr gute Kinaseselektivität gegenüber FLT3 auf.[98-101] Vor allem

Quizartinib **21** wurde als ein einmaliger potenter und selektiver FLT3-Inhibitor charakterisiert.[102] Quizartinib ist ein Typ-II-Inhibitor und weist niedrige nanomolare Aktivität in biochemischen und zellulären Assays auf.[103] Besonders gegenüber verwandten Kinasen wie KIT, PDGFR, RET und CSF1R weist Quizartinib **21** eine über 10-fach höhere Selektivität für FLT3 auf. Das Potential von Quizartinib **21** wurde bereits in klinischen Studien untersucht. Anders als die erste Generation an FLT3-Inhibitoren zeigte Quizartinib **21** in der klinischen Phase I und II erste sehr gute Ergebnisse in der Monotherapie.[104-106] So erlangten 45 % der AML-Patienten eine komplette Remission. Nach einem Rückfall binnen weniger Monate konnten allerdings neue Mutationen in den AML-Blasten nachgewiesen werden.[107] Hierzu zählen Mutationen des *Gatekeeper*-Restes F691 sowie Mutationen innerhalb der Aktivierungsschleife (D835 und Y842). Die molekulare Analyse zeigte, dass 8 Patienten, welche die Mutationen trugen, Resistenzen gegenüber Quizartinib **21** entwickelten.[107]

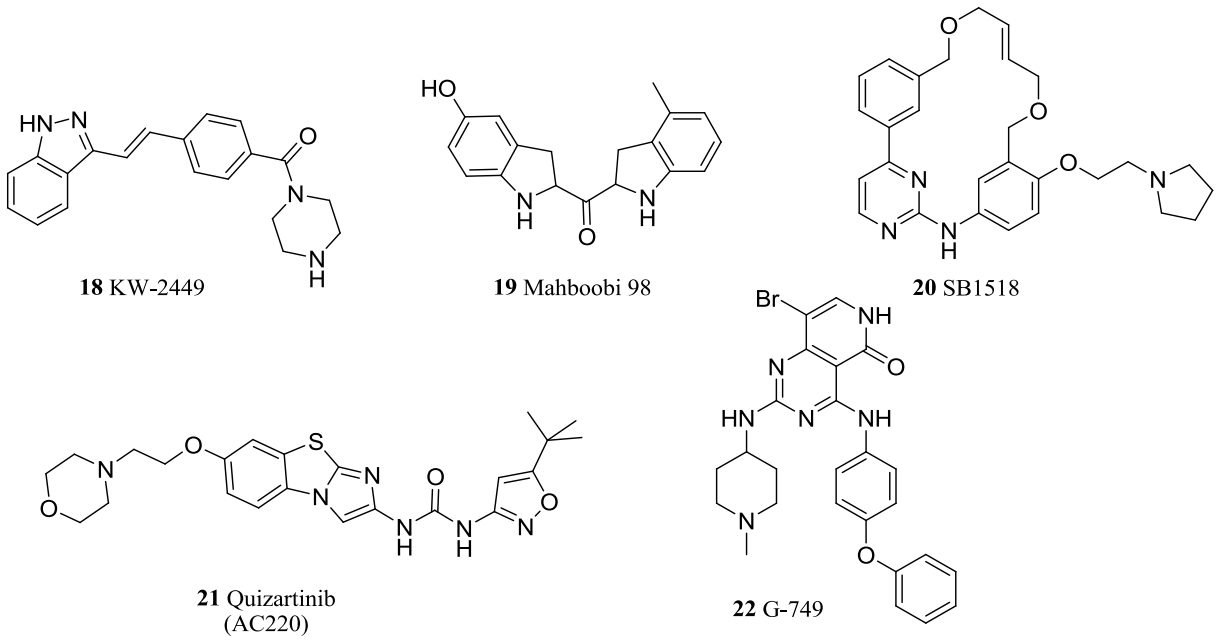

Abbildung 15: FLT3-Inhibitoren der zweiten Generation, welche speziell für FLT3 entwickelt worden sind.

Durch das Problem, dass diese sekundären Mutationen Resistenzen gegenüber Wirkstoffen verleihen können, müssen neue Varianten an FLT3-Inhibitoren gefunden werden, welche aktiv bezüglich dieser Mutanten sind. Der kürzlich publizierte FLT3-Inhibitor G-749 **22** weist potente Inhibition gegenüber FLT3-Mutationen auf (Abbildung 15, Tabelle 3).[101] G-749 **22** zeigt außerdem eine hohe Kinaseselektivität und ist mit biochemischen IC_{50}-Werten von

0,4 nM (wild-Typ-FLT3) und 0,6 nM (FLT3-D835Y) außerordentlich potent. Der Vergleich der zellulären Aktivitäten von G-749 **22**, Midostaurin **15**, Quizartinib **21** und Sorafenib **9** verdeutlicht, dass einzig G-749 **22** starke Aktivität gegenüber den Mutanten aufweist (Tabelle 3). Während Sorafenib **9** inaktiv ist, ist bei Midostaurin **15** und Quizartinib **21** ein signifikanter Abfall der Aktivität gegenüber einzelner Mutanten zu beobachten.[101]

Tabelle 3: Vergleich der Aktivitäten unterschiedlicher FLT3-Inhibitoren im zellulären Assay.[101, 107]

	Ba/F3-Zellen mit FLT3 Mutationen IC_{50} [nM]						
Verbindung	**wt**	**ITD**	**ITD/N676D**	**ITD/F691L**	**ITD/D835Y**	**D835Y**	**D835Y/N676D**
G-749	6	12	21	38	-	3	2
Quizartinib	9	4	36	194	85	52	150
Midostaurin	29	22	129	16	-	11	17
Sorafenib	-	2	-	2316	2081	-	-

Weitere Studien beschreiben einige dieser neuen FLT3-Inhibitoren, welche Aktivität gegenüber den FLT3-Mutationen aufweisen. Hierzu zählen besonders Arbeiten zu SAR-302503[108, 109], Ponatinib[110-113], Crenolanib[114-116] und PLX3397[117, 118].

2 Die Parkinson-Erkrankung

2.1 Einführung und Geschichte

Muhammed Ali (*alias* Cassius Clay) entzündete 1996 zitternd die Olympische Fackel in Atlanta. Ein Zeichen der Willensstärke, aber auch zeigte es den Verfall des einst vor Energie strotzenden Boxers. Cassius Clay litt bereits seit Jahren an der Parkinson-Krankheit.[119]

Im Jahre 1817 beschrieb James Parkinson (1755-1824) in seiner Monographie „*An Essay on the Shaking Palsy*“ (eine Abhandlung über die Schüttellähmung) erstmals Symptome der Parkinson-Krankheit, die er bei sechs seiner Patienten beobachtete.[120] In dieser wissenschaftlichen Abhandlung beschrieb James Parkinson die *paralysis agitans* (Schüttellähmung) als klinisch definiertes Krankheitsbild mit den Kardinalsyndromen Ruhezittern (Tremor), Bewegungsverlangsamung (Bradykinesie) und Gleichgewichtsstörung (posturale Instabilität). Jedoch lag er hierbei nicht ganz richtig. Bei der Parkinson-Erkrankung handelt es sich weder um eine Lähmung, noch wird sie in allen Fällen von einem Schütteln begleitet.[119] Dessen ungeachtet wurde die Krankheit später nach ihm benannt. Erst der französische Neurologe Jean-Martin Charcot (1825-1893) erkannte die Wichtigkeit der Erstbeschreibung von James Parkinson und sprach als Erster von Morbus Parkinson und führte die Muskelstarre (Rigor) als viertes Kardinalsyndrom ein.[121] Demnach ist Morbus Parkinson die häufigste motorische und die zweithäufigste neurodegenerative Erkrankung nach der Alzheimer-Demenz.[122, 123]

Der biochemische Hintergrund der Parkinson-Krankheit wurde in den frühen 60er Jahren des 20. Jahrhunderts aufgeklärt. Forschergruppen erkannten den Mangel des Botenstoffes Dopamin im Gehirn von Parkinson-Patienten, welcher für die motorischen Defizite verantwortlich gemacht wird.[124, 125] Die Ursache der Pathomechanismen dieser neurodegenerativen Erkrankung sind, ca. 200 Jahre nach der Erstbeschreibung der Parkinson-Krankheit, bislang noch unzureichend. Derzeit gibt es noch keine Heilung, lediglich symptomlindernde Medikamente ersetzen im Gehirn den fehlenden Botenstoff Dopamin, können aber die Nervenzellen nicht vor ihrem Absterben bewahren.[126]

Die Formen der Parkinson-Krankheiten werden nach ihren Ursachen unterschieden (Abbildung 16). Bekannt ist, dass die Erkrankung sowohl sporadisch als und auch familiär gehäuft auftreten kann. Mit Abstand das häufigste Parkinson-Syndrom stellt der primäre, sporadische Morbus-Parkinson (auch idiopathisches Parkinson-Syndrom, IPS), ohne bekannte Ursache, mit bis zu 90 % der Fälle dar.[127] Liegt indes eine bestimmte äußere Ursache wie

das Auslösen durch Medikamente oder Tumore vor, wird von einem sekundären oder symptomatischen Parkinson-Syndrom gesprochen. Familiär bedingter Parkinson tritt in 5-10 % der Fälle auf, wobei dieser genetisch vererbt wird.[128]

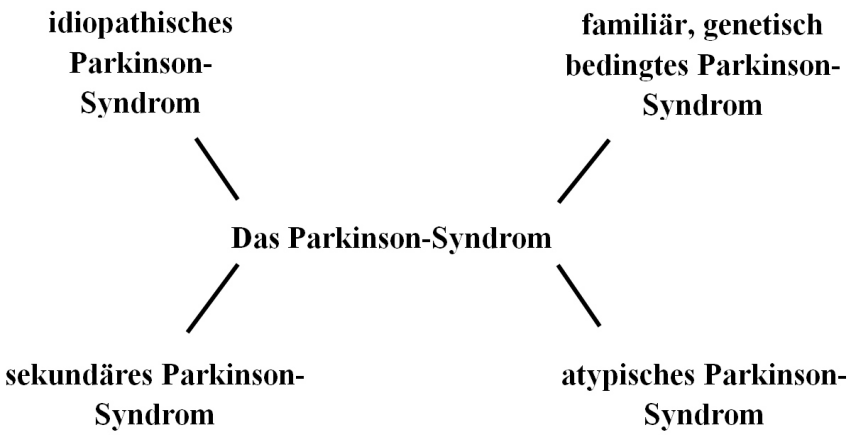

Abbildung 16: Die vier unterschiedlichen Arten des Parkinson-Syndroms. Das IPS, auch Morbus-Parkinson genannt, ist mit ca. 90 % das häufigste aller Parkinson-Syndrome.[127]

In Deutschland tritt der Morbus Parkinson mit einer Prävalenz von 100-200 Fälle pro 100 000 Einwohnern auf.[129] Mit zunehmenden Alter steigt die Anzahl der Neuerkrankungen auf 1-2 % der über 60-Jährigen und auf 4 % der über 80-Jährigen an.[130]

2.2 Die Ätiologie von Morbus Parkinson

Während das sekundäre bzw. symptomatische Parkinson-Syndrom durch unterschiedliche Ursachen ausgelöst wird, ist jedoch nach wie vor ungeklärt wie und warum die idiopathische Form des Parkinson-Syndroms, der Morbus Parkinson, auftritt. Eines der größten Risiken scheint das immer höher werdende Lebensalter zu spielen. Außerdem wird angenommen, dass oxidativer Stress, mitochondriale Dysfunktion und Pestizide wie Rotenon und Paraquat eine Rolle bei der Entstehung von Morbus Parkinson einnehmen.[131-134] Der Beweis, dass Neurotoxine Parkinson-Syndrome auslösen, wurde 1983 erbracht.[135] Langston *et al.* berichteten in den 80er Jahren in Kalifornien über eine Gruppe heroinabhängiger Jugendlicher, welche nach Injektion einer synthetisch hergestellten Ersatzdroge die Symptome der Parkinson-Krankheit, vor allem die der Bewegungsunfähigkeit, aufzeigten. Die chemische Analyse zeigte, dass Verunreinigungen von MPTP **23** (1-Methyl-4-phenyl-1,2,3,6-tetrahydropyridin) Ursache für die Entstehung der Krankheit war, wobei es zu der

Zerstörung dopaminerger Zellen im Gehirn kommt (Abbildung 17). Heutzutage wird MPTP **23** in der Forschung eingesetzt, um die Parkinson-Erkrankung in Tierversuchen an Mäusen, Raten oder Primaten weiter zu untersuchen und zu verstehen.[136-138]

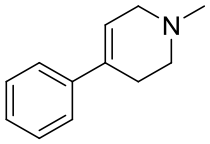

23 MPTP

Abbildung 17: Verunreinigungen von MPTP **23** in synthetisch hergestelltem Heroin lösten 1983 Symptome der Parkinson-Krankheit aus.[135]

2.2.1 Neuropathologie der Parkinson-Erkrankung

Morbus Parkinson gehört zu den neurodegenerativen Erkrankungen, wobei es zum Absterben von Nervenzellen in Gehirnregionen erkrankter Patienten kommt. Die Gehirnregion, die bei Morbus Parkinson am stärksten betroffen ist, befindet sich im Mittelhirn und wird *Substantia nigra pars compacta* (SNpc) (von lat. „schwarze Substanz“) genannt.[139] Bei gesunden Menschen produzieren die Nervenzellen Dopamin und senden es über ihre Fortsätze an das *Corpus Striatum* (von lat. „Streifenkörper“), wo es wieder freigegeben wird. Ein neuropathologisches Merkmal des Morbus-Parkinsons ist der Verlust dieser dopaminerger Neuronen der SNpc. Das *Striatum* gehört zu den Basalganglien, welche eine entscheidende Rolle bei der Initiierung und Aufrechterhaltung von Bewegungen spielen.[140] Der Verlust an Dopamin führt demnach zu Störungen in den Basalganglien was letztendlich zu motorischen und kognitiven Einschränkungen führt. Die Anzahl an sterbenden dopaminergen Neuronen ist nicht genau bekannt, jedoch wird jährlich von einem kontinuierlichen Verlust von ungefähr 10 % ausgegangen.[141] Die Kardinalsymptome der Parkinson-Krankheit manifestieren sich erst dann, wenn bereits 60-70 % dopaminerger Neuronen in der SNpc ihre Funktion eingestellt haben bzw. abgestorben sind.[127] Der Verlust an dopaminergen Neuronen lässt sich *post mortem* oft schon mit bloßem Auge erkennen, da diese einen hohen Gehalt des dunkelgefärbten Pigments Neuromelanin aufweisen. Durch die im Laufe der Jahre zu Grunde gehenden Neuronen verschwindet die Dunkelfärbung und der Hirnstamm wirkt blass.[142]
Ein zweites neuropathologisches Merkmal der Parkinson-Krankheit ist in Form von Proteinablagerungen in den noch intakten Neuronen der SNpc zu finden. Proteinablagerungen sind in der Regel verbunden mit verminderter Löslichkeit und/oder steigender Aggregation

der involvierten Proteine und sind in vielen neurodegenerativen Krankheiten allgegenwärtig.[143] Im Falle der Parkinson-Krankheit sind die charakteristischen Proteinablagerungen in Form von zytoplasmatischen Einschlusskörperchen, den sogenannten *Lewy bodies* (LB) bzw. *Lewy neurites* (LN) zu finden und wurden 1912 erstmals vom Neurologen Friedrich Lewy in Verbindung mit der Krankheit gebracht (Abbildung 18).[144-146] LB und LN sind überwiegend aus einem kleinen, präsynaptischen Protein, genannt α-Synuclein (SNCA), aufgebaut.[145] Die Bedeutung der LB bzw. die Funktion von SNCA ist jedoch noch unklar. LB können ebenfalls in Gehirnen gesunder Patienten sowie in Gehirnen von Patienten mit anderen neurodegenerativen Krankheiten wie die Alzheimer-Demenz oder die *Lewy bodies*-Demenz, welche keine Parkinson-Syndrome hervorrufen, auftreten.[134]

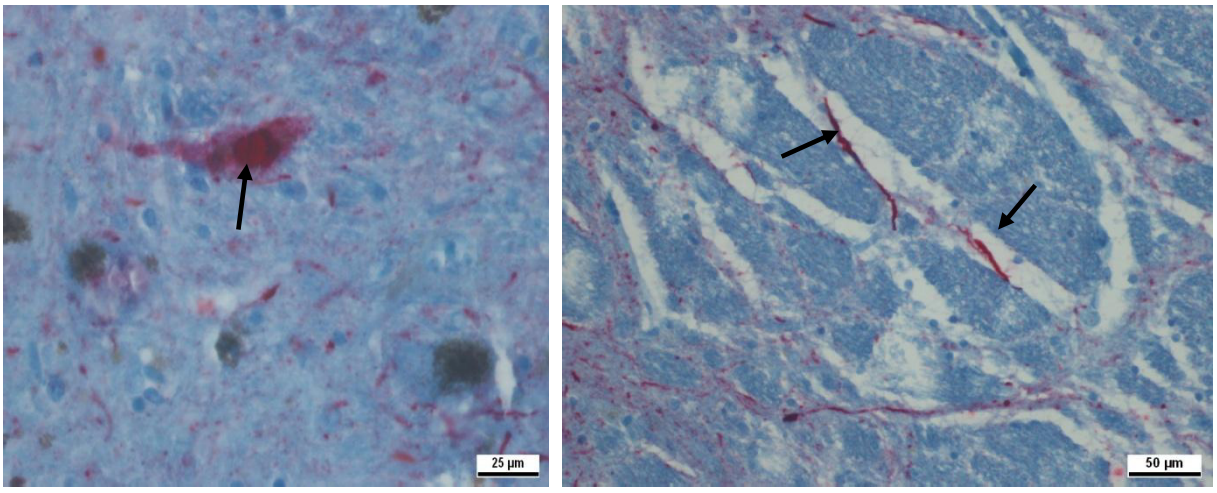

Abbildung 18: Immunhistologische Färbung von α-Synuclein. Links: intrazytoplasmatische *Lewy-bodies* in der immunhistologischen Färbung mit Fuchsinrot. Rechts: *Lewy neurites* im Mittelhirn in der immunhistologischen Färbung mit Fuchsinrot. Mit freundlicher Genehmigung von Dr. med. Roland Heyny-von Haussen (Klinikum Darmstadt).

2.2.2 Gegenwärtige Behandlung der Parkinson-Krankheit

Die Therapie der Parkinson-Krankheit beruht neben der Sprachtherapie, Ergotherapie und psychischer Begleitung der Patienten vor allem auf der medikamentösen Kombinationstherapie. Bislang werden sechs Stoffklassen (L-Dopa, Dopamin-Antagonisten, MAO-B-Hemmer, Amantadin, Anticholinergika und COMT-Hemmer) für die Behandlung eingesetzt (Abbildung 19).[126, 147, 148]

Seitdem Anfang der 60er der Mangel des Neurotransmitters Dopamin **24** in Gehirnen von Parkinson-Patienten festgestellt wurde, legte dies den Grundstein für die erste effektive Behandlung der Erkrankung. Es schien plausibel, dem Körper das fehlende Dopamin **24** mittels medikamentöser Behandlung wieder zuzuführen. Aufgrund der Blut-Hirn-Schranke, zeigten erste Behandlungsversuche mit Dopamin **24** keine Wirkung, da Dopamin **24** nicht in der Lage war, diese zu überwinden. Die Entwicklung von Levodopa, kurz L-DOPA **25**, ist eine Vorstufe des Dopamins **24**. Es konnte die Blut-Hirn-Schranke überwinden und wurde schnell im Gehirn zu Dopamin **24** umgewandelt (Abbildung 19).[149] Unter physiologischen Bedingungen wird L-DOPA **25** aus Tyrosin gewonnen, welches anschließend durch die Katalyse einer Decarboxylase in Dopamin **24** umgewandelt wird. Da sich außerhalb des zentralen Nervensystems ebenfalls Decarboxylasen befinden, wird L-DOPA **25** in Kombination mit Decarboxylasehemmern oder mit COMT-Hemmern (Catechol-O-Methyltransferase) verabreicht. So kann sichergestellt werden, dass L-DOPA **25** nicht schon außerhalb des Gehirns in Dopamin **24** oder in unerwünschte Nebenprodukte umgewandelt wird. Ein effektiver Decarboxylasehemmer ist Carbidopa **26**, welches in Kombination mit L-DOPA eines der effektivsten Medikamente zur Behandlung der Parkinson-Krankheit darstellt.[126, 147] Jedoch führt es in höheren Dosen zu Wirkungsschwankungen und zu Dyskinesien (Störung der Bewegung).[126] Derzeitige Hemmstoffe für COMT sind Tolcapon **27** und Entacapon **28**.[150, 151] Auch hier wird durch Kombination mit L-DOPA eine deutliche Verminderung von Wirkungsschwankungen erzielt.

Selegilin **29** und Rasagilin **30** gehören zu der Gruppe der Monoaminooxidase-B-Hemmer (MAO-B-Hemmer).[126] Das Wirkprinzip von MAO-B beruht auf den Abbau von freigesetzten Dopamin **24** im Gehirn. Wird dieses Enzym gehemmt, erfolgt der Dopaminabbau langsamer, wodurch dessen Wirkung verlängert wird.[149]

Medikamente der Gruppe der Dopaminantagonisten wie Pramipexol **31** ahmen die Funktion bzw. die Wirkung von Dopamin **24** im Gehirn nach. Sie ersetzen die fehlende Funktion des Dopamins **24** und können Symptome der Parkinson-Krankheit beeinflussen.[126, 149]

Amantadin **32** wird selten für die Behandlung von Patienten genommen, da klinische Studien gezeigt haben, dass es nur zu einer moderaten Verbesserung der Symptome kommt.[126]

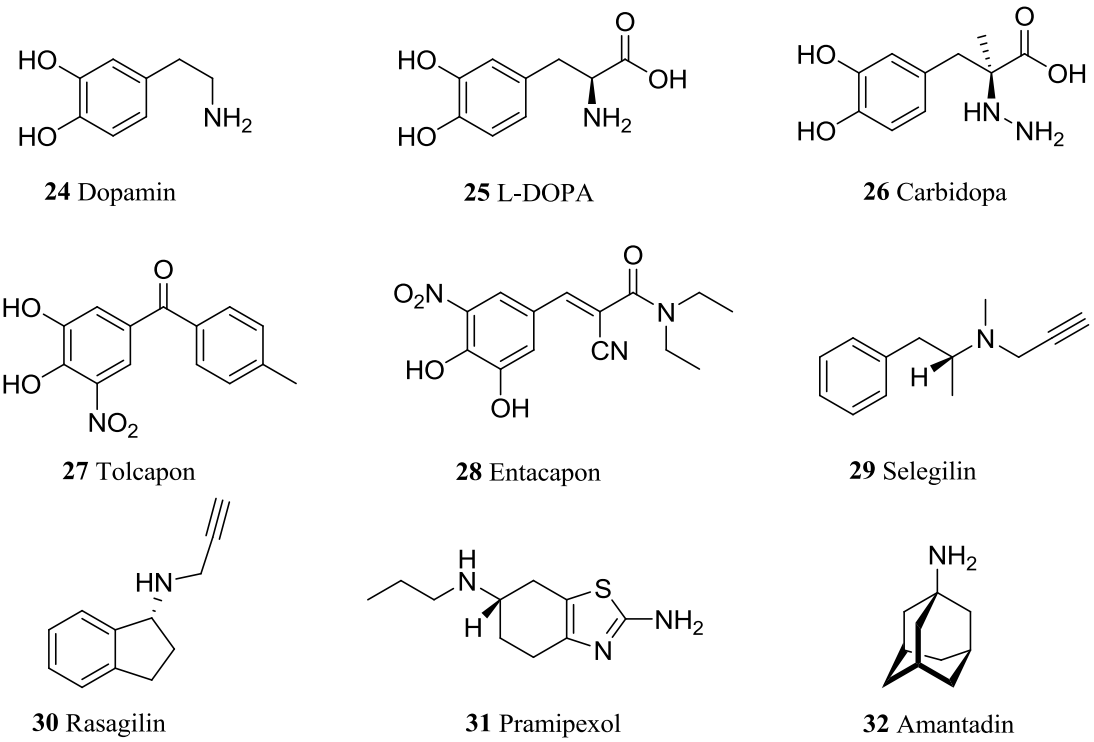

24 Dopamin **25** L-DOPA **26** Carbidopa

27 Tolcapon **28** Entacapon **29** Selegilin

30 Rasagilin **31** Pramipexol **32** Amantadin

Abbildung 19: Auswahl der zurzeit angewendeten Medikamente für die Behandlung der Parkinson-Krankheit.[126, 147, 148, 150, 151]

2.2.3 Genetisch bedingtes Parkinson-Syndrom

Wenngleich die Mehrzahl der Parkinson-Erkrankungen sporadischer Natur sind, sind 5-10 % der Fälle genetisch bedingt und zählen somit zu der familiären Form des Parkinson-Syndroms.[152] Durch die Untersuchung unterschiedlicher Familien konnten Wissenschaftler verschiedene Gene identifizieren, welche mit der Krankheit in Verbindung gebracht worden sind. Bislang sind 18 spezifische, chromosomale Regionen (PARK) beschrieben, wobei ebenso die Mehrheit der korrespondierenden Gene zu den PARK-Loki identifiziert worden ist (Tabelle 4).[152, 153] Die meisten der Gene können dabei autosomal dominant bzw. autosomal rezessiv vererbt werden. Mutationen in sechs dieser Gene wurden bislang als eindeutige Ursache der Parkinson-Erkrankung angesehen und sind zusammen für 30 % der familiären Fälle sowie für 3-5 % der sporadischen Fälle verantwortlich (Abbildung 20).[153, 154] Diese Entdeckung der monogenen Formen der Parkinson-Krankheit in den letzten 20 Jahren eröffnete für Wissenschaftler neue Möglichkeiten den Ursachen der Krankheit sowie deren möglichen Therapie auf den Weg zu gehen.

Tabelle 4: Identifizierte Gene der Parkinson-Krankheit, welche in Verbindung mit der familiären Form gebracht werden.[152, 153] AD: autosomal dominant; AR: autosomal-rezessiv.

PARK-Lokus	Chromosom	Gen	Funktion	Erbgang
PARK1 & 4	4q21	alpha-synuclein (SNCA)	Bestandteil der *Lewy bodies*	AD
PARK2	6q25-27	Parkin	E3 Ubiquitin Protein-Ligase	AR
PARK3	2p13	Unbekannt	Unbekannt	AD
PARK5	4p14	UCHL1	Ubiquitin C-terminale Hydrolase	AD
PARK6	1p35-36	PINK1	Mitochondriale Kinase	AR
PARK7	1p36	DJ-1	Antioxidation	AR
PARK8	12q12	LRRK2	Kinase, GTPase	AD
PARK9	1p36	ATP13A2	Kation-transportierende ATPase	AR
PARK10	1p32	Unbekannt	Unbekannt	AD
PARK11	2q36-37	GIGYF2	Unbekannt	AD
PARK12	Xq21-25	Unbekannt	Unbekannt	X Chromosom
PARK13	2p13	HTRA2	Serin-Protease	Unbekannt
PARK14	22q13.1	PLA2G6	Phospholipasen A2	AR
PARK15	22q12-13	FBXO7	E3 Ubiquitin Protein-Ligase	AR
PARK16	1q32	Unbekannt	Unbekannt	Unbekannt
PARK17	16q11.2	VPS35	Unbekannt	AD
PARK18	3q27.1	EIF4G1	Unbekannt	AD

Zu den Genen, in denen Mutationen verantwortlich für den erblich bedingten Parkinson gemacht werden, zählen Parkin, PINK1 (*phosphatase and tensin homolog (PTEN)-induced putative kinase 1*), DJ-1, SNCA sowie LRRK2 (*leucine-rich repeat kinase 2*) (Abbildung 20). Die wohl meist bekannte Mutation, G2019S, ist in LRRK2 zu finden und trägt zu 5-10 % zur erblich bedingten Form sowie 0,5-2 % zur sporadischen Form bei.[154, 155] In den folgenden Kapiteln wird näher auf SNCA und vor allem auf LRRK2 eingegangen.

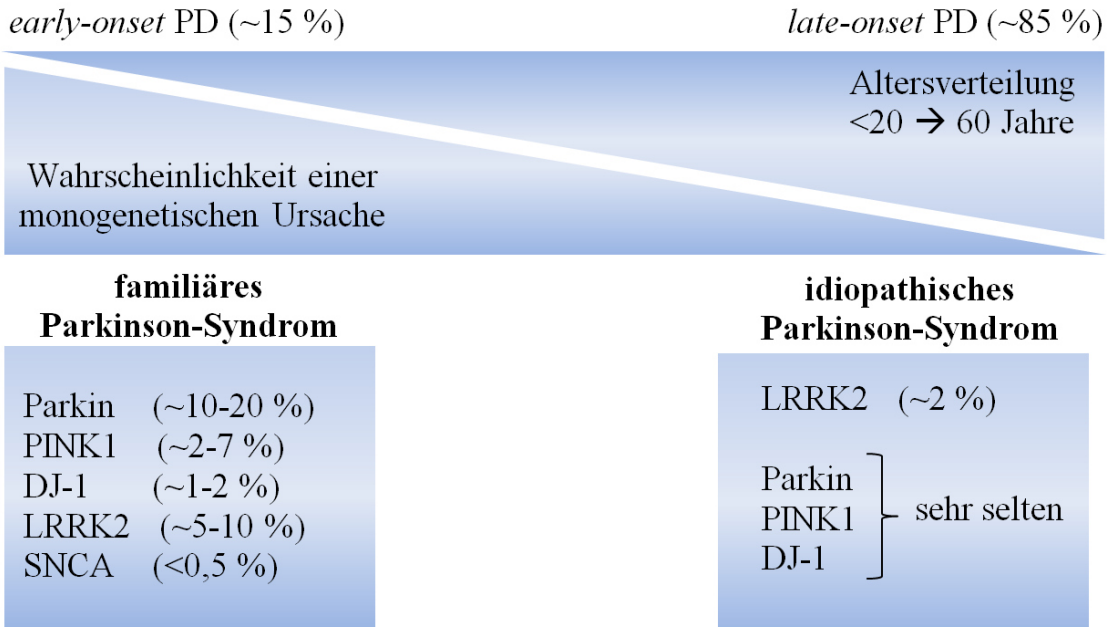

Abbildung 20: Häufigkeit des familiären Parkinson-Syndroms im Vergleich zum idiopathischen Parkinson-Syndrom. In Anlehnung an Klein *et al.*[154]

2.3 α-Synuclein und dessen Rolle in der Parkinson-Krankheit

SNCA war das erste Gen, bei dem 1996 Mutationen definitiv in Verbindung mit dem familiären Parkinson-Syndrom gebracht worden sind.[156] Derzeit sind drei pathogene Punktmutationen, A30P, E46K und A53T, bekannt.[156-158] Zusätzlich wurden bislang insgesamt 17 chromosomale Duplikationen entlang des SNCA-Gens entdeckt, von denen 13 dem familiären und 4 dem idiopathischen Parkinson-Syndrom zugeordnet wurden konnten.[153] Triplikationen des SNCA-Gens wurden in drei unabhängigen Familien gefunden.[159-161]

α-Synuclein ist ein hoch lösliches, nativ ungefaltetes, extrem hitzeresistentes, kleines acides Protein (14 kDa).[162] Die Struktur von α-Synuclein kann in drei individuelle Abschnitte

untergliedert werden. Die hochkonservierte N-terminale Domäne (Reste 1-65) beinhaltet sieben unvollständige Sequenzwiederholungen, jede 11 Aminosäuren lang, welche Variationen der Reste KTEGV aufweist.[153, 162] Alle drei Punktmutationen befinden sich innerhalb dieser Domäne. Da aber die normale Funktion des SNCA-Gens noch unklar ist, ist es auch schwer zu sagen, welchen Einfluss die Mutationen auf dessen Funktion ausüben.[143] Im Zentrum des 140 Aminosäuren kleinen Proteins (Reste 66-95) liegt die hydrophobe NAC-Region (*non-amyloid component*). Diese steht im Verdacht für den Aggregationsprozess verantwortlich zu sein, da sie äußert hydrophob und somit hoch amyloidogen wirkt.[145] Besonders die Aminosäuren 71-82 nehmen eine entscheidende Rolle bezüglich der Aggregationsbildung zu Fibrillen ein.[163] Die C-terminale Domäne (Reste 96-140) besteht überwiegend aus aciden Aminosäuren und ist deshalb stark negativ geladen. Diese wirkt aggregationsinhibierend auf die NAC-Domäne.

Die Funktion von α-Synuclein ist noch nicht erforscht worden. Bekannt ist jedoch, dass fibrilläres α-Synuclein Hauptbestandteil der *Lewy bodies* ist. Seit dieser Entdeckung stellt sich die Frage, ob diese proteinhaltigen Einschlüsse selbst toxisch sind, oder ob diese nur das Endresultat eines neuroprotektiven Mechanismus darstellen.[143] Es werden heutzutage unterschiedliche Mechanismen zur Fibrillenbildung diskutiert.[162] Es wird jedoch angenommen, dass die drei Punktmutationen A30P, E46K und A53T von SNCA die Bildung von stabilen β-Faltblätter fördern und somit die Bildung von Oligomeren und Fibrillen begünstigen.[143, 153] Die Aggregation vom Monomer bis zur Fibrille verläuft dabei schrittweise über die Dimerisierung partiell gefalteter Monomere und über die löslichen toxischen Oligomere (Abbildung 21).[162, 164]

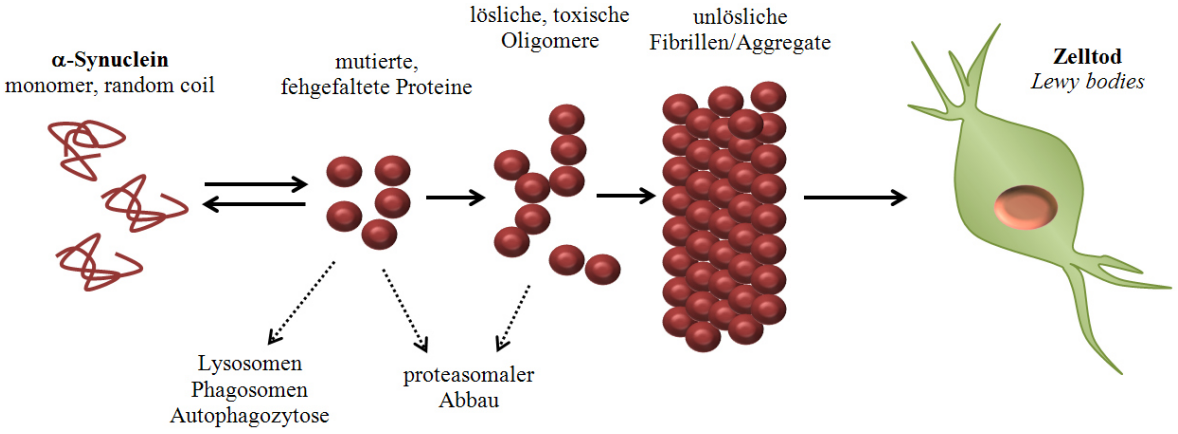

Abbildung 21: Schematische Darstellung der α-Synuclein Aggregation nach Recchia *et al.* und Irwin *et al.*[162, 164]

2.4 LRRK2 als therapeutisches Target zur Behandlung der Parkinson-Krankheit

2.4.1 Nomenklatur, Struktur und Mutationen von LRRK2

2002 identifizierte die Gruppe von Funayama *et al*. in einer japanischen Familie einen neuen Gen-Lokus auf Chromosom 12 (12p11.2-q13.1), welcher als Ursache für autosomal dominantes Parkinson-Syndrom angesehen wird.[165] In den Folgejahren gelang es zwei Forschergruppen gleichzeitig das Gen LRRK2 zu identifizieren und Mutationen mit der Erkrankung in Zusammenhang zu bringen.[166, 167] Mutationen in LRRK2 sind derzeit die häufigste genetische Ursache für das *late-onset* Parkinson-Syndrom.[168] Das Protein LRRK2 wird auch als Dardarin bezeichnet, welches sich von dem Baskischen „*dardara egin*" ableitet und Zittern bedeutet. 51 Exons codieren für ein 2527 Aminosäuren großes Protein mit einem Molekulargewicht von ca. 280 kDa.[168, 169] Es wird überwiegend in Organen (Lunge und Niere), Geweben und im Gehirn exprimiert.[166, 167] Die physiologische Funktion von LRRK2 erstreckt sich über die Kontrolle und Aufrechterhaltung der Länge von Neuriten durch Interaktionen mit Rab5a, die Kontrolle der Proteintranslation durch Phosphorylierung von 4E-BP1, sowie Interaktionen mit α- und β-Tubulinen, welche sich zu Mikrotubuli zusammenlagern.[145] Sequenz-Analysen belegten, dass LRRK2 aus verschiedenen unabhängigen Domänen aufgebaut ist. Hierzu gehören Ankyrin-Wiederholungseinheiten, eine *leucine-rich repeat* Domäne (LRR-Domäne), eine ROC (*Ras of complex*) GTPase-Domäne, gefolgt von einer COR-Domäne (*C-terminal of Ras*), einer Kinase-Domäne und einer C-terminalen WD40-Einheit (Abbildung 22).[170]

Nachdem PARK8 2002 zum ersten Mal beschrieben und 2004 Mutationen im LRRK2-Gen identifiziert worden sind, steigt die Anzahl der veröffentlichten Sequenzvarianten in LRRK2 stetig an. Derzeit sind mehr als 40 LRRK2-Mutationen bekannt, von denen fünf als pathogen gelten.[171, 172] Diese pathogenen Mutationen konzentrieren sich auf die ROC-, COR- und Kinase-Domäne. Dabei besitzt die ROC-Domäne einen Aminosäurerest, an denen multiple Mutationen R1141H, R1141G und R1141C zu finden sind. Die beiden Letzteren gelten als pathogen. Die COR-Domäne enthält eine Mutation an Position Y1699C und die Kinase-Domäne besitzt zwei benachbarte Mutationen an den Stellen G2019S sowie I2020T.[173] Besonderes Interesse gilt dabei der G2019S-Mutation, welche in beiden Fällen, dem familiären und dem sporadischen Parkinson, zu finden ist. Viele Studien haben gezeigt, dass LRRK2-Mutationen zwischen 5-13 % bei familiären und zwischen 1-5 % bei sporadischen

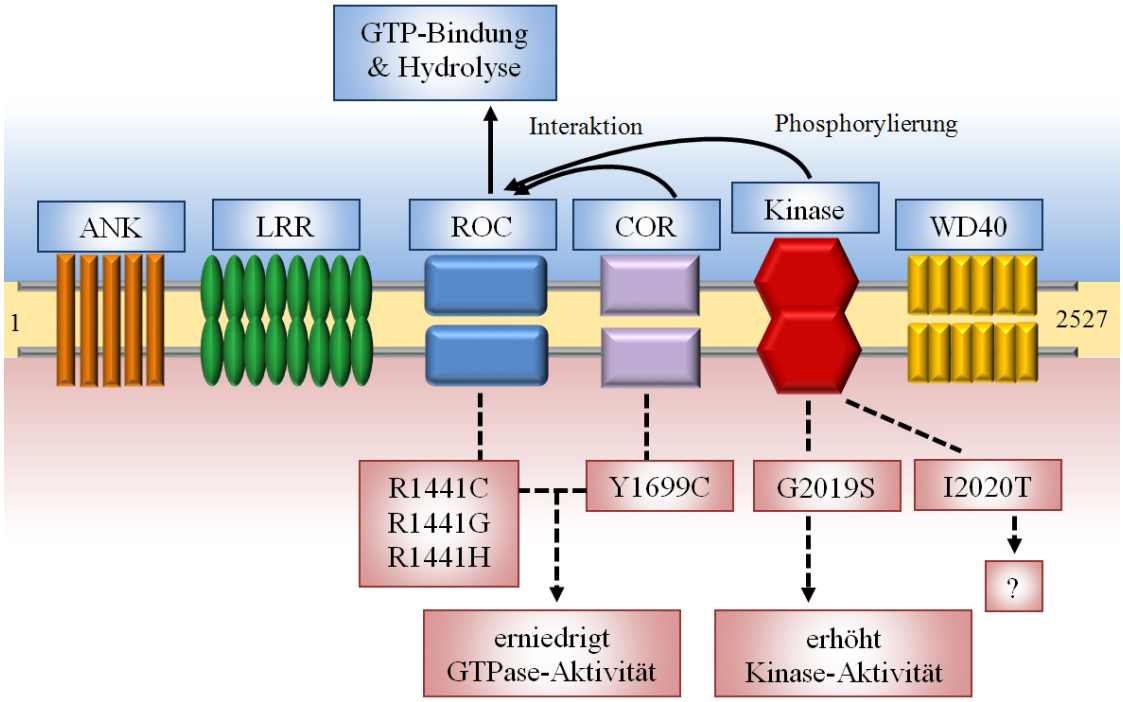

Abbildung 22: Schematische Illustration von LRRK2. Domänen: ANK (*ankyrin-repeat-domain*), LRR (*leucine-rich repeat domain*), ROC (*Ras of complex,* (GTPase)), COR (*C-terminal of Ras*), am C-terminalen Ende befindet sich eine WD40-Einheit. Die meist bekanntesten pathogenen Mutationen sind unterhalb der Struktur gezeigt. Mutationen von R1441 sowie Y1699 erniedrigen die GTPase-Aktivität, wohingegen G2019S die Kinase-Aktvität erhöht. Dies führt dazu, dass die Kinase-Domäne die ROC-Domäne phosphoyliert, obwohl dies *in vivo* noch nicht bestätigt wurde. In Anlehnung an M. Cookson.[173]

Parkinson auftreten.[174] Vom größerem Interesse ist jedoch die Prävalenz der G2019S-Mutation. Sie ist sehr selten in Asien, Südafrika und einigen europäischen Ländern wie Polen, Griechenland und Deutschland zu finden. Jedoch tritt sie gehäuft in einigen ethnischen Gruppen auf. So trägt die G2019S-Mutation mit 13-41 % des sporadischen und mit 30-37 % des familiären Parkinson-Syndroms bei Patienten mit jüdischer oder arabischer Herkunft bei.[174]

2.4.2 LRRK2 und dessen Rolle in der Parkinson-Krankheit

Der pathogene Mechanismus der Parkinson-Krankheit, verursacht durch LRRK2-Mutationen, ist noch ungewiss und nicht verstanden.[153] Ebenso ist die physiologische Funktion von LRRK2 noch nicht genau verstanden. Die Gegenwart einer ROC/GTPase sowie einer Kinase-Domäne lässt jedoch vermuten, dass LRRK2 eine wichtige Rolle in intrazellulären

Signalprozessen einnimmt.[143] Es wird postuliert, dass LRRK2 vorzugsweise eine dimere Konformation einnimmt.[173] Hierdurch sind die unterschiedlichen Domänen, welche die pathogenen Mutationen beinhalten, in der Lage untereinander zu kommunizieren und zu interagieren.[143] Aufgrund der Dimerisierung wird angenommen, dass LRRK2 seine eigene Aktivität reguliert. *In vitro* Studien belegten, dass Mutationen (R1141H, R1141G und R1141C) in der ROC/GTPase sowie eine Mutation (Y1699C) in der COR-Domäne die GTPase-Aktivität verringern, aber nicht die Kinase-Aktivität steigern (Abbildung 22).[175, 176] Im Gegensatz dazu agiert die G2019S-Mutation in der Kinase-Domäne als eine *gain-of-function*-Mutation, indem sie die Kinase-Aktivität im Vergleich zum wild-Typ erhöht.[173, 177] Erkenntnisse bezüglich Modeling zeigten, dass die Glycin zu Serin Substitution LRRK2 dazu zwingen, in der konstitutiv aktiven Form zu bleiben. Dies hat zur Folge, dass die katalytische Seite zugänglich bleibt, was zur erhöhten Kinase-Aktivität führt.[177] I2020T, eine weitere klinisch relevante Mutation, liegt ebenfalls innerhalb der Kinase-Domäne. Jedoch gibt es hier unterschiedliche Angaben, ob diese die Kinase-Aktivität erhöht oder senkt.[177]

2.4.3 Inhibitoren zur Behandlung der Parkinson-Krankheit – Stand der Forschung

Die Identifizierung involvierter Gene in der Parkinson-Krankheit und das vermehrte Verständnis über dessen Funktionen bietet Forschern potentielle Targets zur Behandlung dieser Krankheit. Von diesen Genen hat sich LRRK2 in den letzten Jahren als ein sehr attraktives therapeutisches Target herauskristallisiert.[178] LRRK2 ist 2004 zuerst in Verbindung mit dem familiären Parkinson-Syndrom gebracht worden.[167] Die Bedeutung von LRRK2 wurde 2011 weiter bestätigt, indem es ebenfalls als Risikofaktor für das sporadische Parkinson-Syndrom angesehen wurde.[178] Beweise, die diese Tatsache unterstützen, liegen in der Entdeckung der G2019S-Mutation, welche in der Aktivierungsschleife liegt und die Kinase-Aktivität steigert. Eine Überexpression dieser Mutante ist toxisch *in vitro* und *in vivo*.[178]

Seitdem die in der Kinase-Domäne liegende G2019S-Mutation in Zusammenhang mit der Neurotoxizität und dem Parkinsonsyndrom gebracht wurde, ist die Entwicklung von Kinase-Inhibitoren in den letzten Jahren rasant angewachsen. Die ersten publizierten LRRK2-Inhibitoren wurden durch *screening* von Substanz-Bibliotheken gefunden. Erste Patente wurden 2006 eingereicht. Deng *et al.* verschaffte einen Überblick über die bislang zugänglichen Patente mit dem Fokus der LRRK2-Inhibition.[179] So wurden von 2006-2011

15 Patente vorgelegt. Ende 2013, zwei Jahre später, hat sich die Anzahl der Patente mit 31 mehr als verdoppelt.[178] Dieses neue große Feld der LRRK2-Inhibition spiegelt sich auch in den bislang mit mehr als 25 erschienenen Publikationen unterschiedlicher industrieller und akademischer Arbeitsgruppen wieder.

In diesem Kapitel wird nur ein kleiner Überblick über *small molecules* für die therapeutische Behandlung der Parkinson-Krankheit mit dem Fokus auf Selektivität und gute pharmakologische Eigenschaften gegeben. Einen weiteren Überblick über bekannte LRRK2-Inhibitoren sind in dem kumulativen Teil der Arbeit zu finden.

Eine der bislang vielversprechendsten Leitstrukturen für die LRRK2-Inhibition stellen die Aminopyrimidine dar (Abbildung 23). LRRK2-IN-1 **33** war der erste selektive und potente Inhibitor, der eigens für LRRK2 synthetisiert wurde. Mit biochemischen IC_{50}-Werten von 13 nM und 6 nM gegenüber dem wild-Typ und der G2019S-Mutante ist er ein äußert potenter Inhibitor (Tabelle 5). Jedoch wies er eine rund 400-fache Resistenz gegenüber der LRRK2[A2016T]-Mutation sowie der LRRK2[A2016T + G2019S]-Mutation auf.[180] Die Selektivität von LRRK2-IN-1 **33** wurde in einem Selektivitäts-Panel aus 442 Kinasen ermittelt. Lediglich 12 weitere Kinasen wurden signifikant bei einer Konzentration von 10 µM inhibiert.[180]

TAE684 **34** und HG-10-102-01 **35** wurden in den darauffolgenden Monaten entwickelt.[181,182] Beide weisen eine ähnliche Aktivität gegenüber dem wild-Typ und der G2019S-Mutante auf (Tabelle 5). Im Gegensatz zu LRKK2-IN-1 **33** inhibieren beide Inhibitoren, **34** und **35**, die

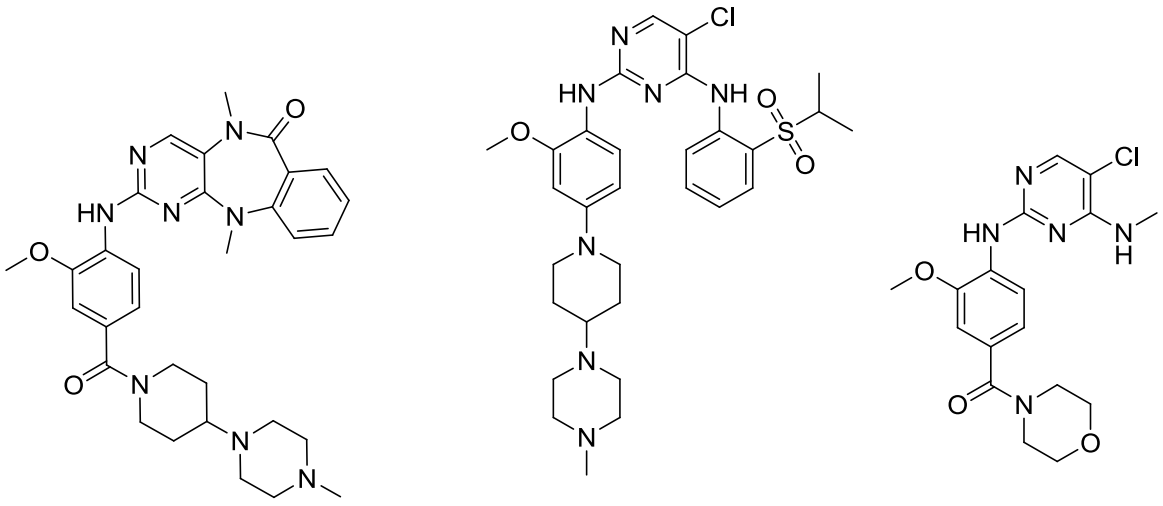

33 LRRK2-IN-1 **34** TAE584 **35** HG-10-102-01

Abbildung 23: Selektive, hochpotente LRRK2-Aminopyrimidin-Inhibitoren.[180-182]

LRRK2[A2016T]-Mutante sowie die LRRK2[A2016T + G2019S]-Mutation im niedrigen nanomolarem Bereich. In einem Kinase-Panel gegenüber 442 Kinasen zeigte sich, dass TAE684 **34** ein potenter Inhibitor mehrerer Kinasen und weniger selektiv als LRRK2-IN-1 **33** ist.[182] HG-10-102-01 **35** hingegen ist besonders selektiv. In einem Panel, bestehend aus 138 Kinasen, wurden nur zwei weitere Kinasen inhibiert.[181] Alle drei Inhibitoren weisen ebenfalls erste gute pharmakologische Eigenschaften auf (Tabelle 5). Auffallend ist, dass HG-10-102-01 **35** eine sehr geringe Plasma-Halbwertszeit von 0,13 h aufweist. Im Vergleich dazu hat TAE684 **34** eine Plasma-Halbwertszeit von 11,3 h. Jedoch zeigte HG-10-102-01 **35** sehr gute pharmakologische Eigenschaften bezüglich der Hirnpenetration und der Dephosphorylierung von Ser910 und Ser935 in Geweben wie Niere, Milz und Gehirn.[181]

Tabelle 5: Vergleich der LRRK2-Inhibtoren bezüglich deren Aktivitäten gegenüber dem wild-Typ, gegenüber Mutationen und ausgewählten pharmakokinetischen Eigenschaften.[180-182]

Verbindung	IC_{50} [nM]				Maus-Pharmakokinetik	
	wild-Typ LRRK2	LRRK2-G2019S	LRRK2-A2016T	LRRK2-A2016T+G2019S	Bioverfügbarkeit (F)[%]	$t_{1/2}$ [h]
LRRK2-IN-1	13	6,0	2450	3080	49	4,5
TAE684	7,8	6,1	63,3	21,9	83	11,3
HG-10-102-01	20,3	3,2	153,7	95,9	67	0,13

Neben den Aminopyrimidinen wurden weitere Stoffklassen wie Arylbenzylamide oder Cyancinnoline als potente und selektive LRRK2-Inhibitoren entwickelt (Abbildung 24). GSK2578215A **36** ist ein Vertreter der Arylbenzylamide. Mit IC_{50}-Werten von 11 nM und 9 nM gegenüber dem wild-Typ und der G2019S-Mutante von LRRK2 ist er ebenfalls ein äußerst potenter Inhibitor.[183] Jedoch weist dieser eine 8-fach reduzierte Aktivität gegenüber der LRRK2[A2016T]-Mutation auf. In einem Kinase-Panel zeigte GSK2578215A **36** eine sehr gute Selektivität. Aus 460 Kinasen wurden lediglich drei weitere bei einer Konzentration von 10 µM inhibiert.[183]

Ähnliche Aktivitäten sind für das Cinnolin-Derivat **37** ermittelt wurden, das sehr gute Aktivitäten gegenüber dem wild-Typ und der G2019S-Mutante von LRRK2 mit IC_{50}-Werten von 7 bzw. 5 nM zeigt. Die Profilierung in einem Panel, bestehend aus 40 Kinasen zeigte gute Selektivität. Nur vier weitere Kinasen neben LRRK2 wurden bei einer Konzentration von 1 µM inhibiert.[184]

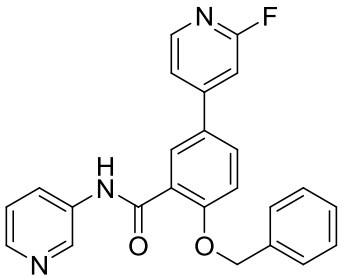

36 GSK2578215A

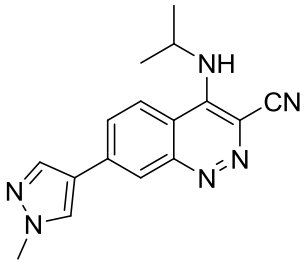

37

Abbildung 24: LRRK2-Inhibitoren der Stoffklassen der Arylbenzylamide **36** und der Cyancinnoline **37**.[183, 184]

Aufgrund des noch sehr neuen Themengebietes der LRRK2-Inhibition ist es bisher noch nicht gelungen, den idealen LRRK2-Inhibitor herzustellen. Deshalb muss das Interesse weiter darin bestehen Verbindungen zu finden, welche aktiv, selektiv und hirngängig sind.

3 Aufgabenstellung und Zielsetzung der Arbeit

Proteinkinasen sind die zweitwichtigsten Targets in der Arzneimittelforschung.[5] Die Entwicklung von potenten und selektiven Inhibitoren ist daher ein wertvoller Ansatzpunkt zur Behandlung von Krankheiten. Die medizinische Chemie knüpft an diesen Punkt an und versucht gezielt Leitstrukturen zu finden. Mit Hilfe von *in silico* Design werden Leitstrukturen oftmals optimiert, um so Wirkstoffe für die gezielte Therapie zu entwickeln.

Die Behandlung der akuten myeloischen Leukämie beruht derzeit ausschließlich auf der Chemotherapie durch Verabreichung von Zytostatika, da die molekulare Pathogenese der AML bislang noch nicht komplett entschlüsselt ist.[49] In den letzten Jahren sind vermehrt Genmutationen des FLT3-Rezeptors in den Vordergrund getreten. Ungefähr 30 % aller AML diagnostizierten Fälle weisen Mutationen dieses Gens auf.[53] Einige potentielle Wirkstoffe befinden sich derzeit in klinischen Studien und haben erste sehr gute Ergebnisse gezeigt.

Die gezielte Behandlung der Parkinson-Krankheit mittels Kinase-Inhibitoren ist noch ein sehr neues Gebiet. Seitdem 2004 die in der LRRK2 Kinase-Domäne liegende G2019S-Mutation in Zusammenhang mit der Neurotoxizität und dem Parkinsonsyndrom gebracht wurde, ist LRRK2 ein wichtiges therapeutisches Target für akademische und industrielle Gruppe geworden.

Im Fokus der vorliegenden Dissertation stehen deshalb das Design und die Synthese potentieller, selektiver ATP-kompetitiver FLT3- und LRRK2-Inhibitoren. Mit Hilfe von *in silico* Design sollen potentielle Wechselwirkungen der Liganden mit den Proteinen erkannt und so die Struktur-Aktivitäts-Beziehung von Indolinon- sowie Chinoxalin-Derivaten untersucht werden. Die erfolgreich hergestellten Verbindungen sollen anschließend *in vitro* und in einem *in vivo* Zebrafisch-Embryo-Toxizitäts-Assay untersucht werden. Durch phänotypische Veränderungen der Zebrafische sollen so Rückschlüsse auf die Toxizität ausgewählter Verbindungen geschlossen werden. Um einen Überblick über die bislang publizierten LRRK2-Inhibitoren zu ermöglichen, sollen zunächst zurückliegende Daten aufgearbeitet, zusammengefasst und evaluiert werden.

4 Kumulativer Teil der Arbeit

4.1 Modifikation einer Inhibitorleitstruktur weg von der γ-Sekretase und hin zu der FLT3 Inhibition

Der Inhalt dieses Kapitels wurde bereits veröffentlicht.[185]

Autoren: Ghislaine Marlyse Okala Amombo, Thomas Kramer, Fabio Lo Monte, Stefan Göring, Matthias Fach, Steven Smith, Stephanie Kolb, Robert Schubenel, Karlheinz Baumann, Boris Schmidt.

Titel: „Modification of a promiscuous inhibitor shifts the inhibition from γ-secretase to FLT-3".

Journal: Bioorganic & Medicinal Chemistry Letters.

DOI: 10.1016/j.bmcl.2012.10.016.

Zusammenfassung:

Die akute myeloische Leukämie ist eine bösartige Erkrankung des blutbildenden Systems mit einer Langzeitüberlebensdauer von 25-70 % bei Patienten unter 60 Jahren. Vor allem Genmutationen des FLT3-Rezeptors sind in den letzten Jahren vermehrt in den Vordergrund gerückt, da diese die meist bekannten und am häufigsten auftretenden Gen-Abnormitäten in der AML darstellen. Rund ein Drittel aller AML-Patienten weist zwei unterschiedliche Klassen aktivierender Mutationen auf. Die meistbekannten Mutationen mit rund 23 % stellen die interne Tandem-Duplikationen in der Juxtamembran-Domäne dar. Die zweite Klasse aktivierender Mutationen sind Punktmutationen innerhalb der Tyrosinkinase-Domäne. Deshalb stellt FLT3 ein interessantes Target zur Behandlung der AML dar. Derzeit werden bereits einige FLT3-Inhibitoren unterschiedlicher Strukturklassen in präklinischen Studien evaluiert und weisen erste Erfolge auf.

Basierend auf dem Indolinon-Grundgerüst wurde in vorangegangenen Arbeiten Inhibitoren der dual spezifischen CK1/γ-Sekretase synthetisiert. Von zwei Indolinon-Derivaten wurde ein Selektivitäts-Panel bestimmt, wobei diese eine Aktivität gegenüber FLT3 aufwiesen. Mit dem Ziel die Aktivität gegenüber FLT3 zu verbessern und gegenüber der γ-Sekretase zu vermindern, wurden mit Hilfe der Struktur-Aktivitäts-Beziehung unterschiedliche Verbindungen hergestellt, welche eine Aktivität bezüglich FLT3 im tiefen nanomolarem

Bereich aufwiesen. Die gegenüber der γ-Sekretase selektivsten FLT3-Inhibitoren waren **16i** sowie **16n**. Der potenteste Inhibitor **16e** wies einen IC_{50}-Wert von 4.1 nM auf. Dieser wurde anschließend in einem Kinase-Panel sowie in einem Zebrafisch-Toxizitäts-Assay evaluiert. Neben FLT3 wurden nur zwei weitere Kinasen (HGK und JAK3) signifikant inhibiert. Der Zebrafisch-Toxizitäts-Assay wies keinerlei Sterblichkeit noch phänotypische Veränderungen auf. Anschließende Docking-Studien in die ATP-Bindungstasche von FLT3 zeigten mögliche Interaktionen mit den Aminosäuren Lys644, Met665, Phe691 und Phe830 auf.

Eigener Beitrag zu dieser Arbeit:
Der synthetische Beitrag lag in den Verbindungen BSc3944 (1), BSc4540 (16a), BSc4541 (16b), BSc4534 (16c), BSc4538 (16d), BSc4657 (16e), BSc4536 (16i), BSc4537 (16j), BSc4539 (16k), BSc4654 (16l), BSc4655 (16m), BSc4661 (16n), BSc4685 (16o), BSc4533 (16p), BSc4532 (16q), BSc4535 (16r), BSc4682 (16z). In Klammer die Verbindungsnummern in der Publikation.
Des Weiteren wurden das molekulare Docking sowie der Zebrafisch-Toxizitäts-Assay von mir durchgeführt.

Bioorganic & Medicinal Chemistry Letters 22 (2012) 7634–7640

Contents lists available at SciVerse ScienceDirect

Bioorganic & Medicinal Chemistry Letters

journal homepage: www.elsevier.com/locate/bmcl

Modification of a promiscuous inhibitor shifts the inhibition from γ-secretase to FLT-3

Ghislaine Marlyse Okala Amombo[a,†], Thomas Kramer[a,†], Fabio Lo Monte[a,†], Stefan Göring[a], Matthias Fach[a], Steven Smith[a], Stephanie Kolb[a], Robert Schubenel[b], Karlheinz Baumann[b], Boris Schmidt[a,*]

[a] Clemens Schöpf-Institute of Organic Chemistry and Biochemistry, Technische Universität Darmstadt, Petersenstr. 22, D-64287 Darmstadt, Germany
[b] F. Hoffmann-La Roche Ltd, Pharmaceutical Division, Preclinical Research CNS, Bldg. 70/345, CH-4070 Basel, Switzerland

ARTICLE INFO

Article history:
Received 14 August 2012
Revised 28 September 2012
Accepted 1 October 2012
Available online 11 October 2012

Keywords:
Acute myeloid leukemia
FLT-3
Kinase inhibitor
γ-Secretase

ABSTRACT

The inhibition of FLT-3 activity is an interesting target for the treatment of acute myeloid leukemia (AML). The serendipitous identification of FLT-3 inhibitors from a CK1/γ-secretase programme provided compounds with dual inhibitory activity. We analyzed the structure–activity relationship of these inhibitors and derivatized them to arrive at compounds with reduced impact on γ-secretase activity and enhanced FLT-3 inhibition.

Acute myeloid leukemia (AML) is an aggressive haematological malignancy with long-term survival rates of 25–70% in patients younger than 60 years and only 5–15% in older patients.[1,2] Activating mutations of FLT-3 (FMS-like tyrosine kinase-3) are abundant molecular abnormalities found in AML.[3] FLT-3 is essential for the normal function of stem cells and the immune system and is primarily expressed in immature hematopoietic cells.[4] It contains an extracellular ligand binding domain, a transmembrane domain, and an intracellular juxtamembrane domain followed by the tyrosine kinase domain, which is interrupted by a kinase insert region.[5,6] Internal-tandem duplications (ITDs) and tyrosine kinase domain (TKD) point mutations are the two major classes of activating FLT-3 mutations identified in AML patients.[7] FLT-3/ITD mutations were estimated to occur in ~23% of de novo AML.[8] Several ATP-competitive FLT-3 inhibitors have been developed for a targeted therapy of this disease.[9] The FLT-3 inhibitors are derived from different structural classes and some of them displayed high potential in preclinical and clinical trials, Scheme 1.[5–10]

The published data suggest that FLT-3 is an attractive therapeutic target for the development of kinase inhibitors for AML and other associated diseases.[11]

Working on the structure–activity relationship of the indolinone scaffold of dual CK1/γ-secretase inhibitors in the context of Alzheimer's disease we additionally profiled the compounds for kinase selectivity. Serendipitously FLT-3 was part of the kinase panel and two substances displayed significant inhibition (98% and 89% at 10 mM) of this tyrosine kinase, Scheme 2.[11]

Regarding this and the fact that FLT-3 is not known to exert effects on the amyloid precursor protein metabolism we focused on optimizing the FLT-3 inhibitory activity of **1** and reducing its modulation of γ-secretase activity. Primary objective of our research was to decrease the effect on γ-secretase and to improve meanwhile the inhibitory activity against FLT-3. The structure of **1** guided the variation of the structure–activity relationship (SAR) study.

The Knoevenagel condensation of indolinones and aldehydes provides a rapid and efficient method to generate a chemical diversity. The Koevenagel products were obtained from microwave irradiated reaction mixtures within 30 min, which was followed by rapid purification. In the first step alkyl or aryl benzyl halides were coupled with 4-hydroxybenzaldhydes **3** under basic conditions to obtain a series of elongated benzaldehydes **4a–n** for the subsequent Knoevenagel condensation.[11,12] A further nucleophilic substitution of the chlorides **4k,l** resulted in the tertiary amines **5a,b** potential intermediate iminium salts were hydrolysed in the aqueous work up.[11] The ether **7** was formed in a microwave heated reactor by substitution of an aromatic fluoride **6** with a 4-(4-methyl-1*H*-imidazole-1-yl)phenol.[13] The 4-fluoro-benzaldehyde **8** was substituted to its corresponding sulfonyl **9** and imidazol benzaldehyde **10**, Scheme 3.[13,14] The phenylimidazoles **7** and **10** were prepared to evaluate this motif, which is frequently employed on γ-secretase

* Corresponding author. Tel.: +49 6151 163075; fax: +49 6151 163278.
E-mail address: Schmidt_boris@t-online.de (B. Schmidt).
† These authors contributed equally to this work.

0960-894X/$ - see front matter © 2012 Elsevier Ltd. All rights reserved.
http://dx.doi.org/10.1016/j.bmcl.2012.10.016

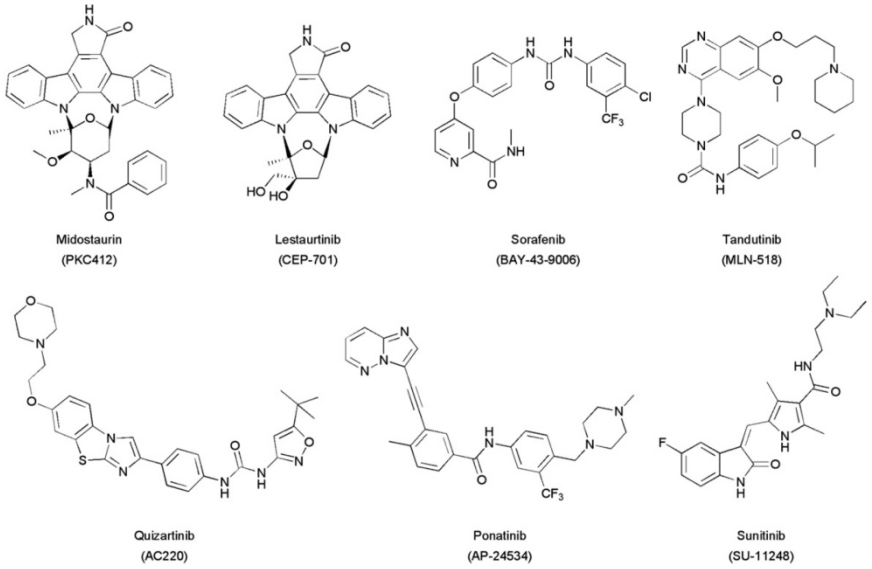

Scheme 1. FLT-3 inhibitors evaluated in preclinical or clinical trials.[5–7,9,10]

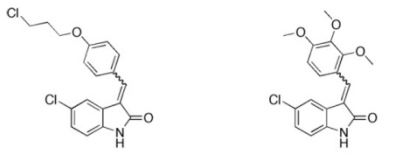

Scheme 2. Screening hits of potential FLT-3 inhibibitors in a kinase panel of 43 kinases.[11]

modulators.[15] The opportunity to obtain fluorescent derivatives was addressed by two derivatives: (A) a two step synthesis resulted in the azobenzene derivative **12**, the 4-aminobenzaldehyde **11** was converted to its diazonium derivative via diazotation and the final azobenzene **12** was formed by an azo coupling reaction.[16] (B) The 9-methyl-9*H*-carbazole **13** was converted to the bulky aldehyde **14** in a two step procedure under Vilsmeier–Haack conditions, Scheme 3.[17]

Commercial aldehydes and the previously synthesized benzaldehydes (Scheme 3) were coupled with the indolinones **15a,b** under microwave supported Knoevenagel conditions, Scheme 4.[11] The resulting products **16a–x** were obtained in yields up to 97%, Table 1. This class of compounds was shown to isomerize within 2 days in methanol, thus no attempts were made to separate the isomers.[11] A further reduction of compound **16e** resulted in 77% yield of product **16y**, Scheme 5a. Finally, the product **16i** was derivatized to obtain the tetrazole **16z** in a moderate yield of 62%, Scheme 5b.[18]

Human recombinant FLT-3 was used in the FLT-3 in vitro kinase assay to ascertain the inhibitory activity. The concentration of the phosphorylated substrate peptide phospho-Ulight-CAGAGAIETDK EYYTVKD (Starting unphosphorylated peptide concentration: 100 nM) was determined after 90 min incubation time at room temperature by the LANCE detection method.[24] All experiments were carried out as technical replicates, the average of two such replicates is listed in Table 1.

The results are expressed as a percent of control (Staurosporine) specific activity ((measured specific activity/control specific activity) × 100) obtained in the presence of the test compounds (10 μM), Table 1. The previously described liquid phase electrochemiluminescence (LPECL) assay was used to measure the Aβ42 isoform to evaluate the compounds for their potency in inhibiting γ-secretase activity, Table 1.[23]

To confirm the FLT-3 inhibition-ratio observed at 10 μM concentration we determined the IC_{50} values of compounds **16e,j,l,n**. The four compounds showed potent inhibition of FLT-3 activity: IC_{50} = 4.1 nM for **16e**, IC_{50} = 14.0 nM for **16j**, IC_{50} = 29.0 nM for **16l** and IC_{50} = 17.0 nM for **16n**, which exceeded the IC_{50} in the Aβ42 generation assay by 3 powers of 10. These activities indicated that we have differentiated FLT-3 inhibition from γ-secretase inhibition.

The most potent γ-secretase inhibitors **16s,v** feature a phenylimidazole, which is frequently encountered in γ-secretase modulators. However, both compounds display reduced FLT-3 inhibition. As indolinones are well known as kinase inhibitors[25,26] we determined the broader selectivity of our most active FLT-3 inhibitor **16e**. The selectivity of compound **16e** was evaluated at a concentration of 1 μM against 50 human protein kinases, Figure 1. Most of the 50 kinases in this panel showed a residual activity higher than 80%, whereas FLT-3 displayed a residual activity of only 14.7%. The only kinases, which were also significantly inhibited by this compound, were the Ser/Thr kinase HGK (MAP4K4) and the Tyr kinase JAK3.

In addition to the H4 APP#9 cell-based toxicity assay, we evaluated the compounds in a zebrafish embryo phenotype assay, which enabled toxicity determination in whole organisms.[27] The embryos were collected and maintained in E2 medium at 28 °C. Compound **16e** was added 4–5 hpf (hours post fertilization) and the phenotypes were compared after 48 hpf. Compound **16e** causes

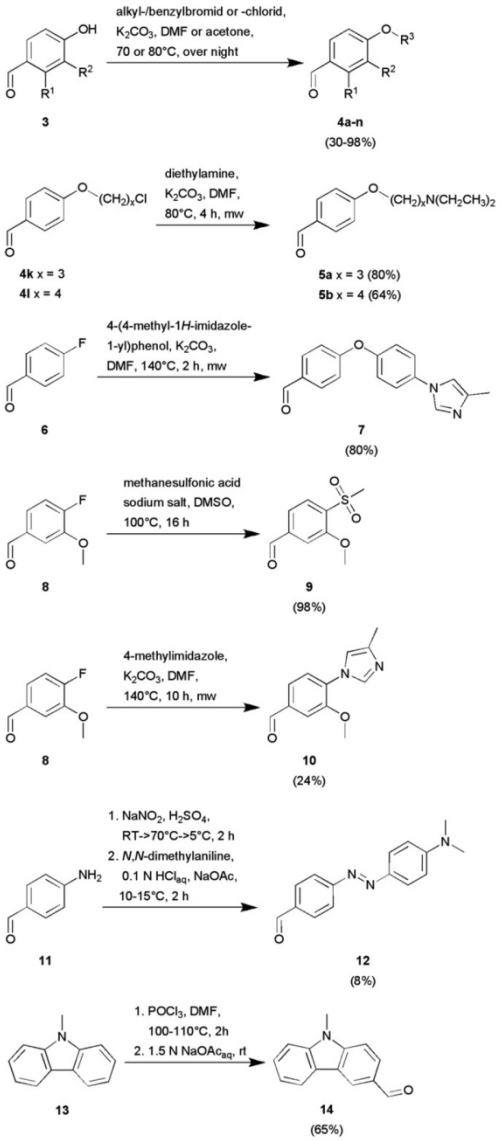

Scheme 3. Aldehyde syntheses (R^1 = H, OMe; R^2 = H, OMe; R^3 = alkyl/benzyl moieties).[11–14,16,17]

a development delay at 20 μM, Figure 2. Compared to the control, zebrafish embryos treated with **16e** were still covered by the chorion. Nevertheless, they did not reveal other abnormalities. The zebrafish embryo assay did not reveal lethality and peculiarities at a concentration below 20 μM of **16e**.

The docking studies (Molegro Virtual Docker 5) of the FLT-3 crystal structure (PDB: 1RJB) and compounds **16e** and **16n**

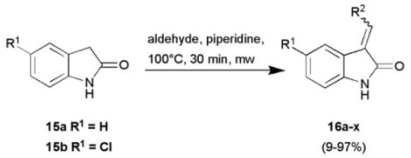

Scheme 4. Synthesis of indolinone derivatives under microwave conditions (R^2 = phenyl moieties).[11,19–22]

revealed potential inhibitor-enzyme interactions, Figure 3.[8] In both cases the docking result indicates four potential interactions. The indolinone motif interacts edge-to-face with the Phe830 of the DFG motif. In addition, the indolinone fits to the FLT-3 hinge region by face-to-face interplay with Phe691 and the hydrogen bonding with Lys644.[8] The phenyl group of the inhibitors interacts with Met665.[28] In addition to these interactions, the rigidity of the bridge between the indolinone and the phenyl moiety may contribute to potent FLT-3 inhibition. Therefore, we synthesized compounds **16e** and **16y**, which differ in orientation and rotational flexibility of the aryl substituent. The FLT-3 in vitro assay results of compounds **16e** (FLT-3 inhibition-ratio = 100%) and **16y** (FLT-3 inhibition-ratio = 47%) revealed a twofold increased FLT-3 inhibition-ratio for **16e** and exemplifying the influence of rigidity. A FLT-3 inhibition comparison of all compounds revealed that an electron donor motif is needed at the end of the elongated, variable alkyl chain. For example compound **16c**, which lacks this motif, showed a decreased inhibition activity compared to **16d,i**. This may be explained by a polar area formed by Glu573 and Gln577, which is in close vicinity. A comparison of the FLT-3 inhibition results and the docking studies offers the possible suggestion that the benzylidene indolinone moiety may occupy the entrance of the ATP-binding site (compound **16a,b,k**) and the elongated alkyl chain ranging from C_2 (**16e**) to C_4 (**16h**) could act as a flexible 'anchor' in the inner side of the ATP-binding pocket, for example, **16d–j**. Furthermore, a comparison of the FLT-3 inhibition results of Table 1 revealed that bulky residues at the phenyl moiety lead to a decreased inhibitory activity.

The inhibitory activity of the synthesized compounds in the γ-secretase assay cannot be correlated to the FLT-3 inhibition-ratio, Figure 4. In the case of compounds **16i** (FLT-3 inhibition-ratio = 96%; IC_{50} (Aβ42) > 40 μM) and **16n** (FLT-3 inhibition-ratio = 87%; IC_{50} (Aβ42) > 160 μM) we expected the same result, but surprisingly, they were not active against the γ-secretase, Table 1 and Fig. 4. In comparison with other compounds, for example, **16d,l** and **16p,r**, the nitrile and alkyl chain combination is important for this selectivity.

Conclusion: we have identified several potent FLT-3 inhibitors based on the scaffold of the screening hit **1**, which display neglible activity on γ-secretase inhibition. The most active compound **16e** did not display significant toxicity in H4 APP#9 cells and the zebrafish embryo phenotype assay. This lack of apparent toxicity may be due to lack of permeation, yet permeation is indicated by the activity in the Aβ42 generation assay. The combination of FLT-3 in vitro results and docking studies revealed likely enzyme-inhibitor interactions with the amino acids Lys644, Met665, Phe691 and Phe830. Further improvement of these FLT-3 inhibitors will focus on the reduction of the log*P* to enhance to pharmacokinetic properties. Our most active FLT-3 inhibitor **16e** exhibits a *C*log*P* value of 5.28, Table 1, which implies impaired solubility.

Table 1
Synthesized indolinones, their chemical properties and in vitro assay results[23,24]

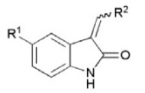

1-2, 16a-x, 16z

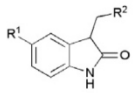

16y

Compound	R^1	R^2	FLT-3 inhibition -ratio[a] (%)	IC_{50} of A_{42} LPECL assay[b] (μM)	Toxicity (μM)[c]	Yield (%)	Clog P[d]
Staurosporine[e]	–	–	100	n.t.[f]	n.t. [f]	–	4.19
Sunitinib[e]	–	–	100	n.t. [f]	n.t. [f]	–	3.00
1	Cl	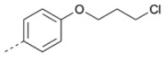	98	4.7	Y (40)	–	5.04
2	Cl		89	–	–	–	3.50
16a	Cl		94	47.6	N (40)	28	3.53
16b	Cl	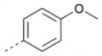	85	>40	N (40)	88	4.12
16c	Cl	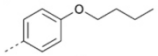	79	>40	N (40)	83	5.71
16d	Cl	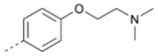	99	7.6	N (40)	65	4.22
16e	Cl	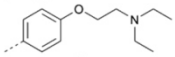	100	17.7	Y (40)	55	5.28
16f	H	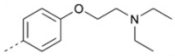	97	–	–	95	4.31
16g	Cl	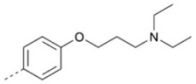	99	–	–	80	5.63
16h	Cl	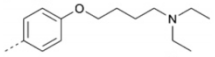	99	–	–	64	5.56
16i	Cl	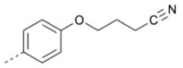	96	>40	Y (40)	90	3.94
16j	Cl	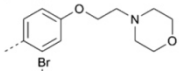	96	11.3	N (40)	84	4.24
16k	Cl	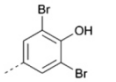	97	15.0	N (40)	97	5.10
16l	Cl	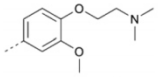	98	11.5	Y (40)	31	3.96
16m	Cl	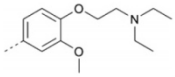	99	11.5	Y (40)	42	5.02
16n	Cl	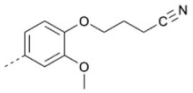	87	>160	N (160)	67	3.68

(*continued on next page*)

Table 1 (*continued*)

Compound	R^1	R^2	FLT-3 inhibition -ratio[a] (%)	IC_{50} of A_{42} LPECL assay[b] (μM)	Toxicity (μM)[c]	Yield (%)	Clog*P*[d]
16o	Cl	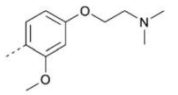	100	10.0	N (40)	71	4.31
16p	Cl	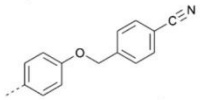	75	27.3	N (40)	93	5.32
16q	Cl	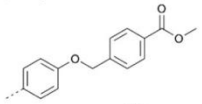	58	38.8	N (40)	70	5.86
16r	Cl	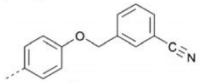	77	>40	N (40)	48	5.32
16s	Cl	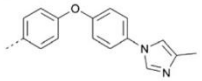	83	5.4	Y (10)	41	5.88
16t	H	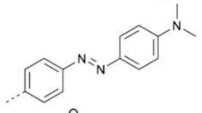	77	>80	N (80)	9	5.55
16u	Cl	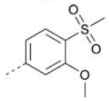	48	7.3	Y (20)	85	2.49
16v	Cl	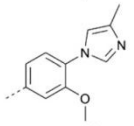	74	6.7	Y (80)	55	4.25
16w	Cl	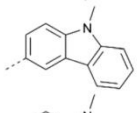	69	19.8	N (80)	17	6.04
16x	H	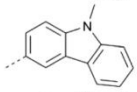	78	27.6	Y (80)	15	5.07
16y	H	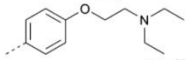	47	–	–	77	3.87
16z	Cl	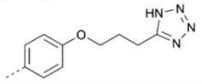	83	17.7	Y (40)	62	3.76

[a] Percent of control (Staurosporine) specific activity ((measured specific activity/control specific activity) × 100); activity at a concentration of 10 μM.
[b] Aβ liquid phase electrochemiluminescence (LPECL) assay, H4 APP#9 cells.
[c] Determined in H4-cells, Y = Yes, N = No.
[d] Calculated by ChemDraw Ultra (9.0.1).
[e] Control.
[f] n.t. = Not tested.

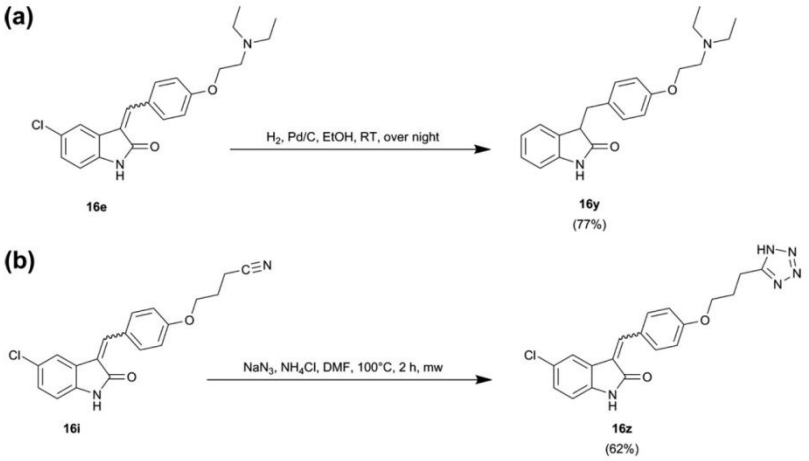

Scheme 5. Post-Knoevenagel modifications: (a) Reduction with H_2 and Pd/C; (b) Tetrazole synthesis under microwave conditions.[18]

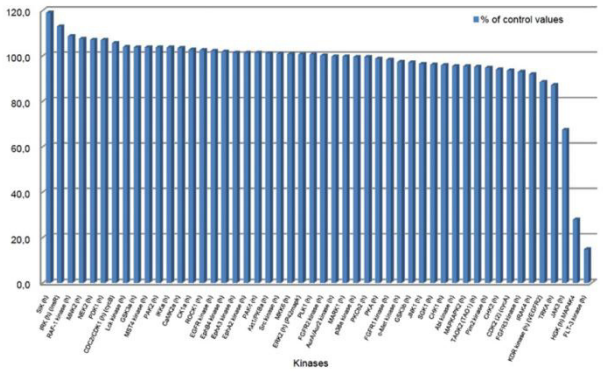

Figure 1. Screening of compound **16e** against a panel of human protein kinases. Each bar represents the activity of one individual protein kinase (determination method: percent of control (Staurosporine) specific activity [(measured specific activity/control specific activity) × 100]). Compound **16e** was tested at a concentration of 1 μM against 50 protein kinases. See the Supplementary data for more details.[24]

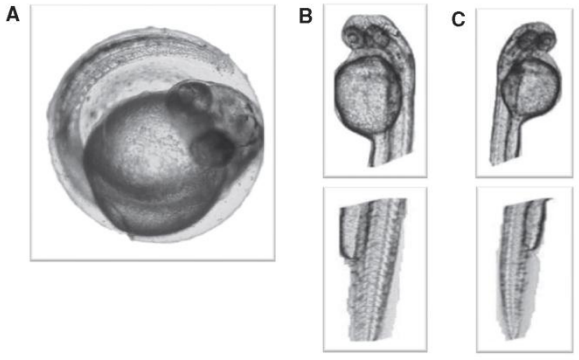

Figure 2. Exposure of zebrafish embryos to (A) 20 μM of **16e**, (B) 5 μM of **16e**, (C) control. The embryos were collected and maintained in E2 medium at 28 °C. Compound **16e** was added 4–5 hpf (hours post fertilization) and the phenotypes were compared after 48 hpf.

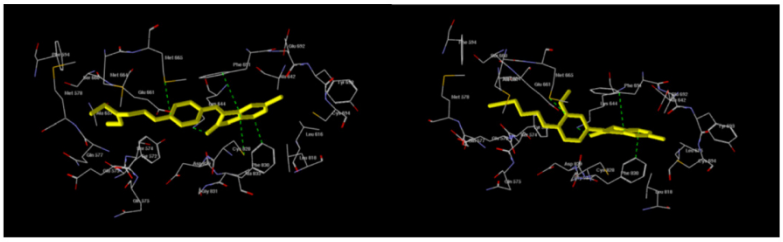

Figure 3. Docking of compound **16e** (left) and **16n** (right) into the PDB crystal structure 1RJB of FLT-3; important interactions are highlighted; Software: Molegro Virtual Docker 5.

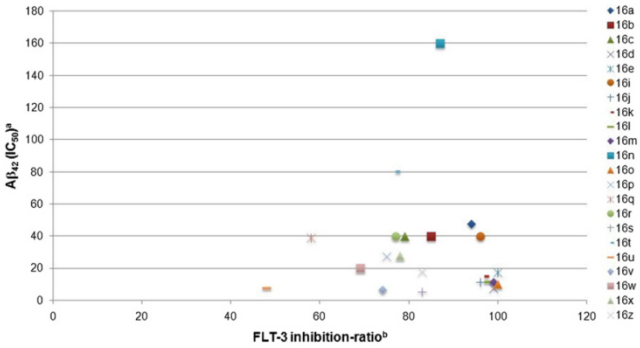

Figure 4. Correlation plot of FLT-3 activity inhibition and Aβ42 inhibition (IC_{50}); [a]values at 40 μM are determined as >40, see Table 1; [b]determination method: percent of control (Staurosporine) specific activity [(measured specific activity/control specific activity) × 100]).

Supplementary data

Supplementary data associated with this article can be found, in the online version, at http://dx.doi.org/10.1016/j.bmcl.2012.10.016.

References and notes

1. Kindler, T.; Lipka, D. B.; Fischer, T. *Blood* **2010**, *116*, 5089.
2. Levis, M.; Small, D. *Expert Opin. Investig. Drugs* **1951**, *2003*, 12.
3. Pratz, K. W.; Levis, M. J. *Curr. Drug Targets* **2010**, *11*, 781.
4. Griffith, J.; Black, J.; Faerman, C.; Swenson, L.; Wynn, M.; Lu, F.; Lippke, J.; Saxena, K. *Mol. Cell* **2004**, *13*, 169.
5. Advani, A. S. *Curr. Pharm. Des.* **2005**, *11*, 3449.
6. Paz, K.; Zhu, Z. *Expert Opin. Ther. Targets* **2005**, *9*, 1147.
7. Zarrinkar, P. P.; Gunawardane, R. N.; Cramer, M. D.; Gardner, M. F.; Brigham, D.; Belli, B.; Karaman, M. W.; Pratz, K. W.; Pallares, G.; Chao, Q.; Sprankle, K. G.; Patel, H. K.; Levis, M.; Armstrong, R. C.; James, J.; Bhagwat, S. S. *Blood* **2009**, *114*, 2984.
8. Mahboobi, S.; Uecker, A.; Sellmer, A.; Cenac, C.; Hocher, H.; Pongratz, H.; Eichhorn, E.; Hufsky, H.; Trumpler, A.; Sicker, M.; Heidel, F.; Fischer, T.; Stocking, C.; Elz, S.; Bohmer, F. D.; Dove, S. *J. Med. Chem.* **2006**, *49*, 3101.
9. Pemmaraju, N.; Kantarjian, H.; Ravandi, F.; Cortes, J. *Cancer* **2011**, *117*, 3293.
10. www.clinicaltrials.gov July 2012.
11. Höttecke, N.; Liebeck, M.; Baumann, K.; Schubenel, R.; Winkler, E.; Steiner, H.; Schmidt, B. *Bioorg. Med. Chem. Lett.* **2010**, *20*, 2958.
12. Strohfeldt, K.; Müller-Bunz, H.; Pampillón, C.; Sweeney, N. J.; Tacke, M. *Eur. J. Inorg. Chem.* **2006**, 4621.
13. Fischer, C.; Munoz, B.; Zultansky, S.; Methot, J.; Zhou, H.; Brown, W. C., WO 2008/156580 A1, 2008.
14. Ulman, A.; Urankar, E. *J. Org. Chem.* **1989**, *54*, 4691.
15. Schmidt, B.; Baumann, S.; Braun, H. A.; Larbig, G. *Curr. Top. Med. Chem.* **2006**, *6*, 377.
16. Perez-Moreno, J.; Zhao, Y.; Clays, K.; Kuzyk, M. G.; Shen, Y.; Qiu, L.; Hao, J.; Guo, K. *J. Am. Chem. Soc.* **2009**, *131*, 5084.
17. Langendoen, A.; Plug, J. P. M.; Koomen, G.-J.; Pandit, U. K. *Tetrahedron* **1989**, *45*, 1759.
18. Lo Monte, F.; Kramer, T.; Boländer, A.; Plotkin, B.; Eldar-Finkelman, H.; Fuertes, A.; Dominguez, J.; Schmidt, B. *Bioorg. Med. Chem. Lett.* **2011**, *21*, 5610.
19. Angell, R.; Reynolds, K.; Lumley, J., WO 2004069998 A2, 2004.
20. Bouerat, L. M. E.; Fensholdt, J.; Nielsen, S. F.; Liang, X.; Havez, S. E.; Andersson, E. C.; Jensen, L.; Hansen, J. R., WO 2005058309 A1, 2005.
21. Jiang, T.; Kuhen, K. L.; Wolff, K.; Yin, H.; Bieza, K.; Caldwell, J.; Bursulaya, B.; Tuntland, T.; Zhang, K.; Karanewsky, D.; He, Y. *Bioorg. Med. Chem. Lett.* **2006**, *16*, 2109.
22. Wood, E.; Crosby, R. M.; Dickerson, S.; Frye, S. V.; Griffin, R.; Hunter, R.; Jung, D. K.; McDonald, O. B.; McNutt, R.; Mahony, W. B.; Peel, M. R.; Ray, J.; Lackey, K. *Anti-Cancer Drug Des.* **2001**, *16*, 1.
23. Narlawar, R.; Perez Revuelta, B. I.; Haass, C.; Steiner, H.; Schmidt, B.; Baumann, K. *J. Med. Chem.* **2006**, *49*, 7588.
24. www.cerep.fr
25. Chen, C. H.; Lee, O.; Yao, C. N.; Chuang, M. Y.; Chang, Y. L.; Chang, M. H.; Wen, Y. F.; Yang, W. H.; Ko, C. H.; Chou, N. T.; Lin, M. W.; Lai, C. P.; Sun, C. Y.; Wang, L. M.; Chen, Y. C.; Hseu, T. H.; Chang, C. N.; Hsu, H. C.; Lin, H. C.; Shih, Y. C.; Chou, S. H.; Hsu, Y. L.; Tseng, H. W.; Liu, C. P.; Tu, C. M.; Hu, T. L.; Tsai, Y. J.; Chen, T. S.; Lin, C. L.; Chiou, S. J.; Liu, C. C.; Hwang, C. S. *Bioorg. Med. Chem. Lett.* **2010**, *20*, 6129.
26. Prakash, C. R.; Raja, S. *Mini Rev. Med. Chem.* **2012**, *12*, 98.
27. Nagel, R. *ALTEX* **2002**, *19*, 38.
28. Salonen, L. M.; Ellermann, M.; Diederich, F. *Angew. Chem.* **2011**, *123*, 4908.

Supplementary Material (ESI) for Bioorganic & Medical Chemistry Letters

Supporting Information

Modification of a promiscuous inhibitor shifts the inhibition from γ-secretase to FLT-3

Ghislaine Marlyse Okala Amombo*[a], Thomas Kramer*[a], Fabio Lo Monte*[a], Stefan Göring[a], Matthias Fach[a], Steven Smith[a], Stephanie Kolb[a], Robert Schubenel[b], Karlheinz Baumann[b] and Boris Schmidt†[a]

[a] *Clemens Schöpf - Institute of Organic Chemistry and Biochemistry, Technische Universität Darmstadt, 64287 Darmstadt, Hessen, Germany, Fax: +496151-163278; Tel: +496151-164531*

[b] *F. Hoffmann-La Roche Ltd, Pharmaceutical Division, Preclinical Research CNS, Bldg. 70/345, CH-4070 Basel, Switzerland,*

† E-mail: schmidt_boris@t-online.de

*These authors contributed equally to this work.

Table of Content:

I. General comments

II. Experimental methods and chemical data

III. FTL-3 *in vitro* assay conducted by Cerep

IV. Selectivity screening of compound **16e** conducted by Cerep

V. γ-Secretase assay and cell-based toxicity assay conducted by Roche

VI. Toxicity assay: Determination of the *in vivo* activity on wt zebrafish embryos

VII. References

I. General comments

The ^{1}H-NMR spectra were recorded on a Bruker AC 300 spectrometer at 300 MHz and Bruker AC 500 spectrometer at 500 MHz. The ^{13}C-NMR spectra were recorded on a Bruker AC 300 spectrometer at 75 MHz and Bruker AC 500 spectrometer at 125 MHz. Chemical shifts are reported as ppm downfield from Me_4Si. Mass spectrometry was performed on a Bruker-Franzen Esquire LC mass spectrometer and a MAT 95 double focussing sector field MS. Microwave experiments were carried out using a Biotage® Initiator™ microwave apparatus. All microwave experiments were carried out in sealed microwave process vials utilizing the standard absorbance level (300 W maximum power). High performance liquid chromatographies were carried out in an Agilent 1100 (column: reversed phase, Zorbax Eclipse XDB-C8, 4.6 x 150 mm; 254 nm). The eluent is composed of: a) H_2O (1% TFA) (A) and acetonitrile (B) with a gradient: 30 to 90% B within 12 min. All reagents and solvents were purchased at ABCR, Acros, Sigma Aldrich and VWR.

II. Experimental methods and chemical data

1. General Procedure for synthesis of benzaldehyds 4a-l[1]

K_2CO_3 (2.40 eq.) and the aldehyde **3** (1.00 eq.) were suspended in acetone or dimethylformamide. Then an alkyl/benzyl bromide/chloride (1.00 eq.) was added. This reaction suspension was stirred at 70°C over night. After complete turnover water was added and the aqueous solution was extracted with chloroform. The combined organic layers were dried with $MgSO_4$ and the solvent was removed in vacuo. The resulting residue was used without further purification, purified by column chromatography on silica gel or recrystallized in an appropriate solvent to provide the desired product.

4-butoxybenzaldehyde 4a[2]

The resulting product is a bright yellow oil (51%). **HPLC**: R_t = 6.85 min. **^{1}H-NMR** ($CDCl_3$, 300 MHz): δ [ppm] = 9.88 (s, 1H), 7.82 (d, 2H, *J* = 8.8 Hz), 6.98 (d, 2H, *J* = 8.8 Hz), 4.05 (t, 2H, *J* = 6.4 Hz), 1.85-1.75 (m, 2H), 1.57-1.44 (m, 2H), 0.99 (t, 3H). **^{13}C-NMR** ($CDCl_3$, 75 MHz): δ [ppm] = 191.0, 164.4, 132.1, 129.9, 114.9, 68.3, 31.2, 19.3, 13.9. **MS** (EI, 70 eV): *m/z* = 178 [M^+].

4-(2-(diethylamino)ethoxy)benzaldehyde 4b[3]

The resulting brown oil (78%) was used in the next step without further analysis.

4-(4-formylphenoxy)butannitrile 4c

The resulting product is a bright yellow oil (65%). **HPLC**: R_t = 4.71 min. **^{1}H-NMR** ($CDCl_3$, 300 MHz): δ [ppm] = 9.89 (s, 1H), 7.84 (d, 2H, *J* = 8.8 Hz), 7.01 (d, 2H, *J* = 8.8 Hz), 4.17 (t, 2H, *J* = 5.7 Hz), 2.61 (t, 2H, *J* = 7.1 Hz), 2.23-2.14 (m, 2H). **^{13}C-NMR** ($CDCl_3$, 75 MHz): δ [ppm] = 190.8, 163.4, 132.2, 130.5, 119.0, 114.9, 65.7, 25.4, 14.3. **MS** (EI, 70 eV): *m/z* = 189 [M^+].

4-(2-morpholinoethoxy)benzaldehyde 4d[4]

The resulting bright yellow oil (52%) was used in the next step without further analysis.

4-((4-formylphenoxy)methyl)benzonitrile 4e

The resulting product is a colorless solid (51%). **HPLC**: R_t = 6.76 min. **^{1}H-NMR** ($CDCl_3$, 500 MHz): δ [ppm] = 9.90 (s, 1H), 7.86 (d, 2H, *J* = 8.8 Hz), 7.70 (d, 2H, *J* = 8.4 Hz), 7.55 (d, 2H, *J* = 8.4 Hz), 7.07 (d, 2H, *J* = 8.8 Hz), 5.21 (s, 2H). **^{13}C-NMR** ($CDCl_3$, 125 MHz): δ [ppm] = 190.8, 163.2, 141.5, 132.7, 132.2, 130.8, 127.7, 118.6, 115.2, 112.3, 69.2, 52.3. **MS** (EI, 70 eV): *m/z* = 237 [M^+].

Methyl 4-((4-formylphenoxy)methyl)benzoate 4f

The resulting product is a colorless solid (43%). **HPLC**: R_t = 6.90 min. **^{1}H-NMR** ($CDCl_3$, 500 MHz): δ [ppm] = 9.89 (s, 1H), 8.07 (d, 2H, *J* = 8.4 Hz), 7.84 (d, 2H, *J* = 8.8 Hz), 7.50 (d, 2H, *J* = 8.4 Hz), 7.07 (d, 2H, *J* = 8.8 Hz), 5.21 (s, 2H), 3.93 (s, 3H). **^{13}C-NMR** ($CDCl_3$, 125 MHz): δ [ppm] = 190.8, 166.8, 163.4, 141.2, 132.2, 130.5, 130.2, 130.2, 127.1, 115.3, 69.7, 52.3. **MS** (EI, 70 eV): *m/z* = 270 [M^+].

3-((4-formylphenoxy)methyl)benzonitrile 4g

The resulting product is a colorless solid (30%). **HPLC**: R_t = 6.76 min. **^{1}H-NMR** ($CDCl_3$, 500 MHz): δ [ppm] = 9.91 (s, 1H), 7.86 (d, 2H, *J* = 8.8 Hz), 7.75 (s, 1H), 7.69-7.64 (m, 2H), 7.54-7.51 (m, 1H), 7.50 (d, 2H, *J* = 8.4 Hz), 7.08 (d, 2H, *J* = 8.8 Hz), 5.18 (s, 2H). **^{13}C-NMR** ($CDCl_3$, 125 MHz): δ [ppm] = 190.8, 163.1, 137.8, 132.2, 132.0, 131.6, 130.9, 130.7, 129.7, 118.6, 115.2, 113.1, 69.0. **MS** (EI, 70 eV): *m/z* = 237 [M^+].

4-(2-(dimethylamino)ethoxy)-3-methoxybenzaldehyde 4h[4]

The resulting bright brown oil (47%) was used in the next step without further analysis.

4-(2-(diethylamino)ethoxy)-3-methoxybenzaldehyde 4i

The resulting bright brown oil (45%) was used in the next step without further analysis.

4-(4-formyl-2-methoxyphenoxy)butannitrile 4j

The resulting product is a bright yellow oil (69%). **HPLC**: R_t = 4.34 min. **^{1}H-NMR** ($CDCl_3$, 500 MHz): δ [ppm] = 9.86 (s, 1H), 7.44 (dd, 1H, *J* = 1.8 Hz, *J* = 8.1 Hz), 7.42 (d, 1H, *J* = 1.8 Hz), 6.98 (d, 1H, *J* = 8.1 Hz), 4.21 (t, 2H, *J* = 5.8 Hz), 3.92 (s, 3H), 2.65 (t, 2H, *J* = 7.1 Hz), 2.25-2.20 (m, 2H). **^{13}C-NMR** ($CDCl_3$, 125 MHz): δ [ppm] = 191.0, 153.4, 150.2, 130.8, 126.7, 119.1, 112.2, 109.6, 66.6, 56.1, 25.5, 14.3.

4-(3-chloropropoxy)benzaldehyde 4k[1]

The resulting product is a colorless oil (98%). **HPLC**: R_t = 6.52 min. **^{1}H NMR** ($CDCl_3$, 500 MHz): δ [ppm] = 9.92 (s, 1H) 7.86 (m, 2H), 7.04 (m, 2H), 4.24 (t, 2H, *J* = 5.9 Hz), 3.78 (t, 2H, *J* = 6.3 Hz), 2.30 (m, 2H). **^{13}C-NMR** ($CDCl_3$, 125 MHz): δ [ppm] = 190.7, 163.7, 132.0, 130.2, 114.8, 64.6, 41.2, 32.0.

4-(4-chlorobutoxy)benzaldehyde 4l

The resulting product is a colorless oil (98%). **HPLC**: R_t = 7.06 min. **^{1}H NMR** ($CDCl_3$, 500 MHz): δ [ppm] = 9.91 (s, 1H), 7.86 (d, 2H, *J* = 8.8 Hz), 7.02 (d, 2H, *J* = 8.7 Hz), 4.12 (t, 2H, *J* = 5.8 Hz), 3.65 (t, 2H, *J* = 6.2 Hz), 2.02 (m, 4H). **^{13}C-NMR** ($CDCl_3$, 125 MHz): δ [ppm] = 190.7, 163.9, 132.0, 130.0, 114.7, 67.4, 44.6, 29.2, 26.5.

2. Synthesis of 4-(2-(dimethylamino)ethoxy)benzaldehyde 4m and 4-(2-(dimethylamino)-ethoxy)-2-methoxybenzaldehyde 4n[5]

For the synthesis of 4-(2-(dimethylamino)ethoxy)benzaldehyde **4m** see the mentioned reference. The resulting brown oil (63%) was used in the next step without further analysis.

For the synthesis of 4-(2-(dimethylamino)ethoxy)-2-methoxybenzaldehyde **4n** see the mentioned reference. The resulting product is a bright brown oil (66%). **HPLC**: R_t = 0.75 min, 1.11 min. **^{1}H-NMR** ($CDCl_3$, 300 MHz): δ [ppm] = 10.28 (s, 1H), 7.79 (d, 1H, J = 8.7 Hz), 6.54 (dd, 1H, J = 2.2 Hz, J = 8.7 Hz), 6.49 (d, 1H, J = 2.2 Hz), 4.13 (t, 2H, J = 5.7 Hz), 3.88 (s, 3H), 2.75 (t, 2H, J = 5.7 Hz), 2.35 (s, 6H). **^{13}C-NMR** ($CDCl_3$, 75 MHz): δ [ppm] = 188.4, 165.5, 163.7, 130.9, 119.3, 106.2, 98.9, 66.4, 58.2, 55.8, 46.0.

3. General Procedure for synthesis of 4-(3-(diethylamino)propoxy)benzaldehyde 5a and 4-(4-(diethylamino)butoxy)benzaldehyde 5b[1]

K_2CO_3 (5.00 eq.) and the alkylchloride **4k** or **4l** (1.00 eq.) were suspended in dimethylformamide. Then diethylamine (5.00 eq.) was added and the mixture heated at 80°C under microwave irradiation for 4 h. After complete turnover ethyl acetate (30 mL) was added. The organic phase was washed with water and dried with $MgSO_4$. The solvent was removed in vacuo. The resulting residue was used in the next step without further purification and analysis.

4. Synthesis of 4-(4-(4-methyl-1*H*-imidazol-1-yl)phenoxy)benzaldehyde 7[6]

A mixture of 4-(4-methyl-1H-imidazol-1-yl)phenole (1.74 g, 10 mmol), 4-fluorobenz-aldehyde **6** (1.24 g, 10 mmol) and anhydrous K_2CO_3 (1.38 g, 10 mmol) in abs. dimethylformamide (5 mL) was heated at 140°C under microwave irradiation for 2 h. The cooled reaction mixture was diluted with ethyl acetate (5 mL), filtered through a plug of silica gel, and washed with ethyl acetate (10-20 mL). The combined organic extracts were concentrated, and the resulting residue was purified by column chromatography on silica gel to provide the desired product in 80% as a brown oil. **HPLC**: R_t = 2.64 min. **^{1}H-NMR** (DMSO-d_6, 500 MHz): δ [ppm] = 9.94 (s, 1H), 8.26 (m, 1H), 7.95 (m, 2H), 7.75 (m, 3H), 7.31 (m, 2H), 7.18 (m, 2H), 2.14 (s, 3H). **^{13}C-NMR** (DMSO-d_6, 125 MHz): δ [ppm] = 191.5, 162.1, 153.2, 135.6, 133.8, 132.0, 131.4, 129.9, 129.3, 122.4, 122.2, 121.5, 118.1, 117.6, 116.0, 13.6. **MS** (EI, 70 eV): m/z = 278 [M^+].

5. Synthesis of 3-methoxy-4-(methylsulfonyl)benzaldehyde 9[7]

Methanesulfinic acid sodium salt (125 mg, 0.81 mmol) and 4-fluoro-3-methoxybenzaldehyde **8** (91.06 mg, 0.89 mmol) were dissolved in dry DMSO (3 mL), under nitrogen. The mixture was stirred at 100°C for 16h and then poured into ice. The formed precipitate was collected by filtration, washed with water and dried to afford 258 mg (98%) of colourless solid. The crude solid was used in next step without any further purification. **HPLC**: R_t = 2.66 min. **^{1}H-NMR** (DMSO-d_6, 500 MHz): δ [ppm] = 10.00 (s, 1H), 8.11 (d, 1H, *J* = 7.9 Hz), 7.53 (dd, 1H, *J* = 1.3 Hz, *J* = 7.9 Hz), 7.49 (d, 1H, *J* = 1.2 Hz), 4.02 (s, 3H), 3.18 (s, 3H). **^{13}C-NMR** (DMSO-d_6, 125 MHz): δ [ppm] = 190.8, 184.4, 157.7, 141.5, 133.5, 130.7, 123.3, 110.9, 56.7, 42.9.

6. Synthesis of 2-methoxy-4-(4-methyl-1H-imidazol-1-yl)benzaldehyde 10[6]

A mixture of 4-fluoro-3-methoxybenzaldehyde **8** (1.22 g, 7.92 mmol) and 4-methylimidazole (1.24 g, 15.07 mmol) in dry dimethylformamide was degassed and flushed with argon for 20 min. Afterwards K_2CO_3 (1.66 g, 11.98 mmol) was added and the reaction suspension was heated at 140°C under microwave irradiation for 10 h. Then water was added and the aqueous solution was extracted with ethyl acetate. The combined organic layers were washed with brine, dried with Na_2SO_4 and the solvent was removed in vacuo. The resulting residue was purified by column chromatography on silica gel (solvent: ethyl acetate) and provide 411 mg (24%) of the orange product. The product was used in the next step without detailed analysis. **HPLC**: R_t = 1.37 min. **MS** (EI, 70 eV): *m/z* = 216 [M^+].

7. Synthesis of (E)-4-((4-(dimethylamino)phenyl)diazenyl)benzaldehyde 12[8]

For the synthesis of compound **12** see the mentioned reference in the publication. Used in the next step without further analysis.

8. Synthesis of 9-methyl-9H-carbazole-3-carbaldehyde 14[9]

For the synthesis of compound **14** see the mentioned reference in the publication. Used in the next step without further analysis.

9. General Procedure for synthesis of 3-substituted indol-2-ones[1]

Equimolar amounts (0.3 mmol) of 5-chlorooxindole/oxindole and aldehyde were dissolved in methanol (1 ml), a drop of piperidine (30 µl) was added and the mixture heated at 100°C under microwave irradiation for 30 min. The reaction mixture was cooled to room

temperature and the resulting precipitate was removed by filtration, carefully washed with methanol and recrystallized at least once from methanol to give the desired product in good yield.

5-chloro-3-(4-(3-chloropropoxy)benzyliden)indolin-2-one 1[1]

The resulting product is a yellow solid (30%). **HPLC**: R_t = 8.06 min, 8.44 min. **^{1}H-NMR** (DMSO-d_6, 500 MHz): δ [ppm] = 10.69 (s, 2H), 8.49 (d, 2H, *J* = 8.9 Hz), 7.89 (s, 1H), 7.80 (d, 1H, *J* = 2.0 Hz), 7.70 (d, 2H, *J* = 8.9 Hz), 7.66 (s, 1H), 7.56 (d, 1H, *J* = 2.0 Hz), 7.27 (dd, 1H, *J* = 2.0 Hz, *J* = 8.3 Hz), 7.20 (dd, 1H, *J* = 2.0 Hz, *J* = 8.3 Hz), 7.13 (d, 2H, *J* = 8.9 Hz), 7.07 (d, 2H, *J* = 8.9 Hz), 6.89 (d, 1H, *J* = 8.3 Hz), 6.81 (d, 1H, *J* = 8.3 Hz), 4.20 (t, 4H, *J* = 5.9 Hz), 3.81 (m, 4H), 2.20 (m, 4H). **^{13}C-NMR** (DMSO-d_6, 125 MHz): δ [ppm] = 168.5, 167.1, 160.6, 160.0, 141.4, 138.8, 138.7, 137.9, 134.8, 131.6, 129.2, 127.5, 127.3, 127.0, 126.3, 125.3, 124.9, 124.8, 123.0, 122.8, 121.4, 119.3, 114.8, 114.3, 111.4, 110.5, 64.6, 64.5, 41.9, 31.6. **MS** (EI, 70 eV): *m/z* = 347 [M$^+$].

5-chloro-3-(4-hydroxybenzylidene)indolin-2-one 16a[10]

The resulting product is an orange solid (28%). **HPLC**: R_t = 5.39 min, 6.15 min. **^{1}H-NMR** (DMSO-d_6, 500 MHz): δ [ppm] = 10.69 (s, 2H), 8.41 (d, 2H, *J* = 8.9 Hz), 7.80 (s, 1H), 7.76 (d, 1H, *J* = 2.0 Hz), 7.60 (m, 4H), 7.25 (dd, 1H, *J* = 2.0 Hz, *J* = 8.3 Hz), 7.15 (dd, 1H, *J* = 2.0 Hz, *J* = 8.3 Hz), 6.88 (m, 3H), 6.80 (m, 3H). **^{13}C-NMR** (DMSO-d_6, 125 MHz): δ [ppm] = 168.8, 167.3, 162.1, 160.7, 141.1, 139.6, 138.7, 138.4, 135.4, 132.1, 128.7, 127.8, 126.9, 125.1, 124.8, 124.8, 124.1, 123.3, 123.1, 121.3, 120.9, 118.8, 116.0, 115.7, 111.2, 110.3. **MS** (EI, 70 eV): *m/z* = 271 [M$^+$].

5-chloro-3-(4-methoxybenzyliden)indolin-2-one 16b[11]

The resulting product is a yellow solid (88%). **HPLC**: R_t = 7.06 min, 7.50 min. **^{1}H-NMR** (DMSO-d_6, 500 MHz): δ [ppm] = 10.69 (s, 2H, $NH_{E/Z}$), 8.49 (d, 2H, *J* = 8.9 Hz), 7.88 (s, 1H), 7.80 (d, 1H, *J* = 2.0 Hz), 7.70 (d, 2H, *J* = 8.9 Hz), 7.66 (s, 1H), 7.56 (d, 1H, *J* = 2.0 Hz), 7.27 (dd, 1H, *J* = 2.0 Hz, *J* = 8.3 Hz), 7.19 (dd, 1H, *J* = 2.0 Hz, *J* = 8.3 Hz), 7.12 (d, 2H, *J* = 8.9 Hz), 7.05 (d, 2H, *J* = 8.9 Hz), 6.89 (d, 1H, *J* = 8.3 Hz), 6.81 (d, 1H, *J* = 8.3 Hz), 3.85 (d, 6H). **^{13}C-NMR** (DMSO-d_6, 125 MHz): δ [ppm] = 168.6, 167.1, 161.6, 160.9, 141.4, 138.3, 137.9, 134.8, 131.6, 129.2, 127.5, 127.3, 126.8, 126.2, 125.3, 124.9, 124.7, 122.9, 122.8, 121.4, 119.3, 114.4, 113.7, 111.4, 110.5, 55.4, 55.4. **MS** (EI, 70 eV): *m/z* = 285 [M$^+$].

3-(4-butoxybenzyliden)-5-chloroindolin-2-one 16c

The resulting product is a yellow solid (83%). **HPLC**: R_t = 8.42 min, 8.71 min. **^{1}H-NMR** (DMSO-d_6, 500 MHz): δ [ppm] = 10.60 (s, 2H), 8.46 (d, 2H, *J* = 8.9 Hz), 7.79 (s, 1H), 7.71 (d, 2H, *J* = 8.9 Hz), 7.65 (s, 1H), 7.63 (d, 1H, *J* = 2.0 Hz), 7.56 (d, 1H, *J* = 2.0 Hz), 7.20 (dd,

1H, J = 2.0 Hz, J = 8.3 Hz), 7.13 (dd, 1H, J = 2.0 Hz, J = 8.3 Hz), 7.05 (d, 2H, J = 8.9 Hz), 6.98 (d, 2H, J = 8.9 Hz), 6.85 (d, 1H, J = 8.3 Hz), 6.78 (d, 1H, J = 8.3 Hz), 4.05 (t, 4H, J = 6.5 Hz), 1.75-1.71 (m, 4H), 1.50-1.43 (m, 4H), 0.96-0.94 (m, 6H). **^{13}C-NMR** (DMSO-d_6, 125 MHz): δ [ppm] = 168.5, 167.1, 161.0, 160.3, 141.3, 138.7, 138.6, 137.6, 134.7, 131.3, 128.8, 127.2, 127.0, 126.6, 126.0, 125.2, 124.9, 124.7, 122.8, 121.4, 119.0, 114.6, 114.0, 111.1, 110.3, 67.4, 67.3, 41.9, 41.9, 30.6, 18.6, 13.6. **MS** (EI, 70 eV): m/z = 327 [M^+].

5-chloro-3-(4-(2-(dimethylamino)ethoxy)benzyliden)indolin-2-one 16d

The resulting product is a yellow solid (65%). **HPLC**: R_t = 3.28 min, 4.38 min. **^{1}H-NMR** (DMSO-d_6, 500 MHz): δ [ppm] = 10.69 (s, 2H), 8.48 (d, 2H, J = 8.9 Hz), 7.89 (s, 1H), 7.80 (d, 1H, J = 2.0 Hz), 7.69 (d, 2H, J = 8.9 Hz), 7.66 (s, 1H), 7.56 (d, 1H, J = 2.0 Hz), 7.27 (dd, 1H, J = 2.0 Hz, J = 8.3 Hz), 7.20 (dd, 1H, J = 2.0 Hz, J = 8.3 Hz), 7.12 (d, 2H, J = 8.9 Hz), 7.05 (d, 2H, J = 8.9 Hz), 6.89 (d, 1H, J = 8.3 Hz), 6.81 (d, 1H, J = 8.3 Hz), 4.16-4.13 (m, 4H), 2.66-2.63 (m, 4H), 2.22 (d, 12H). **^{13}C-NMR** (DMSO-d_6, 125 MHz): δ [ppm] = 168.6, 167.1, 160.9, 160.2, 141.4, 138.8, 137.9, 134.8, 131.6, 129.2, 127.5, 127.3, 126.8, 126.1, 125.3, 125.2 124.9, 124.7, 122.9, 122.8, 121.4, 119.3, 114.8, 114.3, 111.4, 110.5, 66.1, 66.0, 57.6, 57.6, 45.5. **MS** (EI, 70 eV): m/z = 342 [M^+].

5-chloro-3-(4-(2-(diethylamino)ethoxy)benzyliden)indolin-2-one 16e

The resulting product is an orange solid (55%). **HPLC**: R_t = 4.28 min, 4.92 min. **^{1}H-NMR** (DMSO-d_6, 500 MHz): δ [ppm] = 10.69 (s, NH), 8.48 (d, 2H, J = 8.9 Hz,), 7.87 (s, 1H), 7.80 (d, 1H, J = 2.0 Hz), 7.68 (d, 2H, J = 8.9 Hz), 7.66 (s, 1H), 7.56 (d, 1H, J = 2.0 Hz), 7.27 (dd, 1H, J = 2.0 Hz, J = 8.3 Hz), 7.20 (dd, 1H, J = 2.0 Hz, J = 8.3 Hz), 7.11 (d, 2H, J = 8.9 Hz), 7.04 (d, 2H, J = 8.9 Hz), 6.88 (d, 1H, J = 8.3 Hz), 6.81 (d, 1H, J = 8.3 Hz), 4.13-4.10 (m, 4H), 2.80-2.78 (m, 4H), 2.57-2.53 (m, 8H), 0.99-0.96 (m, 12H). **^{13}C-NMR** (DMSO-d_6, 125 MHz): δ [ppm] = 168.5, 167.1, 160.9, 160.2, 141.4, 138.8, 137.9, 134.8, 131.6, 129.1, 127.5, 127.3, 126.7, 126.1, 125.2, 124.8, 124.7, 122.8, 122.8, 121.4, 119.2, 114.8, 114.3, 111.3, 110.5, 66.7, 66.6, 51.2, 47.0, 46.9, 11.9, 11.9. **MS** (EI, 70 eV): m/z = 370 [M^+].

3-(4-(2-(diethylamino)ethoxy)benzylidene)indolin-2-one 16f

The resulting product is a yellow oil (95%). **HPLC**: R_t = 3.00 min, 4.17 min. **^{1}H-NMR** ($CDCl_3$, 500 MHz): δ [ppm] = 8.94 (s, 1H), 8.62 (s, 1H), 8.37 (d, 1H, J = 8.8 Hz), 7.79 (s, 1H), 7.75 (d, 2H, J = 7.7 Hz), 7.67 (m, 2H), 7.49 (m, 1H), 7.29 (s, 1H), 7.22 (m, 2H), 7.00 (m, 2H), 6.91 (m, 5H), 6.62 (d, 1H, J = 16.2 Hz), 4.20 (t, 2H, J = 6.0 Hz), 4.15 (t, 2H, J = 6.1 Hz), 2.98 (m, 4H), 2.74 (m, 8H), 1.14 (m, 12H). **^{13}C-NMR** ($CDCl_3$, 125 MHz): δ [ppm] = 170.6, 168.2, 160.8, 160.1, 143.3, 141.5, 139.4, 137.6, 134.5, 131.5, 130.0, 129.4, 128.2, 127.3,

127.1, 127.1, 125.8, 125.8, 125.0, 123.8, 122.7, 122.0, 121.6, 121.6, 118.8, 115.0, 114.7, 114.4, 110.2, 109.5, 66.5, 66.4, 47.8, 11.5. **MS** (EI, 70 eV): *m/z* = 336 [M^{+}].

5-chloro-3-(4-(3-(diethylamino)propoxy)benzylidene)indolin-2-one 16g

The resulting product is a yellow oil (80%). **HPLC**: R_t = 4.65 min, 5.41 min. **^{1}H-NMR** (DMSO-d_6, 500 MHz): δ [ppm] = 10.71 (s, 1H), 10.70 (s, 1H), 8.50 (d, 1H, *J* = 9.0 Hz), 7.89 (s, 1H), 7.87 (d, 1H, *J* = 8.8 Hz), 7.81 (d, 1H, *J* = 2.8 Hz), 7.71 (d, 2H, *J* = 8.6 Hz), 7.67 (s, 1H), 7.56 (d, 1H, *J* = 2.0 Hz), 7.28 (dd, 1H, *J* = 2.1 Hz, *J* = 8.3 Hz), 7.21 (dd, 1H, *J* = 2.1 Hz, *J* = 8.2 Hz), 7.13 (m, 2H), 7.06 (d, 2H, *J* = 9.0 Hz), 6.91 (d, 1H, *J* = 8.3 Hz), 6.83 (d, 1H, *J* = 8.2 Hz), 4.14 (m, 4H), 2.84 (m, 12H), 1.96 (m, 4H), 1.07 (m, 12H). **^{13}C-NMR** (DMSO-d_6, 125 MHz): δ [ppm] = 169.0, 167.6, 161.3, 160.6, 141.9, 139.3, 138.4, 135.3, 132.1, 129.6, 128.0, 127.8, 127.3, 126.7, 125.8, 125.3, 125.3, 123.4, 123.3, 121.9, 119.7, 115.3, 114.8, 111.9, 111.0, 66.1, 48.8, 46.9, 25.6, 10.9. **MS** (EI, 70 eV): *m/z* = 384 [M^{+}].

5-chloro-3-(4-(4-(diethylamino)butoxy)benzylidene)indolin-2-one 16h

The resulting product is a yellow oil (64%). **HPLC**: R_t = 5.05 min, 5.73 min. **^{1}H-NMR** (DMSO-d_6, 500 MHz): δ [ppm] = 10.72 (d, 2H, *J* = 5.5 Hz), 8.50 (d, 2H, *J* = 8.6 Hz), 7.89 (s, 1H), 7.82 (s, 1H), 7.71 (d, 2H, *J* = 8.4 Hz), 7.67 (s, 1H), 7.57 (s, 1H), 7.28 (d, 2H, *J* = 8.3 Hz), 7.21 (d, 1H, *J* = 7.9 Hz), 7.13 (d, 2H, *J* = 8.4 Hz), 7.06 (d, 1H, *J* = 8.5 Hz), 6.90 (d, 1H, *J* = 8.3 Hz), 6.83 (d, 1H, *J* = 8.2 Hz), 4.12 (s, 4H), 2.77 (s, 12H), 1.79 (d, 4H, *J* = 5.7 Hz), 1.68 (s, 4H), 1.08 (s, 12H). **^{13}C-NMR** (DMSO-d_6, 125 MHz): δ [ppm] = 169.0, 167.6, 161.4, 160.7, 141.9, 139.3, 138.4, 135.3, 132.1, 129.6, 128.0, 127.8, 127.2, 126.6, 125.7, 125.3, 125.2, 123.3, 121.9, 119.7, 115.3, 114.8, 111.9, 111.0, 67.9, 51.6, 46.7, 40.8, 40.6, 40.3, 40.0, 39.7, 39.4, 39.2, 26.6, 22.2, 10.6. **MS** (EI, 70 eV): *m/z* = 398 [M^{+}].

4-(4-((5-chloro-2-oxoindolin-3-yliden)methyl)phenoxy)butannitrile 16i

The resulting product is a yellow solid (90%). **HPLC**: R_t = 6.99 min, 7.48 min. **^{1}H-NMR** (DMSO-d_6, 500 MHz): δ [ppm] = 10.69 (s, 2H), 8.49 (d, 2H, *J* = 8.9 Hz), 7.89 (s, 1H), 7.80 (d, 1H, *J* = 2.0 Hz), 7.70 (d, 2H, *J* = 8.9 Hz), 7.66 (s, 1H), 7.56 (d, 1H, *J* = 2.0 Hz), 7.26 (dd, 1H, *J* = 2.0 Hz, *J* = 8.3 Hz), 7.20 (dd, 1H, *J* = 2.0 Hz, *J* = 8.3 Hz), 7.13 (d, 2H, *J* = 8.9 Hz), 7.06 (d, 2H, *J* = 8.9 Hz), 6.89 (d, 1H, *J* = 8.3 Hz), 6.81 (d, 1H, *J* = 8.3 Hz), 4.14 (t, 4H, *J* = 5.9 Hz), 2.73 (m, 4H), 2.50 (m, 4H). **^{13}C-NMR** (DMSO-d_6, 125 MHz): δ [ppm] = 168.6, 167.1, 160.6, 159.9, 141.4, 138.9, 138.7, 137.8, 134.8, 131.6, 129.2, 127.6, 127.3, 127.0, 126.4, 125.3, 124.9, 123.0, 122.8, 121.4, 120.2, 119.3, 114.8, 114.3, 111.4, 110.5, 66.1, 24.6, 13.4. **MS** (EI, 70 eV): *m/z* = 338 [M^{+}].

5-chloro-3-(4-(2-morpholinoethoxy)benzyliden)indolin-2-one 16j

The resulting product is a yellow solid (84%). **HPLC**: R_t = 3.35 min, 4.65 min. **^{1}H-NMR** (DMSO-d_6, 500 MHz): δ [ppm] = 10.69 (s, 2H), 8.48 (d, 2H, *J* = 8.9 Hz), 7.88 (s, 1H), 7.80 (d, 1H, *J* = 2.0 Hz), 7.69 (d, 2H, *J* = 8.9 Hz), 7.66 (s, 1H), 7.56 (d, 1H, *J* = 2.0 Hz), 7.27 (dd, 1H, *J* = 2.0 Hz, *J* = 8.3 Hz), 7.20 (dd, 1H, *J* = 2.0 Hz, *J* = 8.3 Hz), 7.13 (d, 2H, *J* = 8.9 Hz), 7.06 (d, 2H, *J* = 8.9 Hz), 6.89 (d, 1H, *J* = 8.3 Hz), 6.81 (d, 1H, *J* = 8.3 Hz), 4.21-4.18 (m, 4H), 3.59 (m, 8H), 2.72 (m, 4H), 2.50 (m, 8H). **^{13}C-NMR** (DMSO-d_6, 125 MHz): δ [ppm] = 168.6, 167.1, 160.8, 160.0, 141.4, 138.8, 137.9, 134.8, 131.6, 129.2, 127.5, 127.3, 126.8, 125.3, 124.9, 122.9, 122.8, 121.4, 119.3, 114.9, 114.4, 111.3, 110.5, 66.2, 65.5, 56.9, 53.9. **MS** (EI, 70 eV): *m/z* = 384 [M^-].

5-chloro-3-(3,5-dibromo-4-hydroxybenzylidene)indolin-2-one 16k[12]

The resulting product is an orange solid (97%). **HPLC**: R_t = 6.98 min, 7.65 min. **^{1}H-NMR** (DMSO-d_6, 500 MHz): δ [ppm] = 10.50 (d, 2H), 8.75 (s, 2H), 8.49 (s, 2H), 7.84 (s, 1H), 7.59 (s, 1H), 7.60 (m, 2H), 7.20 (dd, 1H, *J* = 2.0 Hz, *J* = 8.3 Hz), 7.05 (dd, 1H, *J* = 2.0 Hz, *J* = 8.3 Hz), 6.85 (d, 1H, *J* = 8.3 Hz), 6.76 (d, 1H, *J* = 8.3 Hz). **^{13}C-NMR** (DMSO-d_6, 125 MHz): δ [ppm] = 168.9, 167.4, 159.1, 155.3, 138.2, 137.4, 134.2, 128.6 125.1, 124.7, 120.6, 117.6, 114.1, 110.9, 109.9. **MS** (EI, 70 eV): *m/z* = 429 [M^-].

5-chloro-3-(4-(2-(dimethylamino)ethoxy)-3-methoxybenzyliden)indolin-2-one 16l

The resulting product is a dark yellow solid (31%). **HPLC**: R_t = 3.40 min, 4.53 min. **^{1}H-NMR** (DMSO-d_6, 500 MHz): δ [ppm] = 10.67 (s, NH), 8.66 (d, 1H, *J* = 2.1 Hz), 7.87-7.85 (m, 2H), 7.80 (d, 1H, *J* = 2.1 Hz), 7.69 (d, 1H, *J* = 2.1 Hz), 7.65 (s, 1H), 7.35 (d,1H, *J* = 1.9 Hz), 7.32-7.31 (m, 1H), 7.28 (dd, 1H, *J* = 2.1 Hz, *J* = 8.3 Hz), 7.20 (dd, 1H, *J* = 2.1 Hz, *J* = 8.3 Hz), 7.16 (d, 1H, *J* = 8.5 Hz), 7.10 (d, 1H, *J* = 8.5 Hz), 6.89 (d, 1H, *J* = 8.3 Hz), 6.83 (d, 1H, *J* = 8.3 Hz), 4.14 (t, 4H, *J* = 5.9 Hz), 3.83 (s, 3H), 3.81 (s, 3H), 2.65 (m, 4H), 2.23 (s, 6H), 2.22 (s, 6H). **^{13}C-NMR** (DMSO-d_6, 125 MHz): δ [ppm] = 168.6, 167.2, 150.8, 150.0, 148.7, 148.1, 141.4, 139.4, 138.8, 138.2, 129.0, 127.9, 127.4, 127.1, 126.3, 125.3, 124.8, 124.6, 123.6, 122.9, 122.7, 121.7, 119.2, 115.4, 113.1, 112.8, 112.1, 111.4, 110.5, 66.7, 66.6, 67.6, 55.6, 55.4, 45.6. **MS** (EI, 70 eV): *m/z* = 271 [M^+].

5-chloro-3-(4-(2-(diethylamino)ethoxy)-3-methoxybenzyliden)indolin-2-one 16m

The resulting product is a dark yellow solid (42%). **HPLC**: R_t = 4.32 min, 5.07 min. **^{1}H-NMR** (DMSO-d_6, 500 MHz): δ [ppm] = 10.67 (s, NH), 8.66 (d, 1H, *J* = 2.0 Hz), 7.87-7.85 (m, 2H), 7.80 (d, 1H, *J* = 2.0 Hz), 7.69 (d, 1H, *J* = 2.0 Hz), 7.65 (s, 1H), 7.35 (d, 1H, *J* = 1.9 Hz), 7.32-7.31 (m, 1H), 7.28 (dd, 1H, *J* = 2.0 Hz, *J* = 8.3 Hz), 7.20 (dd, 1H, *J* = 2.0 Hz, *J* = 8.3 Hz), 7.16 (d, 1H, *J* = 8.5 Hz), 7.10 (d, 1H, *J* = 8.5 Hz), 6.89 (d, 1H,

J = 8.3 Hz), 6.83 (d, 1H, *J* = 8.3 Hz), 4.11 (m, 4H), 3.83 (s, 3H), 3.81 (s, 3H), 2.80 (m, 4H), 2.56 (m, 8H), 0.98 (m, 12H). **^{13}C-NMR** (DMSO-d_6, 125 MHz): δ [ppm] = 168.6, 167.2, 150.9, 150.0, 148.7, 148.1, 141.4, 139.4, 138.8, 138.2, 129.0, 128.0, 127.4, 127.0, 126.3, 125.3, 124.8, 124.6, 123.6, 122.9, 122.7, 121.7, 119.2, 115.4, 113.2, 112.8, 112.1, 111.4, 110.5, 67.2, 67.1, 55.6, 55.5, 51.2, 47.1, 11.9. **MS** (EI, 70 eV): *m/z* = 400 [M^+].

4-(4-((5-chloro-2-oxoindolin-3-yliden)methyl)-2-methoxyphenoxy)butannitrile 16n

The resulting product is a bright orange solid (67%). **HPLC**: R_t = 6.78 min, 7.24 min. **^{1}H-NMR** (DMSO-d_6, 500 MHz): δ [ppm] = 10.67 (s, NH), 8.67 (d, 1H, *J* = 2.0 Hz), 7.88 (s, 1H), 7.86 (dd, 1H, *J* = 2.0 Hz, *J* = 8.5 Hz), 7.80 (d, 1H, *J* = 2.1 Hz), 7.69 (d, 1H, *J* = 2.1 Hz), 7.66 (s, 1H), 7.37 (d, 1H, *J* = 1.9 Hz), 7.35-7.33 (m, 1H), 7.28 (dd, 1H, *J* = 2.1 Hz, *J* = 8.3 Hz), 7.20 (dd, 1H, *J* = 2.1 Hz, *J* = 8.3 Hz), 7.17 (d, 1H, *J* = 8.5 Hz), 7.12 (d, 1H, *J* = 8.5 Hz), 6.89 (d, 1H, *J* = 8.3 Hz), 6.83 (d, 1H, *J* = 8.3 Hz), 4.13 (t, 4H, *J* = 6.1 Hz), 3.85 (s, 3H), 3.82 (s, 3H), 2.66 (m, 4H), 2.06 (m, 4H). **^{13}C-NMR** (DMSO-d_6, 125 MHz): δ [ppm] = 168.6, 167.2, 150.4, 149.6, 148.8, 148.2, 141.5, 139.3, 138.8, 138.0, 129.1, 127.8, 127.5, 127.4, 126.8, 125.3, 124.8, 123.5, 123.0, 122.8, 121.7, 120.1, 119.2, 115.5, 113.2, 112.5, 111.4, 110.5, 66.7, 66.5, 55.6, 55.5, 24.7, 24.7. **MS** (EI, 70 eV): *m/z* = 368 [M^+].

5-chloro-3-(4-(2-(dimethylamino)ethoxy)-2-methoxybenzyliden)indolin-2-one 16o

The resulting product is a yellow solid (71%). **HPLC**: R_t = 3.58 min, 4.80 min. **^{1}H-NMR** (DMSO-d_6, 500 MHz): δ [ppm] = 10.65 (d, NH), 8.82 (d, 1H, *J* = 8.7 Hz), 7.96 (s, 1H), 7.69 (s, 1H), 7.64-7.62 (m, 2H), 7.43 (d, 1H, *J* = 2.1 Hz), 7.24 (dd, 1H, *J* = 2.1 Hz, *J* = 8.3 Hz), 7.18 (dd, 1H, *J* = 2.1 Hz, *J* = 8.3 Hz), 6.87 (d, 1H, *J* = 8.3 H), 6.80 (d, 1H, *J* = 8.3 H), 6.72 (m, 2H), 6.62 (m, 2H), 4.15 (m, 4H), 3.91 (s, 3H), 3.87 (s, 3H), 2.65 (t, 4H), 2.23 (s, 6H), 2.22 (s, 6H). **^{13}C-NMR** (DMSO-d_6, 125 MHz): δ [ppm] = 168.6, 167.1, 162.9, 162.4, 160.3, 159.6, 141.2, 138.8, 133.7, 133.6, 132.3, 130.8, 128.8, 127.4, 127.3, 125.3, 124.8, 124.3, 123.1, 122.2, 121.4, 118.9, 115.0, 114.9, 111.2, 110.5, 106.0, 105.6, 99.0, 98.1, 66.2, 66.1, 57.7, 56.0, 55.8, 45.6. **MS** (EI, 70 eV): *m/z* = 372 [M^+].

4-((4-((5-chloro-2-oxoindolin-3-yliden)methyl)phenoxy)methyl)benzonitrile 16p

The resulting product is a yellow solid (93%). **HPLC**: R_t = 8.17 min, 8.54 min. **^{1}H-NMR** (DMSO-d_6, 500 MHz): δ [ppm] = 10.70 (s, 2H), 8.49 (d, 2H, *J* = 8.9 Hz), 7.88 (m, 5H), 7.80 (d, 1H, *J* = 2.0 Hz), 7.71 (d, 2H, *J* = 8.9 Hz), 7.69 (s, 1H), 7.67 (d, 4H), 7.53 (d, 1H, *J* = 2.0 Hz), 7.27 (dd, 1H, *J* = 2.0 Hz, *J* = 8.3 Hz), 7.20 (m, 3H), 7.14 (d, 2H, *J* = 8.9 Hz), 6.89 (d, 1H, *J* = 8.3 Hz), 6.81 (d, 1H, *J* = 8.3 Hz), 5.33 (d, 4H, *J* = 2.9 Hz). **^{13}C-NMR** (DMSO-d_6, 125 MHz): δ [ppm] = 168.5, 167.1, 160.2, 159.5, 142.4, 141.4, 138.9, 138.6, 137.7, 134.7,

132.4, 131.6, 129.2, 128.2, 127.6, 127.3, 126.7, 125.3, 125.1, 124.9, 123.2, 122.8, 121.4, 119.3, 118.7, 115.2, 114.7, 111.4, 110.6, 110.5, 68.5, 68.4, 52.1. **MS** (EI, 70 eV): *m/z* = 386 [M^+].

Methyl 4-((4-((5-chloro-2-oxoindolin-3-yliden)methyl)phenoxy)methyl)-benzoate 16q

The resulting product is a yellow solid (70%). **HPLC**: R_t = 8.31 min, 8.66 min. **^{1}H-NMR** (DMSO-d_6, 500 MHz): δ [ppm] = 10.70 (s, 2H), 8.49 (d, 2H, *J* = 8.9 Hz), 8.00 (m, 4H), 7.89 (s, 1H), 7.80 (d, 1H, *J* = 2.0 Hz), 7.70 (d, 2H, *J* = 8.9 Hz), 7.66 (s, 1H), 7.62 (m, 4H), 7.53 (d, 1H, *J* = 2.0 Hz), 7.27 (dd, 1H, *J* = 2.0 Hz, *J* = 8.3 Hz), 7.20 (m, 3H), 7.14 (d, 2H, *J* = 8.9 Hz), 6.89 (d, 1H, *J* = 8.3 Hz), 6.81 (d, 1H, *J* = 8.3 Hz), 5.13 (d, 4H, *J* = 3.0 Hz), 3.86 (s, 6H). **^{13}C-NMR** (DMSO-d_6, 125 MHz): δ [ppm] = 168.5, 167.1, 166.0, 160.4, 159.7, 142.2, 141.4, 138.9, 138.6, 137.8, 134.7, 131.9, 131.6, 129.3, 129.2, 129.1, 127.6, 127.3, 127.2, 126.6, 125.3, 125.0, 124.9, 123.1, 122.8, 121.4, 119.3, 115.2, 114.7, 111.4, 110.5, 68.8, 68.7, 52.1. **MS** (EI, 70 eV): *m/z* = 419 [M^-].

3-((4-((5-chloro-2-oxoindolin-3-yliden)methyl)phenoxy)methyl)benzonitrile 16r

The resulting product is a yellow solid (90%). **HPLC**: R_t = 8.12 min, 8.53 min. **^{1}H-NMR** (DMSO-d_6, 500 MHz): δ [ppm] = 10.70 (s, 2H), 8.50 (d, 2H, *J* = 8.9 Hz), 7.96 (d, 2H), 7.89 (s, 1H), 7.85-7.81 (m, 5H), 7.72 (d, 2H, *J* = 8.9 Hz), 7.67 (s, 1H), 7.63 (m, 2H), 7.54 (d, 1H, *J* = 2.0 Hz), 7.27 (dd, 1H, *J* = 2.0 Hz, *J* = 8.3 Hz), 7.21 (m, 3H), 7.15 (d, 2H, *J* = 8.9 Hz), 6.89 (d, 1H, *J* = 8.3 Hz), 6.81 (d, 1H, *J* = 8.3 Hz), 5.28 (d, 4H, *J* = 3.0 Hz). **^{13}C-NMR** (DMSO-d_6, 125 MHz): δ [ppm] = 168.5, 167.1, 160.2, 159.6, 141.4, 138.9, 138.6, 138.4, 137.8, 134.7, 132.6, 132.5, 131.8, 131.6, 131.2, 129.8, 129.2, 127.6, 127.2, 126.7, 125.3, 125.0, 124.9, 123.2, 122.8, 121.4, 119.3, 118.6, 115.2, 114.7, 111.5, 111.4, 110.5, 68.3, 68.2. **MS** (EI, 70 eV): *m/z* = 386 [M^+].

5-chloro-3-(4-(4-methyl-1H-imidazol-1-yl)phenoxy)benzylidene)indolin-2-one 16s

The resulting product is a yellow solid (41%). **HPLC**: R_t = 5.53 min, 6.15 min. **^{1}H-NMR** (DMSO-d_6, 500 MHz): δ [ppm] = 10.76 (s, 2H), 8.11 (dd, 2H, *J* = 1.3 Hz, *J* = 6.8 Hz), 7.92 (m, 1H), 7.84 (m, 1H), 7.75 (m, 1H), 7.66 (m, 4H), 7.50 (m, 2H), 7.41 (m, 2H), 7.24 (m, 10H), 7.16 (m, 2H), 7.08 (m, 2H), 6.89 (m, 2H), 6.81 (m, 1H), 2.16 (s, 6H). **^{13}C-NMR** (DMSO-d_6, 125 MHz): δ [ppm] = 172.4, 168.87, 167.47, 159.55, 158.97, 154.17, 154.10, 142.0, 139.6, 138.8, 138.5, 137.6, 135.2, 133.9, 132.2, 129.9, 129.6, 129.3, 127.9, 127.7, 127.5, 126.4, 125.9, 125.4, 124.8, 123.0, 122.4, 122.4, 121.9, 121.9, 120.6, 118.4, 117.8, 114.8, 111.9, 111.09, 14.52, 14.04. **MS** (EI, 70 eV): *m/z* = 427 [M^-].

3-(4-(4-(dimethylamino)phenyl)diazenyl)benzylidene)indolin-2-one 16t

The resulting product is a red solid (9%). **^{1}H-NMR** (DMSO-d_6, 500 MHz): δ [ppm] = 10.65 (s, 1H), 7.86 (m, 6H), 7.66 (m, 2H), 7.22 (m, 2H), 6.87 (m, 5H), 3.09 (s, 6H). **^{13}C-NMR** (DMSO-d_6, 125 MHz): δ [ppm] = 168.6, 152.8, 143.0, 142.7, 135.4, 134.9, 130.6, 130.3, 127.9, 125.0, 122.56, 122.0, 121.2, 120.9, 120.8, 111.6, 110.2, 29.8. **MS** (EI, 70 eV): *m/z* = 368 [M^+].

5-chloro-3-(3-methoxy-4-(methylsulfonyl)benzylidene)indolin-2-one 16u

The resulting product is an orange solid (85%). **HPLC**: R_t = 4.75 min, 6.48 min. **^{1}H-NMR** (DMSO-d_6, 500 MHz): δ [ppm] = 10.81 (s, 2H), 8.59 (s, 1H), 8.01 (s, 1H), 7.94 (d, 1H, *J* = 8.0 Hz), 7.88 (m, 3H), 7.72 (s, 1H), 7.63 (s, 1H), 7.50 (d, 1H, *J* = 8.0 Hz), 7.46 (d, 1H, *J* = 2.1 Hz), 7.33 (dd, 1H, *J* = 2.1 Hz, *J* = 8.3 Hz), 7.29 (dd, 1H, *J* = 2.1, *J* = 8.3 Hz), 6.91 (d, 1H, *J* = 8.3 Hz), 6.86 (d, 1H, *J* = 8.3 Hz), 4.02 (s, 3H), 3.32 (s, 3H), 3.31 (s, 3H). **^{13}C-NMR** (DMSO-d_6, 125 MHz): δ [ppm] = 168.4, 167.0, 157.3, 156.7, 142.6, 141.7, 140.7, 140.4, 136.9, 135.9, 130.8, 129.7, 129.6, 129.5, 129.12, 129.1, 128.6, 126.7, 126.1, 125.5, 124.6, 122.9, 122.4, 121.5, 120.9, 116.0, 114.4, 112.1, 111.5, 56.6, 56.3. **MS** (EI, 70 eV): *m/z* = 363 [M^+].

5-chlor-3-(3-methoxy-4-(4-methyl-1H-imidazol-1-yl)benzylidene)indoline 16v

The resulting product is an orange solid (55%). **HPLC**: R_t = 4.10 min, 4.89 min. **^{1}H-NMR** (DMSO-d_6, 500 MHz): δ [ppm] = 10.78 (s, 2H), 8.70 (d, 1H, *J* = 1.7 Hz), 7.99 (s, 1H), 7.96 (d, 1H, *J* = 8.5 Hz), 7.92 (d, 1H, *J* = 1.3 Hz), 7.91 (d, 1H, *J* = 1.3 Hz), 7.86 (d, 1H, *J* = 2.1 Hz), 7.73 (s, 1H), 7.63 (d, 1H, *J* = 2.1 Hz), 7.61 (d, 1H, *J* = 1.5 Hz), 7.57 (d, 1H, *J* = 8.1 Hz), 7.51 (d, 1H, *J* = 8.2 Hz), 7.43 (d, 1H, *J* = 10.4 Hz), 7.32 (dd, 1H, *J* = 2.1 Hz, *J* = 8.3 Hz), 7.26 (m, 3H), 6.92 (d, 1H, *J* = 8.3 Hz), 6.86 (d, 1H, *J* = 8.3 Hz), 3.92 (s, 3H), 3.90 (s, 3H), 2.17 (s, 6H). **^{13}C-NMR** (DMSO-d_6, 125 MHz): δ [ppm] = 170.0, 168.7, 152.6, 154.4, 141.1, 143.6, 139.5, 138.7, 138.6, 138.5, 138.4, 135.6, 135.4, 131.5, 130.2, 129.2, 129.0, 128.7, 128.5, 127.8, 127.7, 127.3, 126.8, 126.7, 125.8, 123.9, 124.1, 121.6, 118.2, 118.0, 117.9, 115.7, 113.3, 112.6, 57.9, 57.7, 50.3, 15.3. **MS** (ESI, 70 eV): *m/z* = 366 [M^+].

5-chloro-3-((9-methyl-9H-carbazol-3-yl)methylene)indolin-2-one 16w

The resulting product is a yellow solid (17%). **HPLC**: R_t = 8.61 min, 8.90 min. **^{1}H-NMR** (DMSO-d_6, 500 MHz): δ [ppm] = 10.70 (s, 1H), 8.12 (d, 1H, *J* = 7.8 Hz), 7.79 (m, 5H), 7.54 (m, 1H), 7.25 (m, 2H), 6.88 (m, 1H), 3.95 (s, 3H). **^{13}C-NMR** (DMSO-d_6, 125 MHz): δ [ppm] = 138.7, 167.3, 142.2, 141.6, 141.3, 140.6, 139.7, 138.6, 131.1, 128.8, 127.7, 127.4, 127.1, 127.5, 126.3, 125.7, 125.2, 124.8, 124.3, 124.0, 123.1, 122.8, 122.2, 121.9, 121.8, 121.0, 120.4, 119.9, 119.7, 118.9, 111.2, 110.4, 109.9, 109.8, 109.5, 29.2. **MS** (EI, 70 eV): *m/z* = 358 [M^+].

3-((9-methyl-9H-carbazol-3-yl)methylene)indolin-2-one 16x[13]

The resulting product is a yellow solid (15%). **HPLC**: R_t = 8.13 min, 8.32 min. **^{1}H-NMR** (DMSO-d_6, 500 MHz): δ [ppm] = 10.51 (s, 1H), 8.51 (m, 1H), 8.16 (d, 1H, *J* = 7.7 Hz), 7.80 (s, 1H), 7.67 (m, 4H), 7.48 (m, 1H), 7.18 (m, 3H), 6.82 (m, 2H), 3.88 (s, 3H). **^{13}C-NMR** (DMSO-d_6, 125 MHz): δ [ppm] = 169.4, 142.9, 141.7, 141.6, 138.1, 131.2, 129.8, 127.7, 126.7, 125.4, 122.9, 122.6, 122.2, 121.9, 121.8, 121.4, 120.9, 119.9, 110.4, 109.9, 29.5. **MS** (EI, 70 eV): *m/z* = 324 [M^-].

10. Synthesis of 3-(4-(2-(diethylamino)ethoxy)benzyl)indolin-2-one 16y

The chlorooxindolinone **16e** (1.00 eq.) was dissolved in EtOH. The resulting solution was fumigated with H_2 and stirred over night under normal pressure. Afterwards, the reaction solution was filtert through Celite®. The solvent was removed in vacuo. The resulting product is a colorless oil (77%). **HPLC**: R_t = 0.75 min. **^{1}H-NMR** ($CDCl_3$, 500 MHz): δ [ppm] = 8.21 (s, 1H), 7.18 (t, 1H, *J* = 7.6 Hz), 7.06 (d, 2H, *J* = 8.5 Hz), 6.97 (t, 1H, *J* = 7.4 Hz), 6.90 (d, 1H, *J* = 7.4 Hz), 6.85 (d, 1H, *J* = 7.7 Hz), 6.73 (d, 2H, *J* = 8.5 Hz), 4.45 (m, 2H), 3.71 (dd, 1H, *J* = 4.6 Hz, *J* = 8.2 Hz), 3.45 (m, 2H), 3.38 (dd, 1H, *J* = 4.5 Hz, *J* = 13.9 Hz), 3.27 (m, 4H), 3.02 (dd, 1H, *J* = 8.2 Hz, *J* = 13.8 Hz), 1.46 (m, 6H). **^{13}C-NMR** ($CDCl_3$, 125 MHz): δ [ppm] = 178.8, 155.9, 141.4, 131.0, 130.7, 128.7, 128.0, 124.7, 122.1, 144.2, 109.7, 62.6, 50.6, 47.5, 47.2 , 47.1, 35.5, 8.6, 8.6. **MS** (EI, 70 eV): *m/z* = 338 [M^+].

11. Synthesis of 3-(4-(3-(1*H*-tetrazol-5-yl)propoxy)benzyliden)-5-chloroindolin-2-one 16z

4-(4-((5-chloro-2-oxoindolin-3-ylidene)methyl)phenoxy)butannitrile **16i** (20 mg, 0.06 mmol), sodium azide (46 mg, 0.71 mmol) und ammonium chloride (38 mg, 0.71 mmol) were added to dimethylformamide (0.7 mL) and stirred for 2 h at 100°C under microwave irradiation. After cooling to room temperature the reaction solution was added to water, acidified with 2N HCl and extracted three times with ethyl acetate. The combined organic layers were dried over sodium sulphate, filtered and the solvent was removed in vacuo. The resulting residue was purified by column chromatography on silica gel to provide the desired product in 62% as brown solid. **HPLC**: R_t = 6.61 min. **^{1}H-NMR** (DMSO-d_6, 500 MHz): δ [ppm] = 12.10 (s, NH), 10.13 (s, NH), 7.95 (s, 1H), 7.28 (d, 1H, *J* = 8.6 Hz), 7.24 (d, 2H, *J* = 8.8 Hz), 7.20 (dd, 1H, *J* = 2.3 Hz, *J* = 8.6 Hz), 7.15 (d, 2H, *J* = 8.8 Hz), 6.77 (d, 1H, *J* = 2.3 Hz) 4.13 (t, 2H, *J* = 6.0 Hz), 2.70 (t, 2H, *J* = 7.1 Hz), 2.08 (m, 2H). **^{13}C-NMR** (DMSO-d_6, 125 MHz): δ [ppm] = 162.3, 157.9, 157.5, 135.4, 131.0, 130.6, 126.4, 126.0, 124.1, 123.6, 121.5, 120.3, 116.7, 115.5, 65.8, 30.8, 24.8. **MS** (EI, 70 eV): *m/z* = 353 (M^+).

III. FTL-3 *in vitro* assay conducted by Cerep

1. Reference compound Data

Assay: FLT-3 Kinase *(h)*

Reference compound: Staurosporine

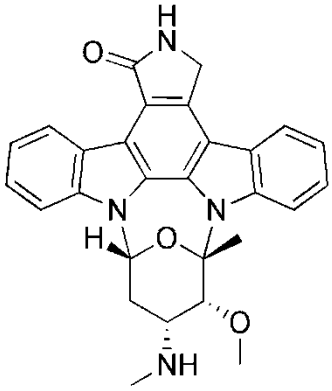

IC_{50} (M) = 9.1E-10

nH = 1.7

2. Experimental conditions

Assay: FLT-3 Kinase *(h)*

Source: human recombinant (insect cells)

Substrate: ATP + Ulight-CAGAGAIETDKEYYTVKD (100 nM)

Incubation: 90 min, RT

Measured Component: Phospho-Ulight- CAGAGAIETDKEYYTVKD

Detection Method: LANCE

3. Analysis and expression of results

The resulted technical replicates are expressed as a percent of control specific activity ((measured specific activity/control specific activity) x 100) obtained in the presence of the compounds.

The IC_{50} value (concentration causing a half-maximal inhibition of control specific activity) and Hill coefficient(s) (nH) were determined by non-linear regression analysis of the inhibition curve generated with mean replicate values using Hill equation curve fitting (Y D + $[(A-D)/(1-(IC_{50})^{nII})]$, where Y = specific activity, D = minimum specific, A = maximum specific activity, C = compound concentration, $C_{50} = IC_{50}$, and nH = slope factor).

This analysis was performed using software developed at Cerep (Hill software) and validated by comparison with data generated by the commercial software SigmaPlot® 4.0 for Windows® (1997 by SPSS inc.).

IV. Selectivity screening of compound 16e conducted by Cerep

The ExpresS Diversity kinase profile is a fast turnaround profile conducted by Cerep. Percentage kinase activities of compound **16e** at 1 μM in panels of human protein kinases determined by Cerep. Measurements were performed in duplicate and the average was taken.

Kinase	% of Control Values[1]	Kinase	% of Control Values[1]
Abl kinase *(h)*	95,4	JAK3 *(h)*	67,3
Akt1/PKBα *(h)*	101,1	JNK1 *(h)*	96,4
AurA/Aur2 kinase *(h)*	99,6	KDR kinase *(h)* (VEGFR2)	88,4
CaMK2α *(h)*	103,4	Lck kinase *(h)*	103,8
CDC2/CDK1 *(h)* (cycB)	105,5	MAPKAPK2 *(h)*	95,3
CDK2 *(h)* (cycA)	93,5	MARK1 *(h)*	99,6
CHK1 *(h)*	95,8	MKK6 *(h)*	100,7
CHK2 *(h)*	94,0	MNK2 *(h)*	107,4
CK1α *(h)*	102,6	MST4 kinase *(h)*	103,7
c-Met kinase *(h)*	97,2	NEK2 *(h)*	106,9
EGFR kinase *(h)*	102,1	p38α kinase *(h)*	99,4
EphA2 kinase *(h)*	101,2	PAK2 *(h)*	103,7
EphA3 kinase *(h)*	101,3	PAK4 *(h)*	101,2
EphB4 kinase *(h)*	101,8	PDK1 *(h)*	106,9
ERK_2 *(h)* ($P42^{mapk}$)	100,6	Pim2 kinase *(h)*	94,7
FGFR1 kinase *(h)*	98,2	PKA *(h)*	98,7
FGFR2 kinase *(h)*	100,1	PKCβ2 *(h)*	99,4
FGFR3 kinase *(h)*	92,9	PLK1 *(h)*	100,5
FLT-3 kinase *(h)*	14,7	RAF-1 kinase *(h)*	108,6
GSK3α *(h)*	103,7	ROCK1 (h)	102,4
GSK3β *(h)*	97,0	SGK1 *(h)*	96,0
HGK *(h)* MAP4K4	27,8	SIK *(h)*	118,9
IKKα *(h)*	103,6	Src kinase *(h)*	100,8
IRAK4 *(h)*	91,8	TAOK2 (TAO1) *(h)*	95,1
IRK *(h)* (InsR)	112,9	TRKA *(h)*	87,0

[1] The results are expressed as a percent of control specific activity ((measured specific activity/control specific activity) x 100) obtained in the presence of the compounds (control = staurosporine).

Assay Kinase	Source	Substrate/Stimulus/Tracer	Incubation	Measured Component
Abl kinase *(h)*	human recombinant (insect cells)	ATP + Ulight-TK peptide (100 nM)	60 min RT	phospho-Ulight-TK-peptide
Akt1/PKBα *(h)*	human recombinant (insect cells)	ATP + CREBtide (CKRREILSRRPSYRK) (25 nM)	60 min RT	phospho-CREBtide (CKRREILSRRPSYRK)
AurA/Aur2 kinase *(h)*	human recombinant (Sf21 cells)	ATP + Ulight-RRRSLLE (100 nM)	15 min RT	phospho-Ulight-RRRSLLE
CaMK2α *(h)*	human recombinant	ATP + Ulight-CGSGSGRPRTSSFAEG (50 nM)	30 min RT	phospho-Ulight-CGSGSGRPRTSSFAEG
CDC2/CDK 1 (h) (cycB)	human recombinant (insect cells)	ATP + Ulight-CFFKNIVTPRTPPPSQGK-amide (100 nM)	15 min RT	phospho-Ulight-CFFKNIVTPRTPPPSQGK-amide
CDK2 *(h)* (cycA)	human recombinant	ATP + Ulight-CFFKNIVTPRTPPPSQGK-amide (50 nM)	30 min RT	phospho-Ulight-CFFKNIVTPRTPPPSQGK-amide
CHK1 *(h)*	human recombinant (insect cells)	ATP + CREBtide (CKRREILSRRPSYRK) (25 nM)	30 min RT	phospho-CREBtide (CKRREILSRRPSYRK)
CHK2 *(h)*	human recombinant (insect cells)	ATP + CREBtide (CKRREILSRRPSYRK) (25 nM)	15 min RT	phospho-CREBtide (CKRREILSRRPSYRK)
CK1α *(h)*	human recombinant	ATP + Ulight-ARTKQTARKSTGGKAPRKQLAGCG (25 nM)	60 min RT	phospho-Ulight-ARTKQTARKSTGGKAPRKQLAGCG
c-Met kinase *(h)*	human recombinant (insect cells)	ATP + Ulight-CAGAGAIETDKEYYTVKD (25 nM)	60 min RT	phospho-Ulight-CAGAGAIETDKEYYTVKD
EGFR kinase *(h)*	human recombinant (insect cells)	ATP + Ulight-CAGAGAIETDKEYYTVKD (100 nM)	15 min RT	phospho-Ulight-CAGAGAIETDKEYYTVKD
EphA2 kinase *(h)*	human recombinant	ATP + Ulight-TK peptide (50 nM)	30 min RT	phospho-Ulight-TK-peptide
EphA3 kinase *(h)*	human recombinant	ATP + Ulight-TK peptide (50 nM)	60 min RT	phospho-Ulight-TK-peptide
EphB4 kinase *(h)*	human recombinant (insect cells)	ATP + Ulight-TK peptide (100 nM)	90 min RT	phospho-Ulight-TK-peptide
ERK2 *(h)* ($P42^{mapk}$)	human recombinant (*E. coli*)	ATP + Ulight-CFFKNIVTPRTPPPSQGK-amide (100 nM)	15 min RT	phospho-Ulight-CFFKNIVTPRTPPPSQGK-amide
FGFR1 kinase *(h)*	human recombinant	ATP + Ulight-CAGAGAIETDKEYYTVKD	60 min RT	phospho-Ulight-CAGAGAIETDKEYYTV

	(insect cells)	(100 nM)		KD
FGFR2 kinase *(h)*	human recombinant	ATP + Ulight-CAGAGAIETDKEYYTVKD (25 nM)	15 min RT	phospho-Ulight-CAGAGAIETDKEYYTVKD
FGFR3 kinase *(h)*	human recombinant	ATP + Ulight-CAGAGAIETDKEYYTVKD (100 nM)	90 min RT	phospho-Ulight-CAGAGAIETDKEYYTVKD
FLT-3 kinase *(h)*	human recombinant (insect cells)	ATP + Ulight-CAGAGAIETDKEYYTVKD (100 nM)	90 min RT	phospho-Ulight-CAGAGAIETDKEYYTVKD
GSK3α *(h)*	human recombinant	ATP + Ulight-CFFKNIVTPRTPPPSQGK-amide (100 nM)	60 min RT	phospho-Ulight-CFFKNIVTPRTPPPSQGK-amide
GSK3β *(h)*	human recombinant	ATP + Ulight-CFFKNIVTPRTPPPSQGK-amide (100 nM)	90 min RT	phospho-Ulight-CFFKNIVTPRTPPPSQGK-amide
HGK *(h)* (MAP4K4)	human recombinant	ATP + Ulight-FLGFTYVAP (50 nM)	90 min RT	phospho-Ulight-FLGFTYVAP
IKKα *(h)*	human recombinant (Sf21 cells)	ATP + Ulight-IkappaB-alpha (100 nM)	30 min RT	phospho-Ulight-IkappaB-alpha
IRAK4 *(h)*	human recombinant (insect cells)	ATP + Ulight-FLGFTYVAP (50 nM)	90 min RT	phospho-Ulight-FLGFTYVAP
IRK *(h)* (InsR)	human recombinant	ATP + Ulight-Poly GAT[EAY(1:1:1)]n (50 nM)	10 min RT	phospho-Ulight-Poly GAT[EAY(1:1:1)]n
JAK3 *(h)*	human recombinant	ATP + Ulight-CAGAGAIETDKEYYTVKD (100 nM)	60 min RT	phospho-Ulight-CAGAGAIETDKEYYTVKD
JNK1 *(h)*	human recombinant (*E. coli*)	ATP + Ulight-CFFKNIVTPRTPPPSQGK-amide (100 nM)	60 min RT	phospho-Ulight-CFFKNIVTPRTPPPSQGK-amide
KDR kinase *(h)* (VEGFR2)	human recombinant (Sf9 cells)	ATP + Ulight-CAGAGAIETDKEYYTVKD (100 nM)	60 min RT	phospho-Ulight-CAGAGAIETDKEYYTVKD
Lck kinase *(h)*	human recombinant (insect cells)	ATP + Ulight-Poly GAT[EAY(1:1:1)]n (25 nM)	30 min RT	phospho-Ulight-Poly GAT[EAY(1:1:1)]n
MAPKAPK 2 *(h)*	human recombinant (*E. coli*)	ATP + CREBtide (CKRREILSRRPSYRK) (25 nM)	15 min RT	phospho-CREBtide (CKRREILSRRPSYRK)
MARK1 *(h)*	human recombinant	ATP + Ulight-RRRSLLE (50 nM)	30 min RT	phospho-Ulight-RRRSLLE
MKK6 *(h)*	human recombinant	ATP + inactive p38a (50 nM)	10 min RT	phospho-p38a
MNK2 *(h)*	human recombinant (Sf21 cells)	ATP + CREBtide (CKRREILSRRPSYRK) (25 nM)	90 min RT	phospho-CREBtide (CKRREILSRRPSYRK)
MST4	human	ATP + Ulight	30 min	Phospho-Ulight-TM-

kinase *(h)*	recombinant	TM- PKC (50 nM)	RT	PKC
NEK2 *(h)*	human recombinant (insect cells)	ATP + Ulight-FLGFTYVAP (50 nM)	60 min RT	phospho-Ulight-FLGFTYVAP
p38α kinase *(h)*	human recombinant (*E. coli*)	ATP + Ulight-CFFKNIVTPRTPPPSQGK-amide (100 nM)	60 min RT	phospho-Ulight-CFFKNIVTPRTPPPSQG Kamide
PAK2 *(h)*	human recombinant (Sf9 cells)	ATP + Ulight-RRRSLLE (50 nM)	60 min RT	phospho-Ulight-RRRSLLE
PAK4 *(h)*	human recombinant (insect cells)	ATP + Ulight-RRRSLLE (50 nM)	30 min RT	phospho-Ulight-RRRSLLE
PDK1 *(h)*	human recombinant (insect cells)	ATP + Ulight-FLGFTYVAP (400 nM)	90 min RT	phospho-Ulight-FLGFTYVAP
Pim2 kinase *(h)*	human recombinant (insect cells)	ATP + CREBtide (CKRREILSRRPSYRK) (25 nM)	60 min RT	phospho-CREBtide (CKRREILSRRPSYRK)
PKA *(h)*	human recombinant (*E. coli*)	ATP + Ulight-RRRSLLE (50 nM)	10 min RT	phospho-Ulight-RRRSLLE
PKCβ2 *(h)*	human recombinant	ATP + CREBtide (CKRREILSRRPSYRK) (25 nM)	15 min RT	phospho-CREBtide (CKRREILSRRPSYRK)
PLK1 *(h)*	human recombinant	ATP + Ulight-FLGFTYVAP (40 nM)	60 min RT	phospho-Ulight-FLGFTYVAP
RAF-1 kinase *(h)*	human recombinant	ATP + Ulight-ARTKQTARKSTGGKAPRKQL AGCG (50 nM)	180 min RT	phospho-Ulight-ARTKQTARKSTGGKA PRKQ LAGCG
ROCK1 *(h)*	human recombinant	ATP + Ulight-RRRSLLE (50 nM)	30 min RT	phospho-Ulight-RRRSLLE
SGK1 *(h)*	human recombinant	ATP + Ulight-RRRSLLE (50 nM)	30 min RT	phospho-Ulight-RRRSLLE
SIK *(h)*	human recombinant (Sf21 cells)	ATP + CREBtide (CKRREILSRRPSYRK) (25 nM)	90 min RT	phospho-CREBtide (CKRREILSRRPSYRK)
Src kinase *(h)*	human recombinant (insect cells)	ATP + Ulight-Poly GAT[EAY(1:1:1)]n (5 nM)	10 min RT	phospho-Ulight-Poly GAT[EAY(1:1:1)]n
TAOK2 (TAO1) *(h)*	human recombinant	ATP + Ulight-FLGFTYVAP (40 nM)	60 min RT	phospho-Ulight-FLGFTYVAP
TRKA *(h)*	human recombinant (insect cells)	ATP + Ulight-Poly GAT[EAY(1:1:1)]n (5 nM)	10 min RT	phospho-Ulight-Poly GAT[EAY(1:1:1)]n

V. γ-Secretase assay and cell-based toxicity assay conducted by Roche

See in the publication Ref. 17.

VI. Toxicity assay: Determination of the *in vivo* activity on wt zebrafish embryos

The wt zebrafish embryos were collected and placed into 24-well plates, ten embryos per well and maintained in E2 medium at 28°C. Compounds were added 5 hpf (50% epiboly) and the embryos allowed to grow in chemical compound solution up to 2 days. The phenotypes were compared using the Axio Scope.A1 microscope system from Carl Zeiss at 48 hpf. - **Animal husbandry.** All animal experiments were conducted and documented according to the federal and local regulation.

VII. References

1. Höttecke, N.; Liebeck, M.; Baumann, K.; Schubenel, R.; Winkler, E.; Steiner, H.; Schmidt, B. *Bioorg. Med. Chem. Lett.* **2010**, *20*, 2958.
2. Marder, S.; Perry, J.; Zhou, W.; Kuebler, S. M.; Cammack, J. K., WO 2002079691 A1, **2002**.
3. Yadav, Y.; Maclean, E. D.; Bhattacharyya, A.; Parmar, V. S.; Balzarini, J.; Barden, C. J.; Too, C. K.; Jha, A. *Eur. J. Med. Chem.* **2011**, *46*, 3858.
4. Nagarapu, L.; Aneesa; Satyender, A.; Chandana, G.; Bantu, R. *J. Heterocycl. Chem.* **2009**, *46*.
5. Strohfeldt, K.; Müller-Bunz, H.; Pampillón, C.; Sweeney, N. J.; Tacke, M. *Eur. J. Inorg. Chem.* **2006**, *2006*, 4621.
6. Fischer, C.; Munoz, B.; Zultansky, S.; Methot, J.; Zhou, H.; Brown, W. C., WO 2008/156580 A1, **2008**.
7. Ulman, A.; Urankar, E. *J. Org. Chem.* **1989**, *54*, 4691.
8. Perez-Moreno, J.; Zhao, Y.; Clays, K.; Kuzyk, M. G.; Shen, Y.; Qiu, L.; Hao, J.; Guo, K. *J. Am. Chem. Soc.* **2009**, *131*, 5084.
9. Langendoen, A.; Plug, J. P. M.; Koomen, G.-J.; Pandit, U. K. *Tetrahedron* **1989**, *45*, 1759.
10. Wood, E.; Crosby, R. M.; Dickerson, S.; Frye, S. V.; Griffin, R.; Hunter, R.; Jung, D. K.; McDonald, O. B.; McNutt, R.; Mahony, W. B.; Peel, M. R.; Ray, J.; Lackey, K. *Anti-cancer Drug Des.* **2001**, *16*, 1.
11. Jiang, T.; Kuhen, K. L.; Wolff, K.; Yin, H.; Bieza, K.; Caldwell, J.; Bursulaya, B.; Tuntland, T.; Zhang, K.; Karanewsky, D.; He, Y. *Bioorg. Med. Chem. Lett.* **2006**, *16*, 2109.
12. Angell, R.; Reynolds, K.; Lumley, J., WO 2004069998 A2, **2004**.
13. Bouerat, L. M. E.; Fensholdt, J.; Nielsen, S. F.; Liang, X.; Havez, S. E.; Andersson, E. C.; Jensen, L.; Hansen, J. R., WO 2005058309 A1, **2005**.

4.2 Computer unterstütztes Design, Synthese und biologische Evaluation von Chinoxalinbisarylharnstoffen als FLT3 Inhibitoren

Der Inhalt dieses Kapitels wird voraussichtlich im November 2014 bei der Fachzeitschrift *Bioorganic & Medicinal Chemistry Letters* zur Publikation eingereicht. Es handelt sich um eine Rohfassung.

Autoren: Stefan Göring*, Dennis Bensinger*, Eva Christine Naumann, Boris Schmidt.

Titel: „Computer-guided design, synthesis and biological evaluation of quinoxalinebisarylureas as FLT3 inhibitors".

Zusammenfassung:

Die akute myeloische Leukämie ist eine bösartige Erkrankung des blutbildenden Systems, welche durch unkontrollierte Ausbreitung von Zellen innerhalb des Knochenmarks gekennzeichnet ist. Die fünf Jahres Überlebensrate liegt für Patienten unter 60 Jahre bei nur 40 %. FLT3 ist das meist bekannte mutierte Gen in der AML und es wurde gezeigt, dass es eine entscheidende Rolle in der Entwicklung und dem Wachstum blutbildender sowie nichtblutbildender Zellen einnimmt. Zwei große Klassen aktivierender Mutationen in FLT3 sind bislang beschrieben worden. FLT3 interne Tandem-Duplikationen in der Juxtamembran-Domäne werden in rund 23 % der AML-Patienten gefunden. Mit 7 % stellen die Punktmutationen an den Aminosäureresten D835 und I836 die zweite Klasse aktivierender Mutationen dar.

Basierend auf den ersten publizierten FLT3-Chinoxalininhibitor AG1295 wurde ein Pharmakophormodell entwickelt, welches als Templat für den Zugang neuer FLT3-Inhibitoren dienen sollte. Mit Hilfe diesem wurde ein *screening* einer Substanz-Datenbank durchgeführt, welches durch weitere virtuelle *screenings* zu Chinoxalin-basierenden FLT3-Inhibitoren führte. Das computergestützte Modell wurde unter Verwendung der Software MOE erstellt. Zur Evaluation dieses Modells wurden 15 Chinoxalin-Derivate synthetisiert und anschließend biologisch getestet. Die aktivsten Verbindungen wiesen einen IC_{50}-Wert im zweistelligen nanomolarem Bereich auf. Eine Verbindung wurde außerdem in einem Zebrafisch-Toxizitäts-Assay untersucht.

Eigener Beitrag zu dieser Arbeit:

Der synthetische Beitrag lag in den Verbindungen BSc5110 (12a), BSc5162 (12c), BSc5163 (12e), BSc5164 (12f), BSc5144 (12h), BSc5145 (12g), BSc5143 (12l). In Klammer die Verbindungsnummern in der Publikation.

Computer-guided design, synthesis and biological evaluation of quinoxalinebisarylureas as FLT3 inhibitors.

Stefan Göring*, Dennis Bensinger*, Eva Naumann and Boris Schmidt†

Clemens Schöpf - Institute of Organic Chemistry and Biochemistry, Technische Universität Darmstadt, 64287 Darmstadt, Hessen, Germany.

** These authors contributed equally to this work.*

† Corresponding author: Tel.: +49 6151 163075; Fax: +49 6151 163278.

E-mail: schmidt_boris@t-online.de.

Keywords: Acute myeloid leukemia, FMS-like tyrosine kinase 3, Pharmacophore, Docking, Quinoxaline, SAR, Zebrafish

Abstract

Activating mutations of FLT3 are present in ~30% of patients with acute myeloid leukemia (AML) and associated with poor prognosis. Point mutations in the tyrosine kinase domain (TKD) are observed as primary mutations or acquired as secondary mutations in FLT3 with internal tandem duplications (FLT3-ITD) after treatment with tyrosine kinase-inhibitors (TKIs). Although dozens of potent inhibitors against FLT3-ITD are reported in literature, activating TKD point mutations especially at residues F691 and D835 remain the leading cause for clinical resistance showing the steady need of new potent inhibitors. Here we report on the discovery and characterization of novel quinoxaline based FLT3 inhibitors. The known TK family III inhibitor **AG1295** represents one of the first tyrphostins showing activitiy in AML disease models but has not been developed to clinical studies due to low inhibitory strength *in vivo*. We discuss the pharmacophore features of a diverse set of known inhibitors as starting point for a new optimization algorithm for type II TKIs starting from an *in silico* design compound library following pharmacophore search and induced-fit docking in the known FLT3 crystal structure. This lead to the design of a set of diverse quinoxalinebisarylurea compounds that have been synthesized and assayed for FLT3 kinase activity. The most promising compounds were further evaluated in a zebrafish embryo phenotype assay.

Introduction

Acute myeloid leukemia (AML) is a malignant disorder of the hematopoietic system, which is characterized by uncontrolled proliferation of cells inside the bone marrow.[1, 2] The five-year survival rate for patients under 60 years is only 40 %.[3] FMS-like tyrosine kinase 3 (FLT3) is a class III receptor tyrosine kinase including FMS, c-KIT and two genes encoding platelet-derived growth factor receptor α and β.[4] It is the most common mutated gene in AML and has been demonstrated to play a crucial role in the development and growth of hematopoietic and nonhematopoietic cells.[5] FLT3 is composed of a N-terminal extracellular ligand-binding domain with five immunoglobulin-like motifs, a transmembrane domain followed by an intracellular juxtamembrane domain and a C-terminal tyrosine kinase domain.[6] The ligand for FLT3 (FL), cloned in 1993[7] is a type I transmembrane protein and is expressed in most tissues including hematopoietic organs (spleen and bone marrow), prostate, ovary, kidney, lung, heart and placenta.[8, 9] After binding of its FL membrane bound FLT3 underlies a quick conformation change with homodimerization and exposing phosphoryl acceptor sites in the tyrosine kinase domain to activate multiple downstream signaling pathways.[8, 10]

Two classes of activating FLT3 mutations have now been identified and are present in about 30 % of AML cases. FLT3 internal tandem duplications (ITDs) occur in the juxtamembrane domain and were identified in approximately 23 % of AML patients.[11] Point mutations at residue D835 or I836 in the activation loop of FLT3 are less frequent and were found in approximately 7 % of AML cases.[3, 9, 12] It is proven that both types of mutations constitutively activate the tyrosine kinase activity.[13]

Smith and coworkers first described the appearance of drug resistant kinase mutations in FLT3-ITD positive AML patients relapsing after treatment with **Quizartinib (AC220)**.[14] They found mutations at the gatekeeper mutation (F691L) and within the activation loop (D835Y, D835V, Y842C, Y842H) conferring high degrees of *in vitro* **Quizartinib** resistance.

Because of the high frequency of drug-resistant AML, there is an intensive focus of developing potent and selective FLT-3 inhibitors.[6, 9, 10, 15-18] Quinoxalines **AG1295** and **AG1296** have been the first inhibitors developed for FLT3 exhibiting an IC_{50} value of about 1 μM (Figure 1).[19, 20] Consecutively, several small molecule FLT3 inhibitors, including **Quizartinib (AC220)**, **Sorafenib (BAY-43-9006)**, **Sunitinib (SU-11248)** and **Midostaurin (PKC412)**, have been discovered and were evaluated *in vitro* and *in vivo* and entered late-stage clinical trials (Figure 1).[10, 20-24] Especially the bisarylurea **AC220** was identified and evaluated as a uniquely potent and selective FLT3 inhibitor by Chao *et al.* in 2009.[25] Despite

high research efforts in academic and industrial groups no targeted drug has been approved for the treatment of FLT3-mutant AML.

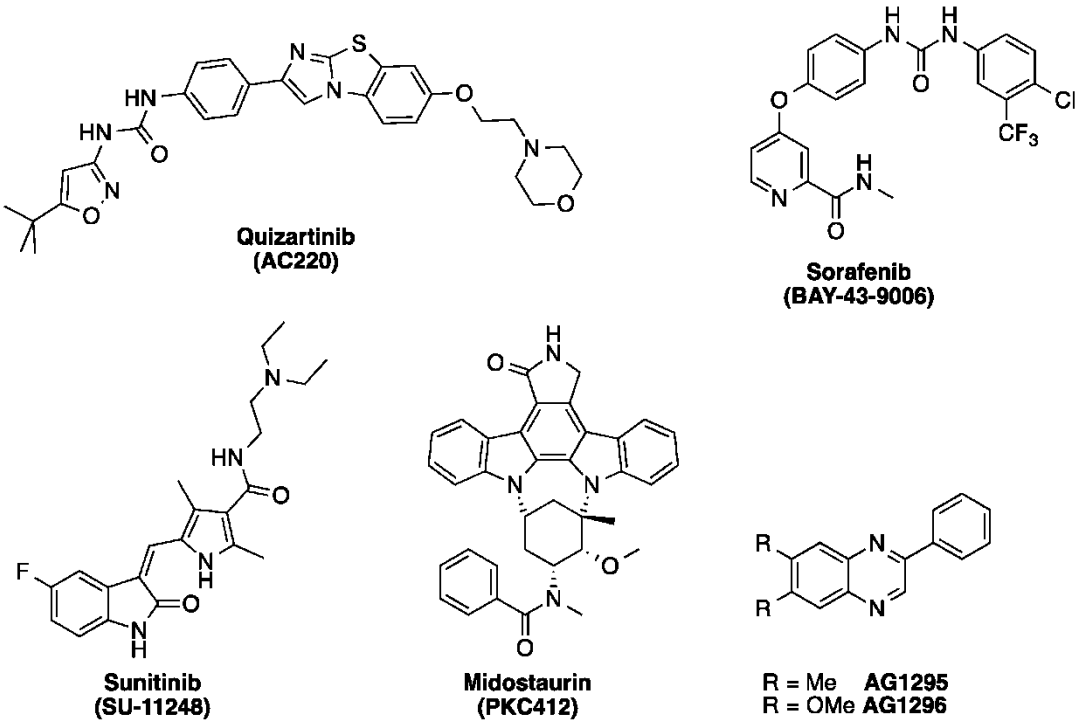

Figure 1: Selected structures of known FLT3 inhibitors.[19-24]

Optimization Strategy

The Quinoxaline scaffold can undergo alternating donor-acceptor interactions with the gatekeeper+1 / gatekeeper+3 amino acids in the hinge region as affirmed by crystallographic observations on other kinases described before (Figure 2, left). Docking of **AG1295** in the FLT3 hinge region implicates that optimal ligand geometry and distances may explain the observed high ligand efficiency due to hydrogen bonding with the hinge backbone and π-π-interactions with the gatekeeper F691 or F830 (Figure 2, right). Substitution at the 4`-phenyl position enables interactions with the DFG-motif by a linking group and occupation of the regulatory domain pocket with aromatic groups as generally observed for TKIs. Due to the ubiquitous occurrence of bisarylureas connected to a hinge binding scaffold, we were interested in a general pharmacophore model for FLT3 type II TKIs binding to a kinase in a DFG_{out}/JM_{out} conformation. This model will be subsequently used to filter a large *in silico* library of

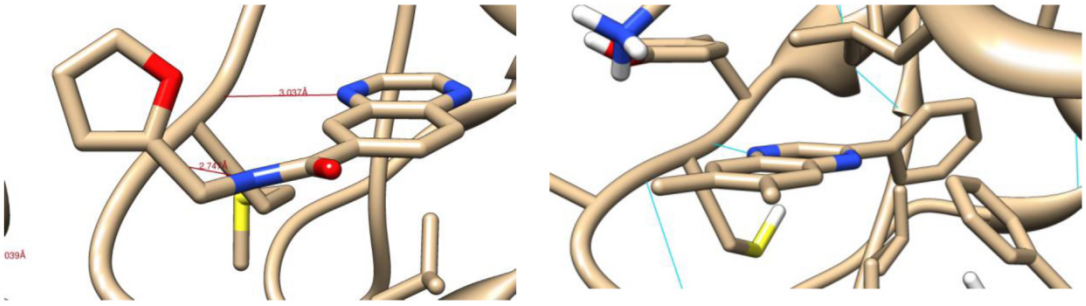

Figure 2: Structure of quinoxaline-based inhibitor in CHK2 (PDB: 4BDC, left) and result of the docking study of **AG1295** in the active site of FLT3 reveals donor-acceptor interactions with the hinge region (right).

bisarylureas created by combination of a hypothetic precursor molecules with amines from our in-house chemical database (figure 3). A ligand-based pharmacophore contains the essential interactions of a ligand with a receptor. We used the freely accessible online databaseincluding 1675 FLT3 inhibitors with corresponding *in vitro* pharmacology listed.[26] For this study eight highly potent inhibitors have been chosen whose binding mode has been solved crystallographically for other kinases or have probably type II inhibition and also contain the bisarylurea-binding motif that served as the starting point for this work (figure 4). In this database 136 molecules with an IC_{50} or K_i value of greater than 1000 nM are randomly selected, which are considered inactive for the preparation of the pharmacophore model.

425 pharmacophore hypotheses are generated, which are sorted by ascending P-value. The accuracy of active compounds (Acc_1) or inactive compounds (ACC_0) is the ratio m_1/N_1 and m_0/N_0 respectively, where N is the total number of molecules and m is the number of molecules that fit the model (actives) or do not fit in the model (inactives). For $Acc_1 = 1$ all active molecules are taken into account while with $ACC_0 = 1$ no inactive molecule fits the pharmacophore hypothesis. The statistical significance of these accuracy values is determined using the chi-square-derived P-value. This is the decadic logarithm of the probability of $\chi 2$ that the accuracy results Acc_1 and ACC_0 were achieved only by chance. Lower P-values indicate higher significance of the accuracy. The generated pharmacophores **A** to **D** contain a donor-projection, acceptor-projection, π-ring-projections and aromatic rings (Table 1). In all structures, the donor groups (NH) of the urea motif are considered as a projection, but not the carbonyl acceptor. By the pharmacophor search for a diverse set of structures the generated hypotheses can be superior to single scaffolds since the projection of π-rings covers ligand structures like a receptor would. In pharmacophor hypothesis **A** each of the connecting phenyl ring as well the various head groups are recognized, which in **B** to **D** is not the case. The

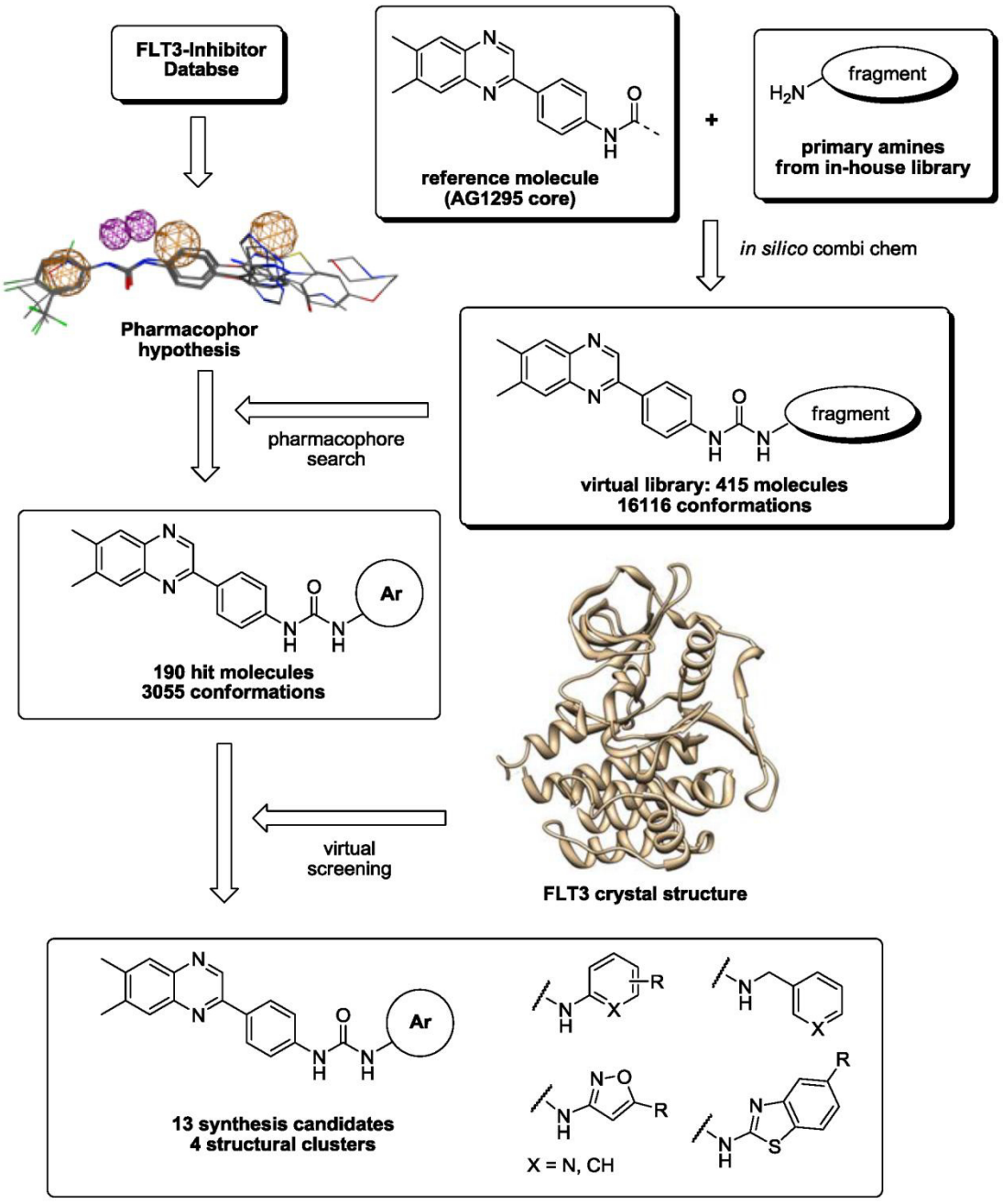

Figure 3: Flowchart for the optimization of quinoxaline-based TKI starting from **AG1295** using pharmacophore elucidation, pharmacophore search and molecular docking.

terminal phenyl ring of the bisarylurea motif is covered as an aromatic ring center (**A**) or a projection (**B** to **D**) with high superposition of all molecular scaffolds. All models show a high exclusion of nearly all inactive molecules (ACC_0 ~ 1) and include, except for the quizartinib derivative **2** the entire active set of molecules.

While the pharmacophore method allows a quick assessment of many molecules using simple parameters, information on possible interactions between ligand and receptor, and an assessment of the size of a binding pocket by docking methods are indispensable. However, only two dissolved crystal structures are available for FLT3. In 2004, Griffith *et al.* described the structure of the cytosolic kinase domain, but not in a complex with an inhibitor or ATP.[26] Due to the position of juxtamembrane domain and activation loop, these are the autophosphorylated, inactive conformation (PDB: 1RJB). The structure of the immunoglobulin-like domains in complex with the FLT3 ligand was presented 2012 by Verstraete *et al.* (PDB: 3QS7, 3QS9).[27] In the next step, hits from the pharmacophore search were rated on an induced fit docking in the kinase structure of FLT3 to assess binding geometry and potential ligand-receptor interactions.

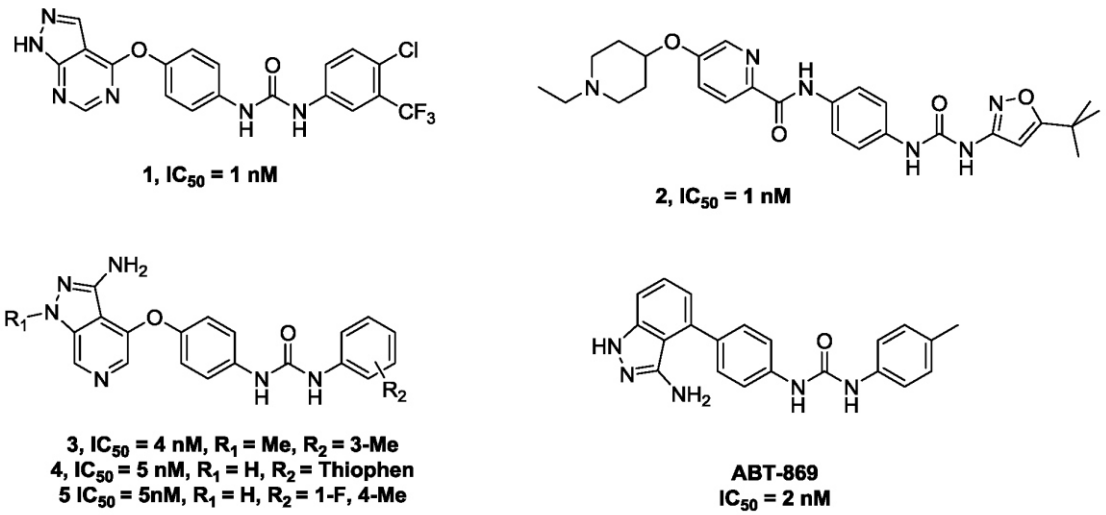

Figure 4: Active set of inhibitors in addition to TKIs in clinical trials (Sorafenib, Quizartinib) to generate pharmacophore hypothesis.

Table 1: Generated pharmacophore hypothesis with lowest p-values. Acc indicates the overall accuracy while the P-value indicates statistical significance. Generated pharmacophores consist of donor-projections (purple), acceptor-projections (cyan) and aromatic rings and projections (orange).

Entry	Pharmacophore	Acc	P-value	Acc_1	Acc_0
A	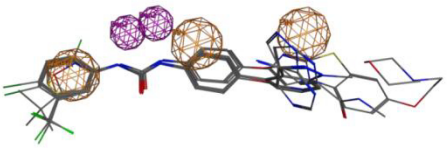	0.9931	-26.2	0.875	1.0000
B	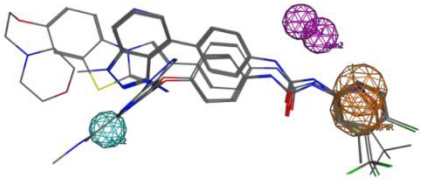	0.9861	-22.6	0.875	0.9926
C	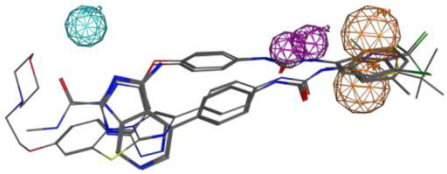	0.9861	-22.6	0.875	0.9926
D	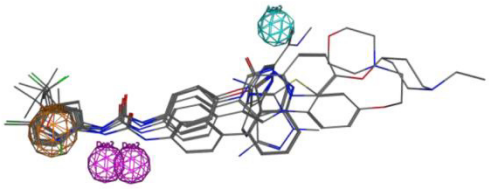	0.9792	-21.3	1.000	0.9779

Subsequently, sterically demanding amine fragments (bicyclics, large side group etc.) could be filtered since placement in the type II conformation was not possible (figure 5). Various functional groups were not counted among the synthesis candidates, since they represent prodrug concepts and thus do not bind in this structure to the kinase (carboxylate) or are potentially toxic (phenols, thiophenol, aromatic amines). Diamine derivatives were also not considered for synthesis as they cannot synthesized selectively (formation of regioisomers) and can be oxidized to toxic *p*-aminophenols, that can modify cellular macromolecules as benzoquinone imines. Also extended Lipinski parameters were used for selection, so

derivatives with log P > 6.0 and a molecular weight greater than 600 Da were discarded. Finally, 13 derivatives were selected for synthesis (Table 2). Like **AG1295**, the quinoxaline motif was oriented toward the protein surface and the aromatic head groups were located in the DFG pocket for the quinoxaline derivatives **12a-m**. Thus, similar interactions could be found within the ATP-binding pocket of FLT3. The benzothiazole derivative **12i** and the phenoxy derivative **12m** are very lipophilic, however, have a higher hydrophobic and aromatic contact surface, which could lead to higher activity. The lowest lipophilicity exhibited the picolyl **12d** and pyridine derivative **12g** which probably also therefore should have a higher solvent-solubility, since π-stacking interactions are weakened in the crystal by the benzylic position. The topological polar surface area (tPSA) regarding nitrogen and oxygen atoms allow an assessment of membrane permeability. Due to the small number of donor and acceptor motif this surface is significantly impaired from 140 $Å^2$.

Several possible interactions were found between the quinoxaline scaffold and the hinge region. Strong hydrogen bonds were observed between nitrogen of the quinoxaline and Cys694, additionally to the hydrogen bond with Glu692. Residue Leu616 forms a hydrogen-π-interaction with the quinoxaline ring. Furthermore the donor-acceptor-motive of the urea forms multiple interactions with the amino acids D829, K644 and E661.

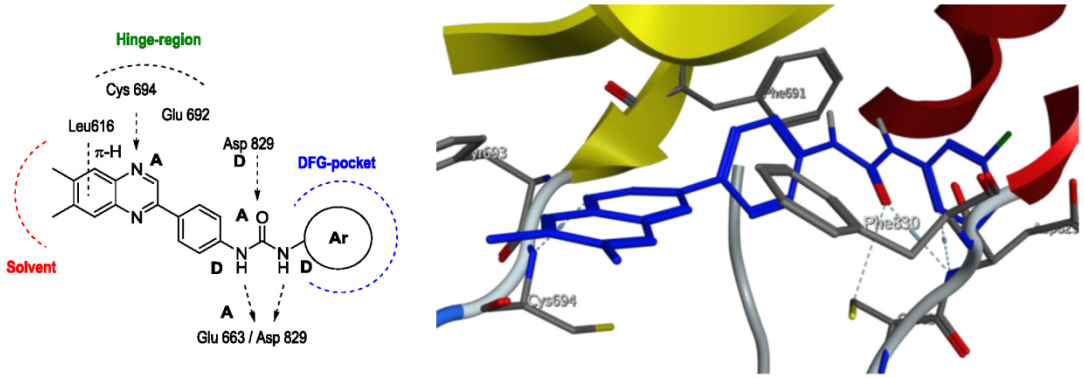

Figure 5: Docking study of compound **12b** performed using MOE 2013.08 and the known FLT3 crystal structure (PDB: 1RJB).[28]

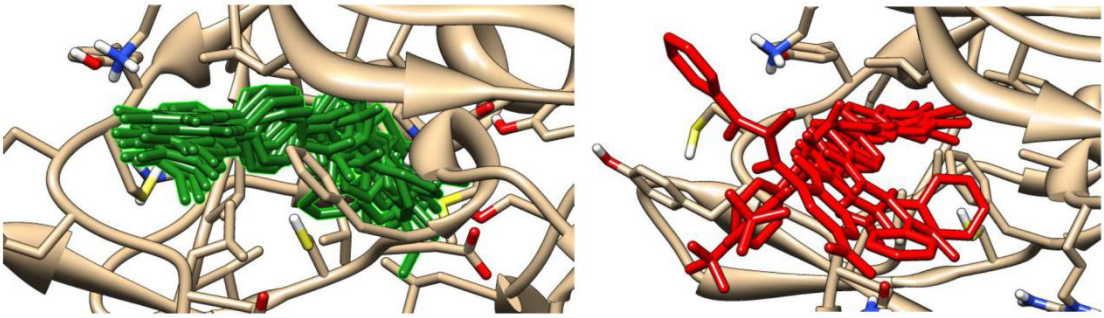

Figure 6: Ensemble of compounds that fit to the hinge region and DFG-pocket (best-scored pose, left) and compounds that could not be docked properly (right).[28]

Synthesis and in vitro Pharmacology

The synthesis of compounds **12a-m** starts with the synthesis of arylgyloxal **7**, which was used for the following coupling to the quinoxaline scaffold. Therefore glyoxale **7** was prepared by oxidation of its corresponding acetophenone **6** using SeO_2 (Scheme 1). The commercial available 4,5-dimethylbenzene-1,2-diamine and the synthesized glyoxal **7** were reacted at 80°C in DMF within 1 hour to the 2-arylquinoxaline derivative **8** and was obtained in good yield of 80 %. The reduction of intermediate **8** to its corresponding amine **9** was performed in the presence of Fe and $FeCl_3$, The final compound **12a** was obtained by *in situ* coupling of amine **9** with isocyanate **10**.

Due to the variations of the selected amines and to simplify the synthesis of the final compounds **12b-m** amine **9** was treated with triphosgene under basic conditions to form its corresponding isocyante **13** thatwas coupled *in situ* with the selected amines to obtain the final quinoxaline derivatives **12b-m** (Scheme 1). The reference compound **AG1295** was synthesized as described by Zall *et al*. via α-ketoaldehydes starting with benzaldehyde and 4,5-dimethylbenzene-1,2-diamine.[29]

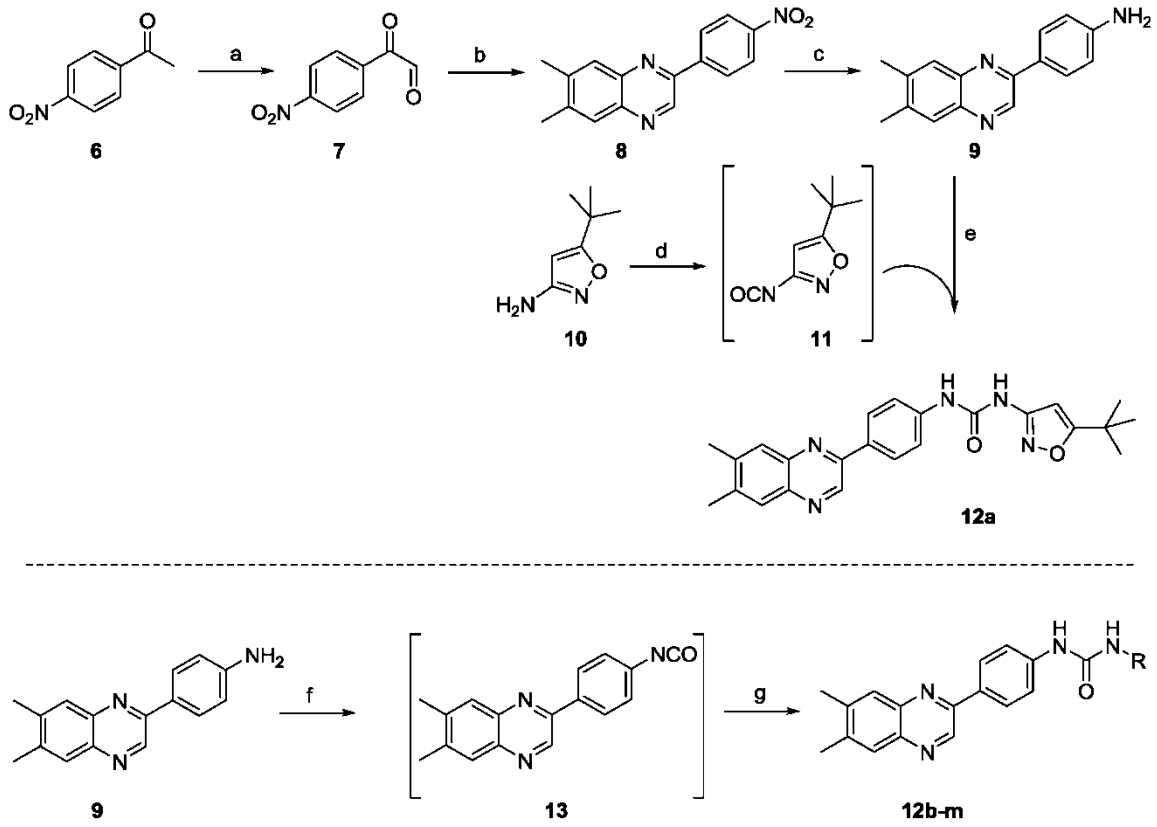

Scheme 1: Reactions and conditions: (a) SeO_2, dioxane/water 3:1, 12h 100°C; (b) diamine, DMF, 1h 80°C, (c) $Fe/FeCl_3$, acetic acid, ethanol, 1h reflux; (d) triphosgene, NEt_3, DCM, 1h -10°C; (e) toluene, 2h reflux; (f) triphosgene, sat. $NaHCO_3$, DCM, 20 min rt; (g) amine, THF, 2h reflux.

To confirm the docking results the obtained quinoxaline derivatives **12a-m** were tested for their ability to inhibit FLT3 kinase activity (Table 2). The results we obtained agreed with our previous docking studies. Thus, six quinoxaline derivatives **12a-f** exhibited an FLT-3 inhibition greater than 50 % at 100 nM. Interestingly, four of them, **12c-f**, contain a methylene bridge between the urea motifs and the aromatic head groups. Comparison of compound **7c** and **12k** proves the importance of the methylene bridge. **12c** exhibited and FLT-3 inhibition of 76 % at 100 nM, whereas compound **12k** lacks this methylene group and the activity decreased to 12 %. The most potent compound **12a** fuses structural elements of **AG1295** and **Quizartinib** and exhibited an inhibition of 80 %. The high activity of **12b** could be caused by the chlorine substitution in para position relative to the nitrogen lowering intramolecular hydrogen bonding strength with the distal urea amine and further allows halogen bonding.

Table 2: FLT3 *in vitro* inhibitory activities of quinoxalines derivatives **12a-m** and their calculated chemical properties.

Compound	R	LogP[a]	tPSA[a]	FLT-3 inhibition at 100 nM[b]
AG1295	-	4.28	24.72	37 %
12a	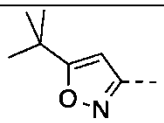	4.66	87.44	80 %
12b	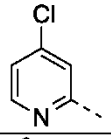	4.69	78.21	76 %
12c	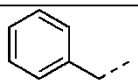	4.83	65.85	76 %
12d	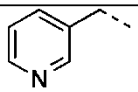	3.49	78.21	72 %
12e	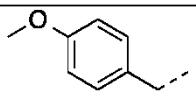	4.70	75.08	67 %
12f	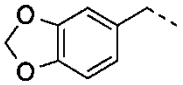	4.60	84.31	65 %
12g	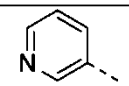	3.42	78.21	42 %
12h	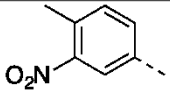	5.04	117.66	41 %
12i	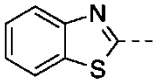	5.71	78.21	20 %
12j	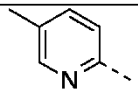	4.62	78.21	13 %
12k	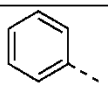	4.76	65.85	12 %
12l	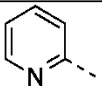	4.13	78.21	0 %
12m	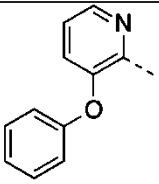	5.67	87.44	0 %

[a] Calculated by ChemBioDraw Ultra (version 13.0.2).

[b] The results are expressed as a percent of control specific activity = (100-(measured specific activity)/(control specific activity))*100; activity at a concentration of 100 nM.

Compared to compound **12l**, which lacks this substitution indicates a multiple drop of FLT3 activity. Next we investigated the role of the dimethyl quinoxline moiety. Based on the most active and promising compound **12a** we substituted the hydrophobic dimethyl groups to their more soluble methoxy or dimethoxy derivatives **18a** and **18b** (Scheme 2). Thus, both nitro compounds **14a** and **14b** were reduced with Pd/C under hydrogen to their corresponding amines **15a** and **15b**, and were directly coupled with the previous synthesized glyoxal **7** to obtain the dimethoxy **16a** and mehoxy **16b** intermediates. After the reduction with Fe and $FeCl_3$ to their amino counterparts **17a** and **17b**, respectively, a solution of isocyanate **11** was added to give the desired products **18a** and **18b**.

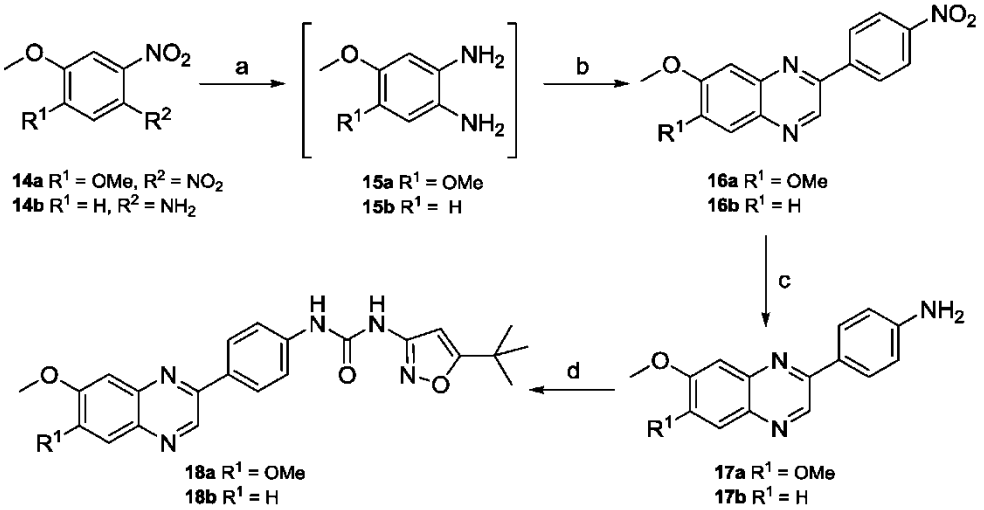

Scheme 2: Reactions and conditions: (a) PD/C, H_2, methanol 4h rt; (b) glyoxal **7**, DMF, 1h 80°C; (c) Fe/$FeCl_3$, acetic acid, methanol, 1h reflux; (d) isocyanate **7**, toluene, 2h reflux.

The results of the FLT3 *in vitro* assay indicated that both compounds exhibited a reduced activity compared to derivative **12a** (Table 3). Nevertheless, the dimethoxy derivative **18a** exhibited a better FLT-3 *in vitro* activity (51 % inhibition at 100 nM) compared to compound **18b** with an inhibition of 30 %.

Table 3: FLT-3 *in vitro* inhibitory activity of compound **18a** and **18b**.

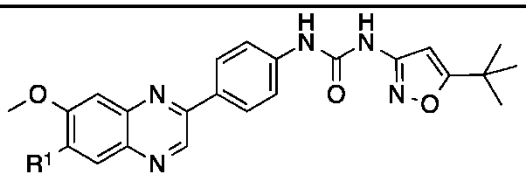

Compound	R^1	Log P[a]	FLT-3 inhibition at 100 nM[b]
13a	OMe	3.43	51 %
13b	H	3.56	30 %

[a] Calculated by ChemBioDraw Ultra (version 13.0.2).

[b] The results are expressed as a percent of control specific activity = (100-(measured specific activity)/(control specific activity)*100); at a inhibitor concentration of 100 nM.

To assess the activity more precisely we determined the IC_{50} values of compounds **12a-c** additionally. IC_{50} values of 71 nM for **12a**, 32 nM for **12b** and 88 nM for compound **12c** were obtained. These confirmed that we have identified a series of highly potent FLT-3 inhibitors based on the quinoxaline scaffold.

Next, we examined compound **12a** and **AG1295** of their *in vivo* activity on zebrafish embryos. In the past decades the zebrafish (*Danio rerio*) has become a useful aquatic vertebrate model to study developmental mechanism with assessing toxicological effects of chemicals and drugs and is standardized international.[30-32] Indeed, the zebrafish has a high fecundity (about 60 to 100 eggs per spawning), rapid embryonic development (about 3 days), a small size and the embryos are transparent and develop outside the body.[32-34] These are advantages to use the zebrafish for the toxicological and pharmacological research. After treating the zebrafish with drugs or chemicals a phenotypic description of the zebrafish is possible and conclusions can be drawn to safety and permeability of the compounds.

In our zebrafish assay the embryos were collected and maintained in E3 medium at 28°C. Compound **12a** was added 24 hpf (hours post fertilization) and the phenotypes were compared after 96 hpf (Figure 6). Lower concentrations from 1 µM to 20 µM of compound **12a** did not reveal any abnormalities compared to the control (Figure 7A-7C). At concentrations of 30 µM and 40 µM the phenotypes changed and 15 % of the zebrafish displayed stunted and crooked tails (Figure 7D-7E). After treating the zebrafish with compound **12a** related, but more pronounced phenotypes were observed at higher concentrations of 50 µM and 100 µM. Stunted and crooked tails were also observed, additionally to the constrained circular movement. At a concentration of 100 µM of tested compound **12a** we observed a development delay (50 % of the zebrafish are not hatched) and all zebrafish exhibited

abnormalities compared to the control (Figure 4H). In addition to the phenotypic description we pursued the lethality of the zebrafish every 24 hours up to 120 hpf (Figure 7). We could observe that at lower concentrations from 1 µM to 40 µM the lethality of the zebrafish embryos were located in a range inside 0 % to 10 %. At increasing concentrations of 50 µM and 100 µM, respectively, the survival rate decreased over the time, for 100 µM the survival rate decreased to 20 %. Related phenotypes were observed for **AG1295**. Below a concentration of 20 µM the zebrafish embryos exhibited no abnormalities compared to the control. At increasing concentration to 100 µM stunted and crooked tails were more pronounced. **AG1295** also displayed similar lethality as observed for compound **7a**. Nevertheless the zebrafish assay did not indicate any abnormalities for compound **7a** at concentrations below 20 µM and indicated no (1 µM) or poor cytotoxicity up to concentrations of 40 µM.

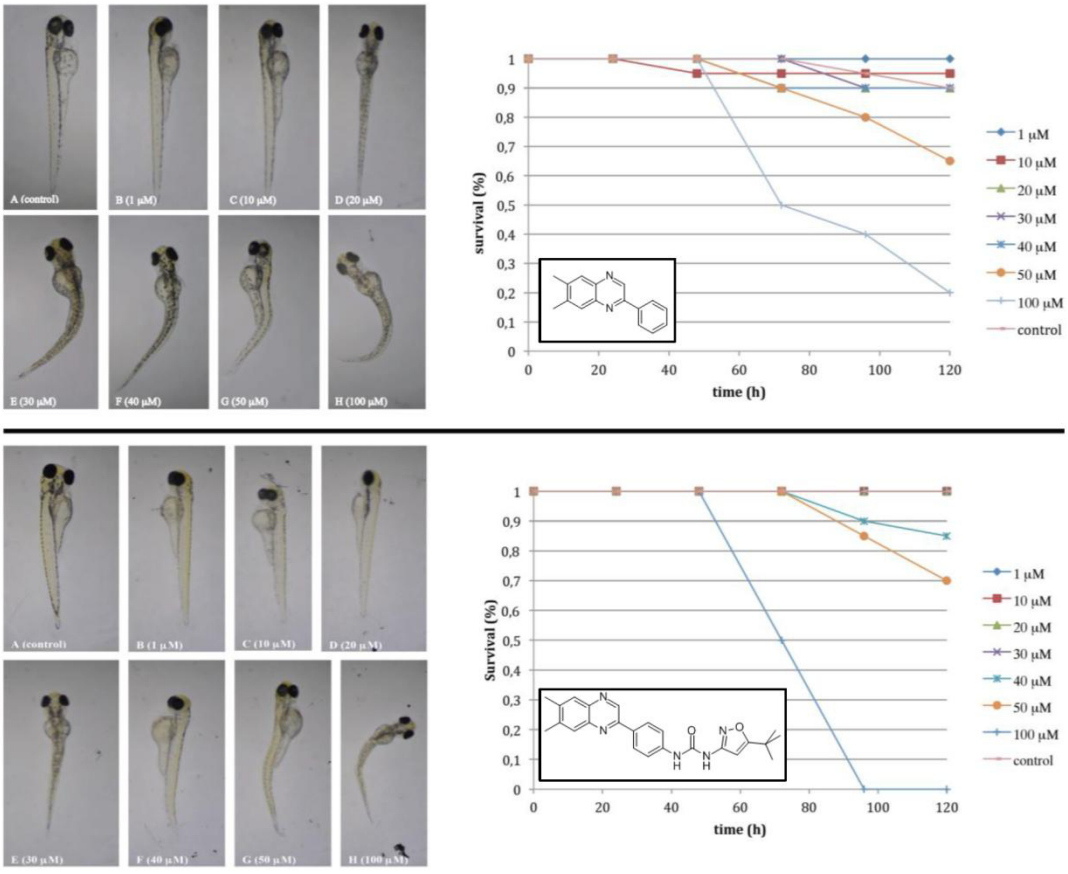

Figure 7: In vivo cytotoxicity of the zebrafish embryos and the survival rate at different time points for compound **12a** (1) and **AG1295** (2). The observed data are expressed as averages of

duplicates. The zebrafish embryos were collected and maintained in E3 medium at 28°C. Compound **12a** and **AG1295** were added 24 hpf (hours post fertilization) and the phenotypes were compared after 96 hpf. (A) Control embryo in 1 % DMSO, (B-H) Zebrafish embryos treated with compound **12a** and **AG1295** in several concentrations of 1 µM (B), 10 µM (C), 20 µM (D), 30 µM (E), 40 µM (F), G (50 µM) and 100 µM (H).

Conclusion

Identification and biological evaluation of quinoxalinebisarylureas as FLT3 inhibitors was the major field in this work. We created a generalized pharmacophore model for type II TKIs inhibiting FLT3 serving as a template for the design of **AG1295**-derived FLT3-Inhibitors. A compound library was searched by this pharmacophore and after subsequent virtual screening we could optimize quinoxaline-based TKIs which led to compounds showing activities in the low nanomolar range. Two of our most active compounds **12a** and **12b** exhibited an IC_{50} value of 71 nM and 32 nM, respectively. During the drug development, safety is one of the most important factors. We have evaluated in our *in vivo* zebrafish embryo phenotype assay the toxicity of compound **12a** compared to **AG1295**. We have observed no significant toxicity below 20 µM for both compounds.

Acknowledgement

The authors thank Christoph Scholz for help with scripting. Dennis Bensinger thanks the Stiftung Industrieforschung (Essen, Germany) for support with a personal scholarship.

References

[1] H.J. Chung, M.R. Kamli, H.J. Lee, J.D. Ha, S.Y. Cho, J. Lee, J.Y. Kong, S.Y. Han, Discovery of quinolinone derivatives as potent FLT3 inhibitors, Biochemical and biophysical research communications, 445 (2014) 561-565.
[2] S. Knapper, FLT3 inhibition in acute myeloid leukaemia, Br. J. Haematol., 138 (2007) 687-699.
[3] M.R. Grunwald, M.J. Levis, FLT3 inhibitors for acute myeloid leukemia: a review of their efficacy and mechanisms of resistance, Int. J. Hematol., 97 (2013) 683-694.
[4] T. Kindler, D.B. Lipka, T. Fischer, FLT3 as a therapeutic target in AML: still challenging after all these years, Blood, 116 (2010) 5089-5102.
[5] A.D. William, A.C. Lee, S. Blanchard, A. Poulsen, E.L. Teo, H. Nagaraj, E. Tan, D. Chen, M. Williams, E.T. Sun, K.C. Goh, W.C. Ong, S.K. Goh, S. Hart, R. Jayaraman, M.K. Pasha, K. Ethirajulu, J.M. Wood, B.W. Dymock, Discovery of the macrocycle 11-(2-pyrrolidin-1-yl-ethoxy)-14,19-dioxa-5,7,26-triaza-tetracyclo[19.3.1.1(2,6). 1(8,12)]heptacosa-1(25),2(26),3,5,8,10,12(27),16,21,23-decaene (SB1518), a potent Janus kinase 2/fms-like tyrosine kinase-3 (JAK2/FLT3) inhibitor for the treatment of myelofibrosis and lymphoma, J. Med. Chem., 54 (2011) 4638-4658.

[6] P. Brown, D. Small, FLT3 inhibitors: a paradigm for the development of targeted therapeutics for paediatric cancer, Eur. J. Cancer, 40 (2004) 707-721, discussion 722-704.
[7] S.D. Lyman, L. James, T. Vanden Bos, P. de Vries, K. Brasel, B. Gliniak, L.T. Hollingsworth, K.S. Picha, H.J. McKenna, R.R. Splett, et al., Molecular cloning of a ligand for the flt3/flk-2 tyrosine kinase receptor: a proliferative factor for primitive hematopoietic cells, Cell, 75 (1993) 1157-1167.
[8] D.L. Stirewalt, J.P. Radich, The role of FLT3 in haematopoietic malignancies, Nat. Rev. Cancer, 3 (2003) 650-665.
[9] D.G. Gilliland, J.D. Griffin, The roles of FLT3 in hematopoiesis and leukemia, Blood, 100 (2002) 1532-1542.
[10] U. Testa, Membrane Tyrosine Kinase Receptor Kit and FLT3 are an Important Targets for the Therapy of Acute Myeloid Leukemia, Current Cancer Therapy Reviews, 9 (2013) 181-219.
[11] M. Nakao, S. Yokota, T. Iwai, H. Kaneko, S. Horiike, K. Kashima, Y. Sonoda, T. Fujimoto, S. Misawa, Internal tandem duplication of the flt3 gene found in acute myeloid leukemia, Leukemia, 10 (1996) 1911-1918.
[12] S. Mahboobi, A. Uecker, A. Sellmer, C. Cenac, H. Hocher, H. Pongratz, E. Eichhorn, H. Hufsky, A. Trumpler, M. Sicker, F. Heidel, T. Fischer, C. Stocking, S. Elz, F.D. Bohmer, S. Dove, Novel bis(1H-indol-2-yl)methanones as potent inhibitors of FLT3 and platelet-derived growth factor receptor tyrosine kinase, J. Med. Chem., 49 (2006) 3101-3115.
[13] M. Levis, J. Allebach, K.F. Tse, R. Zheng, B.R. Baldwin, B.D. Smith, S. Jones-Bolin, B. Ruggeri, C. Dionne, D. Small, A FLT3-targeted tyrosine kinase inhibitor is cytotoxic to leukemia cells in vitro and in vivo, Blood, 99 (2002) 3885-3891.
[14] C.C. Smith, Q. Wang, C.S. Chin, S. Salerno, L.E. Damon, M.J. Levis, A.E. Perl, K.J. Travers, S. Wang, J.P. Hunt, P.P. Zarrinkar, E.E. Schadt, A. Kasarskis, J. Kuriyan, N.P. Shah, Validation of ITD mutations in FLT3 as a therapeutic target in human acute myeloid leukaemia, Nature, 485 (2012) 260-263.
[15] N. Pemmaraju, H. Kantarjian, F. Ravandi, J. Cortes, FLT3 inhibitors in the treatment of acute myeloid leukemia: the start of an era?, Cancer, 117 (2011) 3293-3304.
[16] M. Miano, C. Micalizzi, M. Calvillo, C. Dufour, New targets in pediatric Acute Myeloid Leukemia, Immunol. Lett., 155 (2013) 47-50.
[17] M. Levis, D. Small, FLT3 tyrosine kinase inhibitors, Int. J. Hematol., 82 (2005) 100-107.
[18] S. Kayser, M.J. Levis, FLT3 tyrosine kinase inhibitors in acute myeloid leukemia: clinical implications and limitations, Leuk. Lymphoma, 55 (2014) 243-255.
[19] K.F. Tse, E. Novelli, C.I. Civin, F.D. Bohmer, D. Small, Inhibition of FLT3-mediated transformation by use of a tyrosine kinase inhibitor, Leukemia, 15 (2001) 1001-1010.
[20] M. Levis, K.F. Tse, B.D. Smith, E. Garrett, D. Small, A FLT3 tyrosine kinase inhibitor is selectively cytotoxic to acute myeloid leukemia blasts harboring FLT3 internal tandem duplication mutations, Blood, 98 (2001) 885-887.
[21] J. Cortes, J. Foran, D. Ghirdaladze, M.P. de Vette, M. Zodelava, P. Holman, M.J. Levis, H.M. Katarjian, G. Borthakur, J. James, AC220, a Potent, Selective, Second Generation FLT3 Receptor Tyrosine Kinase (RTK) Inhibitor, in a First-in-Human (FIH) Phase 1 AML Study, Blood (ASH Annual Meeting Abstracts), 114 (2009).
[22] D.J. DeAngelo, R.M. Stone, M.L. Heaney, S.D. Nimer, R.L. Paquette, R.B. Klisovic, M.A. Caligiuri, M.R. Cooper, J.M. Lecerf, M.D. Karol, S. Sheng, N. Holford, P.T. Curtin, B.J. Druker, M.C. Heinrich, Phase 1 clinical results with tandutinib (MLN518), a novel FLT3 antagonist, in patients with acute myelogenous leukemia or high-risk myelodysplastic syndrome: safety, pharmacokinetics, and pharmacodynamics, Blood, 108 (2006) 3674-3681.
[23] W. Fiedler, R. Mesters, H. Tinnefeld, S. Loges, P. Staib, U. Duhrsen, M. Flasshove, O.G. Ottmann, W. Jung, F. Cavalli, R. Kuse, J. Thomalla, H. Serve, A.M. O'Farrell, M. Jacobs,

N.M. Brega, P. Scigalla, D.K. Hossfeld, W.E. Berdel, A phase 2 clinical study of SU5416 in patients with refractory acute myeloid leukemia, Blood, 102 (2003) 2763-2767.
[24] S. Metzelder, Y. Wang, E. Wollmer, M. Wanzel, S. Teichler, A. Chaturvedi, M. Eilers, E. Enghofer, A. Neubauer, A. Burchert, Compassionate use of sorafenib in FLT3-ITD-positive acute myeloid leukemia: sustained regression before and after allogeneic stem cell transplantation, Blood, 113 (2009) 6567-6571.
[25] Q. Chao, K.G. Sprankle, R.M. Grotzfeld, A.G. Lai, T.A. Carter, A.M. Velasco, R.N. Gunawardane, M.D. Cramer, M.F. Gardner, J. James, P.P. Zarrinkar, H.K. Patel, S.S. Bhagwat, Identification of N-(5-tert-butyl-isoxazol-3-yl)-N'-{4-[7-(2-morpholin-4-yl-ethoxy)imidazo[2,1-b][1 ,3]benzothiazol-2-yl]phenyl}urea dihydrochloride (AC220), a uniquely potent, selective, and efficacious FMS-like tyrosine kinase-3 (FLT3) inhibitor, J. Med. Chem., 52 (2009) 7808-7816.
[26] J. Griffith, J. Black, C. Faerman, L. Swenson, M. Wynn, F. Lu, J. Lippke, K. Saxena, The structural basis for autoinhibition of FLT3 by the juxtamembrane domain, Mol. Cell, 13 (2004) 169-178.
[27] K. Verstraete, G. Vandriessche, M. Januar, J. Elegheert, A.V. Shkumatov, A. Desfosses, K. Van Craenenbroeck, D.I. Svergun, I. Gutsche, B. Vergauwen, S.N. Savvides, Structural insights into the extracellular assembly of the hematopoietic Flt3 signaling complex, Blood, 118 (2011) 60-68.
[28] Molecular Operating Environment (MOE), 2013.08; Chemical Computing Group Inc., 1010 Sherbooke St. West, Suite #910, Montreal, QC, Canada, H3A 2R7, 2013., Molecular Operating Environment (MOE), 2013.08; Chemical Computing Group Inc., 1010 Sherbooke St. West, Suite #910, Montreal, QC, Canada, H3A 2R7, 2013.
[29] A. Zall, D. Bensinger, B. Schmidt, Oxidative Homologation of Aldehydes to α-Ketoaldehydes by using Iodoform,

o-Iodoxybenzoic Acid, and Dimethyl Sulfoxide, Eur. J. Org. Chem., (2012) 1439–1447.
[30] M. Giannaccini, A. Cuschieri, L. Dente, V. Raffa, Non-mammalian vertebrate embryos as models in nanomedicine, Nanomedicine: Nanotechnology, Biology, and Medicine, (2014) in press.
[31] E. Lammer, G.J. Carr, K. Wendler, J.M. Rawlings, S.E. Belanger, T. Braunbeck, Is the fish embryo toxicity test (FET) with the zebrafish (Danio rerio) a potential alternative for the fish acute toxicity test?, Comp. Biochem. Physiol. C Toxicol. Pharmacol., 149 (2009) 196-209.
[32] G. Vitale, G. Gaudenzi, A. Dicitore, F. Cotelli, D. Ferone, L. Persani, Zebrafish as an innovative model for neuroendocrine tumors, Endocr. Relat. Cancer, 21 (2014) R67-83.
[33] S. Deeti, S. O'Farrell, B.N. Kennedy, Early safety assessment of human oculotoxic drugs using the zebrafish visualmotor response, J. Pharmacol. Toxicol. Methods, 69 (2014) 1-8.
[34] J. Lee, J.L. Freeman, Zebrafish as a model for investigating developmental lead (Pb) neurotoxicity as a risk factor in adult neurodegenerative disease: A mini-review, NeuroToxicology, (2014) in press.

Supporting Information

Computer-guided design, synthesis and biological evaluation of quinoxalinebisarylureas as FLT3 inhibitors.

Stefan Göring*, Dennis Bensinger*, Eva Naumann and Boris Schmidt†
Clemens Schöpf - Institute of Organic Chemistry and Biochemistry, Technische Universität Darmstadt, 64287 Darmstadt, Hessen, Germany, Fax: +496151-163278; Tel: +496151-164531.
** These authors contributed equally to this work.*
† Corresponding author. Tel.: +49 6151 163075; fax: +49 6151 163278.
E-mail: schmidt_boris@t-online.de.

Table of Content:

I. General comments

II. Experimental methods and chemical data

III. Molecular Docking

IV. FTL-3 *in vitro* assay conducted by Cerep

V. Toxicity assay: Determination of the *in vivo* activity on zebrafish embryos

VI. References

I. General comments

The ^{1}H-NMR spectra were detected on a Bruker AC 300 spectrometer at 300 MHz and Bruker AC 500 spectrometer at 500 MHz. The ^{13}C-NMR spectra were detected on a Bruker AC 300 spectrometer at 75 MHz and Bruker AC 500 spectrometer at 125 MHz. Chemical shifts are reported in ppm and are calibrated to the particular solvent. Mass spectrometry was performed on a Bruker-Franzen Esquire LC mass spectrometer and a MAT 95 double focussing sector field MS. Microwave experiments were carried out using a Biotage® Initiator™ microwave apparatus. All microwave experiments were carried out in sealed microwave process vials utilizing the standard absorbance level (300 W maximum power). Silica gel chromatography was carried out using Merck silica gel 60 (0.015-0.040 mm). High performance liquid chromatographies were carried out in an Agilent 1100 (column: reversed phase, Zorbax Eclipse XDB-C8, 4.6 x 150 mm; 254 nm). The eluent is composed of: a) H_2O (1% TFA) (A) and acetonitrile (1% TFA) (B) with a gradient: 30 to 90% B within 12 min. Automated flash chromatography was performed on a Teledyne ISCO Combi Flash RF 4X using water and acetonitrile solvent mixtures. All commercial available reagents and solvents were purchased at ABCR, Acros, Sigma Aldrich and VWR.

II. Experimental Methods and Chemical Data

2-(4-nitrophenyl)-2-oxoacetaldehyde 3

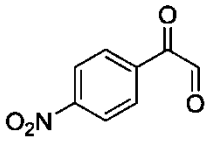

A suspension of SeO_2 (671 mg, 6.05 mmol) in dioxane (6 mL) and water (2 mL) was stirred at 55°C until the solid was dissolved. This was followed by the addition of 1-(4-nitrophenyl)ethanone **2** (200 mg, 1.21 mmol) and the mixture was stirred over night at 100°C. The black solid was filtered off and the solvent from the filtrate was removed under vacuum. The residual amount was diluted in ethyl acetate, was washed two times with water and saturated $NaHCO_3$, dried over $MgSO_4$, filtrated and the solvent was removed under vacuum. The raw product was purified by silica gel column chromatography (cyclohexane/ethyl acetat 1:1) to give 148 mg (68 %) as a yellow solid. **HPLC**: R_t = 1.83 min. **^{1}H-NMR** (DMSO-d_6, 300 MHz): δ [ppm] = 8.41-8.21 (m, 4H), 7.05 (d, 2H, J = 6.8 H). **^{13}C-NMR** (DMSO-d_6, 75 MHz): δ [ppm] = 195.3, 149.8, 138.5, 130.8, 123.5, 90.1.

6,7-dimethyl-2-(4-nitrophenyl)quinoxaline 5

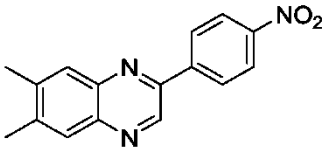

A solution of 2-(4-nitrophenyl)-2-oxoacetaldehyde **3** (140 mg, 0.78 mmol) and 4,5-dimethylbenzene-1,2-diamine (106 mg, 0.78 mmol) in DMF was stirred for 2 hours at 80°C. After cooling to room temperature water was added and the obtained solid was filtrated, dried and gave 174 mg (80 %) as a light yellow solid. **HPLC**: R_t = 7.83 min. **^{1}H-NMR** ($CDCl_3$, 500 MHz): δ [ppm] = 9.28 (s, 1H), 8.41-8.36 (m, 4H), 7.96 (s, 2H), 2.55 (s, 6H). **^{13}C-NMR** ($CDCl_3$, 125 MHz): δ [ppm] = 148.9, 148.7, 142.8, 142.4, 142.3, 141.7, 141.0, 140.2, 129.0, 128.3, 127.8, 124.4, 20.7, 20.6.

4-(6,7-dimethylquinoxalin-2-yl)aniline 6

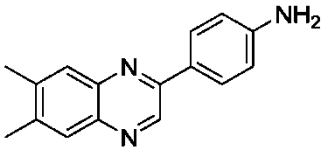

Acetic acid (1.30 mL), Fe (190 mg, 3.39 mmol) and $FeCl_3$ (92 mg, 0.57 mmol) were added to a solution of 6,7-dimethyl-2-(4-nitrophenyl)quinoxaline **5** (158 mg, 0.57 mmol) in ethanol (7 mL) and stirred for 1 hour at 80°C. After cooling to room temperature the solvent was removed and the residual amount was diluted in ethyl acetate and was washed with water. The organic layer was dried over $MgSO_4$, filtered and the solvent was removed under vacuum. After purification by silica gel column chromatography (chloroform/methanol 20:1) 70 mg (50 %) of yellow solid was obtained. **HPLC**: R_t = 3.09 min. **^{1}H-NMR** (DMSO-d_6, 500 MHz): δ [ppm] = 9.28 (s, 1H), 8.02 (d, 2H, *J* = 8.6 Hz), 7.77 (s, 2H), 6.71 (d, 2H, *J* = 8.6 Hz), 5.67 (s, 2H), 2.45 (d, 6H, *J* = 4.2 H). **^{13}C-NMR** (DMSO-d_6, 125 MHz): δ [ppm] = 151.0, 150.5, 142.0, 141.9, 140.4, 140.2, 139.1, 139.3, 128.3, 127.7, 123.3, 113.8, 19.8, 19.6.

1-(5-*tert*-butylisoxazol-3-yl)-3-(4-(6,7-dimethylquinoxalin-2-yl)phenyl)urea 1

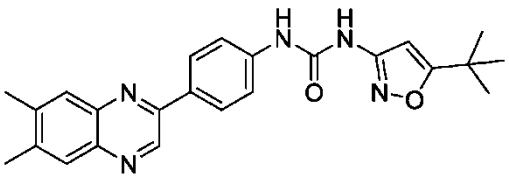

To solution of 5-*tert*-butylisoxazol-3-amine **7** (17 mg, 0.12 mmol) in dichloromethane (2 mL) and triphosgene (10 mg, 0.12 mmol) was added dropwise at -10°C a solution of triethylamine (34 µL, 0.22 mmol) in dichloromethane (0.5 mL). The mixture was stirred for 1 hour at this temperature. Afterwards a solution of 4-(6,7-dimethylquinoxalin-2-yl)aniline **6** (30 mg, 0.12 mmol) in toluene (1 mL) was added and the mixture was stirred for 2 hours at 110°C. After cooling to room temperature water was added and extracted three times with ethyl acetate. The combined organic layers were dried over $MgSO_4$, filtrated and the solvent was removed under vacuum. After purification by silica gel column chromatography (chloroform/methanol 25:1) 28 mg (56 %) of light yellow solid was obtained. **HPLC**: R_t = 8.00 min. **^{1}H-NMR** (DMSO-d_6, 500 MHz): δ [ppm] = 9.58 (s, 1H), 9.42 (s, 1H), 9.07 (s, 1H), 8.29-8.26 (m, 2H), 7.87 (d, 2H, *J* = 11.4 Hz), 7.68-7.65 (m, 2H), 6.54 (s, 1H), 2.49 (d, 6H, *J* = 3.0 Hz), 1.31 (s, 9H). **^{13}C-NMR** (DMSO-d_6, 125 MHz): δ [ppm] = 180.3, 158.2, 151.2,

149.6, 142.3, 140.9, 140.7, 140.3, 139.7, 139.7, 130.3, 127.9, 127.7, 118.5, 92.4, 28.3, 19.8, 19.7. **ESI-MS**: m/z = 438 $[M+Na]^+$.

1-(4-chloropyridin-2-yl)-3-(4-(6,7-dimethylquinoxalin-2-yl)phenyl)urea 10a

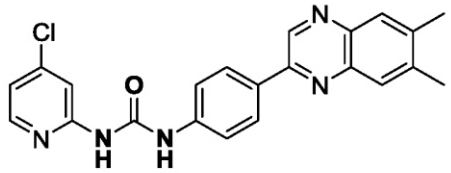

To a biphasic system of triphosgene (35 mg, 0.12 mmol) in dichloromethane (3 mL) and saturated $NaHCO_3$ solution (15 mL) was added dropwise a solution of 4-(6,7-dimethylquinoxalin-2-yl)aniline **6** (84 mg, 0.34 mmol) in dichloromethane (10 mL). The organic phase turned to red and was stirred until no solid was observed. The reaction was stopped by the separation of the organic phase and was dried over $MgSO_4$, filtred and the solvent was removed under vacuum to give a red solid, which was directly used for the next step. The red solid was diluted in THF (4 mL) and was added to a solution of 4-chloropyridin-2-amine (48 mg, 0.37 mmol) in THF (4 mL) and the mixture was stirred under reflux for 2 hours. After cooling to room temperature the solvent was removed and the residue was diluted in a small amount of DMF, refluxed and water was added. The obtained yello solid was filtrated and dried to give 51 mg (36 %). **HPLC**: R_t = 7.40 min. **^{1}H-NMR** (DMSO-d_6, 500 MHz): δ [ppm] = 10.21 (s, 1H), 9.64 (s, 1H), 9.45 (d, 1H, J = 1.2 Hz), 8.35 – 8.29 (m, 3H), 7.92 – 7.86 (m, 2H), 7.80 (d, 1H, J = 1.9 Hz), 7.77 – 7.71 (m, 2H), 7.19 (dd, 1H, J = 5.5, 1.9 Hz), 2.51 – 2.51 (m, 3H), 2.51 – 2.49 (m, 3H). **^{13}C-NMR** (DMSO-d_6, 125 MHz): δ [ppm] = 179.7, 153.7, 151.7, 149.6, 148.9, 144.1, 142.3, 140.7, 140.4, 139.8, 139.7, 130.4, 128.0, 127.7, 118.8, 118.4, 117.9, 111.3, 19.8, 19.8.

1-benzyl-3-(4-(6,7-dimethylquinoxalin-2-yl)phenyl)urea 10b

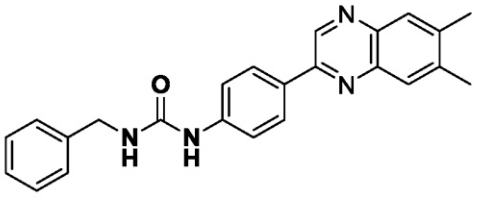

The 1-benzyl-3-(4-(6,7-dimethylquinoxalin-2-yl)phenyl)urea **10b** was obtained as a yellow solid (35 mg, 42 %) using the same procedure as described for **10a** starting from phenylmethanamine (26 µL, 0.24 mmol). **HPLC**: R_t = 7.24 min. **^{1}H-NMR** (DMSO-d_6, 500 MHz): δ [ppm] = 9.39 (s, 1H), 8.88 (s, 1H), 8.22-8.19 (m, 2H), 7.84 (d, 2H, J = 9.1 Hz), 7.64-7.61 (m, 2H), 7.37-7.32 (m, 4H), 7.27-7.24 (m, 1H), 6.74 (t, 1H, J = 5.9 Hz), 4.33 (d,

2H, *J* = 5.9 Hz), 2.47 (d, 6H, *J* = 3.0 Hz). **^{13}C-NMR** (DMSO-d_6, 125 MHz): δ [ppm] = 154.9, 149.8, 142.5, 142.2, 140.6, 140.5, 140.1, 139.6, 139.4, 128.8, 128.3, 127.9, 127.8, 127.7, 127.1, 126.7, 117.7, 42.8, 19.8, 19.7.

1-(4-(6,7-dimethylquinoxalin-2-yl)phenyl)-3-(pyridin-3-ylmethyl)urea 10c

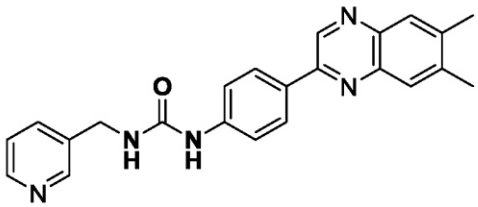

The 1-(4-(6,7-dimethylquinoxalin-2-yl)phenyl)-3-(pyridin-3-ylmethyl)urea **10c** was obtained as a colorless solid (84 mg, 78 %) using the same procedure as described for **10a** starting from pyridin-3-ylmethanamine (33 mg, 0.30 mmol). **HPLC**: R_t = 3.76 min. **^{1}H-NMR** (DMSO-d_6, 500 MHz): δ [ppm] = 9.39 (s, 1H), 9.00 (s, 1H), 8.58 (d, 1H, *J* = 2.2 Hz), 8.49 (dd, 1H, *J* = 4.8, 1.6 Hz), 8.26 – 8.19 (m, 2H), 7.84 (d, 2H, *J* = 8.5 Hz), 7.76 (dt, 1H, *J* = 7.8, 2.0 Hz), 7.68 – 7.59 (m, 2H), 7.39 (dd, 1H, *J* = 7.8, 4.8 Hz), 6.89 (t, 1H, *J* = 6.0 Hz), 4.39 (d, 2H, *J* = 5.9 Hz), 2.49 (s, 6H). **^{13}C-NMR** (DMSO-d_6, 125 MHz): δ [ppm] = 155.0, 149.8, 148.7, 148.0, 142.4, 142.2, 140.6, 140.4, 139.6, 139.4, 135.7, 134.99, 129.0, 127.9, 127.8, 127.7, 123.4, 117.8, 40.5, 19.8, 19.7. **MS** (EI, 70 eV): *m/z* = 383.

1-(4-(6,7-dimethylquinoxalin-2-yl)phenyl)-3-(4-methoxybenzyl)urea 10d

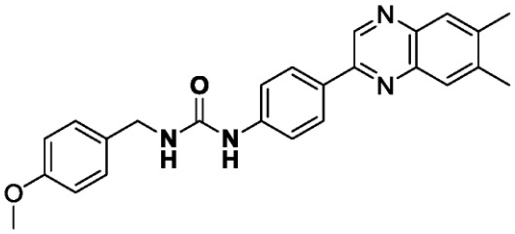

The 1-(4-(6,7-dimethylquinoxalin-2-yl)phenyl)-3-(4-methoxybenzyl)urea **10d** was obtained as a yellow solid (31 mg, 34 %) using the same procedure as described for **10a** starting from (4-methoxyphenyl)methanamine (31µL, 0.24 mmol). **HPLC**: R_t = 7.21 min. **^{1}H-NMR** (DMSO-d_6, 500 MHz): δ [ppm] = 9.39 (s, 1H), 8.83 (s, 1H), 8.21-8.19 (m, 2H), 7.84 (d, 2H, *J* = 9.1 Hz), 7.63-7.60 (m, 2H), 7.27-7.24 (m, 2H), 6.92-6.89 (m, 2H), 6.56 (t, 1H, *J* = 5.8 Hz), 4.25 (d, 2H, *J* = 5.8 Hz), 3.74 (s, 3H), 2.48 (d, 6H, *J* = 3.0 Hz). **^{13}C-NMR** (DMSO-d_6, 125 MHz): δ [ppm] = 158.2, 154.9, 149.9, 142.5, 142.2, 140.6, 140.4, 139.6, 139.4, 132.0, 128.8, 128.5, 127.9, 127.8, 127.7, 117.7, 113.7, 55.1, 42.3, 19.8, 19.7.

1-(benzo[*d*][1,3]dioxol-5-ylmethyl)-3-(4-(6,7-dimethylquinoxalin-2-yl)phenyl)urea 10e

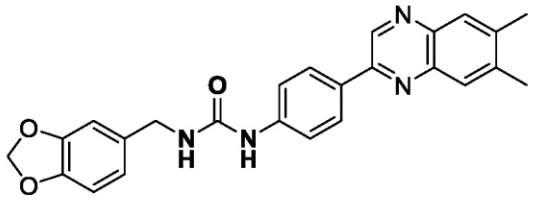

The 1-(benzo[*d*][1,3]dioxol-5-ylmethyl)-3-(4-(6,7-dimethylquinoxalin-2-yl)phenyl)urea **10e** was obtained as a yellow solid (35 mg, 37 %) using the same procedure as described for **10a** starting from benzo[*d*][1,3]dioxol-5-ylmethanamine (36 mg, 0.24 mmol). **HPLC**: R_t = 7.21 min. **^{1}H-NMR** (DMSO-d_6, 500 MHz): δ [ppm] = 9.39 (s, 1H), 8.84 (s, 1H), 8.22-8.19 (m, 2H), 7.84 (d, 2H, *J* = 9.2 Hz), 7.63-7.60 (m, 2H), 6.89 (d, 1H, *J* = 1.6 Hz), 6.87 (d, 1H, *J* = 7.9 Hz), 6.80 (dd, 1H, *J* = 7.9, 1.6 Hz), 6.67 (t, 1H, *J* = 5.9 Hz), 5.98 (s, 2H), 4.23 (d, 2H, *J* = 5.9 Hz), 2.47 (d, 6H, *J* = 3.0 Hz). **^{13}C-NMR** (DMSO-d_6, 125 MHz): δ [ppm] = 154.9, 149.9, 147.2, 146.0, 142.5, 142.2, 140.6, 140.4, 139.6, 139.4, 134.1, 128.8, 127.9, 127.8, 127.7, 120.4, 117.7, 108.0, 107.9, 100.9, 42.6, 19.8, 19.7.

1-(4-(6,7-dimethylquinoxalin-2-yl)phenyl)-3-(pyridin-3-yl)urea 10f

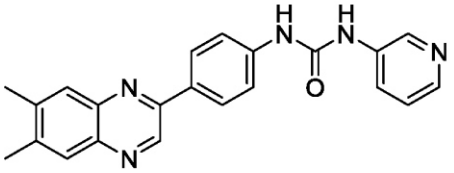

The 1-(4-(6,7-dimethylquinoxalin-2-yl)phenyl)-3-(pyridin-3-yl)urea **10f** was obtained as a yellow solid (84 mg, 67 %) using the same procedure as described for **10a** starting from pyridin-3-amine (32 mg, 0.34 mmol). **HPLC**: R_t = 4.36 min. **^{1}H-NMR** (DMSO-d_6, 500 MHz): δ [ppm] = 9.42 (s, 1H), 9.11 (s, 1H), 8.93 (s, 1H), 8.64 (d, 1H, *J* = 2.3 Hz), 8.28-8.25 (m, 2H), 8.21 (dd, 1H, *J* = 4.6, 1.1 Hz), 7.98-7.96 (m, 1H), 7.86 (d, 2H, *J* = 10.6 Hz), 7.70-7.67 (m, 2H), 7.33 (dd, 1H, *J* = 8.3, 4.7 Hz), 2.48 (d, 6H, *J* = 3.4 Hz). **^{13}C-NMR** (DMSO-d_6, 125 MHz): δ [ppm] = 152.4, 149.7, 143.1, 142.2, 141.4, 140.7, 140.3, 140.2, 139.7, 139.6, 136.2, 129.8, 127.9, 127.7, 125.3, 123.6, 118.4, 19.8, 19.7. **MS** (ES, 70 eV): *m/z* = 369.

1-(4-(6,7-dimethylquinoxalin-2-yl)phenyl)-3-(4-methyl-3-nitrophenyl)urea 10g

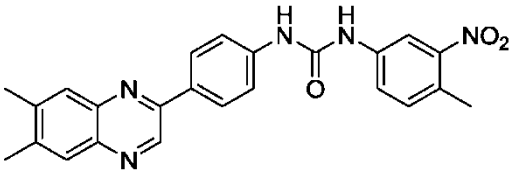

The 1-(4-(6,7-dimethylquinoxalin-2-yl)phenyl)-3-(4-methyl-3-nitrophenyl)urea **10g** was obtained as a light brown solid (65 mg, 45 %) using the same procedure as described for **10a** starting from 4-methyl-3-nitroaniline (52 mg, 0.34 mmol). **HPLC**: R_t = 8.03 min. **^{1}H-NMR** (DMSO-d_6, 500 MHz): δ [ppm] = 9.42 (s, 1H), 9.14 (s, 1H), 9.09 (s, 1H), 8.30 (d, 1H, *J* = 2.3 Hz), 8.28-8.25 (m, 2H), 7.86 (d, 2H, *J* = 11.9 Hz), 7.70-7.76 (m, 2H), 7.59 (dd, 1H, *J* = 8.3, 2.3 Hz), 7.42 (d, 1H, *J* = 8.5 Hz), 2.48 (d, 6H, *J* = 3.3 Hz), 2.46 (s, 3H). **^{13}C-NMR** (DMSO-d_6, 125 MHz): δ [ppm] = 152.2, 149.7, 148.8, 142.3, 141.3, 140.7, 140.3, 139.7, 139.6, 138.5, 133.0, 129.9, 127.9, 127.9, 127.7, 125.7, 123.1, 118.5, 113.4, 19.8, 19.7, 18.9. **MS** (ES, 70 eV): *m/z* = 469.

1-(benzo[*d*]thiazol-2-yl)-3-(4-(6,7-dimethylquinoxalin-2-yl)phenyl)urea 10h

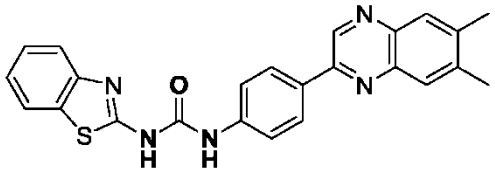

The 1-(benzo[*d*]thiazol-2-yl)-3-(4-(6,7-dimethylquinoxalin-2-yl)phenyl)urea **10h** was obtained as a red solid (51 mg, 43 %) using the same procedure as described for **10a** starting from benzo[*d*]thiazol-2-amine (45 mg, 0.30 mmol). **HPLC**: R_t = 7.89 min. **^{1}H-NMR** (DMSO-d_6, 500 MHz): δ [ppm] = 9.84 (s, 1H), 9.45 (s, 1H), 8.37 – 8.30 (m, 2H), 8.30 (s, 1H), 7.93 (dd, 1H, *J* = 7.9, 1.1 Hz), 7.89 (d, 1H, *J* = 16.1 Hz), 7.82 – 7.74 (m, 2H), 7.68 (d, 1H, *J* = 8.0 Hz), 7.45 – 7.40 (m, 1H), 7.30 – 7.25 (m, 1H), 2.50 (s, 3H), 2.49 (s, 3H). **^{13}C-NMR** (DMSO-d_6, 125 MHz): δ [ppm] = 159.8, 152.5, 149.6, 147.4, 142.3, 140.8, 140.6, 140.35, 139.7, 130.9, 130.6, 128.0, 127.7, 126.0, 122.9, 121.6, 119.1, 118.7, 19.8, 19.8. **MS** (EI, 70 eV): *m/z* = 425.

1-(4-(6,7-dimethylquinoxalin-2-yl)phenyl)-3-(5-methylpyridin-2-yl)urea 10i

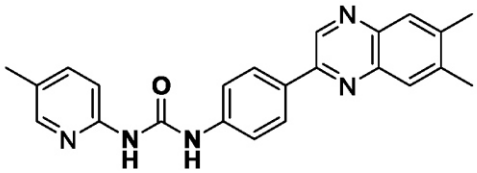

The 1-(4-(6,7-dimethylquinoxalin-2-yl)phenyl)-3-(5-methylpyridin-2-yl)urea **10i** was obtained as a yellow solid (52 mg, 51 %) using the same procedure as described for **10a** starting from 5-methylpyridin-2-amine (31 mg, 0.29 mmol). **HPLC**: R_t = 5.44 min. **^{1}H-NMR** (DMSO-d_6, 500 MHz): δ [ppm] = 10.61 (s, 1H), 9.35 (d, 2H, *J* = 5.0 Hz), 8.26 – 8.17 (m, 2H), 8.10 – 8.02 (m, 1H), 7.79 (d, 2H, *J* = 13.5 Hz), 7.71 – 7.62 (m, 2H), 7.54 (dd, 1H, *J* = 8.5, 2.3 Hz), 7.39 (d, 1H, *J* = 8.4 Hz), 2.42 (s, 3H), 2.41 (s, 3H), 2.18 (s, 3H). **^{13}C-NMR** (DMSO-d_6, 125 MHz): δ [ppm] = 152.1, 150.6, 149.7, 146.5, 142.3, 141.1, 140.7, 140.4, 139.7, 139.6, 139.2, 136.1, 130.1, 127.9, 127.7, 126.5, 118.8, 111.6, 19.8, 19.7, 17.1.

1-(4-(6,7-dimethylquinoxalin-2-yl)phenyl)-3-phenylurea 10j

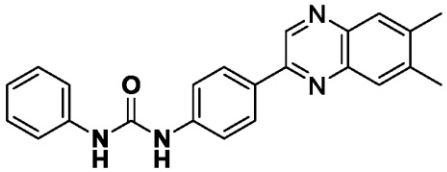

The 1-(4-(6,7-dimethylquinoxalin-2-yl)phenyl)-3-phenylurea **10j** was obtained as a red solid (35 mg, 32 %) using the same procedure as described for **10a** starting from aniline (30 mg, 0.32 mmol). **HPLC**: R_t = 7.31 min. **^{1}H-NMR** (DMSO-d_6, 500 MHz): δ [ppm] = 9.43 (s, 1H), 9.09 (s, 1H), 8.87 (s, 1H), 8.27 (d, 2H, *J* = 8.8 Hz), 7.88 (dd, 2H, *J* = 11.9, 1.1 Hz), 7.69 (d, 2H, *J* = 8.8 Hz), 7.54 – 7.47 (m, 2H), 7.32 (dd, 2H, *J* = 8.5, 7.3 Hz), 7.01 (tt, 1H, *J* = 7.4, 1.2 Hz), 2.50 (s, 6H). **^{13}C-NMR** (DMSO-d_6, 125 MHz): δ [ppm] = 152.4, 149.8, 142.2, 141.8, 140.7, 140.4, 139.7, 139.6, 139.5, 129.5, 128.8, 127.8, 127.7, 122.0, 118.3, 118.2, 19.8, 19.7. **MS** (EI, 70 eV): *m/z* = 386.

1-(4-(6,7-dimethylquinoxalin-2-yl)phenyl)-3-(pyridin-2-yl)urea 10 k

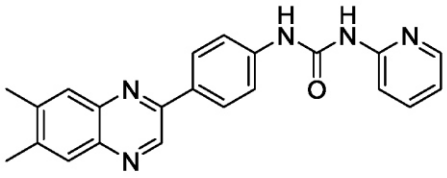

The 1-(4-(6,7-dimethylquinoxalin-2-yl)phenyl)-3-(pyridin-2-yl)urea **10k** was obtained as a green solid (45 mg, 36 %) using the same procedure as described for **10a** starting from pyridin-2-amine (32 mg, 0.34 mmol). **HPLC**: R_t = 5.12 min. **^{1}H-NMR** (DMSO-d_6, 500 MHz): δ [ppm] = 10.73 (s, 1H), 9.52 (s, 1H), 9.43 (s, 1H), 8.33- 8.27 (m, 3H), 7.87 (d, 2H, *J* = 14.6 Hz), 7.79-7.73 (m, 3H), 7.54 (d, 1H, *J* = 8.4 Hz), 7.05-7.03 (m, 1H), 7.49 (d, 6H, *J* = 3.4 Hz). **^{13}C-NMR** (DMSO-d_6, 125 MHz): δ [ppm] = 152.7, 152.0, 149.7, 146.9, 142.3, 141.0, 140.7, 140.3, 139.7, 139.6, 138.6, 130.2, 127.9, 127.7, 118.8, 117.7, 112.0, 19.8, 19.7. **MS** (EI, 70 eV): *m/z* = 369.

1-(4-(6,7-dimethylquinoxalin-2-yl)phenyl)-3-(3-phenoxypyridin-2-yl)urea 10l

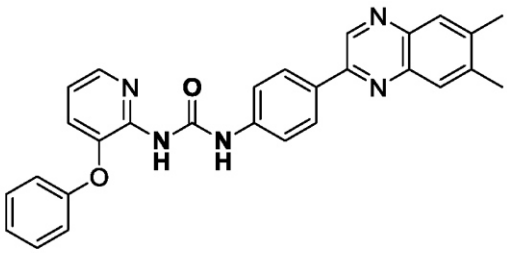

The 1-(4-(6,7-dimethylquinoxalin-2-yl)phenyl)-3-(3-phenoxypyridin-2-yl)urea **10l** was obtained as a yellow solid (63 mg, 42 %) using the same procedure as described for **10a** starting from 3-phenoxypyridin-2-amine (64 mg, 0.35 mmol). **HPLC**: R_t = 7.27 min. **^{1}H-NMR** (DMSO-d_6, 500 MHz): δ [ppm] = 11.95 (s, 1H), 9.46 (s, 1H), 8.37 – 8.25 (m, 3H), 8.00 (dd, 1H, *J* = 5.0, 1.4 Hz), 7.95 – 7.87 (m, 2H), 7.84 (d, 1H, *J* = 8.8 Hz), 7.59 (d, 1H, *J* = 1.5 Hz), 7.55 (dd, 1H, *J* = 8.1, 1.4 Hz), 7.48 – 7.41 (m, 2H), 7.40 – 7.35 (m, 1H), 7.09 (dd, 1H, *J* = 8.0, 5.0 Hz,), 5.31 (s, 2H), 2.52 (s, 3H), 2.51(s, 3H). **^{13}C-NMR** (DMSO-d_6, 125 MHz): δ [ppm] = 175.1, 171.8, 167.4, 166.1, 161.0, 150.7, 143.1, 142.4, 140.8, 140.0, 137.1, 136.1, 128.5, 128.2, 128.00, 127.8, 123.2, 121.2, 119.9, 119.4, 117.9, 112.9, 109.2, 19.8, 19.8.

6,7-dimethoxy-2-(4-nitrophenyl)quinoxaline 13a

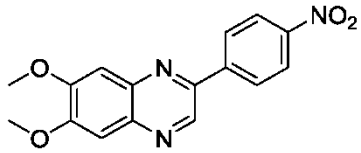

Pd/C (10 %, 30 mg) was added under argon to a stirred solution of 1,2-dimethoxy-4,5-dinitrobenzene **11a** (100 mg, 0.44 mmol) in methanol (5 mL). The mixture was flushed with hydrogen and stirred 4 hours at room temperature. Afterwards the suspension was filtered through a pad of celite and the solvent was concentrated under vacuum to 1 mL. This solution was added to a second solution of 2-(4-nitrophenyl)-2-oxoacetaldehyde **3** (74 mg, 0.45 mmol) in DMF (1.5 mL) and stirred for 1 hour at 80°C. After cooling to room temperature water was added and the obtained brown solid was filtrated, dried and gave 61 mg (44 %). **HPLC**: R_t = 6.87 min. **^{1}H-NMR** ($CDCl_3$, 500 MHz): δ [ppm] = 9.18 (s, 1H), 8.40 (m, 2H), 8.45 (m, 2H), 7.44 (d, 2H, J = 3.0 Hz), 4.11 (d, 6H, J = 2.5 Hz). **^{13}C-NMR** ($CDCl_3$, 125 MHz): δ [ppm] = 154.0, 154.0, 148.7, 147.2, 143.2, 140.0, 139.8, 139.4, 128.0, 124.4, 107.1, 106.4, 56.7, 56.7.

4-(6,7-dimethoxyquinoxalin-2-yl)aniline 14a

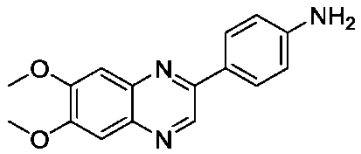

Acetic acid (0.45 mL), Fe (57 mg, 1.02 mmol) and $FeCl_3$ (57 mg, 0.17 mmol) were added to a solution of 6,7-dimethoxy-2-(4-nitrophenyl)quinoxaline **13a** (53 mg, 0.17 mmol) in ethanol (2.5 mL) and stirred for 1 hour at 80°C. After cooling to room temperature the obtained brown solid was filtrated and dried. The filtrate was extracted three times with dichloromethane. The combined organic layers were dried over $MgSO_4$, filtered and the solvent was removed under vacuum to give 46 mg (96 %) of brown solid and was used without further purification. **HPLC**: R_t = 1.73 min. **^{1}H-NMR** (DMSO-d_6, 500 MHz): δ [ppm] = 9.17 (s, 1H), 8.00 (d, 2H, J = 8.4 Hz), 7.35 (d, 2H, J = 4.8 Hz), 6.70 (d, 2H, J = 8.4 Hz), 5.59 (s, 2H), 3,96 (d, 6H, J = 8.9 Hz).

1-(5-*tert*-butylisoxazol-3-yl)-3-(4-(6,7-dimethoxyquinoxalin-2-yl)phenyl)urea 15a

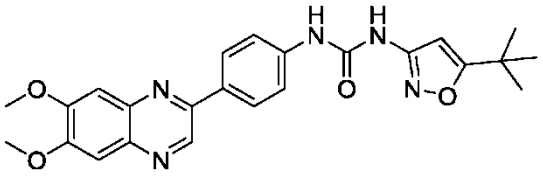

To solution of 5-*tert*-butylisoxazol-3-amine **7** (30 mg, 0.21 mmol) in dichloromethane (2 mL) and triphosgene (16 mg, 0.05 mmol) was added dropwise at -10°C a solution of triethylamine (58 µL, 0.42 mmol) in dichloromethane (1 mL). The mixture was stirred for 1 hour at this temperature. Afterwards a solution of 4-(6,7-dimethoxyquinoxalin-2-yl)aniline **14a** (46 mg, 0.16 mmol) in toluene (1.5 mL) was added and the mixture was stirred for 2 hours at 110°C. After cooling to room temperature water was added and extracted three times with ethyl acetate. The combined organic layers were dried over $MgSO_4$, filtrated and the solvent was removed under vacuum. After purification by flash chromatography (RediSep Column: 13 g C 18 gold, water : acetonitrile = 0 % → 95 % acetonitrile in 12 min) 23 mg (48 %) of a yellow solid was obtained. **HPLC**: R_t = 7.17 min. **^{1}H-NMR** (DMSO-d_6, 500 MHz): δ [ppm] = 9.58 (s, 1H), 9.30 (s, 1H), 9.04 (s, 1H), 8.26-8.23 (m, 2H), 7.67-7.64 (m, 2H), 7.42 (d, 2H, *J* = 7.4 Hz), 6.54 (s, 1H), 3.99 (d, 6H, *J* = 7.2 Hz), 1.31 (s, 9H). **^{13}C-NMR** (DMSO-d_6, 125 MHz): δ [ppm] = 180.3, 158.3, 152.8, 152.1, 151.2, 148.1, 140.5, 140.1, 138.6, 137.9, 130.5, 127.5, 118.5, 106.7, 106.6, 92.5, 56.0, 28.3. **MS** (EI, 70 eV): *m/z* = 447.

7-methoxy-2-(4-nitrophenyl)quinoxaline 13b

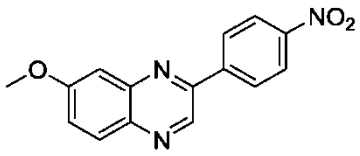

Pd/C (10 %, 54 mg) was added under argon to a stirred solution of 4-methoxy-2-nitroaniline **11b** (180 mg, 1.07 mmol) in methanol (8 mL). The mixture was flushed with hydrogen and stirred 4 hours at room temperature. Afterwards the suspension was filtered through a pad of celite and the solvent was concentrated under vacuum to 1 mL. This solution was added to a second solution of 2-(4-nitrophenyl)-2-oxoacetaldehyde **3** (192 mg, 1.07 mmol) in DMF (3 mL) and stirred for 1 hour at 80°C. After cooling to room temperature water was added and the obtained yellow solid was filtrated, dried and gave 235 mg (78 %). **HPLC**: R_t = 6.87 min. **^{1}H-NMR** ($CDCl_3$, 500 MHz): δ [ppm] = 9.22 (s, 1H), 8.42-8.36 (m, 4H), 8.04 (d, 1H, *J* = 9.0 Hz), 7.48-7.45 (m, 2H), 4.02 (s, 3H). **^{13}C-NMR** ($CDCl_3$, 125 MHz): δ [ppm] = 161.7, 149.5, 149.0, 144.2, 143.0, 140.2, 139.5, 130.3, 128.4, 124.5, 124.4, 107.0, 56.1.

4-(7-methoxyquinoxalin-2-yl)aniline 14b

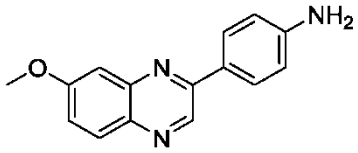

Acetic acid (1.87 mL), Fe (261 mg, 4.68 mmol) and $FeCl_3$ (127 mg, 0.78 mmol) were added to a solution of 7-methoxy-2-(4-nitrophenyl)quinoxaline **13b** (220 mg, 0.78 mmol) in ethanol (10 mL) and stirred for 1 hour at 80°C. After cooling to room temperature the solvent was removed and the residual amount was diluted in dichloromethane and was washed with water. The organic layer was dried over $MgSO_4$, filtered and the solvent was removed under vacuum. After purification by silica gel column chromatography (cyclohexane/ethyl acetate 1:1) 153 mg (78 %) of yellow solid was obtained. **HPLC**: R_t = 2.43 min. **^{1}H-NMR** (DMSO-d_6, 500 MHz): δ [ppm] = 9.23 (s, 1H), 8.07-8.04 (m, 2H), 7.89 (d, 1H, *J* = 9.0 Hz), 7.36-7.32 (m, 2H), 6.73-6.70 (m, 2H), 5.72 (s, 2H), 3.95 (s, 3H). **^{13}C-NMR** (DMSO-d_6, 125 MHz): δ [ppm] = 160.4, 151.3, 151.2, 143.3, 140.2, 136.1, 129.7, 128.5, 123.0, 120.7, 113.8, 106.7, 55.7.

1-(5-*tert*-butylisoxazol-3-yl)-3-(4-(7-methoxyquinoxalin-2-yl)phenyl)urea 15b

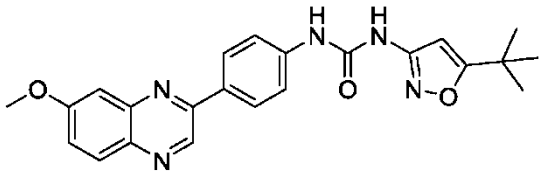

To solution of 5-*tert*-butylisoxazol-3-amine **7** (50 mg, 0.36 mmol) in dichloromethane (5 mL) and triphosgene (36 mg, 0.12 mmol) was added dropwise at -10°C a solution of triethylamine (100 µL, 0.72 mmol) in dichloromethane (1 mL). The mixture was stirred for 1 hour at this temperature. Afterwards a solution of 4-(7-methoxyquinoxalin-2-yl)aniline **14b** (90 mg, 0.36 mmol) in toluene (2 mL) was added and the mixture was stirred for 2 hours at 110°C. After cooling to room temperature water was added and extracted three times with dichloromethane. The solid was diluted in a small amount of DMF and heated to 100°C. Water was added and the obtained light yellow solid was filtrated to give 66 mg (44 %) **HPLC**: R_t = 7.65 min. **^{1}H-NMR** (DMSO-d_6, 500 MHz): δ [ppm] = 9.59 (s, 1H), 9.37 (s, 1H), 9.09 (s, 1H), 8.31-8.32 (m, 2H), 7.98 (d, 1H, *J* = 9.0 Hz), 7.69-7.66 (m, 2H), 7.47-7.43 (m, 2H), 6.54 (s, 1H), 3.98 (s, 3H), 1.31 (s, 9H). **^{13}C-NMR** (DMSO-d_6, 125 MHz): δ [ppm] = 180.3, 160.6, 158.3, 151.2, 150.5, 143.2, 141.1, 140.5, 136.8, 130.1, 129.8, 128.1, 122.1, 118.5, 106.9, 92.5, 55.9, 28.3. **MS** (EI, 70 eV): *m/z* = 417.

III. Molecular Docking

In the following sections, various methods for modeling of small molecules and proteins with the Molecular Operating Environment 2013.08 of the Chemical Computing group are described.[11]

Development of homologous kinase structures

The PDB entries close homologs of FLT3 (PDB: 1RJB) be the function "MOE | Compute kinase Search | | biopolymer" is searched with the default settings (DFG in / out; any alpha.C , Res <2.5 ; Identity > 50%). The sequences (fasta) are taken from the PDB database. The homology models are created with the "SE | Homology model | protein". A force-field is "Amber12 : EHT" (Distance) used. For each PDB entry 25 main chain models are used. The refinement of the models is carried out with the following settings: Intermediates: Medium; Model Scoring: GB / VI; Final model medium. In addition, the calculation in different threads 4 is performed. After creating the models are refined with the "Protonate 3D" and examines deviations from the template in the form of RMSD values and Phi - Psi angles.

Docking of ligands

The protein is prepared with the "Structure Preparation" and "Protonate 3D". Here, the structure of the hydrogen atoms to be added is added protons and error corrected structure. Water molecules are removed for docking. For refinement of the model receptor atoms are fixed in the vicinity of the active site. The ligands are drawn with ChemDraw and transferred to a MOE database; larger amounts of ligand are given out freely available in the respective chapter, taken from databases. (Rescoring 1 Triangle Matcher : London dG (30); Refinement : MMFF94x ForceField ; Rescoring2 : GBVI / ESC dG placement function) to docking individual molecules, the "Induced Fit" protocol. Here, the protein side chains in the refinement step are considered. For docking large ligands numbers is the "Virtual Screening" protocol (Placement Function : Triangle Matcher; rescoring 1 : London dG (30)). Here, the calculation time is omitted, a refinement for the reduction.

Creating Pharmacophores

A database of FLT3 inhibitors is transferred from http://www.bindingdb.org in a MOE database. Inhibitors, for which no IC50 value is described, are deleted. For salts, the smaller molecule or atom is removed and neutralized the protonation of the inhibitors. The database is (8 active , 43 inactive inhibitors) and a test set (110 active , 247 inactive inhibitors) divided into a training set. In the program function "MOE | Compute | pharmacophores | Elucidation" different conformations as "Conformation Import Unique" before pharmacophore creation be

generated. Molecules with an IC50 value of less than 10 nM are classified as active (n = 8), inhibitors with IC50 > 1000 nm as inactive (n = 290). Among the existing standard pharmacophore elements is "Aro | PiN , Radius 1.4, without Limit" added. In addition, the following settings are used: coverage : 0.8 , qcluster : 1.25 , qspacing : 0.6 , o_aro : 1, o_lpa : 1, maxfeatures : 5".

IV. FTL-3 *in vitro* assay conducted by Cerep

1. Reference compound Data

Assay: FLT-3 Kinase *(h)*

Reference compound: Staurosporine

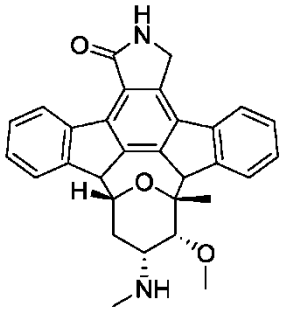

IC_{50} (M) = 9.1E-10

nH = 1.7

2. Experimental conditions

Assay: FLT-3 Kinase *(h)*

Source: human recombinant (insect cells)

Substrate: ATP + Ulight-CAGAGAIETDKEYYTVKD (100 nM)

Incubation: 90 min, RT

Measured Component: Phospho-Ulight- CAGAGAIETDKEYYTVKD

Detection Method: LANCE

3. Analysis and expression of results

The resulted technical replicates are expressed as a percent of control specific activity ((measured specific activity/control specific activity) x 100) obtained in the presence of the compounds.

The IC_{50} value (concentration causing a half-maximal inhibition of control specific activity) and Hill coefficient(s) (nH) were determined by non-linear regression analysis of the

inhibition curve generated with mean replicate values using Hill equation curve fitting (Y D + [(A-D)/(1-(IC_{50})^{nH})], where Y = specific activity, D = minimum specific, A = maximum specific activity, C = compound concentration, C_{50} = IC_{50}, and nH = slope factor).
This analysis was performed using software developed at Cerep (Hill software) and validated by comparison with data generated by the commercial software SigmaPlot® 4.0 for Windows® (1997 by SPSS inc.).

IV. Toxicity assay: Determination of the *in vivo* activity on zebrafish embryos

The zebrafish embryos were collected and placed into 24-well plates, ten embryos per well and maintained in E3 medium at 28°C. Compounds were added 24 hpf and the embryos allowed to grow in chemical compound solution up to 5 days. The phenotypes were compared using the StereoBlue Bino Zoom microscope system from Euromex. Pictures were taken with camera Nikon D5000. **Animal husbandry.** All animal experiments were conducted and documented according to the federal and local regulation.

VI. References

1. *Molecular Operating Environment (MOE), 2013.08; Chemical Computing Group Inc., 1010 Sherbooke St. West, Suite #910, Montreal, QC, Canada, H3A 2R7, 2013.*

4.3 *Small molecule* Kinase-Inhibitoren für LRRK2 und ihre Anwendung in Modellen der Parkinson-Krankheit

Der Inhalt dieses Kapitels wurde bereits veröffentlicht.[186]

Autoren: Thomas Kramer, Fabio Lo Monte, Stefan Göring, Ghislaine Marlyse Okala Amombo, Boris Schmidt.

Titel: „Small Molecule Kinase Inhibitors for LRRK2 and their Application to Parkinson's Disease Models".

Journal: ACS Chemical Neuroscience.

DOI: 10.1021/cn200117j.

Zusammenfassung:

Die Parkinson-Krankheit ist nach der Alzheimer-Krankheit die zweithäufigste neurodegenerative Erkrankung. Unterschiedliche Genmutationen konnten bereits in Verbindung mit dieser Krankheit gebracht werden. Mutationen des Gens PARK8, welches für LRRK2 codiert, stellen die häufigste Ursache für das sporadische und für das familiäre Parkinson-Syndrom dar. LRRK2 ist aus mehreren Domänen aufgebaut und bildet einen großen Proteinkomplex. Mutationen konnten bereits in allen Domänen identifiziert werden. In der Kinase-Domäne befindet sich die am häufigsten vorkommende G2019S-Mutation. Sie ist für die gesteigerte Kinase-Aktivität verantwortlich.

Zurzeit stehen nur sehr wenige *in vitro* und *in vivo* Daten bezüglich LRRK2 zur Verfügung, da es erst seit geraumer Zeit im Fokus akademischer und industrieller Gruppen steht. Dieser Übersichtsartikel befasst sich mit den bereits publizierten ATP-kompetitiven Kinaseinhibitoren und gibt einen Überblick über die bislang identifizierten Mutationen in LRRK2 wieder. Einige Inhibitoren weisen Aktivitäten im nanomolarem Bereich auf und konnten ihre Selektivität in Kinase-Paneln unter Beweis stellen. Jedoch bleibt der limitierende Faktor der Hirngängigkeit, den es zu überwinden gilt. Außerdem werden bestehende Tiermodelle vorgestellt und das Potential von LRRK2 als potentielles Target zur Behandlung der Parkinson-Krankheit kritisch diskutiert.

ACS Chemical Neuroscience

Review

pubs.acs.org/acschemicalneuroscience

Small Molecule Kinase Inhibitors for LRRK2 and Their Application to Parkinson's Disease Models

Thomas Kramer,[†] Fabio Lo Monte,[†] Stefan Göring, Ghislaine Marlyse Okala Amombo, and Boris Schmidt*

Clemens Schöpf - Institute of Organic Chemistry and Biochemistry, Technische Universität Darmstadt, 64287 Darmstadt, Germany

ABSTRACT: Parkinson's disease (PD) is the second most common neurodegenerative disorder. Several single gene mutations have been linked to this disease. Mutations in the gene encoding leucine-rich repeat kinase 2 (LRRK2) indicate LRRK2 as promising therapeutic target for the treatment of PD. LRRK2 mutations were observed in sporadic as well as familial PD patients and have been investigated intensively. LRRK2 is a large and complex protein, with multiple enzymatic and protein-interaction domains, each of which is effected by mutations. The most common mutation in PD patients is G2019S. Several LRRK2 inhibitors have been reported already, although the crystal structure of LRRK2 has not yet been determined. This review provides a summary of known LRRK2 inhibitors and will discuss recent in vitro and in vivo results of these inhibitors.

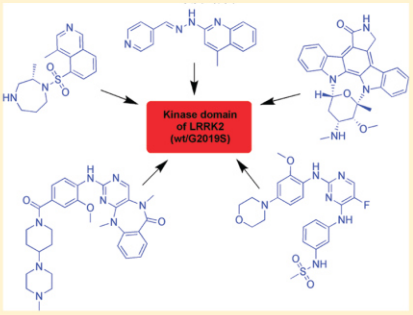

KEYWORDS: *Parkinson's disease, leucine-rich repeat kinase 2 (LRRK2), LRRK2 inhibitors, mutations, animal models*

Parkinson's disease (PD) is the second most prevalent neurodegenerative disorder after Alzheimer's disease, effecting up to ~4% of the population over 80.[1,2] PD is characterized by a large number of motoric and non-motoric symptoms. Four of them are designated as cardinal features: tremor at rest, rigidity, akinesia, and postural instability.[3] PD patients usually develop dementia during the course of the disease and gradually develop depression. The National Institute for Health and Clinical Excellence (NICE, U.K.) published guidelines for the diagnosis and management of patients with PD, which is used by most experts.[2,4] The typical hallmarks of PD in post-mortem brain tissue are loss of dopaminergic neurons of the substantia nigra, associated with the formation of fibrillar aggregates composed of α-synuclein and other proteins (e.g. Lewy bodies).[5,6] Presently, there is no cure for PD and the mainstay therapy is still the drug levodopa (L-Dopa).[2,7] L-Dopa is highly effective in reducing motor symptoms; nevertheless, there are two major problems, the side-effects and that patients become therapy resistant.[7,8] Adenosine A2a receptor antagonists have been shown to reduce PD-like features in animal studies through interaction with the specific dopamine receptor subtype D2 in the basal ganglia, making it more sensitive to dopamine. The adenosine A2a receptor antagonists SYN-115 from Synosia Therapeutics is currently in a phase IIb trial.[7] Other approaches are the metabotropic glutamate receptors (mGluRs), which are members of the G-protein-coupled receptor (GPCR) superfamily. They participate in the modulation of synaptic transmission and neuronal excitability throughout the central nervous system. Several studies indicate the therapeutic utility of mGluR ligands in neurological and psychiatric disorders and make mGluRs promising targets for non-dopaminergic drug discovery in PD. $mGluR_5$ is the target of drug development programmes at major pharmaceutical companies, e.g. Roche and Novartis.[7,9,10]

Several single gene mutations have been identified and linked to PD, for example, DJ-1, UCH-L1, SNCA, PRKN, and LRRK2.[1,2,5,11−14] However, mutations in the LRRK2 gene are the most common cause of familial and sporadic late-onset PD.[15] Since the LRRK2 gene mutations have been linked to PD, several inhibitors were reported to inhibit this kinase. We reviewed the literature and summarized the relevant data.

■ LRRK2: STRUCTURE AND MUTATIONS

The leucine-rich repeat kinase 2 (LRRK2) encodes a large multidomain protein with 2527 amino acids. Several independent domains have been established or predicted for the LRRK2 protein, including an ankyrin-like (ANK) domain, a leucine-rich repeat (LRR) domain, a Ras (renin-angiotensin system) of complex (Roc) domain, which belongs to the Ras GTPase family, followed by a C-terminal of ROC (COR) domain, a kinase (Kinase) domain, and a C-terminal WD40 domain (Figure 1).[16−18]

Beside the structural homology to the MAP kinase kinase kinases (MAPKKK) LRRK2 shares other biochemical features with MAPKKK, like autophosphorylation and interaction with kinase-specific chaperones.[19] LRRK2 is expressed in various brain regions and in several other organs, for example, in the lung, kidney, and heart.[20−22] LRRK2 efficiently phosphorylates

Received: November 25, 2011
Accepted: January 18, 2012
Published: January 18, 2012

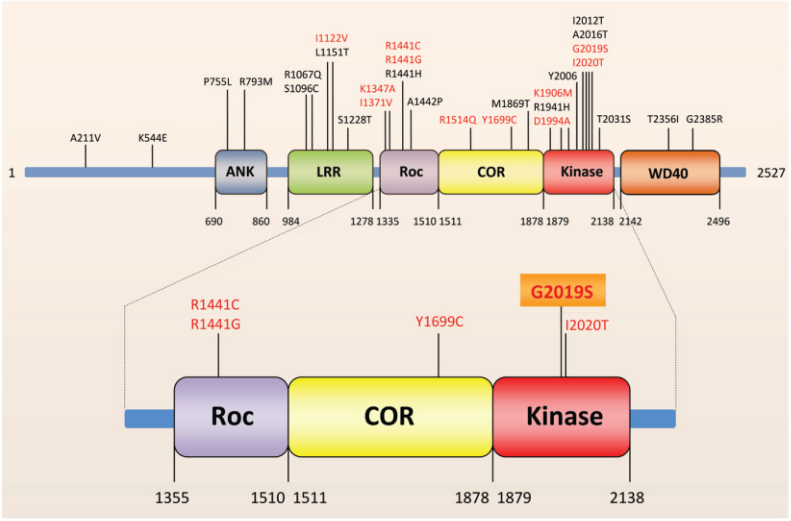

Figure 1. Schematic illustration of domains and most common PD-linked point mutations of LRRK2. Red marked mutations have been linked to altered kinase activity. ANK, ankyrin-like domain; LRR, leucin-rich repeat domain; Roc, Ras of complex domain, which belongs to the Ras GTPase family; COR, C-terminal of Roc domain; Kinase, kinase domain; WD40, C-terminal WD40 domain. The five putatively pathogenic mutations are enlarged.

moesin at Thr^{558} in vitro, raising the idea that moesin may be a physiological substrate of LRRK2. Moreover, ezrin and radixin are phosphorylated by LRRK2, which are involved in moesin binding actin.[23,24] LRRK2 predominantly exists as a dimer under native conditions. The wild-type (wt) LRRK2 dimer displays increased kinase activity versus its monomeric counterpart.[25,26] More than 20 LRRK2 mutations have been linked to autosomal-dominant parkinsonism, and five of them are considered definitely pathogenic (R1441C, R1441G, Y1699C, G2019S, I2020T).[17,18,27] The most common mutation, which is present in more than 85% of PD patients carrying LRRK2 mutations, is G2019S.[28] In some ethnic groups the frequency of the LRRK2-G2019S mutation has been found to be even higher. For example, 13−40% of all PD patients in the Ashkenazi Jewish and northern African Arab population have this mutation, whereas in the Asian population this mutation is much less common.[17,28] The G2019S, R1441C, and R1441G mutations increase the LRRK2 kinase activity and both the kinase as well as the GTPase activities of LRRK2 are required to induce cell death.[6,29−32] The GTPase domain-associated R1441C mutation in combination with the G2019S kinase domain mutation increased the kinase activity up to 7-fold relative to wild-type protein.[33] It was reported that expression of G2019S mutant in Drosophila dendritic arborization neurons causes several dendrite defects, including tau mislocalization in dendrites, tau hyperphosphorylation at the T^{212}/S^{214} sites, dendrite degeneration, and microtubule fragmentation.[34] Furthermore, the LRRK2-G2019S mutant caused a progressive degeneration of nigral dopaminergic neurons in rats.[35] In addition, the autokinase activity of the LRRK2 mutant I2020T was found to be increased in comparison to wild-type.[19] Mutations within or near the GTPase domain including R1514Q, Y1699C, and I1371V increase kinase activity, while the alteration of the lysine residue K1347A leads to an ablation of this. The I1122V mutation in the LRR domain nominally increases kinase activity, whereas the D1994A and K1906M mutations in the kinase domain are able to diminish respectively to inhibit kinase activity.[31] Replacing the kinase domain with a "kinase-dead" version blocks inclusion body formation and delays cell death.[36] In addition, LRRK2 is able to phosphorylate MAPKKK 3, 4, 6, and 7 in vitro. This indicates that MAPKKK are molecular targets of LRRK2 mutants, whereby LRRK2 could be linked to neurotoxicity, cellular stress, and apoptosis.[37,38] LRRK2 provides a potential therapeutic target utilizing the knowledge gained in neuroprotective kinase inhibition.

■ IN VIVO MODELS AND STUDIES

Several studies using in vivo models of LRRK2 fostered the understanding of neurobiology, pathogenesis, and utility of potential therapeutics. The Drosophila model revealed that a LRRK2 loss-of-function mutant leads to significantly impaired locomotive activity and that LRRK2 is critical for the integrity of dopaminergic neurons (DA).[39] Another study showed that transgenic Drosophila harboring G2019S, Y1699C, or G2385 LRRK2 variants exhibit late-onset loss of DA and reduced lifespan.[40] Liu et al. used the GAL4/UAS system to generate transgenic Drosophila expressing either wild-type human LRRK2 or LRRK2-G2019S. They reported that expression of either wild-type human LRRK2 or LRRK2-G2019S in the photoreceptor cells caused retinal degeneration. Furthermore, they observed that expression of LRRK2 or LRRK2-G2019S in neurons produced adult-onset selective loss of dopaminergic neurons and locomotor dysfunction.[41,42] Overexpression of human LRRK2 wild-type, R1441C, and G2019S in DA of transgenic *C. elegans* models was sufficient to induce neurodegeneration and behavioral deficits, whereas knockout of the *C. elegans* LRRK2 homologue, LRK-1, prevents the LRRK2-induced neurodegeneration.[43] The blockage of zebrafish LRRK2 protein by morpholinos caused embryonic lethality and severe development defects such as growth retardation and loss of neurons. In addition, the deletion of the WD40 domain of zebrafish LRRK2 by morpholinos revealed Parkinsonism-like

Table 1. Staurosporine and Derivatives as LRRK2 Inhibitors

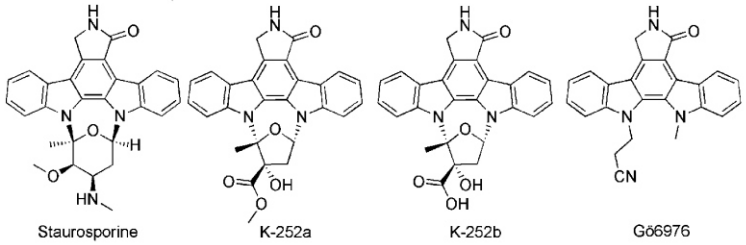

		IC_{50}					
no.	name	wild-type LRRK2	LRRK2-G2019S	substrate	selectivity[a]	in vivo	lit.
1	Staurosporine	~1 nM;[b] 2 nM;[b] 8.2 nM;[d] 40 nM[e]	0.2 nM;[f] 1.8 nM;[c] 40 nM[e]	GST-moesin; LRRKtide; MBP[g]	2		58, 60−62
2	K-252a	~25 nM;[b] 3.6 nM[c]	2.8 nM[c]	LRRKtide			60, 61
3	K-252b	~50 nM[b]		LRRKtide			61
4	Gö6976	~250 nM[b]		LRRKtide			61

[a]Number of all kinases, including LRRK2. [b]Goat GST-LRRK2. [c]GST-LRRK2 (970−2527; wt/G2019S). [d]full-length LRRK2. [e]GST-LRRK2 (wt/G2019S). [f]Full-length Strep-tag LRRK2 (G2019S). [g]Myelin basic protein (MBP).

phenotypes, including loss of dopaminergic neurons in the diencephalon and locomotion defects.[44] Remarkably, another research group failed to reproduce the phenotypic loss of dopaminergic neurons in zebrafish.[45] Nevertheless, the zebrafish model may be a useful vertebrate model. The presence of a LRRK2 protein excess in LRRK2 wild-type and G2019S mice showed exacerbated α-synuclein A53T-mediated cytotoxicity. This result raised the idea that inhibition of LRRK2 expression may provide an applicable strategy to ameliorate α-synuclein-induced neurodegeneration in PD.[46] Expression of full-length LRRK2 wild-type did not induce any significant neuronal loss in the nigrostriatal system of adult rats, whereas expression of human LRRK2-G2019S mutant causes progressive degeneration of nigral dopaminergic neurons.[35] Bacterial artificial chromosome (BAC) transgenic mice expressing LRRK2 wild-type, LRRK2-R1441G, and LRRK2-G2019S have shown evidence of neurodegeneration.[24,47,48] Furthermore, the LRRK2-R1441G BAC transgenic mice revealed tau to be hyperphosphorylated in brain tissues.[48] However, LRRK2 knockout mice lacking the kinase domain of LRRK2 are viable and live a normal life span. Thus, LRRK2 is not essential for mouse development and maintenance of DA.[49] However, expression of the human LRRK2-G2019S mutation in transgenic mice is sufficient to recreate the slowly progressive degeneration of dopaminergic neurons that forms the hallmark pathology of familial and sporadic PD.[50] Several mice studies investigated the potential of LRRK2 as therapeutic strategy for the treatment of PD.[51−57] Two independent lines of LRRK2 germ-line deletion mice indicated that LRRK2 plays an essential role in the regulation of protein homeostasis during aging. Therefore, the authors concluded that LRRK2 inhibition may not represent a suitable therapeutic strategy for the treatment of PD.[54] Another research group created inducible transgenic rats expressing LRRK2 with G2019S substitution and recapitulated the initiation process of dopaminergic dysfunction. However, the mutation was not sufficient to develop dopaminergic neurodegeneration or to induce neuron death in transgenic rats.[57] Data obtained from a R1441C knockin mouse suggested that this mutation impairs stimulated dopamine neurotransmission and D2 receptor function. The R1441C mutation could represent pathogenic precursors preceding dopaminergic degeneration in PD brains.[53] A novel herpes simplex virus (HSV) amplicon-based mouse model of LRRK2 dopaminergic neurotoxicity was developed to determine the efficacy of several LRRK2 kinase inhibitors. Nonetheless, a significant loss of tyrosine hydroxylase-positive neurons was induced due to HSV amplicon-mediated delivery of LRRK2-G2019S, whereas the HSV amplicon-mediated delivery of LRRK2-D1994A caused no neuronal loss. The injection of the LRRK2 kinase inhibitors can attenuate the loss of tyrosine hydroxylase-positive neurons induced by HSV-G2019S. Thus, the inhibition of LRRK2 kinase activity may hold potential to protect against LRRK2 toxicity and consequently for the treatment of neurodegeneration in PD.[58] Hence, LRRK2 kinase inhibition holds potential for the treatment of PD. In the following, we will give a summary of small molecule LRRK2 kinase inhibitors. The inhibition effect of $ROCO^{LRRK2}$ fragments will not be discussed.[59]

■ SMALL MOLECULE KINASE INHIBITORS FOR LRRK2

LRRK2 is a large protein with several discrete domains. It surfaced as a therapeutic target when the kinase activity and the most common LRRK2 mutation, G2019S, were associated with neurotoxicity and PD. The first LRRK2 inhibitors derived from library screening efforts were mostly ATP-competitive. There are only few inhibitors, which were specifically developed to inhibit LRRK2. Thus, the majority of the compounds inhibits more than one kinase at the concentration indicated in the tables. The data in Table 1 derived from a limited number of in vitro assays using wild-type LRRK2 and G2019S-LRRK2. These assays vary in the concentration of LRRK2-constructs, substrate, and ATP; thus, the mere comparison of IC_{50} is misleading. The high sensitive assays utilize radioisotopes, which allow detection of both autophosphorylation and substrate phosphorylation, but are less suitable for high-throughput screening (HTS). High-throughput capability was achieved by time-resolved fluorescence resonance energy transfer (TF-FRET) and the amplified luminescent proximity homogeneous (AlphaScreen) assays.[62] Although truncated LRRK2 and its full-length analog display similar phosphorylation activity, differences have been noticed. This may be a

Table 2. Maleimide Derivatives as LRRK2 Inhibitors

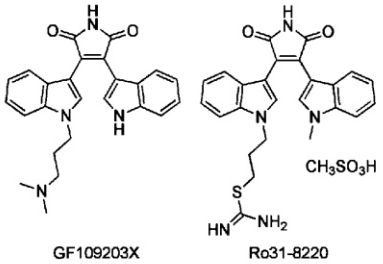

		IC$_{50}$					
no.	name	wild-type LRRK2	LRRK2-G2019S	substrate	selectivity[a]	in vivo	lit.
5	GF109203X	2190 nM[b]	2620 nM[b]	MBP[c]	2		58
6	Ro31-8220	2671 nM;[d] 50 nM[b]	1922 nM;[d] 5160 nM[b]	LRRKtide; MBP[c]	2		58, 60

[a]Number of all kinases, including LRRK2. [b]GST-LRRK2 (wt/G2019S). [c]Myelin basic protein (MBP). [d]GST-LRRK2 (970-2527; wt/G2019S).

Table 3. 5-Iodotubericidin as LRRK2 Inhibitor

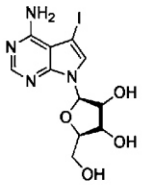

		IC$_{50}$					
no.	name	wild-type LRRK2	LRRK2-G2019S	substrate	selectivity[a]	in vivo	lit.
7	5-iodo-tubericidin	14780 nM[b]	3410 nM[b]	MBP[c]	2		58

[a]Number of all kinases, including LRRK2. [b]GST-LRRK2 (wt/G2019S). [c]Myelin basic protein (MBP).

Table 4. Sorafenib as LRRK2 Inhibitor

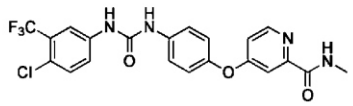

		IC$_{50}$					
no.	name	wild-type LRRK2	LRRK2-G2019S	substrate	selectivity[a]	in vivo	lit.
8	sorafenib	5580 nM[b]	1230 nM[b]	MBP[c]	2	*C. elegans*; Drosophila	58

[a]Number of all kinases, including LRRK2. [b]GST-LRRK2 (wt/G2019S). [c]Myelin basic protein (MBP).

result from the utilization of different substrates, for example, LRRKtide and myelin basic protein (MBP).[60,63]

Staurosporine (**1**) is one of the widely used kinase inhibitors. This unselective compound equipotently inhibited both wild-type LRRK2 and LRRK2-G2019S (truncated and full-length) with an IC$_{50}$ ranging from 0.2 to 40 nM (Table 1).[58,60−62] Its inhibitory effect concerning LRRK2 was determined in different in vitro assays, for example, radioactive, TF-FRET, and AlphaScreen assay. These assays utilized different substrates such as synthetic peptides, for example, LRRKtide and potential physiological substrates: GST-Moesin. Staurosporine (**1**) had a similar inhibitory profile against LRRK1/LRRK2 autophosphorylation and MBP phosphorylation.[58] Its isoindolinone derivatives K-252a/b (**2**/**3**) and Gö6976 (**4**) also inhibited wild-type LRRK2 and LRRK2-G2019S in the nanomolar range, whereas the maleimide analoga GF109203X (**5**) and Ro31-8220 (**6**) inhibited wild-type and LRRK2-G2019S in the low micromolar range only (Table 2).[58,60,61] Ro31-8220 (**6**) is remarkable for the potent inhibition of MBP phosphorylation with an IC$_{50}$ of 50 nM in the TF-FRET assay.

The inhibitory potency of 5-Iodotubericidin (**7**) (Table 3) and Sorafenib (**8**) (Table 4) was more than 4-fold higher for LRRK2-G2019S compared to wild-type LRRK2.[58] Sorafenib (**8**) was up to 50% more selective for wild-type LRRK2 than for wild-type LRRK1. LRRK2-G2019S induced toxicity in rat primary cortical neuronal cultures (TUNEL assay) was completely protected by 5 μM of Sorafenib (**8**). Furthermore, it protected against LRRK2-G2019S-induced neurodegeneration in *C. elegans* and in Drosophila.[64]

The indolinones GW5074 (**9**) and Indirubin-3'-monoxime (**10**) were ∼3-fold more active concerning LRRK2-G2019S than its corresponding wild-type. GW5074 (**9**) and Indirubin-3'-monoxime (**10**) inhibited LRRK2-G2019S with IC$_{50}$'s of 880 nM and ∼1.3 μM, respectively.[58,61] They inhibited the closely related LRRK1 and LRRK2 in a similar manner. GW5074 (**9**) and Indirubin-3'-monoxime (**10**) inhibited LRRK2-mediated

Table 5. Indolinone Dervivatives as LRRK2 Inhibitors

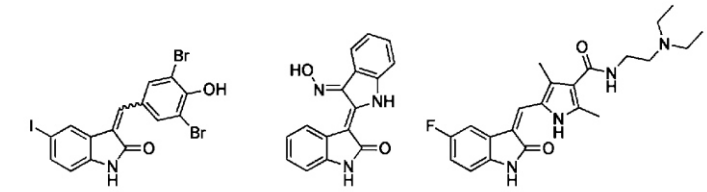

		IC_{50}					
no.	name	wild-type LRRK2	LRRK2-G2019S	substrate	selectivity[a]	in vivo	lit.
9	Raf-1 kinase inhibitor I (GW5074)	~500 nM;[b] 3150 nM[c]	880 nM[c]	LRRKtide; MBP[d]	2	HSV[g] amplicon-based mouse model	58, 61
10	Indirubin-3′-monooxime	4830 nM[c]	1310 nM[c]	MBP[d]	2	HSV[g] amplicon-based mouse model	58
11	Sunitinib	79 nM;[e] 15 nM[f]	19 nM;[e] 26 nM[f]	Nictide; LRRKtide	85		60, 63, 65

[a]Number of all kinases, including LRRK2. [b]Goat GST-LRRK2. [c]GST-LRRK2 (wt/G2019S). [d]Myelin basic protein (MBP). [e]GST-LRRK2 (1326−2527; wt/G2019S). [f]GST-LRRK2 (970−2527; wt/G2019S). [g]Herpes simplex virus.

Table 6. Quinoline Derivatives as LRRK2 Inhibitors

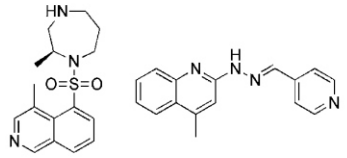

		IC_{50}					
no.	name	wild-type LRRK2	LRRK2-G2019S	substrate	selectivity[a]	in vivo	lit.
12	H-1152	244 nM[b]	600 nM;[c] 150 nM[b]	GST-Moesin; Nictide	85		62, 63, 65
13	Compound 4		4100 nM[d]		13		67

[a]Number of all kinases, including LRRK2. [b]GST-LRRK2 (1326-2527; wt/G2019S). [c]full-length Strep-tag LRRK2 (G2019S). [d]GST-LRRK2 (G2019S).

phosphorylation of LRRKtide and MBP, and additionally the phosphorylation of the eukaryotic translation initiation factor 4E-binding protein (4E-BPI), a putative physiological LRRK2 substrate. Furthermore, they attenuated LRRK2-G2019S induced cell injury and cell death. GW5074 (**9**) rescued the reduction of the density of tyrosine hydroxylase-positive fibers in a herpes simplex virus (HSV) amplicon-based mouse model of LRRK2 dopaminergic neurotoxicity. In addition, GW5074 (**9**) prevented LRRK2-G2019S induced inflammation, increase in isolectin B_4 (ILB4)-positive cells in the striatum and substantia nigra pairs compacta.[58] Both Sorafenib (**8**) and GW5074 (**9**) were found to protect against LRRK2-G2019S-induced neurodegeneration in *C. elegans* and in Drosophila.[64] The well-known kinase inhibitor Sunitinib (**11**) was also investigated concerning its ability to inhibit LRRK2 (Table 5). It inhibited the LRRK2-mediated phosphorylation of Nictide and LRRKtide with an IC_{50} of 15−79 nM (truncated wild-type and LRRK2-G2019S).[60,63,65] The selectivity of Sunitinib (**11**) was profiled in a panel of 85 kinases. Sunitinib (**11**) inhibits LRRK2-G2019S, its wild-type, and 12 further kinases at 1 μM by more than 80%.[60,63,65] However, the less selective Sunitinib (**11**) is capable to suppress the activity of full-length LRRK2 expressed from Swiss-3T3 fibroblast cells.[63] The apparent potency of Sunitinib (**11**) to inhibit wild-type LRRK2 drops to an IC_{50} of 370 nM at cellular ATP concentration (1 mM).[66] In addition, studies of endogenous LRRK2 activity and phosphorylation in EBV-transformed lymphoblastoid cells, derived from a PD patient harboring a homozygous LRRK2-G2019S mutation, revealed that Sunitinib (**11**) inhibited the phosphorylation of Ser^{910} and Ser^{935} more potently than in wild-type cells.[65] A comparable result was observed for the inhibitor H-1152 (**12**) (Table 6). H-1152 (**12**) is a known ROCK2 inhibitor. This compound was profiled in a panel of 85 kinases and found to inhibit Aurora B kinase, BRSK2, wild-type LRRK2, and LRRK2-G2019S at the relevant concentration. H-1152 (**12**) displayed IC_{50}'s ranging from 150 to 600 nM in radioisotope or AlphaScreen phosphorylation assays of wild-type LRRK2 and LRRK2-G2019S. Unfortunately, the structure determination of the LRRK2 kinase domain by X-ray crystallography was not reported yet. A docking analysis of H-1152 (**12**) utilized homology modeling of LRRK2, by superimposing the protein C_α atoms of the LRRK2 model with the reported ROCK1-H-1152 complex. This analysis indicated a backbone interaction with the NH atom of Ala^{1950} (PDB code of ROCK1-H-1152 not published). Furthermore, the two methyl groups of H-1152 (**12**) were observed to make lipophilic contacts with the ATP binding site. The amino acid Ala^{2016} was found to be close to H-1152 (**12**). This can

Table 7. Y-27632 as LRRK2 Inhibitor

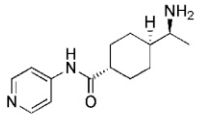

		IC_{50}					
no.	name	wild-type LRRK2	LRRK2-G2019S	substrate	selectivity[a]	in vivo	lit.
14	Y-27632	2300 nM[b]	1800 nM;[c] 1000 nM[b]	GST-Moesin; Nictide	85		62, 63

[a]Number of all kinases, including LRRK2. [b]GST-LRRK2 (1326-2527; wt/G2019S). [c]Full-length Strep-tag LRRK2 (G2019S).

Table 8. Anthracene and Phenanthrene Derivatives as LRRK2 Inhibitors

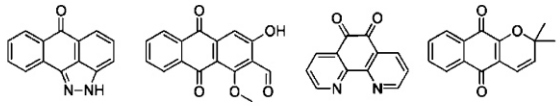

SP600125 Damnacanthal LDN-73794 LDN-22684

		IC_{50}					
no.	name	wild-type LRRK2	LRRK2-G2019S	substrate	substrate selectivity[a]	in vivo	lit.
15	SP600125	3100 nM[b]	5000 nM[b]	MBP[c]	2		58
16	Damnacanthal	7810 nM[b]	9450 nM[b]	MBP[c]	2		58
17	LDN-73794	3500 nM[d]		PLK-peptide	2		68
18	LDN-22684[e]	6900 nM[f]	6100 nM[f]	PLK-peptide			69

[a]Number of all kinases, including LRRK2. [b]GST-LRRK2 (wt/G2019S). [c]Myelin basic protein (MBP). [d]Purified from BAC-transgenic mouse brain. [e]Non-ATP competitive. [f]Human LRRK2 (970-2527; wt/G2019S).

Table 9. Pyrimidine Derivatives as LRRK2 Inhibitors

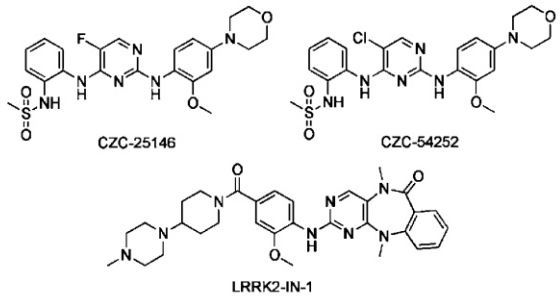

CZC-25146 CZC-54252 LRRK2-IN-1

		IC_{50}					
no.	name	wild-type LRRK2	LRRK2-G2019S	substrate	selectivity[a]	in vivo	lit.
19	CZC-25146	4.76 nM[b]	6.87 nM[b]	LRRKtide	LRRKtide	male CD-1 mice	71
20	CZC-54252	1.28 nM[b]	1.85 nM[b]	LRRKtide	LRRKtide	male CD-1 mice	71
21	LRRK2-IN-1	13 nM[c]	6 nM[c]	Nictide	Nictide	Male C57BL/6 mice	70

[a]Number of all kinases, including LRRK2. [b]Human LRRK2 (wt/G2019S). [c]GST-LRRK2 (1326−2527; wt/G2019S).

contribute to crucial drug resistance, because the IC_{50} of H-1152 (**12**) for the LRRK2 mutant A2016T increased up to ~30-fold.[63] Another commercially available quinoline derivative, Compound 4 (**13**), inhibited the autophosphorylation of LRRK2-G2019S with an IC_{50} of 4.1 μM (Table 6). It was screened in a small kinase panel of 13 kinases at 10 μM concentration. There was no other inhibitory effect, except for MLK1.[67] This observation can be rationalized by the similarity of the kinase domains of MLK and LRRK2. Compound 4 (**13**) was analyzed in a homology model of LRRK2 using the structure of the transforming growth factor-beta (TGF-β) activated kinase 1 (TAK1; PDB code: 2EVA). This homology model of the LRRK2 kinase domain with inhibitor Compound 4 (**13**) indicated hydrogen bond interactions between Compound 4 (**13**) and Ala^{1950}. It was found that the 4-pyridine ring was located in the solvent exposed region of LRRK2. Moreover, a comparison of ATP and Compound 4 (**13**) docking revealed that the 4-methyl quinoline moiety overlapped with the adenine rings of ATP. The treatment of murine dopaminergic SN4741 cells with 10 μM of Compound 4 (**13**) restored their cell survival rates in an oxidative stress-induced test to the level of the control cells. The neurotoxicity test with primary rat cortical neuronal cells revealed cell survival rates of 85% at 10 μM and a significantly increased toxicity at 100 μM.[67] In a kinase panel of 85 kinases the known ROCK inhibitor Y-27632 (**14**) was found to additionally inhibit PRK2,

Table 10. Pharmocokinetic Profile of the Currently Best Published LRRK2 inhibitors CZC-25146 and LRRK2-IN-1[a]

name	route	dose (mg/kg)	T_{max} (h)	C_{max} (ng/mL)	$AUC_{0-\infty}$ (h·ng/mL)	$T_{1/2}$ (h)	CL (mL/min/kg)	V_{ss} (L/kg)	F (%)	BBB penetration (%)	lit.
CZC-25146 (male CD-1 mice)	IV	1	0	154	419−434	1.6	2.3	5.4		4	71
	PO	5	0.25	1357	2878−2894	1			133		
LRRK2-IN-1 (male C57BL/6 mice)	IV	1			2974	4.47	5.6	1.71		not efficiently	70
	PO	10	1.0	1618	14758				49.3		

[a]IV = intravenous injection; PO = oral delivery; T_{max} = time of maximum plasma concentration; C_{max} = maximum plasma concentration; $AUC_{0-\infty}$ = area under the curve (measure of exposure); $T_{1/2}$ = half life; CL = plasma clearance; V_{ss} = volume of distribution; F = oral bioavailability; BBB = blood-brain barrier.

MNK1, wild-type LRRK2 and LRRK2-G2019S at 10 μM (Table 7). Y-27632 (**14**) inhibited truncated LRRK2-G2019S with an IC_{50} of 1 μM in a radioisotope assay. Furthermore, the full-length Strep-tag LRRK2-G2019S was inhibited with an IC_{50} of 1.8 μM in an AlphaScreen assay.[62,63] The anthracene and phenanthrene derivatives SP60012 (**15**), Damnacanthal (**16**), LDN-73794 (**17**), and LDN-22684 (**18**) inhibited LRRK2-G2019S and wild-type LRRK2 in the low micromolar range (Table 8).[58,68,69] LDN-73794 (**17**) was confirmed to be ATP competitive, whereas LDN-22684 (**18**) was found to be a non-ATP competitive inhibitor. Further studies revealed LDN-22684 (**18**) to be neither GTP competitive nor substrate competitive. Hence, it was deduced that LDN-22684 (**18**) is an allosteric LRRK2 inhibitor.[68,69] Three compounds were especially developed to inhibit LRRK2, namely, CZC-25146 (**19**), CZC-54252 (**20**), and LRRK2-IN-1 (**21**) (Table 9).[70,71] CZC-25146 (**19**) and CZC-54252 (**20**) inhibited the activity of recombinant human wild-type LRRK2 with an IC_{50} ranging from ∼1 to ∼5 nM. The G2019S mutant was inhibited with an IC_{50} ranging from ∼2 to ∼7 nM in a TF-FRET assay. In addition, they were screened against a kinase panel of 185 kinases and exhibited good selectivity. CZC-25146 (**19**) inhibited five other kinases, PLK4, GAK, TNK1, CAMKK2, and PIP4K2C, with high potency only, but none of them have been classified as predictors of genotoxicity or hematopoietic toxicity.[72,73] Furthermore, it prevents mutant LRRK2-induced injury of cultured rodent and human neurons with mid-nanomolar potency. In vivo pharmacology established a volume of distribution of 5.4 L/kg and a clearance of 2.3 L/h/kg for CZC-25146 (**19**). Unfortunately, it exhibited a poor brain penetration of just 4% (Table 10).[71]

A HTS and subsequent lead optimization provided the LRRK2 inhibitor LRRK2-IN-1 (**21**). It inhibited both truncated wild-type LRRK2 and LRRK2-G2019S with IC_{50} values of 13 and 6 nM, but LRRK2-A2016T and LRRK2-A2016T+G2019S mutants were found to be ∼400-fold more resistant to LRRK2-IN-1 (**21**) (Table 9).[70] This was explained by a molecular docking study of LRRK2-IN-1 (**21**) bound to a homology model of LRRK2 (A2016T), which revealed an unfavorable steric interaction as observed for H-1152 (**12**). The confirmed reversible ATP competitive inhibitor LRRK2-IN-1 (**21**) was selective in kinase panels containing more than 470 kinases. Surprisingly, under the same conditions as employed for LRRK2, LRRK2-IN-1 lacked inhibition of LRRK1. The kinase panels revealed additional inhibition of DCLK1, DCLK2, as well as MAPK7 and supported IC_{50}'s of greater than 1 μM for AURKB, CHEK2, MKNK2, MYLK (smMLCK), NUAK1, PLK1, and RPS6KA2. LRRK2-IN-1 (**21**) induced a similar dose-dependent Ser^{910} and Ser^{935} dephosphorylation and loss of 14−3−3 binding to endogenous LRRK2 in human-derived neuroblastoma SHSY5Y cells and mouse Swiss3T3 cells. Pharmacokinetic studies of LRRK2-IN-1 (**21**) revealed a half-life of 4.5 h and a bioavailability of 49.3% in mice (Table 10). An insufficient blood-brain barrier (BBB) permeation was concluded from the LRRK2 phosphorylation status in the kidney versus brain, which imposes limits on this "useful first-generation 'tool'".[70]

So far, just a small number of LRRK2 inhibitors have been synthesized and profiled in kinase panels. The best of the reported compounds display both high activity and selectivity. However, these reported best-in-class compounds do not pass the BBB efficiently, which limits their potential in animal models of PD. Maybe the patent literature holds additional treasures, waiting to be released.[74−79]

■ CONCLUSION AND PERSPECTIVES

The importance of the G2019S mutation in the kinase domain of LRRK2 derives from the association with the second most common neurodegenerative disease: Parkinson's disease. The late-onset sporadic classical PD affects almost 2% of the world population over 65 years of age.[80] The availability of suitable HTS assay formats such as TF-FRET or AlphaScreen provided first inhibitors of LRRK2 activity with moderate selectivity. Lead optimization resulted in first generation tools and second-generation inhibitors, which displayed promising pharmacokinetic properties, but are limited by insufficient brain uptake or brain activity. The increase in patent applications (e.g., Glaxo Group Limited and Cellzome Limited) indicates a target on the rise. TTT-3002, a drug candidate of TauTaTis, exhibited good results in LRRK2 inhibition. A phase I clinical trial of TTT-3002 is expected to start in 2011.[74−79,81]

The clinical development of LRRK2 inhibitors is impaired by the lack of public data of relevant pharmacology, biology, and even biomarkers. Moreover, the gain of function in LRRK2 mutations may require fundamentally different dosing regimes for mutation carriers versus other PD patients resulting in personalized medicine. This dosage may very up to 100-fold, implying genomic profiling, patient stratification and a wide therapeutic window. Several in vivo invertebrate models indicate neurotoxic hyperactivity of LRRK2 kinase, but the number of LRRK2 kinase activity studies in mouse models is rather limited. New LRRK2 animal models may provide essential information for target validation and suitable biomarkers for end point identification in drug development. Passage of the blood-brain barrier remains a challenge, yet LRRK2 function may be important outside the CNS. Moreover, the consequences of LRRK2 inhibition are not sufficiently established in animal models or humans to conclude a safe inhibition rate in mutation carriers or normal PD patients nor to rule out therapy resistance in gain of function mutations.

Furthermore, just a small number of substrates has been reported to date and this may increase. Hence, an effective and safe inhibition of LRRK2 kinase activity has yet to be confirmed in vivo, in vitro. Any novel therapy must be evaluated against established PD therapies, which results in either extended or large clinical trials. A robust and approved biomarker may enable shorter or smaller trials; however, this may take years to develop and to gain approval.[82−84] Recently, the LRRK-2 phosphorylation sites Ser^{910}, Ser^{935}, Ser^{955}, and Ser^{973} were suggested as biomarkers for LRRK2 because the treatment of LRRK2 expressing cells with LRRK2-IN-1 (**21**) revealed these phosphorylations to be disrupted. However, the kinases and phosphatases responsible for the regulation of these phosphorylation sites have yet to be identified.[85]

Type-I-kinase inhibitors are notorious for their selectivity problems, which frequently cause adverse events in humans. In addition, drug resistance or diminished activity has been observed, which may be caused by kinase domain mutations. LRRK2 features many mutations, which imposes problems to find a useful drug candidate.[63,70] A new generation of kinase inhibitors, called type-II-inhibitors, may reduce some of these problems.[86,87] They bind to the ATP site and extend into an adjacent allosteric site. This allosteric site is not as highly conserved as the ATP binding site and may provide a strategy to obtain improved selectivity. LRRK2 is a particularly challenging target: the G2019S gain of function mutation requires very efficient inhibition to reduce the activity to the wild-type level. The lack of brain permeable inhibitors leaves an open fundamental question: how much G2019S LRRK2 inhibition is required in vivo? In summary, it can be stated that LRRK2 inhibition provides potential to treat PD, albeit further research and clarification is inevitable.

■ AUTHOR INFORMATION

Corresponding Author

*Fax: +496151-163278. Telephone: +496151-164531. E-mail: schmidt_boris@t-online.de.

Author Contributions

†These authors contributed equally to this work.

Funding

This work was supported by the Technische Universität Darmstadt.

Notes

The authors declare no competing financial interest.

■ REFERENCES

(1) Ross, O. A., and Farrer, M. J. (2005) Pathophysiology, pleiotrophy and paradigm shifts: genetic lessons from Parkinson's disease. *Biochem. Soc. Trans. 33*, 586−590.

(2) Davie, C. A. (2008) A review of Parkinson's disease. *Br. Med. Bull. 86*, 109−127.

(3) Jankovic, J. (2008) Parkinson's disease: clinical features and diagnosis. *J. Neurol. Neurosurg. Psychiatry 79*, 368−376.

(4) Clarke, C. E. (2007) Parkinson's disease. *BMJ - Clin. Rev. 335*, 441−445.

(5) Zimprich, A., Biskup, S., Leitner, P., Lichtner, P., Farrer, M., Lincoln, S., Kachergus, J., Hulihan, M., Uitti, R. J., Calne, D. B., Stoessl, A. J., Pfeiffer, R. F., Patenge, N., Carbajal, I. C., Vieregge, P., Asmus, F., Müller-Myhsok, B., Dickson, D. W., Meitinger, T., Strom, T. M., Wszolek, Z. K., and Gasser, T. (2004) Mutations in LRRK2 cause autosomal-dominant parkinsonism with pleomorphic pathology. *Neuron 44*, 601−607.

(6) Berwick, D. C., and Harvey, K. (2011) LRRK2 signaling pathways: the key to unlocking neurodegeneration? *Trends Cell Biol. 21*, 257−265.

(7) Smith, K. (2010) Treatment frontiers. *Nature - Parkinson's Disease Outlook 466*, 15−18.

(8) Poewe, W. (2006) The natural history of Parkinson's disease. *J. Neurol. 253*, VII/2−VII/6.

(9) Duty, S. (2010) Therapeutic potential of targeting group III metabotropic glutamate receptors in the treatment of Parkinson's disease. *Br. J. Pharmacol. 161*, 271−287.

(10) Niswender, C. M., and Conn, P. J. (2010) Metabotropic glutamate receptors: physiology, pharmacology, and disease. *Annu. Rev. Pharmacol. Toxicol. 50*, 295−322.

(11) Paisán-Ruíz, C., Jain, S., Evans, E. W., Gilks, W. P., Simón, J., van der Brug, M., López de Munain, A., Aparicio, S., Martínez Gil, A., Khan, N., Johnson, J., Martinez, J. R., Nicholl, D., Carrera, I. M., Pena, A. S., de Silva, R., Lees, A., Martí-Massó, J. F., Pérez-Tur, J., Wood, N. W., and Singleton, A. B. (2004) Cloning of the gene containing mutations that cause PARK8-linked Parkinson's disease. *Neuron 44*, 595−600.

(12) Valente, E. M., Abou-Sleiman, P. M., Caputo, V., Muqit, M. M. K., Harvey, K., Gispert, S., Ali, Z., Del Turco, D., Bentivoglio, A. R., Healy, D. G., Albanese, A., Nussbaum, R., González-Maldonado, R., Deller, T., Salvi, S., Cortelli, P., Gilks, W. P., Latchman, D. S., Harvey, R. J., Dallapiccola, B., Auburger, G., and Wood, N. W. (2004) Hereditary early-onset Parkinson's disease caused by mutations in PINK1. *Science 304*, 1158−1160.

(13) Bonifati, V., Rizzu, P., van Baren, M. J., Schaap, O., Breedveld, G. J., Krieger, E., Dekker, M. C. J., Squitieri, F., Ibanez, P., Joosse, M., van Dongen, J. W., Vanacore, N., van Swieten, J. C., Brice, A., Meco, G., van Duijn, C. M., Oostra, B. A., and Heutink, P. (2003) Mutations in the DJ-1 gene associated with autosomal recessive early-onset parkinsonism. *Science 299*, 256−259.

(14) Kitada, T., Asakawa, S., Hattori, N., Matsumine, H., Yamamura, Y., Minoshima, S., Yokochi, M., Mizuno, Y., and Shimizu, N. (1998) Mutations in the parkin gene cause autosomal recessive juvenile parkinsonism. *Nature 392*, 605−608.

(15) Tan, E. K., and Schapire, A. H. (2011) LRRK2 as a therapeutic target in Parkinson's disease. *Eur. J. Neurol. 18*, 545−546.

(16) Deng, J., Lewis, P. A., Greggio, E., Sluch, E., Beilina, A., and Cookson, M. R. (2008) Structure of the ROC domain from the Parkinson's disease-associated leucine-rich repeat kinase 2 reveals a dimeric GTPase. *Proc. Natl. Acad. Sci. U.S.A. 105*, 1499−1504.

(17) Giasson, B. I., and Van Deerlin, V. M. (2008) Mutations in LRRK2 as a cause of Parkinson's disease. *Neurosignals 16*, 99−105.

(18) Mata, I. F., Wedemeyer, W. J., Farrer, M. J., Taylor, J. P., and Gallo, K. A. (2006) LRRK2 in Parkinson's disease: protein domains and functional insights. *Trends Neurosci. 29*, 286−293.

(19) Gloeckner, C. J., Kinkl, N., Schumacher, A., Braun, R. J., ÓNeill, E., Meitinger, T., Kolch, W., Prokisch, H., and Ueffing, M. (2006) The Parkinson disease causing LRRK2 mutation I2020T is associated with increased kinase activity. *Hum. Mol. Genet. 15*, 223−232.

(20) Li, X., Tan, Y., Poulose, S., Olanow, C. W., Huang, X., and Yue, Z. (2007) Leucine-rich repeat kinase 2 (LRRK2)/PARK8 possesses GTPase activity that is altered in familial Parkinson's disease R1441C/G mutants. *J. Neurochem. 103*, 238−247.

(21) Biskup, S., Moore, D. J., Celsi, F., Higashi, S., West, A. B., Andrabi, S. A., Kurkinen, K., Yu, S., Savitt, J. M., Waldvogel, H. J., Faull, R. L. M., Emson, P. C., Torp, R., Ottersen, O. P., Dawson, T. M., and Dawson, V. L. (2006) Localization of LRRK2 to membranous and vesicular structures in mammalian brain. *Ann. Neurol. 60*, 557−569.

(22) Giasson, B. I., Covy, J. P., Bonini, N. M., Hurtig, H. I., Farrer, M. J., Trojanowski, J. Q., and Van Deerlin, V. M. (2006) Biochemical and pathological characterization of Lrrk2. *Ann. Neurol. 59*, 315−322.

(23) Jaleel, M., Nichols, R. J., Deak, M., Campbell, D. G., Gillardon, F., Knebel, A., and Alessi, D. R. (2007) LRRK2 phosphorylates moesin at threonine-558: characterization of how Parkinson's disease mutants affect kinase activity. *Biochem. J. 405*, 307−317.

(24) Li, T., Yang, D., Sushchky, S., Liu, Z., and Smith, W. (2011) Models for LRRK2-Linked Parkinsonism. *Parkinson's Dis. 2011*, 1−16.
(25) Berger, Z., Smith, K. A., and La Voie, M. J. (2010) Membrane localization of LRRK2 is associated with increased formation of the highly active LRRK2 dimer and changes in its phosphorylation. *Biochemistry 49*, 5511−5523.
(26) Greggio, E., Zambrano, I., Kaganovich, A., Beilina, A., Taymans, J., Daniels, V., Lewis, P., Jain, S., Ding, J., Syed, A., Thomas, K. J., Baekelandt, V., and Cookson, M. R. (2008) The Parkinson disease-associated leucine-rich repeat kinase 2 (LRRK2) is a dimer that undergoes intramolecular autophosphorylation. *J. Biol. Chem. 283*, 16906−16914.
(27) Taylor, J. P., Mata, I. F., and Farrer, M., J. (2006) LRRK2: a common pathway for parkinsonism, pathogenesis and prevention? *Trends Mol. Med. 12*, 76−82.
(28) Seol, W. (2010) Biochemical and molecular features of LRRK2 and its pathophysiological roles in Parkinson's disease. *BMB Rep. 43*, 233−244.
(29) Cookson, M. R. (2010) The role of leucine-rich repeat kinase 2 (LRRK2) in Parkinson's disease. *Nat. Rev. Neurosci. 11*, 791−797.
(30) West, A. B., Moore, D. J., Biskup, S., Bugayenko, A., Smith, W. W., Ross, C. A., Dawson, V. L., and Dawson, T. M. (2005) Parkinson's disease-associated mutations in leucine-rich repeat kinase 2 augment kinase activity. *Proc. Natl. Acad. Sci. U.S.A. 102*, 16842−16847.
(31) West, A. B., Moore, D. J., Choi, C., Andrabi, S. A., Li, X., Dikeman, D., Biskup, S., Zhang, Z., Lim, K., Dawson, V. L., and Dawson, T. M. (2007) Parkinson's disease-associated mutations in LRRK2 link enhanced GTP-binding and kinase activities to neuronal toxicity. *Hum. Mol. Genet. 16*, 223−232.
(32) Xiong, Y., Coombes, C. E., Kilaru, A., Li, X., Gitler, A. D., Bowers, W. J., Dawson, V. L., Dawson, T. M., and Moore, D. J. (2010) GTPase activity plays a key role in the pathobiology of LRRK2. *PLoS Genet. 6*, e1000902.
(33) Webber, P. J., Smith, A. D., Sen, S., Renfrow, M. B., Mobley, J. A., and West, A. B. (2011) Autophosphorylation in the Leucine-Rich Repeat Kinase 2 (LRRK2) GTPase Domain Modifies Kinase and GTP-Binding Activities. *J. Mol. Biol. 412*, 94−100.
(34) Lin, C., Tsai, P., Wu, R., and Chien, C. (2010) LRRK2 G2019S mutation induces dendrite degeneration through mislocalization and phosphorylation of tau by recruiting autoactivated GSK3ß. *J. Neurosci. 30*, 13138−13149.
(35) Dusonchet, J., Kochubey, O., Stafa, K., Yound, S. M. Jr, Zufferey, R., Moore, D. J., Schneider, B. L., and Aebischer, P. (2011) A rat model of progressive nigral neurodegeneration induced by the Parkinson's disease-associated G2019S mutation in LRRK2. *J. Neurosci. 31*, 907−912.
(36) Greggio, E., Jain, S., Kingsbury, A., Bandopadhyay, R., Lewis, P., Kaganovich, A., van der Brug, M. P., Belina, A., Blackinton, J., Thomas, K. J., Ahmad, R., Miller, D. W., Kesavapany, S., Singleton, A., Lees, A., Harvey, R. J., Harvey, K., and Cookson, M. R. (2006) Kinase activity is required for the toxic effects of mutant LRRK2/dardarin. *Neurobiol. Dis. 23*, 329−341.
(37) Hsu, C. H., Chan, D., Greggio, E., Saha, S., Guillily, M. D., Ferree, A., Raghavan, K., Shen, G. C., Segal, L., Ryu, H., Cookson, M. R., and Wolozin, B. (2010) MKK6 binds and regulates expression of Parkinson's disease-related protein LRRK2. *J. Neurochem. 112*, 1593−1604.
(38) Gloeckner, C. J., Schumacher, A., Boldt, K., and Uefffing, M. (2009) The Parkinson disease-associated protein kinase LRRK2 exhibits MAPKKK activity and phosphorylates MKK3/6 and MKK4/7, in vitro. *J. Neurochem. 109*, 959−968.
(39) Lee, S. B., Kim, W., Lee, S., and Chung, J. (2007) Loss of LRRK2/PARK8 induces degeneration of dopaminergic neurons in Drosophila. *Biochem. Biophys. Res. Commun. 358*, 534−539.
(40) Ng, C., Mok, S. Z. S., Koh, C., Ouyang, X., Fivaz, M. L., Tan, E., Dawson, V. L., Dawson, T. M., Yu, F., and Lim, K. (2009) Parkin protects against LRRK2 G2019S mutant-induced dopaminergic neurodegeneration in Drosophila. *J. Neurosci. 29*, 11257−11262.
(41) Liu, Z., Wang, X., Yu, Y., Li, X., Wang, T., Jiang, H., Ren, Q., Jiao, Y., Sawa, A., Moran, T., Ross, C. A., Montell, C., and Smith, W. W. (2008) A Drosophila model for LRRK2-linked parkinsonism. *Proc. Natl. Acad. Sci. U.S.A. 105*, 2693−2698.
(42) Smith, W. W. (2010) Leucine-rich kinase 2 (LRRK2) Drosophila Model For Parkinsońs Disease: Wildtype1 (WT1) and G2019S Mutant Flies. U.S. 2010/0175140 A1.
(43) Yao, C., El Khoury, R., Wang, W., Byrd, T. A., Pehek, E. A., Thacker, C., Zhu, X., Smith, M. A., Wilson-Delfosse, A. L., and Chen, S. G. (2010) LRRK2-mediated neurodegeneration and dysfunction of dopaminergic neurons in a Caenorhabditis elegans model of Parkinson's disease. *Neurobiol. Dis. 40*, 73−81.
(44) Sheng, D., Qu, D., Kwok, K. H. H., Ng, S. S., Lim, A. Y. M., Aw, S. S., Lee, C. W. H., Sung, W. K., Lufkin, T., Jesuthasan, S., Sinnakaruppan, M., and Liu, J. (2010) Deletion of the WD40 domain of LRRK2 in Zebrafish causes Parkinsonism-like loss of neurons and locomotive defect. *PLoS Genet. 6*, e1000914.
(45) Ren, G., Xin, S., Zhong, H., and Lin, S (2011) Disruption of LRRK2 does not cause specific loss of dopaminergic neurons in zebrafish. *PLoS Genet. 6*, e20630.
(46) Lin, X., Parisiadou, L., Gu, X., Wang, L., Shim, H., Sun, L., Xie, C., Long, C., Yang, W., Ding, J., Chen, Z. Z., Gallant, P. E., Tao-Cheng, J., Rudow, G., Troncoso, J. C., Liu, Z., Li, Z., and Cai, H. (2009) Leucine-rich repeat kinase 2 regulates the progression of neuropathology induced by Parkinson's-disease-related mutant alpha-synuclein. *Neuron 64*, 807−827.
(47) Li, X., Patel, J. C., Wang, J., Avshalumov, M. V., Nicholson, C., Buxbaum, J. D., Elder, G. A., Rice, M. E., and Yue, Z. (2010) Enhanced striatal dopamine transmission and motor performance with LRRK2 overexpression in mice is eliminated by familial Parkinson's disease mutation G2019S. *J. Neurosci. 30*, 1788−1797.
(48) Li, Y., Liu, W., Oo, T. F., Wang, L., Tang, Y., Jackson-Lewis, V., Zhou, C., Geghman, K., Bogdanov, M., Przedborski, S., Beal, M. F., Burke, R. E., and Li, C. (2009) Mutant LRRK2(R1441G) BAC transgenic mice recapitulate cardinal features of Parkinson's disease. *Nat. Neurosci. 12*, 826−828.
(49) Andreas-Mateos, E., Mejias, R., Sasaki, M., Li, X., Lin, B. M., Biskup, S., Zhang, L., Banerjee, R., Thomas, B., Yang, L., Liu, G., Beal, M. F., Huso, D. L., Dawson, T. M., and Dawson, V. L. (2009) Unexpected lack of hypersensitivity in LRRK2 knock-out mice to MPTP (1-methyl-4-phenyl-1,2,3,6-tetrahydropyridine). *J. Neurosci. 29*, 15846−15850.
(50) Ramonet, D., Daher, J. P. L, Lin, B. M., Stafa, K., Kim, J., Banerjee, R., Westerlund, M., Pletnikova, O., Glauser, L., Yang, L., Liu, Y., Swing, D. A., Beal, M. F., Troncoso, J. C., McCaffery, J. M., Jenkins, N. A., Copeland, N. G., Galter, D., Thomas, B., Lee, M. K., Dawson, T. M., Dawson, V. L., and Moore, D. J. (2011) Dopaminergic neuronal loss, reduced neurite complexity and autophagic abnormalities in transgenic mice expressing G2019S mutant LRRK2. *PloS ONE 6*, e18568.
(51) Melrose, H. L., Dächsel, J. C., Behrouz, B., Lincoln, S. J., Yue, M., Hinkle, K. M., Kent, C. B., Korvatska, E., Taylor, J. P., Witten, L., Liang, Y. Q., Beevers, J. E., Boules, M., Dugger, B. N., Serna, V. A., Gaukhman, A., Yu, X., Castanedes-Casey, M., Braithwaite, A. T., Ogholikhan, S., Yu, N., Bass, D., Tyndall, G., Schellenberg, G. D., Dickson, D. W., Janus, C., and Farrer, M. J. (2010) Impaired dopaminergic neurotransmission and microtubule-associated protein tau alterations in human LRRK2 transgenic mice. *Neurobiol. Dis. 40*, 503−517.
(52) Melrose, H. L., Kent, C. B., Taylor, J. P., Dachsel, J. C., Hinkle, K. M., Lincoln, S. J., Mok, S. S., Culvenor, J. G., Masters, C. L., Tyndall, G. M., Bass, D. I., Ahmed, Z., Andorfer, C. A., Ross, O. A., Wszolek, Z. K., Delldonne, A., Dickson, D. W., and Farrer, M. J. (2007) A comparative analysis of leucine-rich repeat kinase 2 (Lrrk2) expression in mouse brain and Lewy body disease. *Neuroscience 147*, 1047−1058.
(53) Tong, Y., Pisani, A., Martella, G., Karouani, M., Yamaguchi, H., Pothos, E. N., and Shen, J. (2009) R1441C mutation in LRRK2

impairs dopaminergic neurotransmission in mice. *Proc. Natl. Acad. Sci. U.S.A. 106*, 14622−14627.
(54) Tong, Y., Yamaguchi, H., Giaime, E., Boyle, S., Kopan, R., Kelleher, R. J. III, and Shen, J. (2010) Loss of leucine-rich repeat kinase 2 causes impairment of protein degradation pathways, accumulation of alpha-synuclein, and apoptotic cell death in aged mice. *Proc. Natl. Acad. Sci. U.S.A. 107*, 9879−9884.
(55) Wang, L., Xie, C., Greggio, E., Parisiadou, L., Shim, H., Sun, L., Chandran, J., Lin, X., Lai, C., Yang, W., Moore, D. J., Dawson, T. M., Dawson, V. L., Chiosis, G., Cookson, M. R., and Cai, H. (2008) The chaperone activity of heat shock protein 90 is critical for maintaining the stability of leucine-rich repeat kinase 2. *J. Neurosci. 28*, 3384−3391.
(56) Winner, B., Melrose, H. L., Zhao, C., Hinkle, K. M., Yue, M., Kent, C., Braithwaite, A. T., Ogholikhan, S., Aigner, R., Winkler, J., Farrer, M. J., and Gage, F. H. (2011) Adult neurogenesis and neurite outgrowth are impaired in LRRK2 G2019S mice. *Neurobiol. Dis. 41*, 706−716.
(57) Zhou, H., Huang, C., Tong, J., Hong, W. C., Liu, Y., and Xia, X. (2011) Temporal expression of mutant LRRK2 in adult rats impairs dopamine reuptake. *Int. J. Biol. Sci. 7*, 753−761.
(58) Lee, B. D., Shin, J., VanKampen, J., Petrucelli, L., West, A. B., Ko, H. S., Lee, Y., Maguire-Zeiss, K. A., Bowers, W. J., Federoff, H. J., Dawson, V. L., and Dawson, T. M. (2010) Inhibitors of leucine-rich repeat kinase-2 protect against models of Parkinson's disease. *Nat. Med. 16*, 998−1000.
(59) Klein, C. L., Rovelli, G., Springer, W., Schall, C., Gasser, T., and Kahle, P. J. (2009) Homo- and heterodimerization of ROCO kinases: LRRK2 kinase inhibition by the LRRK2 ROCO fragment. *J. Neurochem. 111*, 703−715.
(60) Anand, V. S., Reichling, L. J., Lipinski, K., Stochaj, W., Duan, W., Kelleher, K., Pungaliya, P., Brown, E. L., Reinhart, P. H., Somber, R., Hirst, W., Riddle, S. M., and Braithwaite, S. P. (2009) Investigation of leucine-rich repeat kinase 2: enzymological properties and novel assays. *FEBS J. 276*, 466−478.
(61) Covy, J. P., and Giasson, B. I. (2009) Identification of compounds that inhibit the kinase activity of leucine-rich repeat kinase 2. *Biochem. Biophys. Res. Commun. 378*, 473−477.
(62) Pedro, L., Padrós, J., Beaudet, L., Schubert, H.-D., Gillardon, F., and Dahan, S. (2010) Development of a high-throughput AlphaScreen assay measuring full-length LRRK2(G2019S) kinase activity using moesin protein substrate. *Anal. Biochem. 404*, 45−51.
(63) Nichols, R. J., Dzamko, N., Hutti, J. E., Cantley, L. C., Deak, M., Moran, J., Bamborough, P., Reith, A. D., and Alessi, D. R. (2009) Substrate specificity and inhibitors of LRRK2, a protein kinase mutated in Parkinson's disease. *Biochem. J. 424*, 47−60.
(64) Liu, Z., Hamamichi, S., Lee, B. D., Yang, D., Ray, A., Caldwell, G. A., Caldwell, K. A., Dawson, T. M., Smith, W. W., and Dawson, V. L. (2011) Inhibitors of LRRK2 kinase attenuate neurodegeneration and Parkinson-like phenotypes in Caenorhabditis elegans and Drosophila Parkinson's disease models. *Hum. Mol. Genet. 20*, 3933−3942.
(65) Dzamko, N., Deak, M., Hentati, F., Reith, A. D., Prescott, A. R., Alessi, D. R., and Nichols, R. J. (2010) Inhibition of LRRK2 kinase activity leads to dephosphorylation of Ser(910)/Ser(935), disruption of 14−3-3 binding and altered cytoplasmic localization. *Biochem. J. 430*, 405−413.
(66) Reichling, L. J., and Riddle, S. M. (2009) Leucine-rich repeat kinase 2 mutants I2020T and G2019S exhibit altered kinase inhibitor sensitivity. *Biochem. Biophys. Res. Commun. 384*, 255−258.
(67) Yun, H., Heo, H. Y., Kim, H. H., DooKim, N., and Seol, W. (2011) Identification of chemicals to inhibit the kinase activity of leucine-rich repeat kinase 2 (LRRK2), a Parkinson's disease-associated protein. *Bioorg. Med. Chem. Lett. 21*, 2953−2957.
(68) Liu, M., Dobson, B., Glicksman, M. A., Yue, Z., and Stein, R. L. (2010) Kinetic mechanistic studies of wild-type leucine-rich repeat kinase 2: characterization of the kinase and GTPase activities. *Biochemistry 49*, 2008−2017.
(69) Liu, M., Poulose, S., Schuman, E., Zaitsev, A. D., Dobson, B., Auerbach, K., Seyb, K., Cuny, G. D., Glicksman, M. A., Stein, R. L., and Yue, Z. (2010) Development of a mechanism-based high-throughput screen assay for leucine-rich repeat kinase 2--discovery of LRRK2 inhibitors. *Anal. Biochem. 404*, 186−192.
(70) Deng, X., Dzamko, N., Prescott, A., Davies, P., Liu, Q., Yang, Q., Lee, J.-D., Patricelli, M. P., Nomanbhoy, T. N., Alessi, D. R., and Gray, N. S. (2011) Characterization of a selective inhibitor of the Parkinson's disease kinase LRRK2. *Nat. Chem. Biol. 7*, 203−205.
(71) Ramsden, N., Perrin, J., Ren, Z., Lee, B. D., Zinn, N., Dawson, V. L., Tam, D., Bova, M., Lang, M., Drewes, G., Bantscheff, M., Bard, F., Dawson, T. M., and Hopf, C. (2011) Chemoproteomics-Based Design of Potent LRRK2-Selective Lead Compounds That Attenuate Parkinson's Disease-Related Toxicity in Human Neurons. *ACS Chem. Biol. 6*, 1021−1028.
(72) Olaharski, A. J., Bitter, H., Gonzaludo, N., Kondru, R., Goldstein, D. M., Zabka, T. S., Lin, H., Singer, T., and Kolaja, K. (2010) Modeling bone marrow toxicity using kinase structural motifs and the inhibition profiles of small molecular kinase inhibitors. *Toxicol. Sci. 118*, 266−275.
(73) Olaharski, A. J., Gonzaludo, N., Bitter, H., Goldstein, D., Kirchner, S., Uppal, H., and Kolaja, K. (2009) Identification of a kinase profile that predicts chromosome damage induced by small molecule kinase inhibitors. *PLoS Comput. Biol. 5*, e1000446.
(74) Chan, B., Estrada, A., Sweeney, Z., and Mciver, E. G. (2011) Pyrazolopyridines as inhibitors of the kinase LRRK2. WO 2011/141756 A1.
(75) Kim, J. W., Lee, J., Song, H.-J., Kim, Y., Lee, H. K., Choi, J.-S., Lim, S.-H., and Chang, S. (2011) Kinase Inhibitors. WO 2011/053861 A1.
(76) Lee, J., Song, H.-J., Koh, J. S., Lee, L. K., Kim, Y., Chang, S., Kim, H. W., Chang, S., Lim, S.-H., Choi, J.-S., Kim, J.-H., and Kim, S.-W. (2011) Kinase Inhibitors. WO 2011/060295 A1.
(77) Mciver, E. G., Smiljanic, E., Harding, D. J., and Hough, J. (2010) Compounds (I). WO 2010/106333 A1.
(78) Nichols, P. L., Eatherton, A. J., Bamborough, P., Jandu, K. S., Philips, O. J., and Andreotti, D. (2011) WO 2011/038872 A1.
(79) Ramsden, N. (2009) Use Of LRRK2 Inhibitors For Neurodegenerative Disease. WO 2009/127642 A2.
(80) Correia Guedes, L., Ferreira, J. J., Rosa, M. M., Coelho, M., Bonifati, V., and Sampaio, C. (2010) Worldwide frequency of G2019S LRRK2 mutation in Parkinson's disease: A systematic review. *J. Prak. Rel. Dis. 16*, 237−242.
(81) http://www.tautatis.com/home.html (2011).
(82) Yue, Z. (2012) Genetic mouse models for understanding LRRK2 biology, pathology and pre-clinical application. *Parkinsonism Relat. Disord. 18* (Suppl 1), S180−182.
(83) Yue, Z., and Lachenmayer, M. L. (2011) Genetic LRRK2Models of Parkinson's Disease: Dissecting the Pathogenic Pathway and Exploring Clinical Applications. *Movement Disord. 26*, 1386−1397.
(84) http://www.pdonlineresearch.org/ (2012).
(85) Doggett, E. A., Zhao, J., Mork, C. N., Hu, D., and Nichols, R. J. (2012) Phosphorylation of LRRK2 serines 955 and 973 is disrupted by Parkinsoń disease mutations and LRRK2 pharmacological inhibition. *J. Neurochem. 120*, 37−45.
(86) Davis, M. I., Hunt, J. P., Herrgard, S., Ciceri, P., Wodicka, L. M., Pallares, G., Hocker, M., Treiber, D. K., and Zarrinkar, P. P. (2011) Comprehensive analysis of kinase inhibitor selectivity. *Nat. Biotechnol. 29*, 1046−1051.
(87) Rauh, D. (2010) Inaktive Kinasekonformationen stabilisieren. *Nachr. Chem. 58*, 118−121.

4.4 LRRK2 Kinase-Inhibitoren als neue Medikamente für die Parkinson-Krankheit?

Der Inhalt dieses Kapitels wurde bereits veröffentlicht.[187]

Autoren: Sandra Schulz*, Stefan Göring*, Boris Schmidt, Carsten Hopf.
Titel: „LRRK2 Kinase Inhibitors as New Drugs for Parkinson's Disease?".
Journal: RSC Drug Discovery Series.
DOI: 10.1039/9781849737357-00266.

Zusammenfassung:
Die Parkinson-Krankheit ist eine altersabhängige, verheerende und neurodegenerative Erkrankung. Sie ist durch den Verlust dopaminerger Neuronen in der *Substantia nigra pars compacta* und durch Proteinablagerungen in Form von zytoplasmatischen Einschlusskörperchen, sogenannter *Lewy bodies* bzw. *Lewy neurites* charakterisiert. Die Symptome umfassen motorische und kognitive Störungen wie Tremor, Bradykinese, posturale Instabilität und Rigor. Derzeit gibt es noch keine Heilung, da der pathogene Mechanismus dieser Krankheit noch nicht vollommen entschlüsselt ist. Seitdem die in der Kinase-Domäne liegende G2019S-Mutation in Zusammenhang mit der Neurotoxizität und dem Parkinsonsyndrom gebracht wurde, ist LRRK2 ein wichtiges therapeutisches Target geworden.
Dieses Kapitel gibt Einblicke in den derzeitigen Stand der Inhibition von LRRK2 mittels ATP-kompetitiven Kinase-Inhibitoren. Es werden dabei medizinalchemische Erfolge bezüglich nicht-selektiver und selektiver Inhibition sowie Beispiele aus Patenten näher beleuchtet. Ferner werden erste pharmakokinetische und pharmakodynamische Eigenschaften von LRRK2-Inhibitoren wiedergegeben.
Seit der Entdeckung von LRRK2 im Jahre 2004 ist es bis heute noch nicht gelungen das Protein vollständig kristallographisch darzustellen. Ein Homologie-Modell der Kinase-Domäne von LRRK2 gibt Einsichten in die ATP-Bindungstasche. Relevante Aminosäuren werden für die Interaktion potentieller LRRK2-Inhibitoren näher beleuchtet.
Da LRRK2 auch außerhalb des Gehirns in Geweben wie Herz und Nieren exprimiert wird, wird dessen Rolle außerhalb hinterfragt und kritisch diskutiert.

CHAPTER 11

LRRK2 Kinase Inhibitors as New Drugs for Parkinson's Disease?

SANDRA SCHULZ,[a,b,†] STEFAN GÖRING,[c,†]
BORIS SCHMIDT*[c] AND CARSTEN HOPF*[a,b]

[a] Instrumental Analysis and Bioanalytics, Mannheim University of Applied Sciences, Mannheim, Germany; [b] Center for Applied Research in Biomedical Mass Spectrometry ABIMAS, Mannheim University of Applied Sciences, Mannheim, Germany; [c] Clemens Schöpf-Institute of Organic Chemistry and Biochemistry, Technische Universität Darmstadt, Darmstadt, Germany
*Email: c.hopf@hs-mannheim.de; Schmidt_Boris@t-online.de

11.1 Introduction

Parkinson's disease (PD) is a common, age-related, devastating neurodegenerative disease that is characterized by neuronal cell loss, predominantly in dopaminergic neurons of the *substantia nigra pars compacta*, and by formation of fibrillar conglomerates of lipids and proteins (Lewy bodies) in the surviving neurons.[1] PD affects about 2% of the population older than 60 years.[2] The symptoms include motor and cognitive dysfunction such as postural instability, rigidity, tremor, as well as dementia and depression.[3] The underlying molecular mechanisms of the disease remain poorly understood. Presently, established therapies treat symptoms of the disease, *e.g.*, reduce motor manifestations or alleviate non-motor symptoms, but no PD treatment is able to prevent,

[†]These authors contributed equally to this work

RSC Drug Discovery Series No. 34
Emerging Drugs and Targets for Parkinson's Disease
Edited by Ana Martinez and Carmen Gil

Published by the Royal Society of Chemistry, www.rsc.org

halt or decelerate disease progression.[2] No treatment of its elusive molecular pathogenic mechanisms exists.

Mutations in leucine-rich repeat kinase 2 (LRRK2) are associated with rare autosomal dominant forms of PD. Several non-selective inhibitors with activity against LRRK2 have been identified.[3 7] Most of them have either not been tested for brain penetration or have been found to not enter the brain. A brain-penetrant, non-selective kinase inhibitor, GW5074, is protective in a mouse model of LRRK2-induced neurodegeneration *in vivo*, suggesting that inhibition of LRRK2 kinase activity could be a new treatment option for PD.[6] However, GW5074 is a very non-selective molecule that, among other things, targets several non-kinases. For instance, it displays activity as an allosteric glutamate dehydrogenase inhibitor[8] and as an anti-viral agent with a RAF1 kinase-independent mode of action.[9]

The molecular biology of LRRK2, most notably the consequences of mutations inside (*e.g.*, G2019S) and outside (*e.g.*, R1441C) the kinase domain on kinase activity and LRRK2-induced toxicity *in vitro*, has been summarized in excellent reviews elsewhere.[1,10] Moreover, the current state of validation of LRRK2 as a therapeutic target as well as the question of whether inhibition of LRRK2 kinase activity is the only viable therapeutic strategy for LRRK2-linked PD have been addressed recently.[2,11] Moreover, a comprehensive review of non-selective (as well as the first selective) LRRK2 inhibitors has been provided very recently.[3] We therefore want to focus this book chapter on the following five aspects that are particularly important for LRRK2 kinase-directed drug discovery:

(1) Recent insight into LRRK2 inhibitor structure–activity relationships (SARs) from structural biology studies and molecular modeling;
(2) Recent medicinal chemistry efforts relating to potent and selective LRRK2 kinase inhibitors;
(3) Recent advances in understanding the role of LRRK2 outside the brain and implications for potential mechanism-based toxicity of LRRK2 kinase inhibitors as drugs;
(4) Recent advances in animal models, both invertebrate and vertebrate, for pharmacological evaluation of LRRK2 kinase inhibitors; and
(5) Pharmacokinetics and pharmacodynamics of LRRK2 kinase inhibitors: the current state-of-the-art and future challenges ahead.

11.2 Insight into LRRK2 Inhibitor SARs from Structural Biology Studies and Molecular Modeling

Kinase activity can be controlled by several modes of inhibition. Type I inhibitors, which compete for the ATP-binding site, are usually rather polar and often associated with selectivity problems. This imposes severe obstacles for the chronic treatment of a neurodegenerative disease. Type II inhibitors stabilize the inactive state of the kinase and generally offer benefits in terms of selectivity and

ATP competition. The DFG [Aspartic acid (D), Phenylalanine (F), Glycine (G)] and the APE [Alanine (A), Phenylalanine (P), Glutamic acid (E)] motifs are typical features in the activation loops of kinases. However, in the case of LRRK2, they depend on the availability of a DYG [Aspartic acid (D), Tyrosine (Y), Glycine (G)]-out motif instead of DFG. This DYG motive is changed to DYS [DYG (Aspartic acid (D), Tyrosine (Y), Serine (S)] in the G2019S-LRRK2 mutant. Hence, this modification could be an approach to develop specific LRRK2 kinase inhibitors.[2] However, this mutation results in constitutively active LRRK2, which imposes severe limitations on druggability of such Type II inhibitors in mutation carriers. Selective Type III and Type IV LRRK2 kinase inhibitors have not been reported yet. Again, Type III inhibitors, which stabilize the inactive state of the kinase, are of limited use in LRRK2 mutations which lack the inactive state. Allosteric Type IV inhibitors have not been identified yet. However, the remarkable C2024-C2025 moiety neighboring the DYG/DYS motif may provide a starting point for Type IV inhibition as this motif contributes to conformational stability. The discovery of kinase inhibitors usually progresses by the improvement of a high-throughput-screening (HTS) derived hit series in an iterative process of rational design and molecular docking analysis. This process requires access to robust enzyme structures. Unfortunately, full-length LRRK2 has escaped crystallization so far. Thus construction and use of LRRK2 homology models is the key.[12 17] Choice of structural templates and sequence alignment are the most important parameters for a homology model. The search for closely related kinases by comparison of sequence homology, usually the first choice, has not resulted in robust homology models yet. This enzyme-based approach can be complemented by a ligand-based approach which utilizes inhibitor fingerprinting to search for kinases with similar selectivities. A recent publication by Genentech compared these two approaches and identified a more robust LRRK2 homology model by comparison of inhibitor profiles. The SAR of JAK2 and JAK3 inhibitors with LRRK2 inhibitors suggested JAK2 and JAK3 as privileged templates for homology modeling. The final LRRK2 homology model was constructed from an unpublished JAK2 cocrystal structure.[12] The N-terminal domain of LRRK2 kinase exhibits predominantly β-sheets and an α-helix, whereas the C-terminal domain is organized in α-helices [Figure 11.1(a)]. Several important amino acids are found around the mostly hydrophobic ATP-binding site, which is located at the interface of the N- and C-terminal lobe. Met1947 represents the gatekeeper and forms the rear of the ATP-binding pocket with Lys1906 and Glu1920, whereas the residues Glu1948, Leu1949 and Ala1950 constitute the backbone of the ATP-pocket [Figure 11.1(b)]. The ceiling of the ATP site is created by Phe1883, Leu1885, Val1893 and Ala1904, whereas the residues Ile1933, Gly1953, Ser1954 and Leu2001 form the floor of the ATP-binding pocket.

The analysis of the number of conserved residues *versus* the total number of kinases sharing these indicates a road to selective kinase inhibitors, as eight identical residues in the ATP-binding site are shared by fewer than 20% of all kinases. In keeping with these findings, a detailed binding site sequence analyses has been completed. The list of the 19 amino acid residues in the ATP pocket

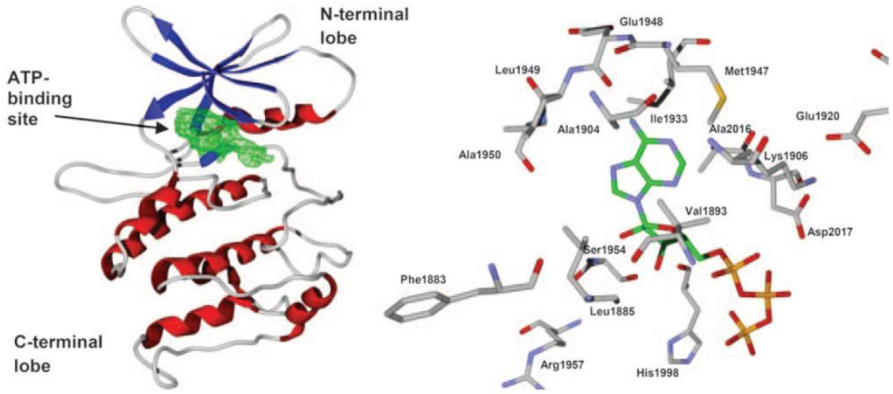

Figure 11.1 (a) Homology model of LRRK2 kinase domain with N- and C-terminal lobes as well as the ATP-binding site (colored in green) at the interface of the two lobes. (b) ATP-binding site of LRRK2 docked with ATP (colored in green) and important amino acids. The homology model was made using the Swiss model server.[18–20] The molecular docking was performed using the software Molegro Virtual Docker 5.

was narrowed down to the most important residues of Phe1883, Leu1949, Ser1954 and Arg1957. Interaction with these four core residues was suggested to provide kinase selectivity of small-molecule inhibitors against LRRK2 regardless of Type I or Type II inhibition.[12] The equilibrium of the active/inactive activation loop is shifted by the G2019S and I2020T mutation towards the active kinase, which imposes limitations on the development of Type II kinase inhibitors, as mutation carriers may not respond to the same dosage regime as non-carriers.

11.3 Medicinal Chemistry for the Design of Potent and Selective LRRK2 Inhibitors

11.3.1 Non-Selective LRRK2 Inhibitors

Almost all LRRK2 inhibitors reported so far have been derived from library screening efforts and act in an ATP-competitive manner. An overview of the different chemotypes is shown in Figure 11.2.

These early LRRK2 hits are all off-target effects of unselective kinase inhibitors and inhibit more than one kinase (Table 11.1). This early data originated from a limited number of *in vitro* assays using wild-type (wt) LRRK2 and G2019S-LRRK2. Unfortunately, these assays vary in the concentration of LRRK2 constructs, substrate and ATP, thus the mere comparison of IC_{50} is misleading. The most sensitive assays utilize radio-isotopes, which allow detection of both autophosphorylation and substrate phosphorylation, but are less suitable for HTS. High-throughput capability was achieved by time-resolved fluorescence resonance energy transfer

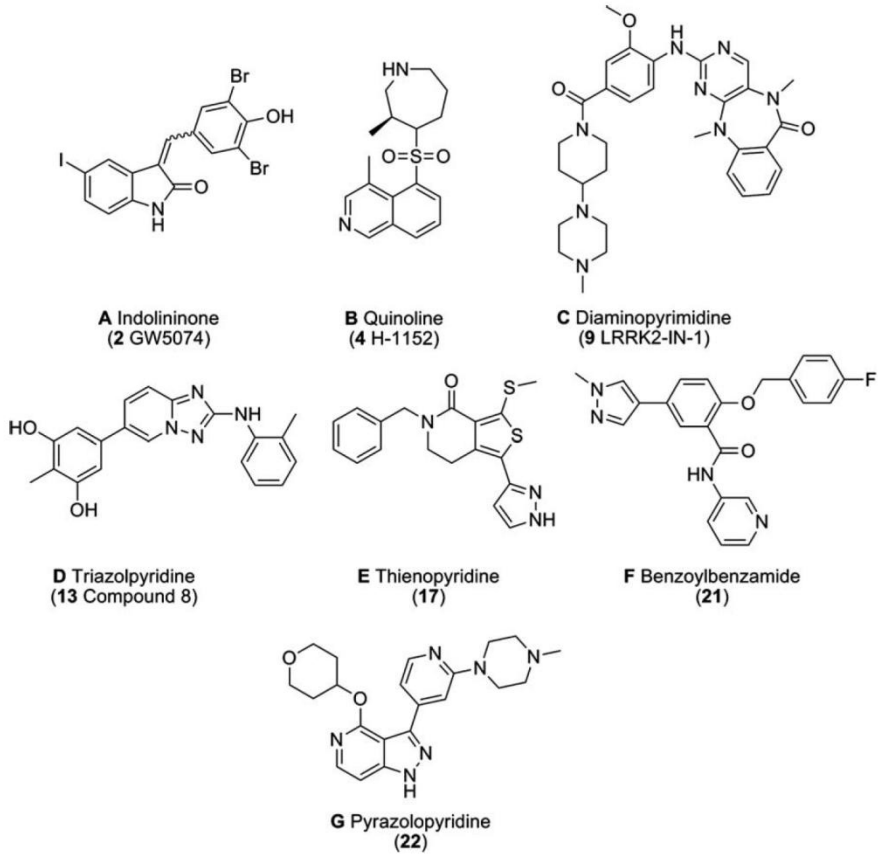

Figure 11.2 Different chemotypes of LRRK2 inhibitors.

(TR-FRET) and the amplified luminescent proximity homogeneous (AlphaScreen) assays.[18] Although truncated LRRK2 and its full-length analog display similar phosphorylation activities, differences have been noted. This may be a result of utilization of different substrates, *e.g.*, LRRKtide and myelin basic protein (MBP).[4,16] Sunitinib (compound **1**), a widely employed kinase inhibitor, inhibits both wt LRRK2 and LRRK2-G2019S (truncated and full-length) with an IC_{50} ranging from 15 to 79 nM (Table 11.1).[4,16,19] The selectivity of sunitinib (**1**) is limited: 12 out of 85 screened kinases are inhibited at 1 μM. However, sunitinib (**1**) is capable of suppressing the activity of full-length LRRK2 expressed from Swiss-3T3 fibroblast cells.[16] The apparent potency of sunitinib (**1**) to inhibit wt LRRK2 drops to an IC_{50} of 370 nM at cellular ATP concentration (1 mM).[20] The indolinones GW5074 (compound **2**) and indirubin-3′-monooxime (compound **3**) are *ca.* three-fold more active against LRRK2-G2019S than the wt kinase, inhibiting the former with IC_{50}s of 880 nM and ~1300 nM, respectively (Table 11.1).[6,21] Closely related LRRK1 and LRRK2 are inhibited in a similar manner, as is phosphorylation of the

Table 11.1 Indolinone derivatives as LRRK2 inhibitors.

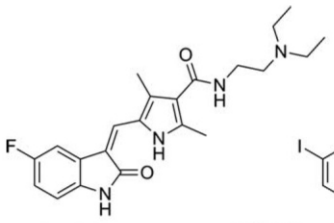

Sunitinib

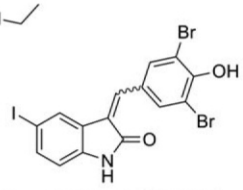

Raf-1 Kinase inhibitor I (GW5074)

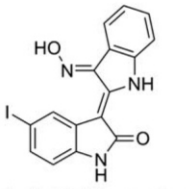

Indirubin-3'-monoxime

No.	*Name*	*Wild-type LRRK2 IC_{50}*	*LRRK2-G2019S IC_{50}*	*Substrate*	*Kinase profile*	*Literature*
1	Sunitinib	79 nM[a] 15 nM[b]	19 nM[a] 26 nM[b]	Nictide LRRKtide	12[f] of 85[g]	Refs. 4, 16 and 19
2	Raf-1 kinase inhibitor I (GW5074)	~500 nM[c] 3150 nM[d]	880 nM[d]	LRRKtide MBP[f]	—	Refs. 6 and 21
3	Indirubin-3'-monooxime	4830 nM[d]	1310 nM[d]	MBP[e]	—	Ref. 6

[a]GST-LRRK2 (1326-2527; wt/G2019S).
[b]GST-LRRK2 (970-2527; wt/G2019S).
[c]Goat GST-LRRK2.
[d]GST-LRRK2 (wt/G2019S).
[e]Myelin basic protein (MBP).
[f]Number of inhibited kinases, including LRRK2.
[g]Total number of tested kinases.

putative LRRK2 substrate, eukaryotic translation initiation factor 4E-binding protein (4E-BPI). As indolinones and indirubines are well established scaffolds for pan-kinase inhibitors, they are frequently employed in kinase programs and thus provide very limited freedom to operate for new kinase programs.[22]

H-1152 (compound **4**) is a known ROCK2 inhibitor. This compound was profiled against a panel of 85 kinases and found to inhibit Aurora B kinase, BRSK2, wild-type LRRK2 and LRRK2-G2019S. H-1152 (**4**) displayed IC_{50}s ranging from 150 to 600 nM in radioisotope or AlphaScreen phosphorylation assays of wt LRRK2 and LRRK2-G2019S (Table 11.2).[18,19] Docking analysis of H-1152 (**4**) utilized a homology model of LRRK2. The carbon atoms of the LRRK2 sequence were superimposed on the reported ROCK1-H-1152 complex. This analysis indicated a backbone interaction with the NH group of Ala1950 (the PDB code of ROCK1-H-1152 has not been published). Furthermore, the two methyl groups of H-1152 (**4**) were observed to make lipophilic contacts with the ATP-binding site. The amino acid Ala2016 was found to be close to H-1152 (**4**). This could contribute to drug resistance, because the IC_{50} of H-1152 (**4**) for the LRRK2 mutant A2016T increased up to *ca.* 30-fold.[16]

Staurosporine (compound **5**) is a well-established pan-kinase inhibitor. It inhibited both wt LRRK2 and LRRK2-G2019S (truncated and full-length) with an IC_{50} ranging from 0.2 to 40 nM (Table 11.3) in different *in vitro* assays, *e.g.*, radioactive, TR-FRET and AlphaScreen assay.[4,6,18,21] These assays utilized different substrates such as synthetic peptides, *e.g.*, LRRKtide and

Table 11.2 H-1152 as an LRRK2 inhibitor.

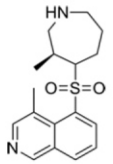

H-1152

No.	*Name*	*Wild-type LRRK2 IC_{50}*	*LRRK2-G2019S*	*Substrate*	*Kinase profile*	*Literature*
4	H-1152	244 nM[a]	600 nM[b] 150 nM[b]	GST-Moesin Nictide	12[c] of 85[d]	Refs. 16, 18 and 19

[a]GST-LRRK2 (1326-2527; wt/G2019S).
[b]Full-length Strep-tag LRRK2 (G2019S).
[c]Number of inhibited kinases, including LRRK2.
[d]Total number of tested kinases.

Table 11.3 Staurosporine and derivatives as LRRK2 inhibitors.

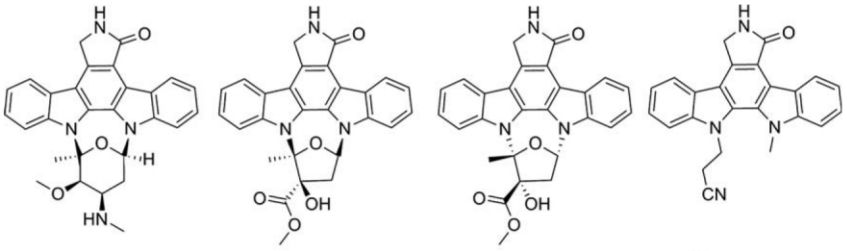

Staurosporine K-252a K-252b Gö6976

No.	*Name*	*Wild-type LRRK2 IC_{50}*	*LRRK2-G2019S IC_{50}*	*Substrate*	*Kinase profile*	*Literature*
5	Staurosporine	~1 nM[a] 2 nM[a] 8.2 nM[c] 40 nM[d]	0.2 nM[e] 1.8 nM[b] 40 nM[d]	GST-Moesin LRRKtide MBP[f]	—	Refs. 4, 6, 18 and 21
6	K-252a	~25 nM[a] 3.6 nM[b]	2.8 nM[b]	LRRKtide	—	Ref. 4 and 21
7	K-252b	~50 nM[a]	—	LRRKtide	—	Ref. 21
8	Gö6976	~250 nM[a]	—	LRRKtide	—	Ref. 21

[a]Goat GST-LRRK2.
[b]GST-LRRK2 (970-2527; wt/G2019S).
[c]Full-length LRRK2.
[d]GST-LRRK2 (wt/G2019S).
[e]Full-length Strep-tag LRRK2 (G2019S).
[f]Myelin basic protein (MBP).

derivatives of potential physiological substrates, *e.g.*, GST-Moesin. Staurosporine (**5**) displayed a similar inhibitory profile against LRRK1/LRRK2 autophosphorylation and MBP phosphorylation.[6] Its isoindolinone derivatives

K-252a/b (compounds **6** and **7**) and Gö6976 (compound **8**) also inhibited wt LRRK2 and LRRK2-G2019S with nM potencies of 3.6 to ~25 nM and ~50 nM, respectively (Table 11.3).[4,21]

11.3.2 Potent and Selective LRRK2 Inhibitors

The pyrimidine derivatives LRRK2-IN-1 (compound **9**), CZC-54252 (compound **10**) and CZC-25146 (compound **11**) were optimized to selectively inhibit LRRK2 (Table 11.4).[23,24] LRRK2-IN-1 (**9**) inhibited both truncated wt LRRK2 and LRRK2-G2019S with IC_{50} values of 13 and 6 nM, but LRRK2-A2016T and LRRK2-A2016T + G2019S mutants were found to be *ca.* 400-fold more resistant to this compound (**9**) (Table 11.4).[23] Molecular docking of LRRK2-IN-1 (**9**) to a homology model of LRRK2-A2016T provided an explanation for resistance of this and the LRRK2-A2016T + G2019S mutants. It revealed an unfavorable steric interaction, which is also present in the H-1152 (**4**) LRRK2 complex.[16] The reversible ATP competitive inhibitor LRRK2-IN-1 (**9**) is selective against a kinase panel of 470 kinases. Surprisingly, LRRK2-IN-1 (**9**) lacked inhibition of LRRK1. The kinase panel revealed additional inhibition of DCLK1, DCLK2 as well as MAPK7 and supported IC_{50}s of greater than 1 μM for AURKB, CHEK2, MKNK2, MYLK (smMLCK), NUAK1, PLK1 and RPS6KA2. LRRK2-IN-1 (**9**) induced a similar dose-dependent Ser910 and Ser935 dephosphorylation and loss of 14-3-3 binding to endogenous LRRK2 in human-derived SHSY5Y neuroblastoma cells and mouse Swiss3T3 cells.

CZC-54252 (**10**) and CZC-25146 (**11**) inhibited the activity of recombinant human wt LRRK2 with an IC_{50} of ~1 to 5 nM. The G2019S mutant was inhibited with an IC_{50} ranging from ~2 to 7 nM in a TR-FRET assay. Potency against the native LRRK2 protein complex in tissue extracts was only slightly lower. In addition, CZC-54252 (**10**) and CZC-25146 (**11**) exhibited good selectivity against 185 native kinases in cell and tissue extracts in a Kinobeads assay (Table 11.4).[24,25] CZC-25146 (**11**) inhibited only five other kinases, PLK4, GAK, TNK1, CAMKK2 and PIP4K2C, with comparable potency, none of them classified as predictors of genotoxicity or hematopoietic toxicity.[26,27] Furthermore, it prevented mutant LRRK2-induced injury of cultured rodent and human neurons with nM potency.

The inhibitor TAE684 (compound **12a**), which fuses structural elements of LRRK-IN-1 (**9**) and the CZC series, inhibited wt LRRK2 and LRRK2-G2019S with IC_{50}s of 7.8 and 6.1 nM, respectively. Although the potencies of TAE684 (**12a**) were similar to LRRK2-IN-1 (**9**), the former compound also inhibited the LRRK2-A2016T and LRRK2-A2016T + G2019S mutants with IC_{50} values of 93.3 and 21.9 nM, respectively (Table 11.4). This finding could be rationalized in a molecular docking study with LRRK2-A2016T. While both TAE684 (**12a**) and LRRK2-IN-1 (**9**) share the aminopyrimidine scaffold, the molecular model suggested that the isopropylsulfone moiety of TAE684 (**12a**) is able to avoid steric contact with the A2016T residue.[28] Furthermore, the selectivity of TAE684 (**12a**) was evaluated against a kinase panel of 442

Table 11.4 Diaminopyrimidine derivatives LRRK2-IN-1, CZC-54252, CZC-25146, TAE684 and HG-10-102-01 as potent and selective LRRK2 inhibitors.

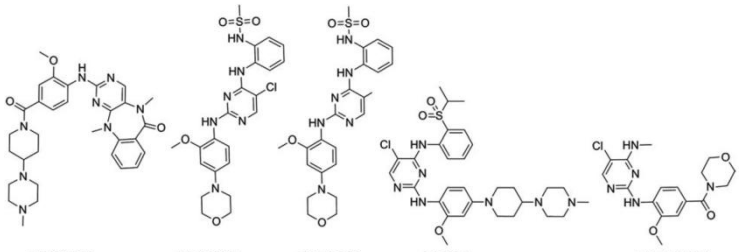

No.	*Name*	*Wild-type LRRK2 IC_{50}*	*LRRK2-G2019S IC_{50}*	*LRRK2-A2016T*	*LRRK2-A2016T + G2019S*	*Substrate*	*Kinase profile*	*Literature*
9	LRRK2-IN-1	13 nM[a]	6 nM[a]	2450 nM[a]	3080 nM[a]	Nictide	12[c] of 442[d]	Ref. 23
10	CZC-54252	1.28 nM[b]	1.85 nM[b]	—	—	LRRKtide	10[c] of 184[d]	Ref. 24
11	CZC-25146	4.76 nM[b]	6.87 nM[b]	—	—	LRRKtide	5[c] of 184[d]	Ref. 24
12a	TAE684	7.8 nM[a]	6.1 nM[a]	93.3 nM[a]	21.9 nM[a]	Nictide	6[c] of 102[d]	Ref. 28 and 29
12b	HG-10-102-01	20.3 nM[a]	3.2 nM[a]	153.1 nM[a]	95.9 nM[a]	Nictide	2[c] of 451[d]	Ref. 30

[a]GST-LRRK2 (1326-2527; wt/G2019S/A2016T/G2019S + A2016T).
[b]Human LRRK2 (wt/G2019S).
[c]Number of inhibited kinases, including LRRK2.
[d]Total number of tested kinases.

kinases. This screen revealed that TAE684 (**12a**) is a potent inhibitor of several kinases like CAMKKβ, CHK2, FGF-1R, NUAK1, PBK and TSSK1 in a low nM range.[28,29] The next generation inhibitor in this series is HG-10-102-01 (compound **12b**), which is characterized by improved ligand efficiency at apparently retained selectivity. The inhibitory activity of HG-10-102-01 (**12b**) of wt LRRK2 and LRRK2-G2019S was comparable to LRRK2-IN-1 (**9**) with IC_{50} values of 20.3 and 3.2 nM, respectively. In contrast to LRRK2-IN-1 (**9**) the inhibitor HG-10-102-01 (**12b**) displayed an increased inhibition against the A2016T mutant.[30] Furthermore, HG-10-102-01 (**12b**) was evaluated against panels of 138 and 451 kinases, respectively (Table 11.4). At a concentration of 10 μM HG-10-102-01 (**12b**) displayed good selectivity against the panel of 138 kinases, as only MLK1 and MNK2 were inhibited by greater than 80%. HG-10-102-01 (**12b**) was evaluated further against 451 kinases and revealed excellent selectivity at a concentration of 1 μM, the only exception being the inhibition of one mutant form of c-Kit (L576P).[30]

The triazolopyridine Compound 8 (compound **13**) and the aminopyrimidine **14a** were identified by HTS as potent LRRK2 G2019S inhibitors. The triazolopyridine (**13**) exhibited a K_i value of 10 nM against LRRK2-G2019S (Table 11.5) and had chemical properties suitable for CNS penetration.[12] The aminopyridine **14a** is characterized by a slightly higher ligand efficiency, yet the scaffold is well established in kinase inhibition and thus provides little freedom to operate. Compound 8 (**13**) was tested against a kinase panel of 63 kinases at 1 μM and exhibited good selectivity. Abl was the only kinase which was also inhibited greater than 50% in addition to wt LRRK2 and LRRK2-G2019S. A homology model was developed on the basis of inhibitor fingerprinting and identified JAK3 and to a lesser extent JAK2 as kinases with similar ligand selectivity for a set of 100 triazolopyridines. JAK2 was selected as a template for the LRRK2 model due to the availability of a high-resolution structure determination of JAK2 cocrystals. The docking of Compound 8 (**13**) to the LRRK2 homology model elucidated the binding mode to the ATP pocket, which is indicative of a kinase Type I inhibitor.[12] The 2-aminotriazole establishes strong hydrogen bond contacts with the residue Ala1950. The essential dimethylphenol moiety interacts with the rear of the ATP pocket and forms hydrogen bonds between Lys1906 and Glu1920 with the hydroxyl group and hydrophobic interactions between the phenol and the gatekeeper Met1947 (Figure 11.3). Unfortunately, the dimethylphenol pharmacophore could not be replaced without loss of potency. This lead was abandoned due to the poor drug metabolism and pharmacokinetic (DMPK) properties associated with the phenol moiety.[12]

Compound 15 (compound **14c**) exhibited a K_i value of 3 nM and excellent selectivity against a panel of 63 kinases at 1 μM. FLT-3, the only kinase found to be effected, was inhibited by 53%.[12] The addition of the substituent R^2 (Table 11.5) to the diaminopyrimidines provided improved selectivity of LRRK2 *versus* JAK2 inhibition. This is probably due to the induction of a dihedral twist that destabilizes the JAK2 inhibiting conformer.

Table 11.5 Triazolopyridine and diaminopyridine derivatives as potent and selective LRRK2 inhibitors.

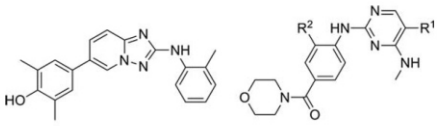

Compound 8 14a-h

No.	*Name*	R^1	R^2	*Wild-type LRRK2* K_i	*LRRK2-G2019S* K_i	*JAK2* K_i	*Substrate*	*Kinase profile*	*Literature*
13	Compound 8	—	—	—	10 nM	405 nM	LRRKtide	2[a] of 63[b]	Ref. 12
14a	—	Cl	H	—	6 nM	7 nM	LRRKtide	—	Ref. 12
14b	—	Cl	CH_3	—	7 nM	> 3200 nM	LRRKtide	—	Ref. 12
14c	Compound 15	Cl	OCH_3	—	3 nM	> 3200 nM	LRRKtide	1[a] of 63[b]	Ref. 12
14d	—	Cl	Br	—	13 nM	> 3200 nM	LRRKtide	—	Ref. 12
14e	—	Br	OCH_3	—	1 nM	3000 nM	LRRKtide	—	Ref. 12
14f	—	F	OCH_3	—	71 nM	> 3200 nM	LRRKtide	—	Ref. 12
14g	—	CF_3	OCH_3	—	1 nM	> 3200 nM	LRRKtide	—	Ref. 12
14h	—	CN	OCH_3	—	13 nM	> 3200 nM	LRRKtide	—	Ref. 12

[a]Number of inhibited kinases, including LRRK2.
[b]Total number of tested kinases.

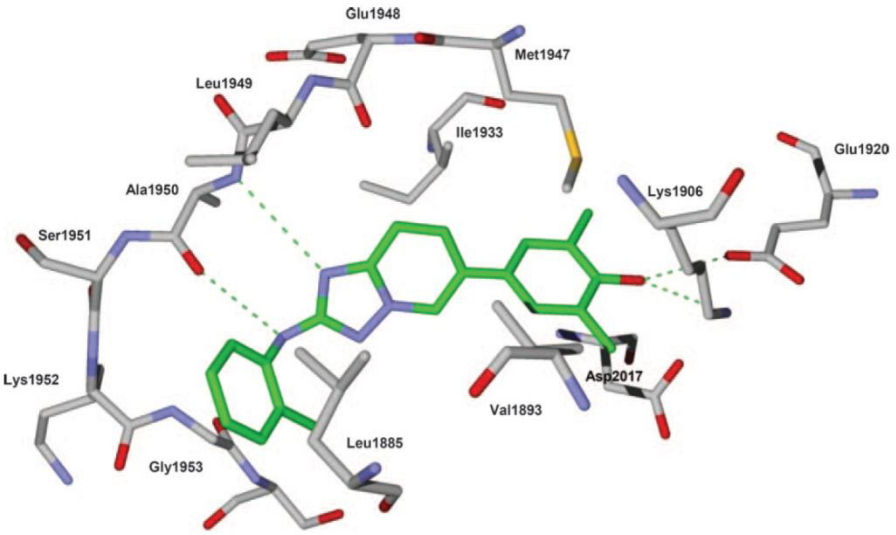

Figure 11.3 Compound 8 (compound **13**) (green) in the ATP-binding pocket of LRRK2. Important protein interactions are shown as green dashed lines. The homology model was made using the Swiss model server.[18–20] The molecular docking was performed using the software Molegro Virtual Docker 5.

11.3.3 Examples from Recently Published Patent Applications

Recently, patent applications by GlaxoSmithKline (GSK), the Medical Research Council (MRC) and Genentech were published.[31 34] The cyclic thieno[3,4-*c*]pyridine derivatives (compounds **15**–**18**) inhibited LRRK2-G2019S in a low nM range (IC_{50}s from 1.3 to 3.2 nM, Table 11.6).[33] LRRK2 inhibitors bearing the benzyloxybenzamide moiety were published by GSK (Table 11.7). Compounds **19**–**21** exhibited similar potencies (LRRK2-G2019S IC_{50}s from 3 to 8 nM) as the thieno[3,4-*c*]pyridines (**15**–**18**).[34] Pyrazolo-pyridines (compounds **22**–**25**) published by Genentech exhibited K_i values of 3 to 35 nM (Table 11.8).[32] Unfortunately, the selectivity of these patented compounds against kinase panels was not disclosed.

11.4 The Role of LRRK2 Outside the Brain and Implications for Potential Mechanism-Based Toxicity of LRRK2 Inhibitors as Drugs

LRRK2 is a large multi-domain phosphoprotein.[35] Several mutations of the catalytic core region of LRRK2 have been unequivocally linked to late-onset autosomal dominant PD[36] and variations around the lrrk2 locus are a risk factor for idiopathic PD[37], with G2019S being the most prevalent in PD patients carrying a LRRK2 mutation (reviewed in ref. 3). Since the G2019S

Table 11.6 Thieno[3,4-*c*]pyridin-4(5*H*)-one derivatives as LRRK2 inhibitors.

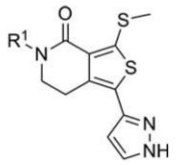

15–18

No.	R^1	*Wild-type LRRK2 IC_{50}*	*LRRK2-G2019S IC_{50}*	*Substrate*	*Kinase profile*	*Literature*
15		—	1.7 nM	LRRKtide	—	Ref. 33
16	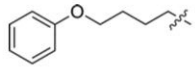	—	3.2 nM	LRRKtide	—	Ref. 33
17	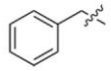	—	1.3 nM	LRRKtide	—	Ref. 33
18		—	2.0 nM	LRRKtide	—	Ref. 33

Table 11.7 Benzyloxybenzamide derivatives as LRRK2 inhibitors.

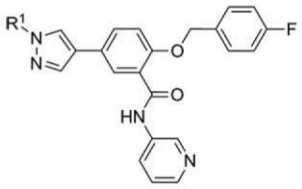

19-21

No.	R^1	*Wild-type LRRK2 IC_{50}*[a]	*LRRK2-G2019S IC_{50}*[a]	*Substrate*	*Kinase profile*	*Literature*
19	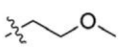	—	6 nM	LRRKtide	—	Ref. 34
20	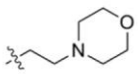	—	8 nM	LRRKtide	—	Ref. 34
21	Me	—	3 nM	LRRKtide	—	Ref. 34

[a]6His-Tev-LRRK2 (1326-2527).

mutation increases kinase activity,[38] treating LRRK2-linked PD with kinase inhibitors appears to be a very promising therapeutic approach. However, little is known about the underlying molecular mechanisms of PD pathophysiology.

Table 11.8 Pyrazolopyridine derivatives as LRRK2 inhibitors.

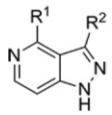

No.	R^1	R^2	K_i[a]	*Substrate*	*Kinase profile*	*Literature*
22	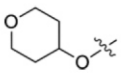	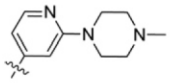	6 nM	LRRKtide	—	Ref. 32
23	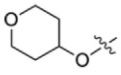	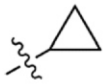	35 nM	LRRKtide	—	Ref. 32
24	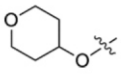		13 nM	LRRKtide	—	Ref. 32
25	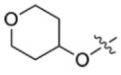	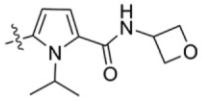	3 nM	LRRKtide	—	Ref. 32

[a]LRRK2 wt (Invitrogen cat# PV4882), LRRK2 G2019S (Invitrogen cat # PV4874).

But also the normal function of this protein and its role outside the brain remain poorly understood. The fact that LRRK2 is not only expressed in various parts of the brain but also in several peripheral tissues including lung, heart and kidney[35] leads to the suspicion that LRRK2 inhibition might cause adverse events which have to be considered early on in on-going attempts to develop LRRK2 selective kinase inhibitors.

The availability of LRRK2 knock-out (KO) mice has recently given insight into novel aspects of the physiological role of LRRK2 and its peripheral biology.[39,40] Tong *et al.* investigated the normal function of LRRK2 by generating two independent lines of germ-line deletion mice and studying potential effects over a time period of 20 months of mouse development.[40] In the brain, the dopaminergic system remained unaffected and no apparent neurodegeneration was detected. Tyrosine hydroxylase immunostaining of the brain revealed normal numbers and morphology of dopaminergic neurons. Striatal dopamine and α-synuclein levels were not significantly altered in comparison to wt mice. In contrast, kidneys of aging (20-month old) LRRK2 KO mice developed striking changes, and a disturbed protein homeostasis was observed. Loss of LRRK2 led to significant age-dependent kidney abnormalities, including renal atrophy and a 60-fold increased accumulation and aggregation of α-synuclein. Furthermore, protein degradation mediated by the ubiquitin–proteasome system was found to be impaired in the absence of LRRK2, leading to an accumulation of ubiquitinated proteins. In addition,

accumulation of lipofuscin granules was observed in kidneys, indicating an impaired autophagy/lysosomal pathway in aging LRRK2 KO mice. The absence of LRRK2, moreover, led to a striking increase in inflammatory responses and apoptosis in mouse kidneys. These dramatic effects in kidney but not in brain may be related to the *ca.* six-fold higher LRRK2 expression in the former.[41] Furthermore, in the brain, LRRK1, a functional homolog of LRRK2 in vertebrates, might compensate for the absence of LRRK2. [35,40] Taken together, LRRK2 plays a crucial role *in vivo* and is involved in regulating protein degradation in an age-dependent manner.[40] For the development of LRRK2 inhibitors as potential treatments of PD, this is critically important, as the full inhibition of LRRK2 may cause mechanism-based renal toxicity.

The essential role of LRRK2 in the kidney was recently confirmed by a team at Novartis.[39] Three different mutant mouse lines were generated, in order to elucidate the essential functions of LRRK2 *in vivo*. The mouse lines were either carrying the pathogenic G2019S mutation inducing an elevated kinase activity (knock-in, KI) or the point mutation D1994S, which inactivates kinase activity (kinase-dead, KD). Additionally, a KO mouse line was generated.[39] As had been observed earlier,[40] LRRK2 mutant brain tissue did not exhibit any neuropathology or quantitative changes compared to wt littermates. However, kidneys were grossly affected in KO and also in KD mice. Both mutant lines developed kidney darkening, tubular dilatation and an elevated lipofuscin accumulation starting at the age of five months. In addition, KO and KD mice presented an early-onset (1.5 month) increase in size and number of secondary lysosomes in the proximal tubule cells. KO mutants, in addition, displayed pathophysiological changes in the lung (microvacuoles and lamellar bodies in lung Type II pneumocytes). These findings further support the essential function of LRRK2 in protein homeostasis. Impaired autophagy was not clearly detected by Herzig *et al.*[39] In contrast to earlier results,[40] LC3 levels, a marker for autophagy, remained unchanged in all mutant lines. mTOR and TCS2 protein levels were reduced in KD and increased in KO and KI mice. In KD mice the level of full-length LRRK2 protein was dramatically reduced in the kidney. The same was noted in wt mice after administration of a LRRK2-selective kinase inhibitor.[39] This may be an important finding for LRRK2 drug discovery, as it illustrates the important role of kinase activity for maintenance of normal LRRK2 protein levels and, hence, normal kidney function. Interestingly, in heterozygous KO mice the reduction of LRRK2 levels was more subtle.[39] In summary, absence of kinase activity is associated with kidney abnormalities and perturbed protein and lysosome homeostasis.[39] Taken together, this extends earlier findings for KO mutants[40] to KD mutants suggesting that protein homeostasis in kidneys depends on LRRK2 kinase activity and not (just) a putative scaffolding role of the LRRK2 protein. Full inhibition of kinase activity might thus not be a suitable therapeutic approach, since it may cause toxic effects in the kidney. However, further investigation, especially of heterozygote animals, is needed to understand this matter properly.

Apart from its essential role in protein homeostasis and kidney morphology and function, LRRK2 has been suggested to be involved in several immunological functions. LRRK2 is expressed in various tissues of the immune system such as the thymus and spleen[35] and in subsets of immune cells.[42,43] LRRK2 mRNA has been detected in human peripheral blood mononuclear cells (hPBMCs), in circulating $CD19^+$ B cells and in $CD14^+$ monocytes. In particular, the monocyte subpopulation $CD14^+CD16^+$ displays high levels of LRRK2 expression, whereas in $CD14^+CD16^-$ cells LRRK2 protein levels are very low. Since $CD14^+CD16^+$ monocytes are augmented in inflammatory processes and considered to be more mature, it is believed that LRRK2 plays a role in monocyte maturation. Additionally, monocyte differentiation experiments revealed that levels of LRRK2 protein remain high in macrophages and dendritic cells after the maturation process is complete.[42] Earlier studies had shown that LRRK2 expression is regulated during B cell differentiation and maturation, as different protein levels of LRRK2 were found in the B-lymphocyte subtypes pre-B, B1 and B2.[43,44] LRRK2 expression in hPBMCs is significantly increased after treatment with IFN-γ, consistent with the fact that the lrrk2 gene contains a consensus binding site for interferon response factors.[42,45] LRRK2 mRNA and protein levels are particularly up-regulated by IFN-γ in isolated monocytes. A weaker and more variable response was recently also observed after IFN-β and TNFα treatment,[42] in contrast to earlier results that did not detect up-regulation of LRRK2 upon TNFα stimulation in THP-1 cells.[45] No increase in LRRK2 expression was detected when hPBMCs were treated with interleukins IL-1β, IL-2, IL-15 or with the insulin-like growth factor IGF-1. The fact that LRRK2 is expressed in monocytes, macrophages, dendritic cells and B cells and that its expression is highly regulated by IFN-γ suggest a role in the immune system. Signal transduction cascades that LRRK2 is involved in as well as its precise role in function of the immune system remain to be established. Recent evidence, however, suggests that LRRK2 can be phosphorylated at Ser910 and Ser935 by canonical (IKKalpha and IKKbeta) and IKK-related (IKKepsilon and TBK1) kinases following activation *via* the MyD88 pathway.[46] This finding implies that inhibition of phosphorylation on Ser910 and Ser935 may not be a specific pharmacodynamic biomarker of LRRK2 inhibition. Consequently, Ser910 and Ser935 phosphorylation data needs to be interpreted with care and may not be the quintessential readout for efficacy of LRRK2 inhibitors *in vivo*.

In summary, LRRK2 is involved in B cell and monocyte maturation and differentiation processes. This implies the possibility of mechanism-based toxicity of LRRK2 inhibitors for PD. Kidney, blood and immune function or potentially toxicity need to be monitored carefully during drug discovery and development. Interestingly, in the case of papillary renal and thyroid carcinomas, down-regulation of LRRK2 expression induced increased cell death[47] and in the brain LRRK2 kinase inhibition attenuated microglial inflammatory responses,[48] illustrating once again the complexity of protein function and the consequences of (sometimes only subtle) changes in the expression level.

11.5 Invertebrate and Vertebrate Animal Models for Pharmacological Evaluation of LRRK2 Inhibitors

Pharmacological validation of LRRK2 as a druggable target for PD and testing of efficacy of possible PD therapeutics requires adequate animal models with a PD-like phenotype. For (mutant) LRRK2-induced PD a limited number of relevant *in vivo* models has been described. The lrrk2 gene is highly conserved across species, providing the opportunity to study LRRK2-related diseases in invertebrate and vertebrate animal models.

Invertebrate LRRK2-linked PD animal models have been published for *Drosophila melanogaster* and for *Caenorhabditis elegans*. *Drosophila* possesses a single ortholog (CG5483) of human LRRK2. Several research groups have generated transgenic loss-of-function *Drosophila* mutants using the GAL4/UAS system, taking advantage of the yeast GAL4 transcription factor which binds specifically to an upstream activation sequence. Under the control of the promoter-GAL4 it is therefore possible to express transgenes in specific cells or various tissues.[49] LRRK loss-of-function mutants exhibited impaired locomotive activity and degeneration of dopaminergic (DA) neurons in *Drosophila*.[50] Overexpression of human wt LRRK2 or the LRRK2-G2019S mutant in fly neurons produced late-onset selective loss of DA neurons in the brain, locomotor deficiencies and early mortality with LRRK2-G2019S causing increased autophosphorylation and a more severe Parkinsonism-like phenotype in comparison to wt LRRK2.[51]

C. elegans contains LRK-1, the ortholog of human LRRK2. In deletion mutants, LRK-1 was identified to be involved in polarized sorting of synaptic vesicle proteins to axons by excluding these proteins from the dendrite-specific Golgi Transport machinery.[52] Overexpression of human wt LRRK2 or the mutants R1441C and G2019S in *C. elegans* DA neurons causes age-dependent neurodegeneration, a decrease of dopamine levels, locomotion impairment and behavioral deficits *in vivo*.[53] As observed for *Drosophila*, the mutant worms display a more severe phenotype than wt, providing additional evidence of the importance of appropriate GTPase and kinase activity in PD pathogenesis.

Drosophila and *C. elegans* invertebrate LRRK2 PD models resemble several key features of human PD and might thus offer suitable short-term models of PD pathogenesis and underlying molecular mechanisms. As many genetic tools are available for these model organisms and large-scale genetic screens are feasible, *Drosophila* and *C. elegans* provide the possibility of carrying out inexpensive and rapid compound screens. However, both organisms lack a mammal-like blood–brain barrier. Furthermore, LRRK2 protein–protein interactions that may contribute to the function of human LRRK2, and thus to PD pathogenesis, may not be evolutionarily conserved.

In zebrafish, XM_682700 has been identified as ortholog of human LRRK2. The blockage of zebrafish LRRK2 (zLRRK2) protein by morpholino reagents led to embryonic lethality and severe developmental deficiencies such as growth retardation and loss of neurons. Interestingly, deletion of only the WD40

domain of zLRRK2 by morpholino-directed targeting of the splicing machinery induces Parkinsonism-like phenotypes such as loss of DA neurons in the diencephalon, and locomotor dysfunction.[54] It may therefore provide a useful small vertebrate disease model for PD.

The most common vertebrate models for LRRK2-linked Parkinsonism are rodent models. LRRK2 transgenic mice have been generated that show some neurochemical and behavioral abnormalities yet mostly lack specific PD characteristics like DA neuronal cell loss in the *substantia nigra*.[40,55 58] One exception is a transgenic mouse model expressing human LRRK2 with the mutation G2019S which demonstrated a modest age-dependent degeneration of DA neurons.[59]

Conditional expression of wt LRRK2 or LRRK2-G2019S in double transgenic mice under the control of the calcium/calmodulin-dependent protein kinase II (CaMK II) promoter failed to trigger neurodegeneration of DA neurons and PD-like behavioral phenotypes.[56] Bacterial artificial chromosome (BAC) transgenic mice expressing wt LRRK2 or the mutants R1441G and G2019S show evidence of an age-dependent decrease of dopamine release and axonal pathology of the nigrostriatal dopaminergic projection[55] or a decrease in striatal dopamine content and release.[58] However, no loss of DA neurons in the *substantia nigra* was observed. Human LRRK2 wt and LRRK2 mutant G2019S BAC transgenic mice generated by Melrose *et al.* revealed abnormal dopamine neurotransmission in both wt and mutant transgenic mice demonstrated by a reduction in extracellular dopamine levels and augmented phosphorylation of the microtubule binding protein tau in G2019S mutant mice.[57] Li *et al.* reported hyperphosphorylation of tau in brain tissue and age-dependent motor activity deficits in mutant LRRK2 R1441G BAC transgenic mice.[55] A possible pathophysiological interaction between the PD-related genes LRRK2 and α-synuclein was shown by Lin *et al.* who generated double transgenic mice co-expressing human LRRK2 and α-synuclein.[56] The overexpression of either wt or PD-related G2019S LRRK2 in A53T α-synuclein transgenic mice significantly accelerated the progression of neuropathological abnormalities, while the presence of excess LRRK2 alone did not exacerbate neurodegeneration. Furthermore, LRRK2 promoted the accumulation and aggregation of α-synuclein in A53T mice. Conversely, the silencing of LRRK2 suppressed the accumulation and aggregation of α-synuclein and by this means delayed the progression of neuropathology in A53T mice.[56] These findings suggest that LRRK2 inhibition is a potential therapeutic option for attenuating α-synuclein-induced neurodegeneration, but some controversy remains.[60] In summary, whereas various LRRK2 mouse models have shed some light on pathobiology of wt and mutant LRRK2 in PD, the observed phenotypes, in particular those relating to neurodegeneration, may prove too subtle for disease models of PD that can be used for robust measurement of the efficacy of LRRK2 inhibitors. Moreover, onset of phenotypic changes is usually late, indicating the need for long-term inhibitor studies, which are not a preferred option – at least not in early drug discovery.

A promising, rapid-onset rodent model, however, was generated by transient expression of the LRRK2-G2019S mutant in mouse brain using herpes simplex virus (HSV) amplicons or adeno-associated virus (AAV) vectors for LRRK2 gene delivery into the *striatum* and the *substantia nigra*.[6] Overexpression of LRRK2 mutant induced a significant loss of tyrosine hydroxylase (TH) positive neurons in the *substantia nigra*. LRRK2 wt and, interestingly, the KD mutant LRRK2-G2019S, D1994A did not trigger any signs of neurodegeneration. An *in vivo* efficacy study with non-selective LRRK2 inhibitors in this animal model revealed that the application of moderately potent kinase inhibitors, GW5074 and indirubin-3'-monooxime, were effective in attenuating the neuronal cell loss suggesting that LRRK2 kinase inhibition may be a viable therapeutic strategy for PD.[6]

The AAV mouse model offers an *in vivo* model for LRRK2-induced loss of DA neurons in the *substantia nigra*, a hallmark of PD, only three weeks after stereotactic injection into the *striatum*.[6] It may therefore be suitable for subchronic evaluation of LRRK2 inhibitor drug candidates, since other rodent models usually take months (if ever) to produce PD-like phenotypes. However, because of the known non-selectivity of the tool compounds used in this study, the results are still a matter of debate.[61] Rapidly induced neurodegeneration could also be a drawback, since it might not be a relevant model for human PD as a late-onset disease. Nevertheless, the AAV mouse model is currently the only rodent model where degeneration of DA neurons is robustly observed and may therefore be considered the model of choice. If the described animal models are relevant for idiopathic PD remains unclear, but currently no animal model is able to fully recapitulate a disease.

11.6 Pharmacokinetics and Pharmacodynamics of LRRK2 Inhibitors: The Current State-of-the-Art

Few potent and selective LRRK2 inhibitors have been reported to date and little is known about their pharmacokinetic properties (Table 11.9). Oral bioavailability of these leads is generally 50% and higher indicating that oral administration is a possible route for future target validation and efficacy studies. However, both the reported Novartis[39] and Genentech[12] LRRK2 inhibitors have plasma half-lives of less than one hour, which significantly restricts their use in *in vivo* studies. The structure of the Novartis/NIBR compound has not been disclosed. LRRK2-IN-1[23] and TAE684[28] display extended plasma half-lives of 4.5 and 11.3 h, respectively, as well as significantly higher compound exposure expressed as (AUC blood h^{-1} ng mL^{-1}; Table 11.9) after oral administration than other compounds. CZC-25146,[24] although it cleared more rapidly than the former two compounds, is extensively distributed in tissue and reaches a maximal plasma concentration of 1357 ng mL^{-1} at an oral dose of 5 mg kg^{-1} *vs.* 1618 ng mL^{-1} at an oral dose of 10 mg kg^{-1} for LRRK2-IN-1. Furthermore, compound exposure to CZC-25146 at a 5 mg kg^{-1} dose is about half that of TAE684 at twice that dose suggesting that CZC-25146 may also be useful as a probe compound for

Table 11.9 Pharmacokinetics (PK) of current potent and selective LRRK2 inhibitors. n.r. = not reported.

		CZC-25146	*LRRK2-IN-1*	*NIBR Inhibitor*	*Cpd 15*	*TAE684*
Mouse PK (1 mg kg^{-1} i.v.)	Clearance/L^{-1} h^{-1} kg^{-1}	2.3	0.3	3.0	—	1.0
	Volume of distribution V_{ss}/L kg^{-1}	5.4	1.7	1.7	—	14.5
	$t_{1/2}$ /h	1.6	4.5	0.4	0.2	11.3
	C_{max}/ng mL^{-1}	154	—	—	—	—
	AUC_{last}/h ng^{-1} mL^{-1}	419	2974	—	—	772
Mouse PK (p.o.)	Oral dose/mg kg^{-1}	5	10	3	—	10
	$t_{1/2}$/h	1	—	—	—	—
	t_{max}/h	0.25	1	—	—	—
	AUC_{last} blood/h ng^{-1} mL^{-1}	2878	14758	573	—	6374
	C_{max} blood/ng mL^{-1}	1357	1618	312	—	—
	C_{max} brain/ng g^{-1}	—	—	672	—	—
	Oral bioavailability (F)/%	133	49	57	—	83
	Wt mouse total brain-to-plasma ratio	~0.04	n.r.[a]	—	1.4	2.3[b]
	p-gp/BCRP double KO mouse total brain-to-plasma ratio	—	—	—	2.9	—
Mouse PK (30 mg kg^{-1} i.p.)	Total plasma concentration at 1 h/μM	—	—	—	8.4	—
	Total brain concentration at 1 h/μM	—	—	—	6.2	—
Literature		Refs. 66 and 24	Ref. 23	Ref. 39	Ref. 12	Ref. 28

[a]Following administration of LRRK2-IN-1, no dephosphorylation of LRRK2 Ser910 or Ser935 was observed in the brain, suggesting that very little or none of the compound penetrated into the brain.
[b]Despite high total brain-to-plasma ratio, suggesting good penetration into the brain, no dephosphorylation of LRRK2 Ser910 or Ser935 was observed in the brain; the reasons for this unexpected result are currently unknown.

future *in vivo* studies. However, whereas CZC-25146 and LRRK2-IN-1 may be useful in *in vivo* studies addressing LRRK2 (inhibitor) function in peripheral organs including kidney and the immune system, they lack a key feature of potential PD drugs: brain penetration.

Two recent LRRK2 inhibitors, Genentech's Compound 15 and TAE684, are brain-penetrant. The former features a total brain-to-plasma ratio of 1.4, which is even higher (2.9) in the p-glycoprotein (p-gp)/ATP-binding cassette subfamily G member 2 (ABCG2/BCRP) double KO mice suggesting that the compound is a moderate substrate of brain efflux transporters.[12] However, 1 h after intraperitoneal dosing at 30 mg kg^{-1}, a compound concentration of 6.2 μM was measured in brain, suggesting that sufficient compound exposure could be obtained at least for acute pharmacodynamic biomarker studies. For TAE684 an even higher total brain-to-plasma ratio was measured (2.3). Nevertheless, despite this evidence for good penetration into the brain, dephosphorylation of LRRK2 Ser910 or Ser935, a potential pharmacodynamics biomarker[23] (but see ref. 46), was only observed in the periphery (*e.g.*, kidney), and not in brain. The reasons for this unexpected result are currently unknown.[28] It should be noted that lack of brain penetration of LRRK2-IN-1 had not been demonstrated, only inferred from lack of LRRK2 Ser910 or Ser935 dephosphorylation,[23] a finding that may have to be revisited in light of the TAE684 study. Future LRRK2 inhibitor drug discovery will have to focus on improving the brain penetration and metabolic stability of selective compounds and on defining suitable biomarkers for acute studies of compound pharmacodynamics in the brain. A very recent study, currently in press, reports a pyrimidine analog, HG-10-102-01, as a potent and selective inhibitor of wt LRRK2 and the G2019S mutant. It inhibited LRRK2 Ser910 and Ser935 phosphorylation at submicromolar concentrations in cells and, as the first compound reported to date, in mouse brain, albeit at high intraperitoneal doses of 50 mg kg^{-1}.[30]

11.7 Will LRRK2 Kinase Inhibitors be Developed into Drugs (for the Treatment of Parkinson's Disease)?

The availability of suitable HTS assay formats such as TR-FRET or AlphaScreen has provided initial inhibitors of LRRK2 activity with moderate selectivity. Lead optimization has resulted in first-generation tools and second-generation inhibitors, which display promising pharmacokinetic properties, but are limited by insufficient brain uptake or brain activity. The increase in patent applications (*e.g.*, GSK and Genentech) indicates a "target on the rise". TTT-3002, a staurosporine derivative in clinical development by TauTaTis, allegedly exhibited good results in LRRK2 inhibition. A Phase I clinical trial of TTT-3002 was expected to start in 2011.[62] However, staurosporines are notorious for their lack of selectivity and the precise status of the compound is unknown.[31,34,63 66]

Clinical development of LRRK2 inhibitors is hampered by the lack of (public) data of the relevant pharmacology, biology and even biomarkers.

For example, it is not known at present whether any of the published potent and selective LRRK2 inhibitors (Tables 11.4 and 11.5) display overt toxicity when chronically administered to animals. If so, given the industry's effort, it would seem fair to assume that any compound-based toxicity could eventually be overcome during drug discovery by further lead optimization. Hence, three main questions need to be addressed:

(1) Patient stratification: Would an ideal LRRK2 kinase inhibitor be a potential drug for all PD patients? Or only for those patients carrying LRRK2 mutations? Or only for those patients carrying activating mutations in the kinase domain, *e.g.*, LRRK2 G2019S?
(2) Mechanism-based toxicity: Given the high expression levels of LRRK2 in peripheral organs such as the kidney and in various blood cells, is LRRK2 inhibition expected to be associated with mechanism-based toxicity that would drastically limit its utility as a treatment for any chronic disease? If so, would such toxicity only be observed if LRRK2 was fully inhibited or could it be mitigated by appropriate dosing regimes? What therapeutic index could be expected for a best-in-class LRRK2 inhibitor?
(3) Utility in other therapy areas besides PD: Given the high expression levels of LRRK2 in peripheral organs such as kidney and in various blood cells, could LRRK2 inhibition be a therapeutic option for diseases other than PD?

11.7.1 Patient Stratification

Since an initial report suggesting that PD-associated mutations in LRRK2 link enhanced GTP-binding and kinase activities to neuronal toxicity,[67] it has generally been assumed that mutations inside the kinase domain of LRRK2 are indeed associated with increased kinase activity that may be attenuated by LRRK2 inhibitors as therapeutics. In contrast, the question of whether mutations outside the kinase domain, *e.g.*, within the GTPase domain, are linked to increased kinase activity and, hence, neurotoxicity is still a matter of debate.[1] Interestingly, use of the selective LRRK2 inhibitor CZC-25146 blocked neurotoxicity induced by LRRK2 R1441C, a mutation outside the kinase domain, in cultured human cortical neurons.[24] To complicate matters further, it has recently been shown that a risk factor for PD, the G2385R mutation in LRRK2's C-terminal WD40 domain, is associated with a partial loss of kinase function and that deletion of the entire C-terminus abolishes kinase function altogether.[68] This study therefore suggests that the simple assumption LRRK2 inhibitor = PD treatment or LRRK2 inhibitor = treatment for patients with testable PD mutations is probably not valid and needs to be thoroughly tested experimentally. On the other hand, careful examination of the precise correlation between the type of mutation, increased kinase activity and therefore possible patient benefit, may result in commercial opportunities for pharmaceutical/diagnostics companies in the field of

companion diagnostics. Carriers of gain-of-function mutations in LRRK2 may require fundamentally different dosing regimens to other PD patients. One possible avenue for future drug discovery in the field is therefore that of personalized/stratified medicine.

Moreover, the gain-of-function mutation G2019S may impact the potential of Type II kinase inhibitors, as the equilibrium of the active/inactive state is shifted to the former, which may reduce the efficacy of Type II kinase inhibitors in the mutation carriers.

11.7.2 Mechanism-Based Toxicity

Pronounced expression of LRRK2 in kidney and defined immune cells (but also in other organs)[35,39,42 44] invariably leads to the question of whether or not LRRK2 inhibition may be associated with unwanted effects such as immunosuppression or renal toxicity. The verdict is still out, but it can be assumed that the currently available potent, selective and (reasonably) metabolically stable LRRK2 inhibitors[23,24,28] will be instrumental in addressing this question. Brain penetration is not required for most of these studies; hence, several probe compounds could be tested side-by-side.

11.7.3 Utility in Other Therapy Areas Besides Parkinson's Disease

Molecular and cell biology work a few years ago suggested that LRRK2 be involved in the interferon-γ (IFN-γ) response.[45] A recent detailed study by a Merck–Serono team reported that LRRK2 expression in human peripheral blood mononuclear cells (hPBMCs) is increased after treatment with IFN-γ and -β as well as TNFα, but not by interleukins IL-1β, IL-15, IL-2 or insulin-like growth factor IGF-1.[42] More importantly, treatment of purified monocytes with the selective LRRK2 inhibitor LRRK2-IN-1 decreased IFN-γ-induced CD14 and CD16 expression with half-maximal effective concentrations of *ca.* 10 and 1 μM, respectively.[42] The significance of this finding is two-fold: On the one hand does it provide pharmacological evidence for the potential utility of LRRK2 inhibitors as treatment for immunological diseases that are mitigated by these cytokines. From a drug discovery and development perspective, the results suggest that easily accessible immune cells could be useful in the discovery of clinically useful pharmacodynamic biomarkers for LRRK2 inhibitors. Furthermore, mitigating a possible immunological component of PD may be a complementary function that could enhance the clinical efficacy of LRRK2 inhibitors.

Recently, LRRK2 was found to be a negative regulator of the transcription factor NFAT, an important regulator of the immune system, and to control the severity of inflammatory bowel disease (IBD). A LRRK2 KO led to more severe clinical symptoms of IBD and KO mice were more susceptible to experimental colitis.[69] However, Liu *et al.* showed with a KD mutant that

LRRK2-based NFAT regulation is a kinase-independent mechanism and thus may not present difficulties in LRRK2 kinase inhibitor development.

Since LRRK2 expression may be associated with IBD[69] and several cytokines are up-regulated in PD patients,[70] LRRK2 appears to play an important role in the immunological processes of these diseases and its inhibition might have the potential to attenuate progression of these diseases. Indeed, very recently a study using cultured microglia revealed that LRRK2 activity is increased in microglial inflammation and that inhibition of LRRK2 kinase activity by the selective LRRK2-IN-1 inhibitor attenuated inflammatory signaling in cultured microglia, as assessed by decreased TNF release, decreased lipopolysaccharide (LPS)-induced p38 phosphorylation, decreased LPS-induced increase in microglia process length, and decreased microglial chemotaxis.[48] These pharmacological findings are well supported by LRRK2 knock-down studies in cultured murine microglia.[71] As a consequence, brain-penetrant LRRK2 inhibitors may be tested in animal models of neuroinflammation outside of PD.

References

1. M. R. Cookson, *Nat. Rev. Neurosci.*, 2010, **11**, 791.
2. B. D. Lee, V. L. Dawson and T. M. Dawson, *Trends Pharmacol. Sci.*, 2012, **33**, 365.
3. T. Kramer, F. Lo Monte, S. Göring, B. Okala Amombo and B. Schmidt, *ACS Chem. Neurosci.*, 2012, **2**, 151.
4. V. S. Anand, L. J. Reichling, K. Lipinski, W. Stochaj, W. Duan, K. Kelleher, P. Pungaliya, E. L. Brown, P. H. Reinhart, R. Somberg, W. D. Hirst, S. M. Riddle and S. P. Braithwaite, *FEBS J.*, 2009, **276**, 466.
5. G. Drewes, C. Hopf and V. Reader, *US Pat.*, 2009220992, 2009.
6. B. D. Lee, J. H. Shin, J. Vankampen, L. Petrucelli, A. B. West, H. S. Ko, Y. I. Lee, K. A. Maguire-Zeiss, W. J. Bowers, H. J. Federoff, V. L. Dawson and T. M. Dawson, *Nat. Med.*, 2010, **16**, 998.
7. M. Liu, B. Dobson, M. A. Glicksman, Z. Yue and R. L. Stein, *Biochemistry*, 2010, **49**, 2008.
8. M. Li, C. J. Smith, M. T. Walker and T. J. Smith, *J. Biol. Chem.*, 2009, **284**, 22988.
9. M. Arita, T. Wakita and H. Shimizu, *J. Gen. Virol.*, 2008, **89**, 2518.
10. T. Gasser, *Expert Rev. Mol. Med.*, 2009, **11**, e22.
11. I. N. Rudenko, R. Chia and M. R. Cookson, *BMC Med.*, 2012, **10**, 20.
12. H. Chen, B. K. Chan, J. Drummond, A. A. Estrada, J. Gunzner-Toste, X. Liu, Y. Liu, J. Moffat, D. Shore, Z. K. Sweeney, T. Tran, S. Wang, G. Zhao, H. Zhu and D. J. Burdick, *J. Med. Chem.*, 2012, **55**, 5536.
13. M. Liu, S. Kang, S. Ray, J. Jackson, A. D. Zaitsev, S. A. Gerber, G. D. Cuny and M. A. Glicksman, *Biochemistry*, 2011, **50**, 9399.
14. I. Marin, *Mol. Biol. Evol.*, 2006, **23**, 2423.
15. I. F. Mata, W. J. Wedemeyer, M. J. Farrer, J. P. Taylor and K. A. Gallo, *Trends Neurosci.*, 2006, **29**, 286.

16. R. J. Nichols, N. Dzamko, J. E. Hutti, L. C. Cantley, M. Deak, J. Moran, P. Bamborough, A. D. Reith and D. R. Alessi, *Biochem. J.*, 2009, **424**, 47.
17. H. Yun, H. Y. Heo, H. H. Kim, N. DooKim and W. Seol, *Bioorg. Med. Chem. Lett.*, 2011, **21**, 2953.
18. L. Pedro, J. Padros, L. Beaudet, H. D. Schubert, F. Gillardon and S. Dahan, *Anal. Biochem.*, 2010, **404**, 45.
19. N. Dzamko, M. Deak, F. Hentati, A. D. Reith, A. R. Prescott, D. R. Alessi and R. J. Nichols, *Biochem. J.*, 2010, **430**, 405.
20. L. J. Reichling and S. M. Riddle, *Biochem. Biophys. Res. Commun.*, 2009, **384**, 255.
21. J. P. Covy and B. I. Giasson, *Biochem. Biophys. Res. Commun.*, 2009, **378**, 473.
22. N. Hottecke, M. Liebeck, K. Baumann, R. Schubenel, E. Winkler, H. Steiner and B. Schmidt, *Bioorg. Med. Chem. Lett.*, 2010, **20**, 2958.
23. X. Deng, N. Dzamko, A. Prescott, P. Davies, Q. Liu, Q. Yang, J. D. Lee, M. P. Patricelli, T. K. Nomanbhoy, D. R. Alessi and N. S. Gray, *Nat. Chem. Biol.*, 2011, **7**, 203.
24. N. Ramsden, J. Perrin, Z. Ren, B. D. Lee, N. Zinn, V. L. Dawson, D. Tam, M. Bova, M. Lang, G. Drewes, M. Bantscheff, F. Bard, T. M. Dawson and C. Hopf, *ACS Chem. Biol.*, 2011, **6**, 1021.
25. M. Bantscheff, D. Eberhard, Y. Abraham, S. Bastuck, M. Boesche, S. Hobson, T. Mathieson, J. Perrin, M. Raida, C. Rau, V. Reader, G. Sweetman, A. Bauer, T. Bouwmeester, C. Hopf, U. Kruse, G. Neubauer, N. Ramsden, J. Rick, B. Kuster and G. Drewes, *Nat. Biotechnol.*, 2007, **25**, 1035.
26. A. J. Olaharski, H. Bitter, N. Gonzaludo, R. Kondru, D. M. Goldstein, T. S. Zabka, H. Lin, T. Singer and K. Kolaja, *Toxicol. Sci.*, 2010, **118**, 266.
27. A. J. Olaharski, N. Gonzaludo, H. Bitter, D. Goldstein, S. Kirchner, H. Uppal and K. Kolaja, *PLoS Comput. Biol.*, 2009, **5**, e1000446.
28. J. Zhang, X. Deng, H. G. Choi, D. R. Alessi and N. S. Gray, *Bioorg. Med. Chem. Lett.*, 2012, **22**, 1864.
29. M. I. Davis, J. P. Hunt, S. Herrgard, P. Ciceri, L. M. Wodicka, G. Pallares, M. Hocker, D. K. Treiber and P. P. Zarrinkar, *Nat. Biotechnol.*, 2011, **29**, 1046.
30. H. G. Choi, J. Zhang, X. Deng, J. M. Hatcher, M. P. Patricelli, Z. Zhao, D. R. Alessi and N. S. Gray, *ACS Med. Chem.*, 2012.
31. B. Chan, A. Estrada, Z. Sweeney and E. G. McIver, *Pat.*, WO 2011/141756 A1, 2011.
32. B. Chan, H. Chen, A. Estrada, D. Shore, Z. Sweeney and E. McIver, *Pat.*, WO 2012/038743 A1, 2012.
33. J. A. Miccauley, H. A. Rajapakse, T. J. Greshock, J. Sander, B. Kim, V. L. Rada, J. T. Kern, H. H. Stevenson and M. T. Bilodeau, *Pat.*, WO 2012/058193 A1, 2012.
34. P. L. Nichols, A. J. Eatherton, P. Bamborough, K. S. Jandu, O. J. Philips and D. Andreotti, *Pat.*, WO 2011/038872 A1, 2011.

35. M. Westerlund, A. C. Belin, A. Anvret, P. Bickford, L. Olson and D. Galter, *Neuroscience*, 2008, **152**, 429.
36. A. Zimprich, S. Biskup, P. Leitner, P. Lichtner, M. Farrer, S. Lincoln, J. Kachergus, M. Hulihan, R. J. Uitti, D. B. Calne, A. J. Stoessl, R. F. Pfeiffer, N. Patenge, I. C. Carbajal, P. Vieregge, F. Asmus, B. Muller-Myhsok, D. W. Dickson, T. Meitinger, T. M. Strom, Z. K. Wszolek and T. Gasser, *Neuron*, 2004, **44**, 601.
37. International Parkinson Disease Genomics Consortium, *Lancet*, **377**, 641.
38. A. B. West, D. J. Moore, S. Biskup, A. Bugayenko, W. W. Smith, C. A. Ross, V. L. Dawson and T. M. Dawson, *Proc. Natl. Acad. Sci. U. S. A.*, 2005, **102**, 16842.
39. M. C. Herzig, C. Kolly, E. Persohn, D. Theil, T. Schweizer, T. Hafner, C. Stemmelen, T. J. Troxler, P. Schmid, S. Danner, C. R. Schnell, M. Mueller, B. Kinzel, A. Grevot, F. Bolognani, M. Stirn, R. R. Kuhn, K. Kaupmann, P. H. van der Putten, G. Rovelli and D. R. Shimshek, *Hum. Mol. Genet.*, 2011, **20**, 4209.
40. Y. Tong, H. Yamaguchi, E. Giaime, S. Boyle, R. Kopan, R. J. Kelleher and J. Shen, *Proc. Natl. Acad. Sci. U. S. A.*, 2010, **107**, 9879.
41. S. Biskup, D. Moore, A. Rea, B. Lorenz-Deperieux, C. Coombes, V. Dawson, T. Dawson and A. West, *BMC Neurosci.*, 2007, **8**, 102.
42. J. Thevenet, R. Pescini Gobert, R. Hooft van Huijsduijnen, C. Wiessner and Y. J. Sagot, *PLoS One*, 2011, **6**, e21519.
43. M. Kubo, Y. Kamiya, R. Nagashima, T. Maekawa, K. Eshima, S. Azuma, E. Ohta and F. Obata, *J. Neuroimmunol.*, 2010, **229**, 123.
44. T. Maekawa, M. Kubo, I. Yokoyama, E. Ohta and F. Obata, *Biochem. Biophys. Res. Commun.*, 2010, **392**, 431.
45. A. Gardet, Y. Benita, C. Li, B. E. Sands, I. Ballester, C. Stevens, J. R. Korzenik, J. D. Rioux, M. J. Daly, R. J. Xavier and D. K. Podolsky, *J. Immunol.*, 2010, **185**, 5577.
46. N. Dzamko, F. Inesta-Vaquera, J. Zhang, C. Xie, H. Cai, S. Arthur, L. Tan, H. Choi, N. Gray, P. Cohen, P. Pedrioli, K. Clark and D. R. Alessi, *PLoS One*, 2012, **7**, e39132.
47. B. D. Looyenga, K. A. Furge, K. J. Dykema, J. Koeman, P. J. Swiatek, T. J. Giordano, A. B. West, J. H. Resau, B. T. Teh and J. P. MacKeigan, *Proc. Natl. Acad. Sci. U. S. A.*, 2011, **108**, 1439.
48. M. S. Moehle, P. J. Webber, T. Tse, N. Sukar, D. G. Standaert, T. M. DeSilva, R. M. Cowell and A. B. West, *J. Neurosci.*, 2012, **32**, 1602.
49. A. H. Brand and N. Perrimon, *Development*, 1993, **118**, 401.
50. S. B. Lee, W. Kim, S. Lee and J. Chung, *Biochem. Biophys. Res. Commun.*, 2007, **358**, 534.
51. Z. Liu, X. Wang, Y. Yu, X. Li, T. Wang, H. Jiang, Q. Ren, Y. Jiao, A. Sawa, T. Moran, C. A. Ross, C. Montell and W. W. Smith, *Proc. Natl. Acad. Sci. U. S. A.*, 2008, **105**, 2693.
52. A. Sakaguchi-Nakashima, J. Y. Meir, Y. Jin, K. Matsumoto and N. Hisamoto, *Curr. Biol.*, 2007, **17**, 592.

53. C. Yao, R. El Khoury, W. Wang, T. A. Byrd, E. A. Pehek, C. Thacker, X. Zhu, M. A. Smith, A. L. Wilson-Delfosse and S. G. Chen, *Neurobiol. Dis.*, 2010, **40**, 73.
54. D. Sheng, D. Qu, K. H. H. Kwok, S. S. Ng, A. Y. M. Lim, S. S. Aw, C. W. H. Lee, W. K. Sung, E. K. Tan, T. Lufkin, S. Jesuthasan, M. Sinnakaruppan and J. Liu, *PLoS Genet.*, 2010, **6**, e1000914.
55. Y. Li, W. Liu, T. F. Oo, L. Wang, Y. Tang, V. Jackson-Lewis, C. Zhou, K. Geghman, M. Bogdanov, S. Przedborski, M. F. Beal, R. E. Burke and C. Li, *Nat. Neurosci.*, 2009, **12**, 826.
56. X. Lin, L. Parisiadou, X. L. Gu, L. Wang, H. Shim, L. Sun, C. Xie, C. X. Long, W. J. Yang, J. Ding, Z. Z. Chen, P. E. Gallant, J. H. Tao-Cheng, G. Rudow, J. C. Troncoso, Z. Liu, Z. Li and H. Cai, *Neuron*, 2009, **64**, 807.
57. H. L. Melrose, J. C. Dächsel, B. Behrouz, S. J. Lincoln, M. Yue, K. M. Hinkle, C. B. Kent, E. Korvatska, J. P. Taylor, L. Witten, Y. Q. Liang, J. E. Beevers, M. Boules, B. N. Dugger, V. A. Serna, A. Gaukhman, X. Yu, M. Castanedes-Casey, A. T. Braithwaite, S. Ogholikhan, N. Yu, D. Bass, G. Tyndall, G. D. Schellenberg, D. W. Dickson, C. Janus and M. J. Farrer, *Neurobiol. Dis.*, 2010, **40**, 503.
58. X. Li, J. C. Patel, J. Wang, M. V. Avshalumov, C. Nicholson, J. D. Buxbaum, G. A. Elder, M. E. Rice and Z. Yue, *J. Neurosci.*, 2010, **30**, 1788.
59. D. Ramonet, J. P. L. Daher, B. M. Lin, K. Stafa, J. Kim, R. Banerjee, M. Westerlund, O. Pletnikova, L. Glauser, L. Yang, Y. Liu, D. A. Swing, M. F. Beal, J. C. Troncoso, J. M. McCaffery, N. A. Jenkins, N. G. Copeland, D. Galter, B. Thomas, M. K. Lee, T. M. Dawson, V. L. Dawson and D. J. Moore, *PLoS One*, 2011, **6**, e18568.
60. M. C. Herzig, M. Bidinosti, T. Schweizer, T. Hafner, C. Stemmelen, A. Weiss, S. Danner, N. Vidotto, D. Stauffer, C. Barske, F. Mayer, P. Schmid, G. Rovelli, P. H. van der Putten and D. R. Shimshek, *PLoS One*, 2012, **7**, e36581.
61. L. Osherovich, *SciBX: Science–Business eXchange*, 2010, **3**.
62. http://www.tautatis.com/home.html.
63. J. W. Kim, J. Lee, H.-J. Song, Y. Kim, H. K. Lee, J.-S. Choi, S.-H. Lim and S. Chang, *Pat.*, WO 2011/053861 A1, 2011.
64. J. Lee, H.-J. Song, J. S. Koh, L. K. Lee, Y. Kim, S. Chang, H. W. Kim, S. Chang, S.-H. Lim, J.-S. Choi, J.-H. Kim and S.-W. Kim, *Pat.*, WO 2011/060295 A1, 2011.
65. E. G. Mciver, E. Smiljanic, D. J. Harding and J. Hough, *Pat.*, WO 2010/106333 A1, 2010.
66. N. G. Ramsden, *Pat.*, WO2009127642 A2, 2009.
67. A. B. West, D. J. Moore, C. Choi, S. A. Andrabi, X. Li, D. Dikeman, S. Biskup, Z. Zhang, K. L. Lim, V. L. Dawson and T. M. Dawson, *Hum. Mol. Genet.*, 2007, **16**, 223.
68. I. N. Rudenko, A. Kaganovich, D. N. Hauser, A. Beylina, R. Chia, J. Ding, D. Maric, H. Jaffe and M. R. Cookson, *Biochem. J.*, 2012, **446**, 99.

69. Z. Liu, J. Lee, S. Krummey, W. Lu, H. Cai and M. J. Lenardo, *Nat. Immunol.*, 2011, **12**, 1063.
70. B. Brodacki, J. Staszewski, B. Toczyłowska, E. Kozłowska, N. Drela, M. Chalimoniuk and A. Stępien, *Neurosci. Lett.*, 2008, **441**, 158.
71. B. Kim, M. S. Yang, D. Choi, J. H. Kim, H. S. Kim, W. Seol, S. Choi, I. Jou, E. Y. Kim and E. H. Joe, *PLoS One*, 2012, **7**, e34693.

4.5 Indolinon-basierende LRRK2-Kinase-Inhibitoren mit einer wichtigen Wasserstoffbrücke

Der Inhalt dieses Kapitels wurde bereits veröffentlicht.

Autoren: Stefan Göring, Jean-Marc Taymans, Veerle Baekelandt, Boris Schmidt.
Titel: „Indolinone based LRRK2 kinase inhibitors with a key hydrogen bond".
Journal: Bioorganic & Medicinal Chemistry Letters.
DOI: 10.1016/j.bmcl.2014.08.049.

Zusammenfassung:
Die Parkinson-Krankheit ist nach der Alzheimer-Krankheit die zweithäufigste neurodegenerative Erkrankung. Sie ist klinisch durch eine Zahl von Symptomen gekennzeichnet wie Tremor, Bradykinese, posturale Instabilität und Rigor gekennzeichnet. Spezifische neuropathologische Kennzeichen sind der Verlust dompaminerger Zellen in der *Substantia nigra pars compacta* sowie die Formation intrazellulärer Fibrillen und *Lewy bodies* in den überlebenden Neuronen.
Die *leucine-rich-repeat kinase 2* (LRRK2) ist ein multidomänen-Komplex, bestehend aus 2527 Aminosäuren. Mindestens fünf Mutationen (R1441C, R1441G, Y1699C, G2019S, I2020T) stehen derzeit unter Verdacht der Pathogenität und sind im katalytischen Zentrum von LRRK2 lokalisiert. Konvergierende Studien belegen, dass die Inhibition der LRRK2-Kinase ein wichtiges therapeutisches Konzept für die Behandlung der Parkinson-Krankheit darstellt. Die G2019S-Mutation in der Kinase-Domäne erhöht die Kinase-Aktivität um das 2-3-fache. Aufgrund dessen könnte die Entwicklung potenter und selektiver Kinase-Inhibitoren eine wichtige Strategie für die Behandlung darstellen.
Vorarbeiten zu FLT3 führten zu einem hochselektiven und potenten FLT3-Inhibitor mit einem IC_{50}-Wert von 4,1 nM. Aufgrund dessen struktureller Ähnlichkeit zu den bekannten LRRK2-Inhibitoren GW5047 und Sunitinib fokussierten wir unser Interesse auf die LRRK2-Inhibition. Es konnten durch Analyse der Struktur-Aktivitäts-Beziehungen eine Reihe von potenten Indolinon-basierenden LRRK2-Inhibitoren entwickelt werden. Die drei vielversprechendsten Inhibitoren **15a**, **20b** und **26d** weisen einen IC_{50}-Wert von 15 nM, 31 nM bzw. 46 nM auf. Dockingstudien von **15b** in die ATP-Bindungstasche zeigten eine

essentielle Wasserstoffbrücke der 4-Hydroxyl-Einheit mit den Aminosäuren E1920 sowie D2017. Die Synthese von **26b** lieferte den Beweis dafür. Der Vergleich der Aktivitäten zeigte eine starke Abnahme von 0,015 µM auf größer 10 µM. Zusätzlich wurde die Aktivität gegenüber der LRRK2-G2019S-Mutation von **15b** bestimmt. Diese lag mit 10 nM im selben Bereich wie für den wild-Typ. Die Bestimmung der Selektivität von **15b** wurde gegenüber 46 humanen Kinasen untersucht. Lediglich zwei weitere Kinasen wurden bei einer Konzentration von 1 µM signifikant inhibiert. Das Zebrafisch-Toxizitäts-Assay zeigte, dass **15b** keine signifikante Toxizität unterhalb von 10 µM aufwies.

Eigener Beitrag zu dieser Arbeit:
Der synthetische Beitrag lag in allen Verbindungen. Des Weiteren wurden das molekulare Docking sowie das Zebrafisch-Toxizitäts-Assay von mir durchgeführt.

Bioorganic & Medicinal Chemistry Letters 24 (2014) 4630–4637

Contents lists available at ScienceDirect

Bioorganic & Medicinal Chemistry Letters

journal homepage: www.elsevier.com/locate/bmcl

Indolinone based LRRK2 kinase inhibitors with a key hydrogen bond

Stefan Göring [a,†], Jean-Marc Taymans [b], Veerle Baekelandt [b], Boris Schmidt [a,*]

[a] Clemens Schöpf—Institute of Organic Chemistry and Biochemistry, Technische Universität Darmstadt, 64287 Darmstadt, Hessen, Germany
[b] KU Leuven, Laboratory for Neurobiology and Gene Therapy, Leuven B-3000, Belgium

ARTICLE INFO

Article history:
Received 11 June 2014
Revised 20 August 2014
Accepted 21 August 2014
Available online 29 August 2014

Keywords:
Parkinson's disease
Leucine-rich repeat kinase 2 (LRRK2)
LRRK2-inhibitors
Zebrafish phenotype

ABSTRACT

The most prevalent leucine-rich repeat kinase 2 (LRRK2) mutation G2019S is associated with Parkinson's disease (PD). It enhances kinase activity and has been identified in both familial and sporadic cases. Kinase activity was reported to be required for LRRK2 mutants to exert their toxic effects. Hence LRRK2 kinase inhibition may be a promising therapeutic target for PD. Here we report on the discovery and characterization of indolinone based LRRK2 inhibitors. Indolinone **15b**, the most potent and selective inhibitor of the present series, is characterized by an IC_{50} of 15 nM against wild-type LRRK2 and 10 nM against the LRRK2 G2019S mutant, respectively. Compound **15b** was further evaluated in a kinase panel including 46 human protein kinases and in a zebrafish embryo phenotype assay, which enabled toxicity determination in whole organisms.

Parkinson's disease (PD) is after Alzheimer's disease the second most common, age related, neurodegenerative disorder, affecting about 2% of the population older than 60 years.[1] It is characterized clinically by a number of symptoms, for example, tremor at rest, bradykinesia, rigidity and postural instability. Specific neuropathological hallmarks for PD are the neuronal cell loss in dopaminergic neurons of the substantia nigra pars compacta and the formation of intracellular fibrils and Lewy bodies in the surviving neurons. A major component of Lewy bodies is α-synuclein.[2] To date the underlying molecular mechanism of PD remains poorly understood and there is no cure for this disease.

The leucine-rich repeat kinase 2 (LRRK2) is a multi-domain protein and consists of 2527 amino acids. Several independent domains are known for the LRRK2 protein including both a serine/threonine kinase and a GTPase domain. Several mutations have been identified inside the protein, at least five of them (R1441C, R1441G, Y1699C, G2019S and I2020T) are currently assumed to be pathogenic and are localized in the catalytic core.[3–5] The most prevalent mutation is the glycine to serine amino acid substitution, which is present in more than 85% of familial PD patients carrying LRRK2 mutations.[6]

Converging studies point to the inhibition of LRRK2 kinase activity as a therapeutic concept. First, the G2019S mutation in the kinase domain increases the kinase activity 2- to 3-fold compared to its wild type counterpart.[7–9] This effect may guide the pharmacological development of kinase inhibitors for a potential PD therapy. Second, the cellular toxicity of acute overexpression of LRRK2 clinical mutants is ablated when these mutations are combined with mutations inactivating the kinase activity, both in cell culture and primary neurons,[7,10] as well as in viral vector mediated brain overexpression in rodents.[11,12] Although pharmacological studies have begun to indicate that LRRK2 kinase inhibition may be beneficial in reversing LRRK2 mediated toxicity,[12] further confirmation studies with more potent and specific LRRK2 inhibitors are required.[13,14]

At present different chemotypes of LRRK2 inhibitors are known (Fig. 1). Compounds of several structural families as indolinone **1** (GW5074),[12] the diaminopyridines **2** (LRRK2-IN-1),[15] **3** (TAE684)[16] and **4** (HG-10-102-01),[17] the cinnoline derivative **5**[18] or the triazolpyridine **6**[19] are potent LRRK2 kinase inhibitors. Especially the LRRK2 inhibitor HG-10-102-01 **4** exhibited good selectivity and pharmacokinetic properties regarding brain penetration and dephosphorylated Ser910 and Ser935 in tissues including kidney, spleen and brain.[17]

Nevertheless, the ideal LRRK2 inhibitor has not yet been reported. Thus the interest to explore activities of multiple classes of compounds that provide desirable characteristics such as potency, selectivity, cellular activity and brain penetrance, to name a few, remains in focus.[3]

In a previous study we have reported the inhibition of the FMS-like tyrosine kinase-3 (FLT-3) by substituted indolinones.[20] FLT-3 is involved and aberrantly active in acute myeloid leukemia (AML).[21,22] Working on FLT-3 inhibitors we have identified a highly

* Corresponding author. Tel.: +49 6151 163075, +49 6151 164531; fax: +49 6151 163278.
E-mail address: schmidt_boris@t-online.de (B. Schmidt).
† Tel.: +49 6151 164531; fax: +49 6151 163278.

http://dx.doi.org/10.1016/j.bmcl.2014.08.049
0960-894X/

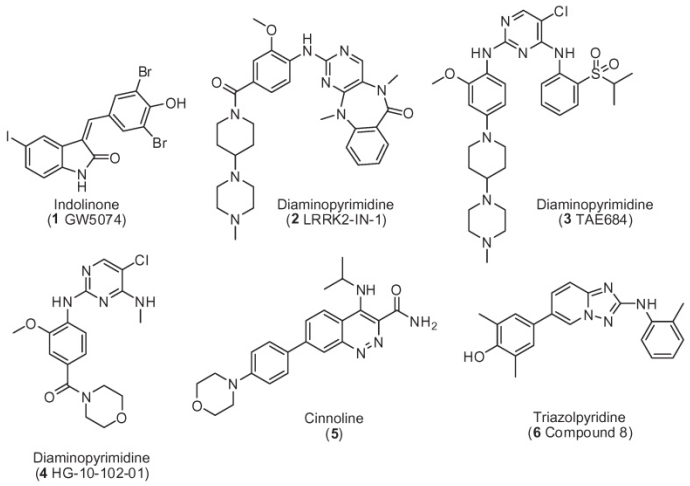

Figure 1. Selected chemotypes as lead structures for the development of new LRRK2 inhibitors.[12,15–19]

active and selective compound based on the indolinone scaffold (Fig. 2). The indolinone **7** exhibited an IC_{50} value for FLT-3 in the low nanomolar range. Additionally, the selectivity of indolinone derivative **7** was determined at a concentration of 1 μM against 50 human protein kinases.[20] Beside FLT-3 only two other kinases (MAP4K4 and JAK3) were also inhibited by this compound. Unfortunately, LRRK2 was not part of this kinase screening. Due to the structural analogy of compound **7** to the known LRRK2 inhibitors **1** (GW5074) and Sunitinib, a well-known multi-kinase inhibitor, we refocused our interest on the inhibition of LRRK2. A recent publication by Novartis confirmed the efficiency of indolinones as selective and brain penetrant LRRK2 inhibitors.[23]

In the absence of a full-length LRRK2 crystal structure analysis, the use and construction of LRRK2 homology models is the key for structure based design. In order to gain insight in how the indolinone derivative **7** interacts with the ATP-binding pocket of LRRK2 we performed docking studies of **7** in a LRRK2 homology model. Based on the sequence identity with the LRRK2 kinase domain, the tyrosine-kinase like kinase B-Raf (PDB 4DBN) was selected as template to model LRRK2 kinase. The alignment between the LRRK2 kinase domain and B-Raf kinase was performed using the automatic mode of the Swiss Model server.[24,25] The final homology model was visualized using Molegro Virtual Docker 6. The validity of docking compounds onto a modeled structure of LRRK2 kinase was recently demonstrated using a kinome-wide kinase inhibitor panel correlating docking scores to compound.[26]

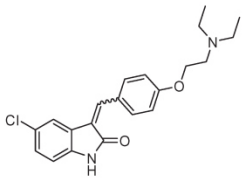

7
IC_{50} (FLT3) = 4.1 nM

Figure 2. Highly potent and selective indolinone inhibitor for FLT3.[20]

This model revealed that the indolinone moiety favorably interacts with the backbone of LRRK2 ATP pocket. Additionally an important interaction was observed with the diethylaminoethoxy anchor. The nitrogen of the diethylamine group interacts with the rear of the ATP-binding pocket and forms a strong hydrogen bond to K1906 in addition to several hydrophobic interactions with amino acids in the close surroundings of the phenol moiety. To confirm the docking results of indolinone derivative **7** in the LRRK2 homology model the potency of this compound was determined against LRRK2 in an in vitro peptide substrate based kinase activity assay at concentrations of 10 and 1 μM (assay information is available in the Supplementary data and referenced in 27 and 26). Those results agreed with our hypothesis and previous docking studies. Thus, indolinone **7** reduces in vitro LRRK2 activity by more than 50% relative to control for both concentrations (Table 1). At 10 and 1 μM of compound, residual LRRK2 kinase activities of 12% and 11% were observed, respectively. To assess the activity of compound **7** more precisely we determined the IC_{50} value additionally. An IC_{50} value of 0.265 μM clearly demonstrated the submicromolar potency of compound **7** and consequently indolinones as LRRK2 inhibitors. Based on these encouraging results indolinone **7** was an attractive lead structure for further structure–activity-relationship (SAR) optimization.

Additional indolinone derivatives were synthesized by known conditions using a Knoevenagel condensation between indolinone and the corresponding aldehydes in methanol and a catalytic amount of piperidine. The Knoevenagel condensation is a reliable and quick method to establish chemical diversity for the variation of the SAR study based on compound **7**. The synthesis is outlined in Scheme 1. The first step provides the aldehydes for the subsequent Knoevenagel condensation. Hence, the alkyl and aryl benzyl halides were connected with derivatives of 4-hydroxybenzaldehydes **8a**–**c**

Table 1
LRRK2 activity of compound **7**

Compound	LRRK2 activity		IC_{50}
	10 μM of compd	1 μM of compd	
7	12%	11%	0.265 μM

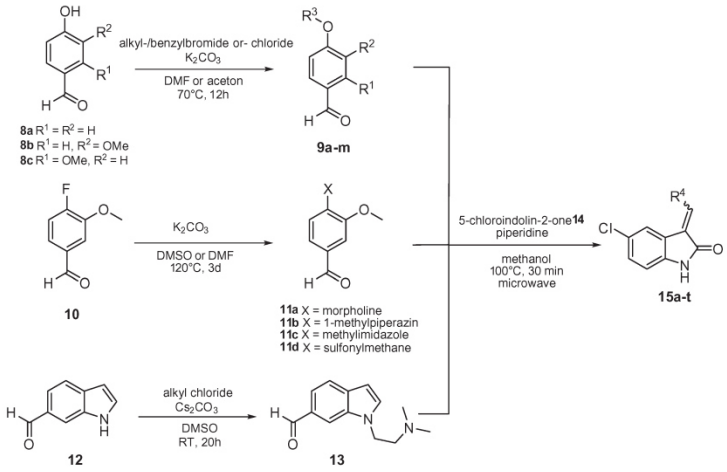

Scheme 1. Synthesis of aldehydes derivatives for the following Knoevenagel condensation.

Table 2
Synthesized indolinone derivatives and their in vitro LRRK2 inhibitory activity

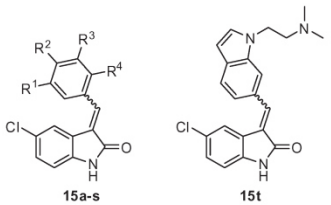

Compound	R^1	R^2	R^3	R^4	LRRK2 activity		IC_{50} (μM)
					10 μM of compd (%)	1 μM of compd (%)	
Staurosporine*	–	–		–	2	5	–
LRRK2-IN-1*	–	–		–	5	13	0.0035
15a	F	OH	F	H	2	5	0.261
15b	Br	OH	Br	H	4	3	0.015
15c	H	OH	H	H	8	12	12
15d	H	2-Morpholinoethoxy	OMe	H	9	8	0.163
15e	H	2-(Dimethylamino)ethoxy	H	H	3	22	0.466
15f	H	H	H	H	16	27	10
15g	H	2-Morpholinoethoxy	H	H	15	37	0.205
15h	H	2-(Diethylamino)ethoxy	OMe	H	24	26	–
15i	H	Acetamide	H	H	28	26	10
15j	H	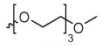	OMe	H	24	26	–
15k	H	4-Methylpiperazin-1-yl	OMe	H	26	32	–
15l	H	4-Morpholino	OMe	H	33	22	–
15m	H	OMe	H	H	42	47	–
15n	H	2-(Dimethylamino)ethoxy	H	OMe	29	62	–
15o	H	3-(1*H*-tetrazol-5-yl)propoxy	H	H	38	85	–
15p	H	4-Methyl-1*H*-imidazol-1-yl	OMe	H	41	52	–
15q	H	Tosyl	OMe	H	48	50	–
15r	H	4-Methoxybenzonitrile	H	H	74	52	–
15s	H	Methyl 4-(methoxy)benzoate	H	H	85	89	–
15t	–	–	–	–	26	56	–

* Control.

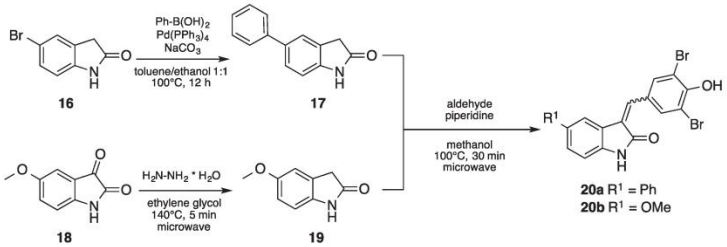

Scheme 2. Synthesis of compounds **20a** and **20b**.

under basic conditions to obtain a number of structurally diverse compounds **9a**–**m** in good yields (see Supporting information).[20] Furthermore 4-fluoro-3-methoxybenzaldehyde **10** was connected to the corresponding cyclic amines **11a**–**c** and to its corresponding sulfonyl derivative **11d**. An aminoalkylation of 1*H*-indole-6-carbaldehyde **12** resulted in aldehyde **13**. The final condensation was carried out in a microwave reactor. The reaction of 5-chloroindolin-2-one **14** with the commercial and synthesized aldehydes yielded the indolinone derivatives **15a**–**t** in good yields up to 97% (Table 2).

The obtained indolinone derivatives **15a**–**t** were tested for their ability to inhibit LRRK2 kinase activity (assay conditions available in Supplementary data).[26,27] Indeed most of the synthesized indolinone derivatives **15a**–**t** exhibited good in vitro activity reducing LRRK2 activity below 50% at 10 μM (Table 2). Two exceptions are the derivatives **15r** and **15s**, which were unable to significantly reduce the in vitro LRRK2 activity (reduction to 74% and 85%, respectively). This may be caused by the length and the size of the second phenyl ring. On the contrary, indolinone derivatives which have no or a short substitution at the 4-hydroxyl of the phenol exhibited high potency against LRRK2 at a concentration of 10 μM. Three of them, the derivatives **15a**–**b** and **15d**, also reduced LRRK2 activity below 10% in the presence of 1 μM test compound. Additionally we determined the IC_{50}'s of selected indolinone derivatives (Table 2). Compound **15b** is highly potent against LRRK2 with an IC_{50} value of 15 nM. Interestingly, indolinone derivative **15b** is closely related to the known brain-penetrant, non-selective LRRK2 inhibitor GW5074 **1**, only the substitution to chlorine in the 5th position of the indol ring is different (Fig. 1). Remarkably this compound **15b** exhibited a 53-fold higher activity against LRRK2 than GW5074 **1** (IC_{50} of 880 nM).[12] Further impacts on the activity of derivative **15b** have substitutions in the 3rd and 5th position of the phenol ring. Compounds **15c** and **15f**, which lack substitutions in this position, displayed a dramatic decrease in LRRK2 inhibitory activity (IC_{50} = 12 μM and IC_{50} = 10 μM, respectively) in comparison to the compounds **15a**–**b** and **15d**.

The chlorine of lead compound **15b** was further substituted (Scheme 2). Two residues with different sizes were chosen to analyze the impact regarding LRRK2 activity on this position. Intermediate **17** was generated via Suzuki coupling between 5-bromoindolin-2-one **16** and benzeneboronic acid. Furthermore isatin **18** was reduced using hydrazine monohydrate to yield indolinone derivative **19**. The final compounds **20a** and **20b** were coupled via Knoevenagel condensation. The LRRK2 activities of compounds **20a** and **20b** are given in Table 3. Derivative **20a**, carrying the phenyl residue, exhibited a 6-fold decrease in LRRK2 activity (0.204 μM) compared to its corresponding methoxy derivative **20b** with 0.031 μM LRRK2 inhibitory activity.

Next, docking studies were performed to analyze the potential binding mode of the most active LRRK2 inhibitor **15b**. Models of compound **15b** docked into the ATP-binding site of LRRK2 are shown in Figures 3A and B. The indolinone core favorably interacts with the backbone of LRRK2. Especially glutamic acid 1948 is close to the N–H motif of the indole and forms a strong hydrogen bond, whereas the chlorine of the indolinone core binds towards the solvent exposed region of the ATP-binding site (Fig. 3A and B). More important are the interactions of the 3,5-dibromo-4-phenol moiety with the rear of the mostly hydrophobic binding pocket (Fig. 3A and B). Hydrophobic interactions were observed between the phenol ring and the gatekeeper residue M1947 in addition to several hydrophobic interactions with the 3,5-dibromo substitutions (e.g., L1924 and G1888). The 4-hydroxy group of the phenol turns

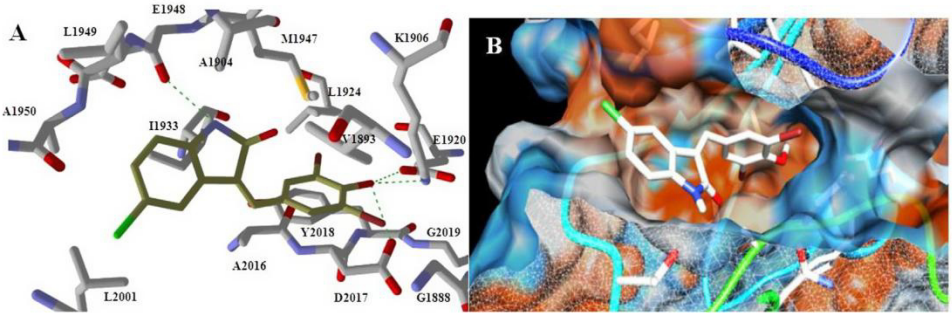

Figure 3. Suggested binding mode of compound **15b**. The homology model of LRRK2 was made using the Swiss Model server.[24,25] The molecular docking was performed using the software Molegro Virtual Docker 6. (A) Compound **15b** (brown) docked in the ATP-binding site of LRRK2. Important interactions are shown as green dashed lines. (B) Surface illustration of the ATP-binding site of LRRK2 and the ligand **15b** (white).

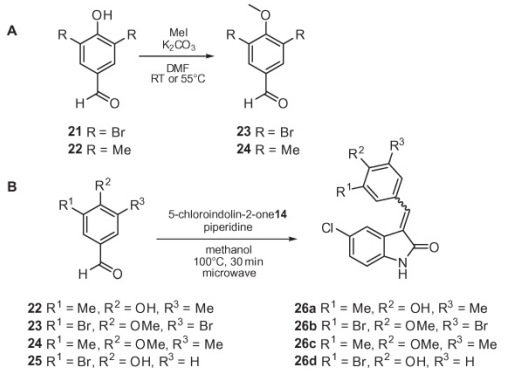

Scheme 3. (A) Methylation of aldehydes **21** and **22** to its corresponding counterparts **23** and **24**. (B) Connecting the aldehydes with indolinone **14** via Knoevenagel condensation.

Table 3
Indolinone derivatives **20a** and **20b** and their in vitro LRRK2 inhibitory activity

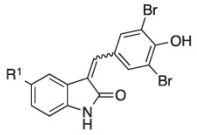

Compound	R^1	IC_{50} (μM)
20a	Ph	0.204
20b	OMe	0.031

Table 4
Synthesized indolinone derivatives and their in vitro LRRK2 inhibitory activity

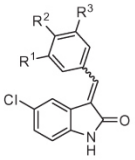

Compound	R^1	R^2	R^3	IC_{50} (wt LRRK2) (μM)	IC_{50} (LRRK2 G2019S)
15b	Br	OH	Br	0.015	0.010 μM
26a	Me	OH	Me	0.194	–
26b	Br	OMe	Br	>10	–
26c	Me	OMe	Me	1.5	–
26d	Br	OH	H	0.046	0.064 μM

out to be particularly important. As already speculated by Chen et al.,[19] the 4-hydroxyl of the triazolpyridine **6** (Fig. 1) may act as a donor and as an acceptor, but this has not been proven. This interaction is also clearly represented in Figure 3A. On the one hand the 4-hydroxyl group of compound **15b** is donating two hydrogen bonds to the conserved residues E1920 and D2017, whereas it also acts as an acceptor by forming a strong H-bond with K1906.

To confirm the docking results and to confirm the importance of the hydroxyl group in the 4th position of the phenol ring a second round of derivatization was performed. A replacement of the hydroxyl should result in loss of LRRK2 inhibitory activity. Therefore additional indolinone derivatives were synthesized (outlined in Scheme 3 and Table 4). The easiest way to establish the role of a hydroxyl in this position is replacement of the hydrogen atom by a methyl group. Therefore, in the presence of methyl iodide and potassium carbonate compound **21** was converted to its corresponding aldehyde **23**. Substitutions in the 3rd and 5th position of the phenol ring also influence LRRK2 inhibitory activity. The commercial 4-hydroxy-3,5-dimethylbenzaldehyde **22**, its corresponding methylated counterpart **24** and the commercial aldehyde **25** which carries only one bromine in the 3rd position were also coupled under the same Knoevenagel conditions with indolinone **14** in good yields between 77% and 89% (Scheme 3, Table 3).

The obtained indolinone derivatives **26a–d** were also tested for their ability to inhibit LRRK2 kinase activity in vitro (Table 4). As expected, the methylation of the phenol oxygen resulted in a dramatic loss of in vitro LRRK2 activity. The comparison of compounds **15b** and **26b** indicates a multiple drop of LRRK2 inhibitory activity from 0.015 μM to >10 μM. This was also confirmed by the indolinone derivatives **26a** and **26c**, respectively. The 3,5-dimethyl-4-hydroxy moiety of compound **26a** exhibited a reduced activity with an IC_{50} of 0.194 μM relative to compound **15b** (IC_{50} = 15 nM), but showed a 7 times higher activity concerning its corresponding methylated form **26c** with an IC_{50} of 1.5 μM (Table 3). This confirms the importance of a hydroxyl in position R^2 (Table 1 and Table 3) for the inactivating activity of indolinone based compounds. Remarkably compound **26d**, which carries one bromine only, exhibited also high potency against LRRK2 with an IC_{50} value of 0.046 μM.

G2019S, the most common disease-causing mutation in LRRK2 dramatically increased kinase activity. Additionally to the wild-type LRRK2 activity we determined the LRRK2 activity against the G2019S mutant for compounds **15b** and **26d** (Table 4). Both compounds inhibited the LRRK2 G2019S mutant in a similar manner as obtained for wild type LRRK2 with 0.010 μM for compound **15b** and 0.064 μM for compound **26d**, respectively.

The indolinone scaffold is well known of its activity in inhibiting several different classes of kinases. Therefore we next examined the kinase selectivity of lead compound **15b**. The kinase selectivity of compound **15b** was assessed against a panel (ExpresS Diversity kinase profile) of 46 human protein kinases (Fig. 4). At a concentration of 1 μM compound **15b** merely inhibited the serine/threonine kinases of HGK (MAPAK4) and Pimp2 with a residual activity below 30%. These results suggest that **15b** is a selective LRRK2 inhibitor, however further profiling against additional kinases are needed.

After the evaluation of the in vitro activity of this set of indolinone derivatives the most potent and promising compounds **15b** and **26d** were additionally tested for their in vivo activity on zebrafish embryos. The zebrafish (*Danio rerio*) has become a useful vertebrate model for assessing toxicological effects of chemicals and drugs and is standardized international.[28,29] Rapid development of the embryos, their small size, high fecundity and the ease of husbandry are advantages of zebrafish for a pharmacological and toxicological research.[28,30,31] Treatment of the zebrafish embryo with chemicals or drugs a phenotypic description of the zebrafish development provides data for compound permeability and safety.

The zebrafish embryos were collected and maintained in E3 medium at 28 °C. The indolinone derivatives **15b** and **26d** were added at 24 hpf (hours post fertilization) and the phenotypes were compared at 96 hpf (Fig. 5). At 20 μM compound **15b** caused a reduced growth compared to concentrations of 1, 5, 10 μM and the control (Fig. 5A–D and I). The zebrafish displayed stunted and crooked tails at a higher concentration of 30 μM. The lethality of the zebrafish was observed every 24 h up to 120 hpf. Above a

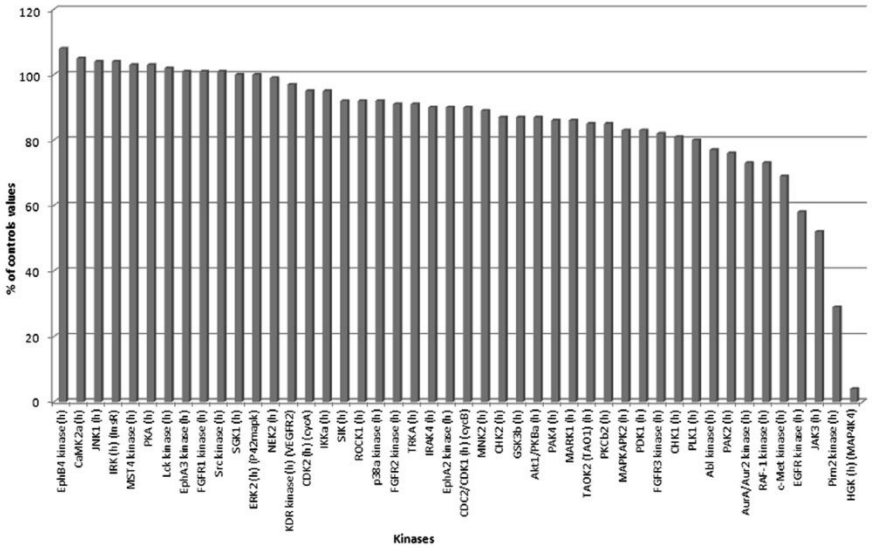

Figure 4. Screening of compound **15b** against 46 human protein kinases at 1 μM. Each bar represents the activity of one individual protein kinase (see Supplementary data for more details).

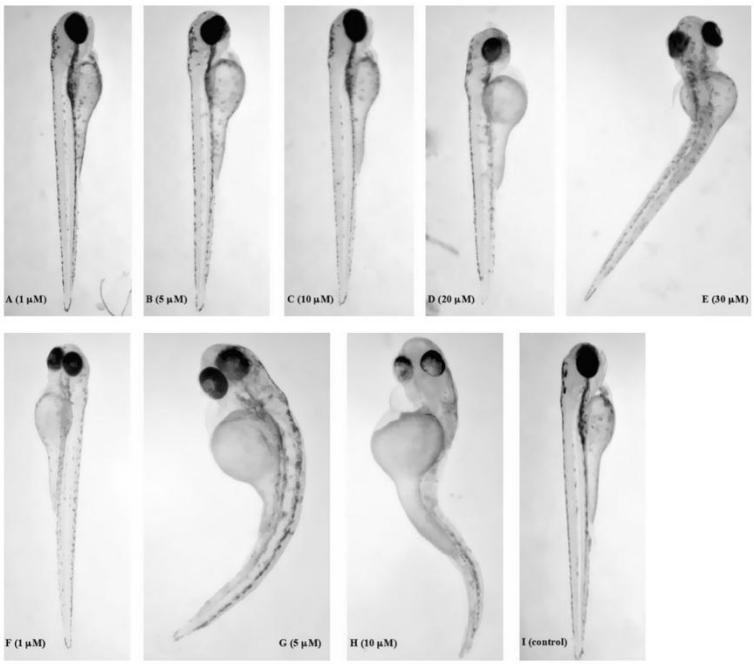

Figure 5. In vivo cytotoxicity with zebrafish embryos. The zebrafish embryos were collected and maintained in E3 medium at 28 °C. Compounds **15b** and **26d** were added 24 hpf (hours post fertilization) and the phenotypes were compared after 96 hpf. (A–E) Zebrafish embryos treated with compound **15b** in different concentrations of 1 μM (A), 5 μM (B), 10 μM (C), 20 μM (D) and 30 μM (E). (F–H) Exposure of the zebrafish embryos to 1 μM, 5 μM and 10 μM of **26d**. **26d** caused stunted and crooked tail at 5 μM, which is more pronounced at 10 μM. (I) Control embryo in 1% DMSO.

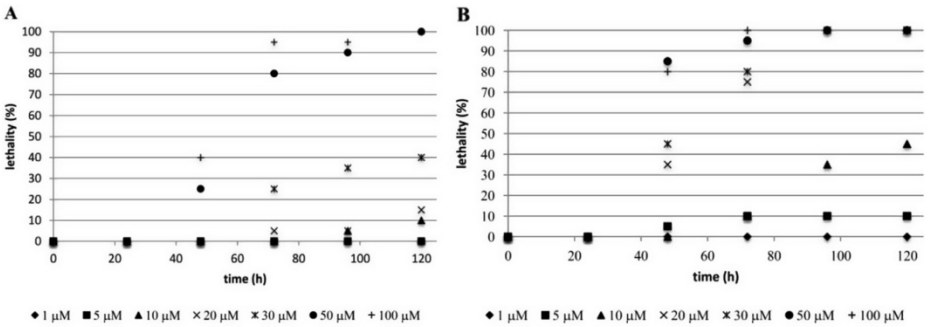

Figure 6. Lethality representation of the zebrafish embryos at different time points for indolinone derivative **15b** and **26d**. The observed data are expressed as averages of duplicates. (A) Lethality caused by compound **15b**. (B) Lethality caused by compound **26d**.

concentration of 30 μM **15b** we observed an increased lethality over time (Fig. 6A). After 120 hpf the lethality for concentrations of 50 μM and 100 μM of compound **15b** exhibited 100%, whereas at 30 μM 40% of the zebrafish embryos died. The zebrafish assay did not indicate any abnormalities and lethality at a concentration below 10 μM (Fig. 5A–D and 6). Related, but more distinct phenotypes were observed for compound **26d**. Reduced growth and stunted and crooked tails were already observed at a concentration of 5 μM, and this is more pronounced at 10 μM (Fig. 5G and H). Indolinone derivative **26d** also displayed a higher in vivo toxicity compared to **15b** (Fig. 6B). At a concentration above 10 μM the lethality increased dramatically over time. After 48 hpf the lethality of the zebrafish embryos increased over 80% for concentrations of 20 and 30 μM, respectively. Therefore, there is a window of safe treatment doses of these compounds situated below 5 μM and above 15 μM which may be used in evaluating neuroprotective effects.

The observed deformities of the zebrafish indicated evidences of exposure and cell penetration of the indolinone derivatives **15b** and **26d**. Nevertheless, it cannot be ruled out that the defects on the axis is an off-target effect via glycogen synthase kinase-3 (GSK-3) inhibition. It is known that Wnt signaling, and thus GSK-3 activity, plays a crucial role in the development of metazoan and was confirmed for known GSK-3 inhibitors, which interrupt zebrafish development.[32–34] Interestingly, the eyeless phenotype caused by GSK-3 inhibitors,[35,36] was not observed for both indolinone derivatives. Hence, we tested both compounds at 10 μM against GSK-3α and GSK-3β to find out whether they have the GSK-3 activity (assay information's are available in Supplementary data). Compound **15b** exhibited a moderate activity (GSK-3α = 59%, GSK-3β = 73%), whereas compound **26d** is inactive against both proteins (GSK-3α = 30%, GSK-3β = 19%). These results indicated that the observed phenotypes are not linked up with GSK-3 activity. Especially for compound **15b** the deformities of the phenotypes were observed at higher concentrations of 20 and 30 μM, respectively.

Therefore, the results of the zebrafish embryo phenotype assay indicate sufficient cell permeation of the compounds **15b** and **26d**.

In conclusion we have synthesized and evaluated a series of potent indolinones as LRRK2 inhibitors. Two of our most active and promising compounds **15b** and **26d** are characterized by an IC_{50} value of 15 and 46 nM against wild-type LRRK2 and 10 and 64 nM against the LRRK2 G2019S mutant, respectively. The combination of the docking studies and the LRRK2 in vitro results of **15b** illustrate the inhibitor-enzyme interaction with the ATP-binding pocket. We established that the hydrogen bond between the 4-hydroxy group of the phenol and the conserved residues E1920 and D2017 is essential for LRRK2 inhibition. During the development of drugs, safety is one of the most important factors. In our in vivo zebrafish embryo phenotype assay we have evaluated the toxicity of both compounds. We observed that indolinone derivative **15b** displayed no significant toxicity below 10 μM, whereas compound **26d** displayed an increased toxicity over time.

Further improvements are required to pursue with more detail phenotypic testing of analogues compounds in vivo and enable development in preclinical models.

Acknowledgment

The authors thank the Hans und Ilse Breuer Stiftung for financial support.

Supplementary data

Supplementary data associated with this article can be found, in the online version, at http://dx.doi.org/10.1016/j.bmcl.2014.08.049.

References and notes

1. Lee, B. D.; Dawson, V. L.; Dawson, T. M. *Trends Pharmacol. Sci.* **2012**, *33*, 365.
2. Tong, Y.; Shen, J. *Neuron* **2009**, *64*, 771.
3. Kramer, T.; Lo Monte, F.; Göring, S.; Okala Amombo, G. M.; Schmidt, B. *ACS Chem. Neurosci.* **2012**, *3*, 151.
4. Taymans, J. M.; Cookson, M. R. *BioEssays: News Rev. Mol., Cell. Dev. Biol.* **2010**, *32*, 227.
5. Cookson, M. R. *Nat. Rev. Neurosci.* **2010**, *11*, 791.
6. Seol, W. *BMB Rep.* **2010**, *43*, 233.
7. Greggio, E.; Jain, S.; Kingsbury, A.; Bandopadhyay, R.; Lewis, P.; Kaganovich, A.; van der Brug, M. P.; Beilina, A.; Blackinton, J.; Thomas, K. J.; Ahmad, R.; Miller, D. W.; Kesavapany, S.; Singleton, A.; Lees, A.; Harvey, R. J.; Harvey, K.; Cookson, M. R. *Neurobiol. Dis.* **2006**, *23*, 329.
8. Nichols, R. J.; Dzamko, N.; Morrice, N. A.; Campbell, D. G.; Deak, M.; Ordureau, A.; Macartney, T.; Tong, Y.; Shen, J.; Prescott, A. R.; Alessi, D. R. *Biochem. J.* **2010**, *430*, 393.
9. West, A. B.; Moore, D. J.; Biskup, S.; Bugayenko, A.; Smith, W. W.; Ross, C. A.; Dawson, V. L.; Dawson, T. M. *Proc. Natl. Acad. Sci. U.S.A.* **2005**, *102*, 16842.
10. Daniels, V.; Baekelandt, V.; Taymans, J. M. *Neuro-Signals* **2011**, *19*, 1.
11. Dusonchet, J.; Kochubey, O.; Stafa, K.; Young, S. M., Jr.; Zufferey, R.; Moore, D. J.; Schneider, B. L.; Aebischer, P. *J. Neurosci.* **2011**, *31*, 907.
12. Lee, B. D.; Shin, J. H.; VanKampen, J.; Petrucelli, L.; West, A. B.; Ko, H. S.; Lee, Y. I.; Maguire-Zeiss, K. A.; Bowers, W. J.; Federoff, H. J.; Dawson, V. L.; Dawson, T. M. *Nat. Med.* **2010**, *16*, 998.
13. Taymans, J. M. *Expert Opin. Ther. Pat.* **2014**, *24*, 727.
14. Vancraenenbroeck, R.; Lobbestael, E.; Maeyer, M. D.; Baekelandt, V.; Taymans, J. M. *CNS Neurol. Disord.: Drug Targets* **2011**, *10*, 724.
15. Deng, X.; Dzamko, N.; Prescott, A.; Davies, P.; Liu, Q.; Yang, Q.; Lee, J. D.; Patricelli, M. P.; Nomanbhoy, T. K.; Alessi, D. R.; Gray, N. S. *Nat. Chem. Biol.* **2011**, *7*, 203.

16. Zhang, J.; Deng, X.; Choi, H. G.; Alessi, D. R.; Gray, N. S. *Bioorg. Med. Chem. Lett.* **2012**, *22*, 1864.
17. Choi, H. G.; Zhang, J.; Deng, X.; Hatcher, J. M.; Patricelli, M. P.; Zhao, Z.; Alessi, D. R.; Gray, N. S. *ACS Med. Chem. Lett.* **2012**, *3*, 658.
18. Garofalo, A. W.; Adler, M.; Aubele, D. L.; Bowers, S.; Franzini, M.; Goldbach, E.; Lorentzen, C.; Neitz, R. J.; Probst, G. D.; Quinn, K. P.; Santiago, P.; Sham, H. L.; Tam, D.; Truong, A. P.; Ye, X. M.; Ren, Z. *Bioorg. Med. Chem. Lett.* **2013**, *23*, 71.
19. Chen, H.; Chan, B. K.; Drummond, J.; Estrada, A. A.; Gunzner-Toste, J.; Liu, X.; Liu, Y.; Moffat, J.; Shore, D.; Sweeney, Z. K.; Tran, T.; Wang, S.; Zhao, G.; Zhu, H.; Burdick, D. J. *J. Med. Chem.* **2012**, *55*, 5536.
20. Amombo, G. M.; Kramer, T.; Lo Monte, F.; Göring, S.; Fach, M.; Smith, S.; Kolb, S.; Schubenel, R.; Baumann, K.; Schmidt, B. *Bioorg. Med. Chem. Lett.* **2012**, *22*, 7634.
21. Mahboobi, S.; Uecker, A.; Sellmer, A.; Cenac, C.; Hocher, H.; Pongratz, H.; Eichhorn, E.; Hufsky, H.; Trumpler, A.; Sicker, M.; Heidel, F.; Fischer, T.; Stocking, C.; Elz, S.; Bohmer, F. D.; Dove, S. *J. Med. Chem.* **2006**, *49*, 3101.
22. Schmidt-Arras, D.; Schwable, J.; Bohmer, F. D.; Serve, H. *Curr. Pharm. Des.* **2004**, *10*, 1867.
23. Troxler, T.; Greenidge, P.; Zimmermann, K.; Desrayaud, S.; Druckes, P.; Schweizer, T.; Stauffer, D.; Rovelli, G.; Shimshek, D. R. *Bioorg. Med. Chem. Lett.* **2013**, *23*, 4085.
24. Arnold, K.; Bordoli, L.; Kopp, J.; Schwede, T. *Bioinformatics* **2006**, *22*, 195.
25. Kiefer, F.; Arnold, K.; Kunzli, M.; Bordoli, L.; Schwede, T. *Nucleic Acids Res.* **2009**, *37*, D387.
26. Vancraenenbroeck, R.; De Raeymaecker, J.; Lobbestael, E.; Gao, F.; De Maeyer, M.; Voet, A.; Baekelandt, V.; Taymans, J. M. *Front. Mol. Neurosci.* **2014**, *7*, 51.
27. Taymans, J. M.; Vancraenenbroeck, R.; Ollikainen, P.; Beilina, A.; Lobbestael, E.; De Maeyer, M.; Baekelandt, V.; Cookson, M. R. *PLoS ONE* **2011**, *6*, e23207.
28. Giannaccini, G.; Cuschieri, A.; Dente, L.; Raffa, V. *Nanomed: Nanotechnol., Biol., Med.* **2014**, *10*, 703–719.
29. Lammer, E.; Carr, G. J.; Wendler, K.; Rawlings, J. M.; Belanger, S. E.; Braunbeck, T. *Comp. Biochem. Physiol. C* **2009**, *149*, 196.
30. Deeti, S.; O'Farrell, S.; Kennedy, B. N. *J. Pharmacol. Toxicol. Methods* **2014**, *69*, 1.
31. Taylor, K. L.; Grant, N. J.; Temperley, N. D.; Patton, E. E. *Cell Commun. Signal* **2010**, *8*, 11.
32. Atilla-Gokcumen, G. E.; Williams, D. S.; Bregman, H.; Pagano, N.; Meggers, E. *Chembiochem: Eur J. Chem. Biol.* **2006**, *7*, 1443.
33. Lo Monte, F.; Kramer, T.; Gu, J.; Anumala, U. R.; Marinelli, L.; La Pietra, V.; Novellino, E.; Franco, B.; Demedts, D.; Van Leuven, F.; Fuertes, A.; Dominguez, J. M.; Plotkin, B.; Eldar-Finkelman, H.; Schmidt, B. *J. Med. Chem.* **2012**, *55*, 4407.
34. Paquet, D.; Bhat, R.; Sydow, A.; Mandelkow, E. M.; Berg, S.; Hellberg, S.; Falting, J.; Distel, M.; Koster, R. W.; Schmid, B.; Haass, C. *J. Clin. Invest.* **2009**, *119*, 1382.
35. Finkielsztein, A.; Kelly, G. M. *Biol. Cell* **2009**, *101*, 661. 664 p following 678.
36. Zhong, H.; Zou, H.; Semenov, M. V.; Moshinsky, D.; He, X.; Huang, H.; Li, S.; Quan, J.; Yang, Z.; Lin, S. *Mol. BioSyst.* **2009**, *5*, 1356.

Supporting Information

Indolinone based LRRK2 kinase inhibitors with a key hydrogen bond

Stefan Göring[a], Jean-Marc Taymans[b], Veerle Baekelandt[b] and Boris Schmidt [a, †]

[a] *Clemens Schöpf - Institute of Organic Chemistry and Biochemistry, Technische Universität Darmstadt, 64287 Darmstadt, Hessen, Germany, Fax: +496151-163278; Tel: +496151-164531.*

[b] *KU Leuven, Laboratory for Neurobiology and Gene Therapy, Leuven B-3000, Belgium.*

† Corresponding author. Tel.: +49 6151 163075; fax: +49 6151 163278.

E-mail: schmidt_boris@t-online.de.

Table of Content:

I. General comments

II. Experimental methods and chemical data

III. FTL-3 *in vitro* assay conducted by Cerep

IV. GSK-3α and GSK-3β *in vitro* assay conducted by Cerep

V. LRRK2 *in vitro* assay

VI. Selectivity screening of compound **15b** conducted by Cerep

VII. Toxicity assay: Determination of the *in vivo* activity on zebrafish embryos

VIII. Modeling of the kinase domain

IX. References

I. General comments

The ^{1}H-NMR spectra were detected on a Bruker AC 300 spectrometer at 300 MHz and Bruker AC 500 spectrometer at 500 MHz. The ^{13}C-NMR spectra were detected on a Bruker AC 300 spectrometer at 75 MHz and Bruker AC 500 spectrometer at 125 MHz. Chemical shifts are reported in ppm and are calibrated to the particular solvent. Mass spectrometry was performed on a Bruker-Franzen Esquire LC mass spectrometer and a MAT 95 double focussing sector field MS. Microwave experiments were carried out using a Biotage® Initiator™ microwave apparatus. All microwave experiments were carried out in sealed microwave process vials utilizing the standard absorbance level (300 W maximum power). Silica gel chromatography was carried out using Merck silica gel 60 (0.015-0.040 mm). High performance liquid chromatographies were carried out in an Agilent 1100 (column: reversed phase, Zorbax Eclipse XDB-C8, 4.6 x 150 mm; 254 nm). The eluent is composed of: a) H_2O (1% TFA) (A) and acetonitrile (1% TFA) (B) with a gradient: 30 to 90% B within 12 min. All commercial available reagents and solvents were purchased at ABCR, Acros, Sigma Aldrich and VWR.

II. Experimental methods and chemical data

Compounds 7, **15e-h and 15m-s** were prepared as described in literature.[1]

Syntheses of benzaldehyd derivatives

2-(2-(2-methoxyethoxy)ethoxy)ethyl 4-methylbenzenesulfonate

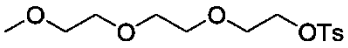

To a solution of NaOH (332 mg 8.3 mmol) in water (0.51 mL) was added 2-(2-(2-methoxyethoxy)ethoxy)ethanol (1.05 g, 6.4 mmol) and THF (0.52 mL). The mixture was cooled to 0°C and a solution of 4-methylbenzene-1-sulfonyl chloride (1.34 g, 7.0 mmol) in THF (1.56 mL) was added. After stirring over night at room temperature the mixture was quenched with water and extracted with DCM (3 x 10 mL). The combined organic layers were washed with 2N HCL (15 mL) and saturated NaCl solution (15 mL), dried over $MgSO_4$, filtrated and concentrated in vacuum. The residue was purified by silica gel chromatography (dichlormethane : methanol 10:1) to give 1.71 g (84%) as a colorless oil. **HPLC**: R_t = 5.45 min. **^{1}H-NMR** ($CDCl_3$, 300 MHz, 300 K): δ [ppm] = 7.77 (d, *J* = 8.3 Hz, 2H), 7.32 (d, *J* = 8.1 Hz, 2H), 4.13 (t, *J* = 4.8 Hz, 2H), 3.66 (t, *J* = 4.8 Hz, 2H), 3.60-3.56 (m, 6H), 3.52-3.48 (m, 2H), 3.34 (s, 3H), 2.42 (s, 3H).

4-(2-(2-(2-methoxyethoxy)ethoxy)ethoxy)benzaldehyde

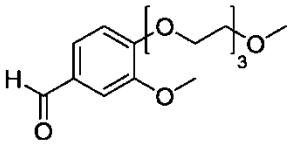

K_2CO_3 (330 mg, 2.39 mmol) and 4-hydroxy-3-methoxybenzaldehyde (240 mg, 1.58 mmol) were suspended in acetone (4 mL). Then 2-(2-(2-methoxyethoxy)ethoxy)ethyl 4-methylbenzenesulfonate (500 mg, 1.58 mmol) was added. This reaction suspension was stirred at 60°C over night. After complete turnover water was added and the aqueous solution was extracted two times with chloroform. The combined organic layers were dried with $MgSO_4$ and the solvent was removed in vacuo. The resulting residue was purified by column chromatography on silica gel (cyclohexane : ethyl acetat 1:5) to give 126 mg (27%) as a colorless oil. **HPLC**: R_t = 3.33 min. **^{1}H-NMR** ($CDCl_3$, 300 MHz): δ [ppm] = 9.84 (s, 1H), 7.44-7.39 (m, 2H), 7.01 (d, 1H, *J* = 8.0 Hz), 4.27 (m, 2H), 3.94-3.90 (m, 5H), 3.76-3.72 (m, 2H), 3.68-3.62 (m, 4H), 3.55-3.51 (m, 2H), 3.36 (s, 3H). **^{13}C-NMR** ($CDCl_3$, 75 MHz):

δ [ppm] = 191.0, 154.1, 150.1, 130.5, 126.7, 112.2, 109.6, 72.1, 71.1, 70.8, 70.7, 69.5, 68.7, 59.2, 56.1.

3,5-dibromo-4-methoxybenzaldehyde

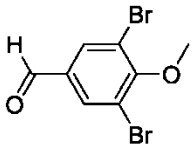

Potassium carbonate (100 mg, 0.72 mmol) was added to a solution of 3,5-dibromo-4-hydroxybenzaldehyde (100 mg, 0.36 mmol) and methyl iodide (51 µL, 0.81 mmol) in DMF (1.5 mL). The mixture was stirred at 55°C for 3 h. After cooling to room temperature water (8 mL) was added and the resulting precipitate was filtered and dried in vacuum to give 85 mg (81%) as a colorless solid. **HPLC**: R_t = 7.04 min. **^{1}H-NMR** ($CDCl_3$, 500 MHz): δ [ppm] = 9.86 (s, 1H), 8.03 (s, 2H), 3.97 (s, 3H). **^{13}C-NMR** ($CDCl_3$, 125 MHz): δ [ppm] = 188.5, 159.3, 134.4, 134.1, 119.5, 61.0.

4-methoxy-3,5-dimethylbenzaldehyde

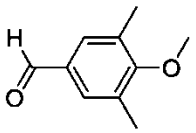

To a solution of 4-hydroxy-3,5-dimethylbenzaldehyde (100 mg, 0.67 mmol) and potassium carbonate (111 mg, 0.80 mmol) in DMF (1.5 mL) was added methyl iodide (50 µL, 0.80 mmol). The reaction mixture was stirred at room temperature for 18 h. After complete turnover ethyl acetate (10 mL) was added and the solution was washed two times with water and brine. The organic layer was dries over $MgSO_4$, filtered and the solvent was removed in vacuum. The residue was purified by silica gel chromatography (cyclohexane : ethyl acetate 6:1) to give 67 mg (61%) as a colorless oil. **HPLC**: R_t = 5.56 min. **^{1}H-NMR** ($CDCl_3$, 500 MHz): δ [ppm] = 9.88 (s, 1H), 7.55 (s, 2H), 3.78 (s, 3H), 2.35 (s, 6H). **^{13}C-NMR** ($CDCl_3$, 125 MHz): δ [ppm] = 191.8, 162.6, 132.4, 132.1, 130.9, 59.9, 16.3.

3-methoxy-4-(4-methylpiperazin-1-yl)benzaldehyde

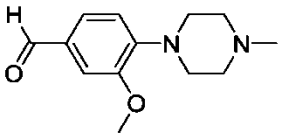

A solution of 4-fluoro-3-methoxybenzaldehyde (100 mg, 0.65 mmol), 1-methylpiperazine (65 mg, 0.65 mmol) and potassium carbonate (90 mg, 0.65 mmol) in DMSO (0.6 mL) was stirred at 100°C for 3 days. The reaction mixture was diluted with water and extracted with diethyl ether (3 x 15 mL). The combined organic layers were dried over $MgSO_4$, filtrated and concentrated in vacuum to give 85 mg (56%) as a yellow solid. **HPLC**: R_t = 0.75 min, 1.13 min. **^{1}H-NMR** ($CDCl_3$, 300 MHz, 500 K): δ [ppm] = 9.84 (s, 1H), 7.41 (dd, 1H, *J* = 1.8 Hz, *J* = 8.1 Hz), 7.37 (d, 1H, *J* = 1.8 Hz), 7.00 (d, 1H, *J* = 8.1 Hz), 3.92 (s, 3H), 3.25 (s, 4H), 2.62-2.61 (m, 4H), 2.36 (s, 3H). **^{13}C-NMR** ($CDCl_3$, 125 MHz): δ [ppm] = 191.2, 152.3, 147.5, 131.0, 126.7, 117.5, 109.3, 55.8, 55.2, 50.1, 46.3.

3-methoxy-4-morpholinobenzaldehyde

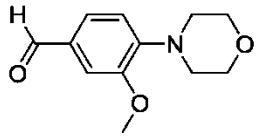

This compound was synthesized as described for compound 4-(4-methylpiperazin-1-yl)benzaldehyde. After recrystallization from ethanol 30 mg (21%) of an orange solid were obtained. **HPLC**: R_t = 3.57 min. **^{1}H-NMR** ($CDCl_3$, 500 MHz, 300 K): δ [ppm] = 9.85 (s, 1H), 7.43 (dd, 1H, *J* = 1.8 Hz, *J* = 8.1 Hz), 7.39 (d, 1H, *J* = 1.8 Hz), 6.96 (d, 1H, *J* = 8.1 Hz), 3.93 (s, 3H), 3.90-3.88 (m, 4H), 3.22-3.20 (m, 4H). **^{13}C-NMR** ($CDCl_3$, 125 MHz): δ [ppm] = 191.1, 152.3, 147.2, 131.3, 126.7, 117.2, 109.5, 67.1, 55.9, 50.6.

1-(2-(dimethylamino)ethyl)-1*H*-indole-6-carbaldehyde

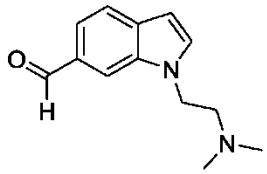

To a solution of 1*H*-indole-6-carbaldehyde (200 mg, 1.38 mmol) in DMSO (2 mL) was added Cs_2CO_3 (897 mg, 2.75 mmol) and the mixture was stirred for 30 minutes at room temperature. Following a solution of 2-dimetylaminoethyl chloride hydrochloride (239 mg, 1.65 mmol) in DMSO (2 mL) was added slowly and the reaction was stirred for another 20 hours at room temperature. After the conversation has taken place ethyl acetate (10 mL) was added. The organic layer was separated and washed with water (2 x 5 mL) and brine (2 x 5 mL), dried over $NaSO_4$, filtered and the solvent was reduced under pressure. The residue was purified by silica gel chromatography (dichlormethane : methanol 95:5) to give 155 mg (52%) as a

yellow oil. **HPLC**: R_t = 0.76 min, 1.34 min. **^{1}H-NMR** ($CDCl_3$, 500 MHz): δ [ppm] = 9.88 (s, 1H), 7.55 (s, 2H), 3.78 (s, 3H), 2.35 (s, 6H). **^{13}C-NMR** ($CDCl_3$, 125 MHz): δ [ppm] = 191.8, 162.6, 132.4, 132.1, 130.9, 59.9, 16.3.

Syntheses of indolinone derivatives

5-phenylindolin-2-one 17

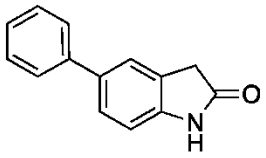

5-Bromo-2-oxindole **16** (150 mg, 0.71 mmol), benzeneboronic acid (113 mg, 0.92 mmol), tetrakis(triphenylphosphine)palladium(0) (61 mg, 0.05 mmol) and Natriumcarbonat (250 mg, 2.41 mmol) were suspended in toluene (1.5 mL) and ethanol (1.5 mL) and refluxed for 12 h at 100°C. Water was added and extracted 3 times with ethyl acetate. The combined organic layers were wash with 1N hydrochlorid acid, brine, dried over $MgSO_4$, filtered and concentrated in vacuum to give 75 mg (51%) as a light brown solid and was used for the next step without further structure determination.

5-methoxyindolin-2-one 19

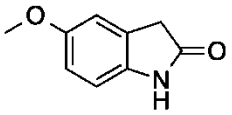

To a suspension of 5-methoxyindoline-2,3-dione (250 mg, 1.41 mmol) in ethylene glycol (1 mL) were added hydrazine monohydrate (140 µL) and KOH (79 mg, 1.41 mmol). The mixture was heated under microwave irradiation at 140°C for 5 minutes. Water was added and the mixture was neutralized with 1N HCl. The obtained suspension was extracted 3 times with ethyl acetate. The combined organic layers were dried over $MgSO_4$, filtered and concentrated in vacuum to give 186 mg (81%) as a yellow solid and was used for the next step without further structure determination.

General procedure for synthesis of 3-substituted indole-2-ones

A suspension of indolinone (0.3 mmol), aldehyde (0.3 mmol) and pyridine (30 µL) in methanol (1 mL) were heated under microwave irradiation at 100°C for 30 minutes. The reaction mixture was cooled to room temperature and the resulting precipitate was removed by filtration, carefully washed with methanol and dried *in vacuo*. When no precipitate was observed methanol was removed under vacuum and the residue was purified by silica gel chromatography to give the desired product.

5-chloro-3-(3,5-difluoro-4-hydroxybenzylidene)indolin-2-one 15a

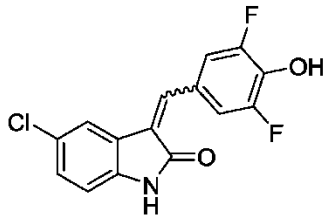

According to the general procedure 52 mg (57%) as an orange solid were obtained.

HPLC: R_t = 5.75 min, 6.58 min. **^{1}H-NMR** (DMSO-d_6, 500 MHz, 300 K): δ [ppm] = 10.76 (s, 1H), 10.72 (s, 1H), 8.30 (d, 2H, *J* = 10.6 Hz), 7.80 (s, 1H), 7.74 (d, 1H, *J* = 2.1 Hz), 7.56 (s, 1H), 7.50 (d, 1H, *J* = 2.1 Hz), 7.46-7.44 (m, 2H), 7.29 (dd, 1H, *J* = 2.1, 8.3 Hz), 7.21 (dd, 1H, *J* = 2.1, 8.3 Hz), 6.89 (d, 1H, *J* = 8.3), 6.82 (d, 1H, *J* = 8.3). **^{13}C-NMR** (DMSO-d_6, 125 MHz): δ [ppm] = 169.2, 167.0, 153.1, 150.6, 144.2, 141.6, 138.9, 137.2, 137.2, 136.0, 135.9, 132.2, 129.5, 127.8, 126.9, 125.3, 124.9, 122.4, 121.7, 119.3, 116.2, 116.0, 113.5, 113.3, 111.5, 110.7. **MS** (EI, 70 eV): *m/z* = 307 [M^+].

5-chloro-3-(3,5-dibromo-4-hydroxybenzylidene)indolin-2-one 15b

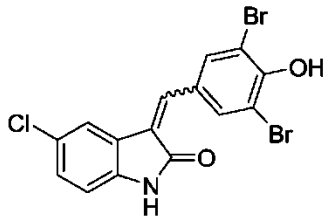

According to the general procedure 99 mg (97%) as an orange solid were obtained.

HPLC: R_t = 6.98 min, 7.65 min. **^{1}H-NMR** (DMSO-d_6, 500 MHz, 300 K): δ [ppm] = 10.69 (s, 2H), 8.48 (d, 2H, *J* = 8.9 Hz), 7.88 (s, 1H), 7.80 (d, 1H, *J* = 2.0 Hz), 7.69 (d, 2H, *J* = 8.9 Hz), 7.66 (s, 1H), 7.56 (d, 1H, *J* = 2.0 Hz), 7.27 (dd, 1H, *J* = 2.0 Hz, *J* = 8.3 Hz), 7.20 (dd, 1H, *J* = 2.0 Hz, *J* = 8.3 Hz), 7.13 (d, 2H, *J* = 8.9 Hz), 7.06 (d, 2H, *J* = 8.9 Hz), 6.89 (d, 1H, *J* = 8.3 Hz), 6.81 (d, 1H, *J* = 8.3 Hz), 4.21-4.18 (m, 4H), 3.59 (m, 8H), 2.72 (m, 4H), 2.50 (m, 8H).

^{13}C-NMR (DMSO-d_6, 125 MHz): δ [ppm] = 168.6, 167.1, 160.8, 160.0, 141.4, 138.8, 137.9, 134.8, 131.6, 129.2, 127.5, 127.3, 126.8, 125.3, 124.9, 122.9, 122.8, 121.4, 119.3, 114.9, 114.4, 111.3, 110.5, 66.2, 65.5, 56.9, 53.9. **MS** (EI, 70 eV): *m/z* = 429 [M^+].

3-benzylidene-5-chloroindolin-2-one 15c

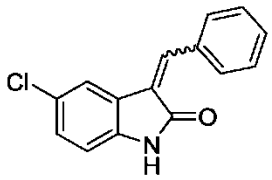

According to the general procedure 60 mg (79%) as a yellow solid were obtained.

HPLC: R_t = 6.92 min. **^{1}H-NMR** (DMSO-d_6, 500 MHz, 300 K): δ [ppm] = 10.73 (s, 1H), 7.73 (s, 1H), 7.69 (m, 2H), 7.57-7.49 (m, 3H), 7.39 (d, 1H, *J* = 2.1 Hz), 7.28 (dd, 1H, *J* = 8.3, 2.1 Hz), 6.89 (d, 1H, *J* = 8.3 Hz). **^{13}C-NMR** (DMSO-d_6, 125 MHz): δ [ppm] = 168.2, 141.7, 137.7, 134.0, 130.0, 129.6, 129.1, 128.6, 126.9, 124.9, 122.5, 121.7, 111.5. **MS** (EI, 70 eV): *m/z* = 255 [M^-].

5-chloro-3-(3-methoxy-4-(2-morpholinoethoxy)benzylidene)indolin-2-one 15d

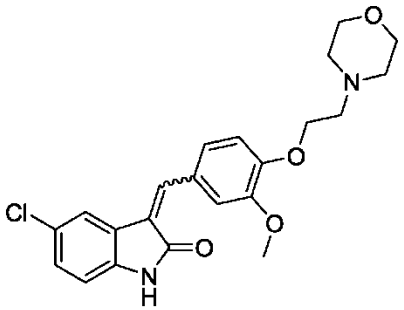

According to the general procedure 24 mg (31%) as a yellow solid were obtained.

HPLC: R_t = 3.76 min, 4.62 min. **^{1}H-NMR** (DMSO-d_6, 500 MHz, 300 K): δ [ppm] = 10.66 (s, 2H), 8.66 (d, 1H, *J* = 2.1 Hz), 7.87-7.85 (m, 2H), 7.80 (d, 1H, *J* = 2.1 Hz), 7.69 (d, 1H, *J* = 2.1 Hz), 7.65 (s, 1H), 7.35 (d, 1H, *J* = 1.9 Hz), 7.33-7.31 (m, 1H), 7.28 (dd, 1H, *J* = 2.1 Hz, *J* = 8.3 Hz), 7.20 (dd, 1H, *J* = 2.1 Hz, *J* = 8.3 Hz), 7.16 (d, 1H, *J* = 8.5 Hz), 7.11 (d, 1H, *J* = 8.5 Hz), 6.89 (d, 1H, *J* = 8.3 Hz), 6.83 (d, 1H, *J* = 8.3 Hz), 4.18 (t, 4H, *J* = 5.9 Hz), 3.83 (s, 3H), 3.81 (s, 3H), 3.58 (t, 8H, *J* = 4.6 Hz), 2.74-2.71 (m, 4H), 2.5-2.49 (m, 8H). **^{13}C-NMR** (DMSO-d_6, 125 MHz): δ [ppm] = 168.6, 167.2, 150.8, 149.9, 148.7, 148.1, 141.4, 139.4, 138.8, 138.1, 129.1, 127.9, 127.4, 127.2, 126.4, 125.3, 124.8, 124.6, 123.6, 122.9, 122.8,

121.7, 119.2, 115.5, 113.2, 113.0, 112.3, 111.4, 110.5, 66.3, 66.2, 56.9, 56.9, 53.7. **MS** (EI, 70 eV): m/z = 414 [M^+].

N-(4-((5-chloro-2-oxoindolin-3-ylidene)methyl)phenyl)acetamide 15i

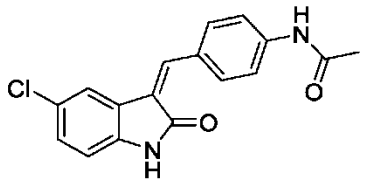

According to the general procedure 81 mg (87%) as a yellow solid were obtained.

HPLC: R_t = 7.67 min. **^{1}H-NMR** (DMSO-d_6, 500 MHz, 300 K): δ [ppm] = 10.68 (s, 2H), 10.23 (s, 2H), 8.42 (d, 2H, J = 8.8 Hz), 7.85 (s, 1H), 7.80 (d, 1H, J = 2.1 Hz), 7.75 (d, 2H, J = 8.7 Hz), 7.69-7.67 (m, 4H), 7.64 (s, 1H), 7.54 (d, 1H, J = 2.1 Hz), 7.27 (d, 1H, J = 2.1, 8.3 Hz), 7.21 (d, 1H, J = 2.1, 8.3 Hz), 6.88 (d, 1H, J = 8.3 Hz), 6.82 (d, 1H, J = 8.3 Hz), 2.09 (s, 3H), 2.09 (s, 3H). **^{13}C-NMR** (DMSO-d_6, 125 MHz): δ [ppm] = 168.9, 168.5, 167.0, 141.8, 141.4, 141.1, 139.0, 138.6, 137.7, 133.6, 130.6, 129.3, 128.7, 128.3, 127.8, 127.2, 125.4, 125.3, 124.9, 123.7, 122.7, 121.6, 119.4, 118.7, 118.1, 111.4, 110.6, 24.2, 24.1. **MS** (EI, 70 eV): m/z = 312 [M^+].

5-chloro-3-(3-methoxy-4-(2-(2-(2-methoxyethoxy)ethoxy)ethoxy)benzylidene)indolin-2-one 15j

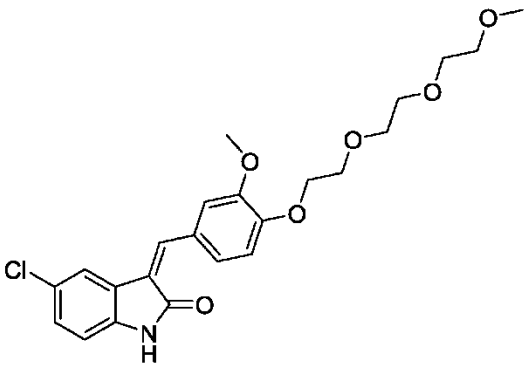

According to the general procedure 57 mg (63%) as a dark yellow solid were obtained.

HPLC: R_t = 6.15 min, 6.72 min. **^{1}H-NMR** (DMSO-d_6, 500 MHz, 300 K): δ [ppm] = 10.66 (s, 2H), 8.67 (d, 1H, J = 2.0 Hz), 7.88-7.85 (m, 2H), 7.80 (d, 1H, J = 2.1 Hz), 7.69 (d, 1H, J = 2.1 Hz), 7.66 (s, 1H), 7.36 (d, 1H, J = 1.9 Hz), 7.33-7.31 (m, 1H), 7.28 (dd, 1H, J = 2.1 Hz, J = 8.3 Hz), 7.20 (dd, 1H, J = 2.1 Hz, J = 8.3 Hz), 7.15 (d, 1H, J = 8.5 Hz), 7.10 (d, 1H, J = 8.5 Hz), 6.89 (d, 1H, J = 8.3 Hz), 6.83 (d, 1H, J = 8.3 Hz), 4.19-4.18 (m, 4H), 3.84 (s, 3H), 3.82 (s, 3H), 3.79-3.77 (m, 4H), 3.62-3.59 (m, 4H), 3.55-3.51 (m, 8H), 3.44-3.42 (m,

4H), 3.23 (m, 6H). **^{13}C-NMR** (DMSO-d_6, 125 MHz): δ [ppm] = 168.6, 167.2, 150.7, 149.9, 148.6, 148.1, 141.4, 139.4, 138.8, 138.1, 129.0, 127.8, 127.4, 127.2, 126.4, 125.3, 124.8, 124.7, 123.6, 122.8, 122.8, 121.7, 119.2, 115.4, 113.1, 112.8, 112.1, 111.3, 110.5, 71.3, 70.0, 69.8, 69.6, 68.8, 68.8, 68.0, 67.8, 58.0, 55.5, 55.4. **MS** (EI, 70 eV): *m/z* = 447 [M$^-$].

5-chloro-3-(3-methoxy-4-(4-methylpiperazin-1-yl)benzylidene)indolin-2-one 15k

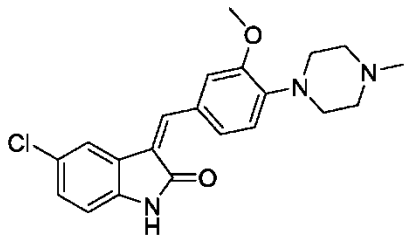

According to the general procedure 70 mg (85%) as an orange solid were obtained.

HPLC: R_t = 3.61 min, 4.53 min. **^{1}H-NMR** (DMSO-d_6, 500 MHz, 300 K): δ [ppm] = 10.63 (s, 1H), 10.59 (s, 1H), 8.65 (d, 1H, *J* = 1.9 Hz), 7.81 (s, 1H), 7.78 (dd, 1H, *J* = 1.9 Hz, *J* = 8.5 Hz), 7.75 (d, 1H, *J* = 2.1 Hz), 7.73 (d, 1H, *J* = 2.1 Hz), 7.63 (s, 1H), 7.30-7.28 (m, 2H), 7.23 (dd, 1H, *J* = 2.1 Hz, *J* = 8.3 Hz), 7.15 (dd, 1H, *J* = 2.1 Hz, *J* = 8.3 Hz), 6.99 (d, 1H, *J* = 8.2 Hz), 6.92 (d, 1H, *J* = 8.2 Hz), 6.87 (d, 1H, *J* = 8.3 Hz), 6.81 (d, 1H, *J* = 8.3 Hz), 3.87 (s, 3H), 3.84 (s, 3H), 3.15-3.13 (m, 8H), 2.89-2.47 (m, 8H), 2.23 (d, 6H). **^{13}C-NMR** (DMSO-d_6, 125 MHz): δ [ppm] = 168.7, 167.2, 151.1, 150.4, 143.9, 143.3, 141.3, 139.3, 138.6, 138.1, 128.7, 127.8, 127.7, 127.5, 127.1, 127.1, 125.2, 124.8, 124.1, 123.8, 122.9, 122.3, 121.6, 118.9, 117.6, 116.8, 115.3, 112.9, 111.2, 110.3, 55.4, 55.3, 54.7, 54.6, 49.4, 49.3, 45.8. **MS** (EI, 70 eV): *m/z* = 383 [M$^-$].

5-chloro-3-(3-methoxy-4-morpholinobenzylidene)indolin-2-one 15l

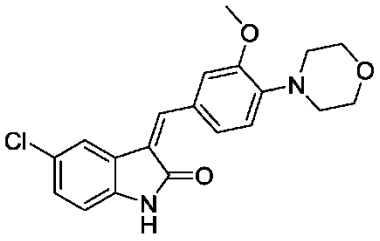

According to the general procedure 16 mg (35%) as an orange solid were obtained.

HPLC: R_t = 5.92 min, 6.48 min. **^{1}H-NMR** (DMSO-d_6, 500 MHz, 300 K): δ [ppm] = 10.68 (s, 1H), 10.65 (s, 1H), 8.66 (d, 1H, *J* = 1.9 Hz), 7.86 (s, 1H), 7.83 (dd, 1H, *J* = 1.9 Hz, *J* = 8.5 Hz), 7.80 (d, 1H, *J* = 2.1 Hz), 7.72 (d, 1H, *J* = 2.1 Hz), 7.65 (s, 1H), 7.35-7.32 (m, 2H), 7.28 (dd, 1H, *J* = 2.1 Hz, *J* = 8.3 Hz), 7.20 (dd, 1H, *J* = 2.1 Hz, *J* = 8.3 Hz), 7.02 (d, 1H, *J* = 8.2

Hz), 6.95 (d, 1H, *J* = 8.2 Hz), 6.89 (d, 1H, *J* = 8.3 Hz), 6.83 (d, 1H, *J* = 8.3 Hz), 3.87 (s, 3H), 3.85 (s, 3H), 3.75-3.73 (m, 8H), 3.14-3.10 (m, 8H). **^{13}C-NMR** (DMSO-d_6, 125 MHz): δ [ppm] = 168.7, 167.2, 151.2, 150.5, 143.8, 143.1, 141.4, 139.3, 138.7, 138.2, 129.0, 128.0, 127.8, 127.5, 127.5, 127.3, 125.2, 124.8, 124.3, 123.8, 122.9, 122.5, 121.7, 119.1, 117.6, 116.8, 115.3, 113.1, 111.3, 110.5, 66.2, 66.2, 55.5, 55.4, 50.1, 49.9. **MS** (EI, 70 eV): *m/z* = 370 [M^+].

5-chloro-3-((1-(2-(dimethylamino)ethyl)-1*H*-indol-6-yl)methylene)indolin-2-one 15t

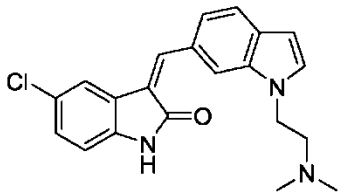

According to the general procedure 188 mg (82%) as an orange solid were obtained.

HPLC: R_t = 4.32 min, 5.21 min. **^{1}H-NMR** (DMSO-d_6, 500 MHz, 300 K): δ [ppm] = 10.72 (s, 2H), 9.11 (s, 1H), 8.08 (s, 1H), 8.02 (dd, 1H, *J* = 1.1 Hz, *J* = 8.4 Hz), 7.94 (s, 1H), 7.88 (s, 1H), 7.86 (d, 1H, *J* = 2.1 Hz), 7.72 (d, 1H, *J* = 2.1 Hz), 7.70 (m, 1H), 7.62 (m, 2H), 7.58 (d, 1H, *J* = 3.1 Hz), 7.39 (dd, 1H, *J* = 1.0 Hz, *J* = 8.2 Hz), 7.27 (dd, 1H, *J* = 2.1 Hz, *J* = 8.3 Hz), 7.20 (dd, 1H, *J* = 1.0 Hz, *J* = 8.2 Hz), 6.90 (d, 1H, *J* = 8.3 Hz), 6.84 (d, 1H, *J* = 8.2 Hz), 6.53 (d, 1H, *J* = 3.1 Hz), 6.50 (d, 1H, *J* = 3.0 Hz), 2.71 (t, 4H, *J* = 6.7 Hz), 2.65 (t, 4H, *J* = 6.6 Hz), 2.51 (m, 12H). **^{13}C-NMR** (DMSO-d_6, 125 MHz): δ [ppm] = 169.1, 167.7, 141.7, 141.7, 140.6, 135.7, 133.3, 132.6, 130.2, 129.3, 127.6, 126.9, 125.1, 124.8, 124.7, 123.5, 121.5, 121.1, 120.3, 119.5, 115.1, 112.3, 111.7, 110.8, 101.6, 101.5, 59.2, 58.8, 45.6, 44.1. **MS** (EI, 70 eV): *m/z* = 365 [M^+].

3-(3,5-dibromo-4-hydroxybenzylidene)-5-phenylindolin-2-one 20a

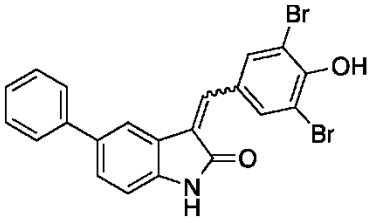

According to the general procedure 25 mg (18%) as an orange solid were obtained.

HPLC: R_t = 7.78 min, 8.21 min. **^{1}H-NMR** (DMSO-d_6, 500 MHz, 300 K): δ [ppm] = 10.72 (s, 1H), 10.68 (s, 1H), 8.82 (s, 2H), 8.05-8.03 (m, 3H), 7.89-7.87 (m, 2H), 7.69-7.67 (m, 2H),

7.57-7.52 (m, 5H), 7.48-7.41 (m, 4H), 7.35-7.30 (m, 2H), 6.98 (d, 1H, J = 8.1 Hz), 6.92 (d, 1H, J = 8.1 Hz). **MS** (EI, 70 eV): m/z = 471 [M^+].

3-(3,5-dibromo-4-hydroxybenzylidene)-5-methoxyindolin-2-one 20b

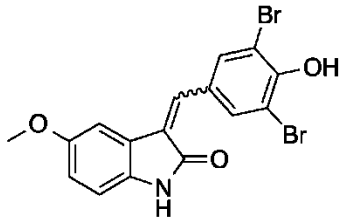

According to the general procedure 67 mg (52%) as an orange solid were obtained.
HPLC: R_t = 6.30 min, 6.74 min. **^{1}H-NMR** (DMSO-d_6, 500 MHz, 300 K): δ [ppm] = 10.42 (s, 1H), 10.37 (s, 1H), 8.79 (s, 2H), 7.94 (s, 2H), 7.71 (s, 1H), 7.47 (s, 1H), 7.33 (d, 1H, J = 2.4 Hz), 7.13 (d, 1H, J = 2.4 Hz), 6.85 (dd, 1H, J = 2.5, 8.5 Hz), 6.79 (m, 2H), 6.73 (d, 1H, J = 8.4 Hz), 3.76 (s, 3H), 3.66 (s, 3H). **MS** (EI, 70 eV): m/z = 425 [M^+].

5-chloro-3-(4-hydroxy-3,5-dimethylbenzylidene)indolin-2-one 21a

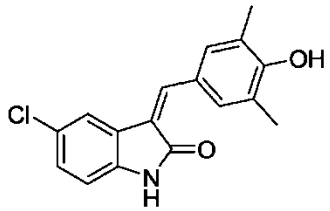

According to the general procedure 61 mg (89%) as an orange solid were obtained.
HPLC: R_t = 6.49 min, 6.96 min. **^{1}H-NMR** (DMSO-d_6, 500 MHz, 300 K): δ [ppm] = 10.63 (s, 1H), 10.58 (s, 1H), 9.05 (s, 2H), 8.19 (s, 2H), 7.75-7.74 (m, 2H), 7.64 (d, 1H, J = 1.9 Hz), 7.57 (s, 1H), 7.35 (s, 2H), 7.24 (dd, 1H, J = 8.3, 2.1 Hz), 7.16 (dd, 1H, J = 8.3, 2.1 Hz), 6.87 (d, 1H, J = 8.3 Hz), 6.80 (d, 1H, J = 8.3 Hz), 2.23 (s, 6H), 2.21 (s, 6H). **^{13}C-NMR** (DMSO-d_6, 125 MHz): δ [ppm] = 168.7, 167.1, 156.8, 155.7, 141.2, 139.6, 138.7, 138.6, 133.8, 130.3, 128.7, 127.6, 127.0, 125.4, 125.1, 124.7, 124.6, 123.8, 123.8, 123.1, 121.6, 121.4, 118.9, 111.2, 110.3, 16.6, 16.4. **MS** (EI, 70 eV): m/z = 299 [M^+].

5-chloro-3-(3,5-dibromo-4-methoxybenzylidene)indolin-2-one 21b

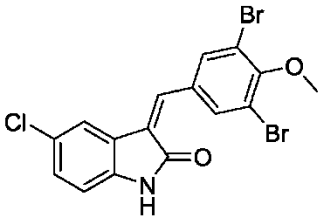

According to the general procedure 82 mg (77%) as an orange solid were obtained.

HPLC: R_t = 8.88 min. **^{1}H-NMR** (DMSO-d_6, 500 MHz, 300 K): δ [ppm] = 10.81 (s, 1H), 8.76 (s, 2H), 7.86 (s, 1H), 7.77 (d, 1H, *J* = 1.6 Hz), 7.26 (dd, 1H, *J* = 8.3, 1.9 Hz), 6.84 (d, 1H, *J* = 8.3 Hz), 3.87 (s, 3H). **^{13}C-NMR** (DMSO-d_6, 125 MHz): δ [ppm] = 166.8, 154.8, 139.7, 136.1, 134.7, 132.8, 128.9, 127.1, 126.3, 125.6, 120.1, 117.1, 111.0, 60.6. **MS** (EI, 70 eV): *m/z* = 443 [M^-].

5-chloro-3-(4-methoxy-3,5-dimethylbenzylidene)indolin-2-one 21c

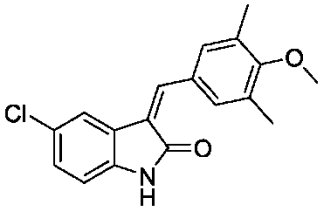

According to the general procedure 78 mg (83%) as an orange solid were obtained.

HPLC: R_t = 7.67 min. **^{1}H-NMR** (DMSO-d_6, 500 MHz, 300 K): δ [ppm] = 10.69 (s, 1H), 7.59 (s, 1H), 7.53 (d, 1H, *J* = 2.1 Hz), 7.40 (s, 2H), 7.26 (dd, 1H, *J* = 8.3, 2.1 Hz), 6.88 (d, 1H, *J* = 8.3 Hz), 3.73 (s, 3H), 2.28 (s, 6H). **^{13}C-NMR** (DMSO-d_6, 125 MHz): δ [ppm] = 169.4, 158.2, 141.5, 137.6, 131.0, 130.1, 129.3, 125.8, 124.8, 122.7, 121.8, 111.4, 59.5, 15.7. **MS** (EI, 70 eV): *m/z* = 313 [M^+].

3-(3-bromo-4-hydroxybenzylidene)-5-chloroindolin-2-one 21d

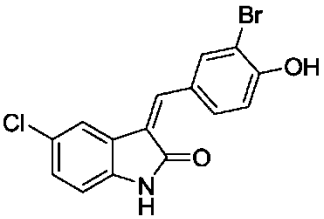

According to the general procedure 85 mg (81%) as an orange solid were obtained.

HPLC: R_t = 6.25 min, 6.90 min. **^{1}H-NMR** (DMSO-d_6, 500 MHz, 300 K): δ [ppm] = 11.11 (s, 1H), 11.01 (s, 1H), 10.68 (d, 2H, *J* = 6.7 Hz), 8.95 (d, 1H, *J* = 2.1 Hz), 8.23 (dd, 1H, *J* = 8.7, 2.1 Hz), 7.89 (d, 1H, *J* = 1.8 Hz), 7.81 (s, 1H), 7.78 (d, 1H, *J* = 2.1 Hz), 7.61-7.59 (m, 2H),

7.52 (d, 1H, J = 2.1 Hz), 7.28 (dd, 1H, J = 8.3, 2.1 Hz), 7.20 (dd, 1H, J = 8.3, 2.1 Hz), 7.10 (d, 1H), J = 8.5 Hz), 7.04 (d, 1H, J = 8.5 Hz), 6.88 (d, 1H, J = 8.3 Hz), 6.82 (d, 1H, J = 8.3 Hz). **^{13}C-NMR** (DMSO-d_6, 125 MHz): δ [ppm] = 168.4, 167.1, 156.7, 156.0, 141.5, 137.6, 137.1, 136.7, 134.4, 134.1, 130.5, 129.1, 127.6, 127.1, 126.9, 126.3, 125.2, 124.9, 123.2, 122.7, 121.5, 119.3, 116.4, 115.9, 111.4, 111.3, 110.6, 109.6. **MS** (EI, 70 eV): m/z = 351 [M^+].

III. FTL-3 *in vitro* assay conducted by Cerep

See in publication reference.[1]

IV. GSK-3α and GSK-3β *in vitro* assay conducted by Cerep[2]

1. Reference compound data

Reference compound: Staurosporine

GSK-3α IC_{50} = 28 nM

GSK-3β IC_{50} = 50 nM

2. Experimental conditions for GSK-3α

Source:	human recombinant
Substrate:	ATP + Ulight-CFFKNIVTPRTPPPSQGK-amide (100 nM)
Measured component:	phospho-Ulight-CFFKNIVTPRTPPPSQGK-amide
Incubation:	60 min/RT
Detection method:	LANCE

3. Experimental conditions for GSK-3β

Source:	human recombinant
Substrate:	ATP + Ulight-CFFKNIVTPRTPPPSQGK-amide (100 nM)
Measured component:	phospho-Ulight-CFFKNIVTPRTPPPSQGK-amide
Incubation:	90 min/RT
Detection method:	LANCE

V. LRRK2 *in vitro* assay

Materials and Methods:

In vitro kinase assay: LRRK2 kinase activity was assessed using an isotopic peptide substrate assay essentially as described in reference.[3, 4]

In short, recombinant LRRK2 was incubated with 6 µCi γ-32P-ATP (3000 Ci/mmol; Perkin Elmer (USA)), 200 µM LRRKtide (RLGRDKYKTLRQIRQ)[5] (Enzo Life Sciences (USA)), 10 µM ATP and kinase inhibitor (see below) or dimethylsulfoxide (DMSO) solvent per 40 µl reaction in 1x kinase buffer for 30 min at 30°C. The composition of 1x kinase buffer is: Tris 25 mM pH 7.5, $MgCl_2$ 10 mM, dithiothreitol (DTT) 2 mM, Triton 0,02%, beta-glycerophosphate 5 mM, Na_3VO_4 0.1 mM. DMSO content of each *in vitro* kinase reaction was 1 %. The LRRK2 enzyme used was GST-tagged truncated LRRK2 containing residues 970 to 2527 (Life Technologies). Reactions were performed in triplicate for each condition and spotted to P81 Whatman phosphocellulose paper (GE Healthcare) and washed 4 times 10 min in 75 mM phosphoric acid. LRRKtide phosphorylation levels were measured via autoradiography using a Storm 840 phosphorescence scanner (GE Healthcare).[6] Phosphorylation was quantified by densitometric analysis using Aida analyzer v1.0 (Raytest, Straubenhardt, Germany) or ImageJ software (NIH, USA). LRRKtide phosphorylation levels were plotted vs. the log of the compound concentration using GraphPad Prism v5 software (Graphpad Software Inc., San Diego, CA, USA) and inhibition curves were fitted using the least squares method from which IC_{50} values were derived.

VI. Selectivity screening of compound 15b conducted by Cerep[2]

The ExpresS Diversity kinase profile is a fast turnaround profile conducted by Cerep. Percentage kinase activities of compound **15b** at 1 μM in panels of human protein kinases determined by Cerep. Measurements were performed in duplicate and the average was taken.

Kinase	% of Control Values[1]	Kinase	% of Control Values[1]
Abl kinase *(h)*	77	JNK1 *(h)*	104
Akt1/PKBα *(h)*	87	KDR kinase *(h)* (VEGFR2)	97
AurA/Aur2 kinase *(h)*	73	Lck kinase *(h)*	102
CaMK2α *(h)*	105	MAPKAPK2 *(h)*	83
CDC2/CDK1 *(h)* (cycB)	90	MARK1 *(h)*	86
CDK2 *(h)* (cycA)	95	MNK2 *(h)*	89
CHK1 *(h)*	81	MST4 kinase *(h)*	103
CHK2 *(h)*	87	NEK2 *(h)*	99
c-Met kinase *(h)*	69	p38α kinase *(h)*	92
EGFR kinase *(h)*	58	PAK2 *(h)*	76
EphA2 kinase *(h)*	90	PAK4 *(h)*	86
EphA3 kinase *(h)*	101	PDK1 *(h)*	83
EphB4 kinase *(h)*	108	Pim2 kinase *(h)*	29
ERK_2 *(h)* ($P42^{mapk}$)	100	PKA *(h)*	103
FGFR1 kinase *(h)*	101	PKCβ2 *(h)*	85
FGFR2 kinase *(h)*	91	PLK1 *(h)*	80
FGFR3 kinase *(h)*	82	RAF-1 kinase *(h)*	73
GSK3β *(h)*	87	ROCK1 (h)	92
HGK *(h)* (MAP4K4)	4	SGK1 *(h)*	100
IKKα *(h)*	95	SIK *(h)*	92
IRAK4 *(h)*	90	Src kinase *(h)*	101
IRK *(h)* (InsR)	104	TAOK2 (TAO1) *(h)*	85
JAK3 *(h)*	52	TRKA *(h)*	91

[1] The results are expressed as a percent of control specific activity ((measured specific activity/control specific activity) x 100) obtained in the presence of the compounds (control = staurosporine).

Assay Kinase	Source	Substrate/Stimulus/Tracer	Incubation	Measured Component
Abl kinase *(h)*	human recombinant (insect cells)	ATP + Ulight-TK peptide (100 nM)	60 min RT	phospho-Ulight-TK-peptide
Akt1/PKBα *(h)*	human recombinant (insect cells)	ATP + CREBtide (CKRREILSRRPSYRK) (25 nM)	60 min RT	phospho-CREBtide (CKRREILSRRPSYRK)
AurA/Aur2 kinase *(h)*	human recombinant (Sf21 cells)	ATP + Ulight-RRRSLLE (100 nM)	15 min RT	phospho-Ulight-RRRSLLE
CaMK2α *(h)*	human recombinant	ATP + Ulight-CGSGSGRPRTSSFAEG (50 nM)	30 min RT	phospho-Ulight-CGSGSGRPRTSSFAEG
CDC2/CDK 1 (h) (cycB)	human recombinant (insect cells)	ATP + Ulight-CFFKNIVTPRTPPPSQGK-amide (100 nM)	15 min RT	phospho-Ulight-CFFKNIVTPRTPPPSQGK-amide
CDK2 *(h)* (cycA)	human recombinant	ATP + Ulight-CFFKNIVTPRTPPPSQGK-amide (50 nM)	30 min RT	phospho-Ulight-CFFKNIVTPRTPPPSQGK-amide
CHK1 *(h)*	human recombinant (insect cells)	ATP + CREBtide (CKRREILSRRPSYRK) (25 nM)	30 min RT	phospho-CREBtide (CKRREILSRRPSYRK)
CHK2 *(h)*	human recombinant (insect cells)	ATP + CREBtide (CKRREILSRRPSYRK) (25 nM)	15 min RT	phospho-CREBtide (CKRREILSRRPSYRK)
c-Met kinase *(h)*	human recombinant (insect cells)	ATP + Ulight-CAGAGAIETDKEYYTVKD (25 nM)	60 min RT	phospho-Ulight-CAGAGAIETDKEYYTVKD
EGFR kinase *(h)*	human recombinant (insect cells)	ATP + Ulight-CAGAGAIETDKEYYTVKD (100 nM)	15 min RT	phospho-Ulight-CAGAGAIETDKEYYTVKD
EphA2 kinase *(h)*	human recombinant	ATP + Ulight-TK peptide (50 nM)	30 min RT	phospho-Ulight-TK-peptide
EphA3 kinase *(h)*	human recombinant	ATP + Ulight-TK peptide (50 nM)	60 min RT	phospho-Ulight-TK-peptide
EphB4 kinase *(h)*	human recombinant (insect cells)	ATP + Ulight-TK peptide (100 nM)	90 min RT	phospho-Ulight-TK-peptide
ERK2 *(h)* ($P42^{mapk}$)	human recombinant (*E. coli*)	ATP + Ulight-CFFKNIVTPRTPPPSQGK-amide (100 nM)	15 min RT	phospho-Ulight-CFFKNIVTPRTPPPSQGK-amide
FGFR1 kinase *(h)*	human recombinant (insect cells)	ATP + Ulight-CAGAGAIETDKEYYTVKD (100 nM)	60 min RT	phospho-Ulight-CAGAGAIETDKEYYTVKD
FGFR2 kinase *(h)*	human recombinant	ATP + Ulight-CAGAGAIETDKEYYTVKD (25 nM)	15 min RT	phospho-Ulight-CAGAGAIETDKEYYTVKD
FGFR3 kinase *(h)*	human recombinant	ATP + Ulight-CAGAGAIETDKEYYTVKD	90 min RT	phospho-Ulight-CAGAGAIETDKEYYTV

		(100 nM)		KD
GSK3β *(h)*	human recombinant	ATP + Ulight-CFFKNIVTPRTPPPSQGK-amide (100 nM)	90 min RT	phospho-Ulight-CFFKNIVTPRTPPPSQGK-amide
HGK *(h)* (MAP4K4)	human recombinant	ATP + Ulight-FLGFTYVAP (50 nM)	90 min RT	phospho-Ulight-FLGFTYVAP
IKKα *(h)*	human recombinant (Sf21 cells)	ATP + Ulight-IkappaB-alpha (100 nM)	30 min RT	phospho-Ulight-IkappaB-alpha
IRAK4 *(h)*	human recombinant (insect cells)	ATP + Ulight-FLGFTYVAP (50 nM)	90 min RT	phospho-Ulight-FLGFTYVAP
IRK *(h)* (InsR)	human recombinant	ATP + Ulight-Poly GAT[EAY(1:1:1)]n (50 nM)	10 min RT	phospho-Ulight-Poly GAT[EAY(1:1:1)]n
JAK3 *(h)*	human recombinant	ATP + Ulight-CAGAGAIETDKEYYTVKD (100 nM)	60 min RT	phospho-Ulight-CAGAGAIETDKEYYTVKD
JNK1 *(h)*	human recombinant (*E. coli*)	ATP + Ulight-CFFKNIVTPRTPPPSQGK-amide (100 nM)	60 min RT	phospho-Ulight-CFFKNIVTPRTPPPSQGK-amide
KDR kinase *(h)* (VEGFR2)	human recombinant (Sf9 cells)	ATP + Ulight-CAGAGAIETDKEYYTVKD (100 nM)	60 min RT	phospho-Ulight-CAGAGAIETDKEYYTVKD
Lck kinase *(h)*	human recombinant (insect cells)	ATP + Ulight-Poly GAT[EAY(1:1:1)]n (25 nM)	30 min RT	phospho-Ulight-Poly GAT[EAY(1:1:1)]n
MAPKAPK 2 *(h)*	human recombinant (*E. coli*)	ATP + CREBtide (CKRREILSRRPSYRK) (25 nM)	15 min RT	phospho-CREBtide (CKRREILSRRPSYRK)
MARK1 *(h)*	human recombinant	ATP + Ulight-RRRSLLE (50 nM)	30 min RT	phospho-Ulight-RRRSLLE
MNK2 *(h)*	human recombinant (Sf21 cells)	ATP + CREBtide (CKRREILSRRPSYRK) (25 nM)	90 min RT	phospho-CREBtide (CKRREILSRRPSYRK)
MST4 kinase *(h)*	human recombinant	ATP + Ulight TM- PKC (50 nM)	30 min RT	Phospho-Ulight-TM-PKC
NEK2 *(h)*	human recombinant (insect cells)	ATP + Ulight-FLGFTYVAP (50 nM)	60 min RT	phospho-Ulight-FLGFTYVAP
p38α kinase *(h)*	human recombinant (*E. coli*)	ATP + Ulight-CFFKNIVTPRTPPPSQGK-amide (100 nM)	60 min RT	phospho-Ulight-CFFKNIVTPRTPPPSQGKamide
PAK2 *(h)*	human recombinant (Sf9 cells)	ATP + Ulight-RRRSLLE (50 nM)	60 min RT	phospho-Ulight-RRRSLLE
PAK4 *(h)*	human recombinant (insect cells)	ATP + Ulight-RRRSLLE (50 nM)	30 min RT	phospho-Ulight-RRRSLLE
PDK1 *(h)*	human	ATP + Ulight-FLGFTYVAP	90 min	phospho-Ulight-

	recombinant (insect cells)	(400 nM)	RT	FLGFTYVAP
Pim2 kinase *(h)*	human recombinant (insect cells)	ATP + CREBtide (CKRREILSRRPSYRK) (25 nM)	60 min RT	phospho-CREBtide (CKRREILSRRPSYRK)
PKA *(h)*	human recombinant (*E. coli*)	ATP + Ulight-RRRSLLE (50 nM)	10 min RT	phospho-Ulight-RRRSLLE
PKCβ2 *(h)*	human recombinant	ATP + CREBtide (CKRREILSRRPSYRK) (25 nM)	15 min RT	phospho-CREBtide (CKRREILSRRPSYRK)
PLK1 *(h)*	human recombinant	ATP + Ulight-FLGFTYVAP (40 nM)	60 min RT	phospho-Ulight-FLGFTYVAP
RAF-1 kinase *(h)*	human recombinant	ATP + Ulight-ARTKQTARKSTGGKAPRKQL AGCG (50 nM)	180 min RT	phospho-Ulight-ARTKQTARKSTGGKAP RKQ LAGCG
ROCK1 *(h)*	human recombinant	ATP + Ulight-RRRSLLE (50 nM)	30 min RT	phospho-Ulight-RRRSLLE
SGK1 *(h)*	human recombinant	ATP + Ulight-RRRSLLE (50 nM)	30 min RT	phospho-Ulight-RRRSLLE
SIK *(h)*	human recombinant (Sf21 cells)	ATP + CREBtide (CKRREILSRRPSYRK) (25 nM)	90 min RT	phospho-CREBtide (CKRREILSRRPSYRK)
Src kinase *(h)*	human recombinant (insect cells)	ATP + Ulight-Poly GAT[EAY(1:1:1)]n (5 nM)	10 min RT	phospho-Ulight-Poly GAT[EAY(1:1:1)]n
TAOK2 (TAO1) *(h)*	human recombinant	ATP + Ulight-FLGFTYVAP (40 nM)	60 min RT	phospho-Ulight-FLGFTYVAP
TRKA *(h)*	human recombinant (insect cells)	ATP + Ulight-Poly GAT[EAY(1:1:1)]n (5 nM)	10 min RT	phospho-Ulight-Poly GAT[EAY(1:1:1)]n

VII. Toxicity assay: Determination of the *in vivo* activity on zebrafish embryos

The zebrafish embryos were collected and placed into 24-well plates, ten embryos per well and maintained in E3 medium[7] at 28°C. Compounds were added 24 hpf and the embryos allowed to grow in chemical compound solution up to 5 days. The phenotypes were compared using the StereoBlue Bino Zoom microscope system from Euromex. Pictures were taken with camera Nikon D5000. **Animal husbandry.** All animal experiments were conducted and documented according to the federal and local regulation.

VIII. Modeling of the kinase domain

The residues 1850-2050 of human LRRK2 were used to find structures with known sequences. The swiss model server (automatic mode) was used to perform an alignment to template sequences.[8, 9] The B-Raf crystal structure (PDB 4DBN) was uses as template. The kinase domain was modeled using Molegro Virtual Docker 6. Only one model was built and no optimizations were performed. The docking was performed manually.

IX. References and notes

[1] G. M. Amombo, T. Kramer, F. Lo Monte, S. Göring, M. Fach, S. Smith, S. Kolb, R. Schubenel, K. Baumann, B. Schmidt, *Bioorg. Med. Chem. Lett.* **2012**, *22*, 7634-7640.

[2] http://www.cerep.fr.

[3] J. M. Taymans, R. Vancraenenbroeck, P. Ollikainen, A. Beilina, E. Lobbestael, M. De Maeyer, V. Baekelandt, M. R. Cookson, *PloS one* **2011**, *6*, e23207.

[4] R. Vancraenenbroeck, J. De Raeymaecker, E. Lobbestael, F. Gao, M. De Maeyer, A. Voet, V. Baekelandt, J. M. Taymans, *Front. Mol. Neurosci.* **2014**, *7*, 51.

[5] M. Jaleel, R. J. Nichols, M. Deak, D. G. Campbell, F. Gillardon, A. Knebel, D. R. Alessi, *Biochem. J.* **2007**, *405*, 307-317.

[6] C. J. Asensio, R. C. Garcia, *Anal. Biochem.* **2003**, *319*, 21-33.

[7] C. Nüsslein-Volhard, R. Dahm, 1 ed., Oxford University Press, **2001**.

[8] K. Arnold, L. Bordoli, J. Kopp, T. Schwede, *Bioinformatics* **2006**, *22*, 195-201.

[9] F. Kiefer, K. Arnold, M. Kunzli, L. Bordoli, T. Schwede, *Nucleic Acids Res.* **2009**, *37*, D387-392.

4.6 Zusätzlich bearbeitete Themen neben dem Schwerpunkt der FLT3- und LRRK2-Inhibition

4.6.1 Membran-verankerte γ-Sekretase Modulatoren mit Terpen abgeleiteten Resten

Der Inhalt dieses Kapitels wurde bereits veröffentlicht.[188]

Autoren: Eva Christine Naumann*, Stefan Göring*, Isabella Ogorek, Sascha Weggen, Boris Schmidt.

Titel: „Membrane anchoring γ-secretase modulators with terpene-derived moieties".

Journal: Bioorganic & Medicinal Chemistry Letters.

DOI: 10.1016/j.bmcl.2013.04.070.

Zusammenfassung:

Die Alzheimer-Krankheit ist die meist bekannteste, fortschreitende und derzeit irreversible Form der Demenz. Charakteristische neuropathologische Merkmale sind zwei verschiedene Arten von Proteinablagerungen. Bei den betroffenen Patienten bilden sich intrazelluläre, neurofibrilläre Bündel (*neurofibrillary tangles,* NFTs) und extrazelluläre, amyloide Plaques. Durch den Abbau eines membranständigen, amyloiden Vorläuferproteins APP durch die β-Sekretase und im Folgenden durch die γ-Sekretase werden Plaques in unterschiedlichen Längen von 38, 40 und 42 Aminosäuren gespalten. $A\beta_{42}$ ist dabei das weitaus toxischere Plaque, da es durch den höheren Anteil an Aminosäuren schneller zur Aggregation neigt und sich so frühzeitig Oligomere ausbilden können. Eine vielversprechende Strategie für die Behandlung der Alzheimer-Demenz ist deshalb die Modulation der γ-Sekretase.

In vorrangegangenen Studien konnte gezeigt werden, dass die Gegenwart eines lipophilen Restes sowie einer Säurefunktion am Carprofen-Grundgerüst möglicherweise entscheidend für die Modulation der γ-Sekretase ist. Motivierend durch diese Ergebnisse synthetisierten wir neue Carprofen- bzw. Tocopherol-basierende Derivate mit Terpen-Einheiten, um die Modulation der γ-Sekretase zu verbessern. Es konnten verschiedene Substanzen hergestellt werden, welche inhibitorische Aktivitäten zwischen 4 µM und 57 µM aufwiesen. Da die Verbindungen einen amphiphilen Charakter, aufgrund der Säurefunktion und des langen hydrophoben Restes, aufwiesen, musste die Bildung von Mizellen ausgeschlossen werden. Experimente zur dynamischen Lichtstreuung wurden durchgeführt, um die Formation von

Mizellen oder Aggregaten im relevanten Konzentrationsbereich von 5-100 µM auszuschließen.

Eigener Beitrag zu dieser Arbeit:
Der synthetische Beitrag lag in den Verbindungen BSc4099 (5a), BSc4118 (5b). In Klammer die Verbindungsnummern in der Publikation.
Des Weiteren wurden Experimente zur dynamischen Lichtstreuung von mir durchgeführt.

Bioorganic & Medicinal Chemistry Letters 23 (2013) 3852–3856

Contents lists available at SciVerse ScienceDirect

Bioorganic & Medicinal Chemistry Letters

journal homepage: www.elsevier.com/locate/bmcl

Membrane anchoring γ-secretase modulators with terpene-derived moieties

Eva Christine Naumann [a,†], Stefan Göring [a,†], Isabella Ogorek [b], Sascha Weggen [b], Boris Schmidt [a,*]

[a] Clemens Schöpf-Institute of Organic Chemistry and Biochemistry, Technische Universität Darmstadt, 64287 Darmstadt, Germany
[b] Department of Neuropathology, Heinrich-Heine-University, 40225 Düsseldorf, Germany

ARTICLE INFO

Article history:
Received 19 February 2013
Revised 24 April 2013
Accepted 27 April 2013
Available online 7 May 2013

Keywords:
Alzheimer's disease
γ-Secretase modulator
Tocopherol
Membrane anchoring

ABSTRACT

Modulation of γ-secretase activity is a promising therapeutic strategy for the treatment of Alzheimer's disease. Herein we report on the synthesis of carprofen- and tocopherol-derived small-molecule modulators carrying terpene moieties as lipophilic membrane anchors. Additionally, these modulators are equipped with an acidic moiety, which contributes to the desired modulatory effect on the γ-secretase with decreased formation of $A\beta_{42}$ and increased $A\beta_{38}$ production.

Alzheimer's disease (AD) is an incurable neurodegenerative disorder and the most prevalent form of age-associated dementia. The number of approximately 36 million dementia sufferers is expected to rise significantly in the next decades as a consequence of increased life exspectancy.[1]

The pathological hallmarks of AD are two kinds of protein deposits in the brain: extracellular amyloid-β-plaques and intracellular neurofibrillary tangles, which cause neuronal loss and neurodegeneration, leading to widespread brain atrophy and break down of neuronal signal communication pathways.[2–4] This causes the major AD associated clinical symptom cognitive decline.[5,6]

The sequential proteolytic cleavage of APP (amyloid precursor protein) by the β- and γ-secretase is responsible for the release of amyloid-β (Aβ) peptides and the formation of Aβ-plaques in the brain (amyloidogenic pathway): APP cleavage by the β-secretase generates the extracellular soluble domain sAPPβ and the transmembrane fragment C99, which is subsequently processed by the γ-secretase to form Aβ-peptides of varying length (mostly $A\beta_{37}$–$A\beta_{42}$).[7–9] Aβ-plaques mainly consist of $A\beta_{42}$ and $A\beta_{40}$. Depending on their length Aβ-peptides tend to aggregate and accumulate in the brain. $A\beta_{38}$ is a more soluble fragment, whereas the more hydrophobic $A\beta_{42}$ species has a higher tendency to aggregate.[10–13] According to the amyloid-hypothesis, the aggregation-prone $A\beta_{42}$ peptides are the central drivers of the pathological process in AD.

Clinical trials with γ-secretase inhibitors, that reduce the overall activity of the enzyme, have failed, most likely because the proteolytic activity of γ-secretase is involved in essential physiological processes such as the Notch-signaling pathway.[14–16] The γ-secretase is an aspartyl protease, a membrane-bound complex of four essential proteins: Presenilin-1 or 2, Nicastrin, *Anterior pharynx defective-1* and *Presenilin enhancer-2*.[17] In contrast modulation of the γ-secretase function is a more promising therapeutic approach for the treatment of AD. Modulation of the γ-secretase has been demonstrated to reduce the production of $A\beta_{42}$ and to increase the formation of shorter Aβ-peptides like $A\beta_{38}$, which have a lower tendency to aggregate. Some non-steroidal anti-inflammatory drugs (NSAIDs) were identified as the first γ-secretase modulators (GSMs). Sulindac sulfide, indomethacin, ibuprofen and *R*-flurbiprofen cause a reduction in $A\beta_{42}$ levels and an increase of $A\beta_{38}$ in vitro and in vivo.[18–20] However *R*-flurbiprofen failed in clinical studies because of low potency.[21]

Recently we reported on NSAID-derived carbazole and carprofen derivatives as GSMs.[22,23] The presence of both a lipophilic and an acidic moiety on the carbazole or the carprofen scaffold seemed to be crucial for the modulatory effect on γ-secretase. The most active derivatives display activities in the low micromolar range (Fig. 1). We assumed that the lipophilic chain acts like a membrane anchor and the acidic moiety might interact with the basic lysine[624], which is postulated to be an important determinant of amyloid β peptide length in the juxtamembrane region of APP.[24]

Motivated by these results we synthesized new carprofen derivatives in order to improve the modulatory effect on γ-secretase. The hypothesis of lipophilic anchoring in the lipid membrane

* Corresponding author. Tel.: +49 6151 164531; fax: +49 6151 163278.
E-mail address: schmidt_boris@t-online.de (B. Schmidt).
† These authors contributed equally to this work.

0960-894X/$ - see front matter © 2013 Elsevier Ltd. All rights reserved.
http://dx.doi.org/10.1016/j.bmcl.2013.04.070

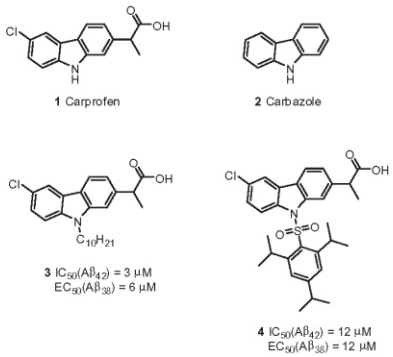

Figure 1. Carprofen (**1**), carbazole (**2**) and two selected γ-secretase modulators (**3**, **4**).[25]

suggested the introduction of natural lipophilic chains with terpene-related structures like the farnesyl- and the phytyl moiety on the carprofen core. Phytol- and farnesol-derived compounds are natural components of essential oils or of chlorophyll. Tocopherol, a terpene-derived natural compound, located in cell membranes, is an effective antioxidant and anti-inflammatory agent and protects cell membranes from oxidative damage.[26] It was proposed as a therapeutic agent for AD and other neurodegenerative disorders, and clinical trials have already been performed based on the hypothesis that AD might be caused by oxidative stress.[26,27] Studies indicated that α-tocopherol levels are significantly altered in the brain of AD patients.[28,29] Changes of the tocopherol levels in the brain might be affected by the APOE status.[30] The major risk factor for late-onset AD is a polymorphism of the APOE gene on chromosom 19.[31] Smoking or non-smoking carriers of the APOE4 isoform displayed remarkable differences in the pharmacokinetics of enantiopure and all-rac-α-tocopherol with its eight stereoisomers.[32] The animal food additive all-rac-α-tocopherol, with its various stereoisomers, is ingested by humans via comsumption of animal fats.[33] These observations encouraged us to investigate the impact of enantiopure and all-rac-α-tocopherol analogues on GSM activity. The new carprofen derivatives **5a–b** were prepared by a one step synthesis (Scheme 1). The reaction of the carprofen **1** and the corresponding phytyl- and farnesyl halogenides **6** and **7** yielded the carprofen derivatives **5a–b**. The phytyl- and farnesyl

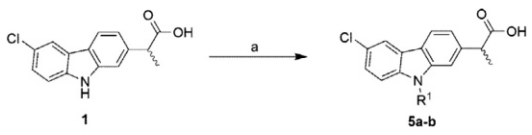

Scheme 1. Synthesis of carprofen derivatives. Reagents and conditions: (a) NaH, R^1-X, THF, 0 °C to rt. A cell-based assay was used to quantify the GSM activity of novel derivatives and to determine the altered generation of $A\beta_{38}$, $A\beta_{40}$ and $A\beta_{42}$ peptides (see Supplementary data).

halogenides **6** and **7** were generated from the commercially available phytol (mix of *cis*/*trans*-isomers) **8** and *trans*,*trans*-farnesol **9** (see Supplementary data).

Indeed the carprofen derivatives **5a–b** showed GSM activity in the low micromolar range (Table 1). The carprofen derivative **5a** (IC_{50} ($A\beta_{42}$) = 4 μM) was the most active GSM and derivative **5b** (IC_{50} ($A\beta_{42}$) = 23 μM) also lowered $A\beta_{42}$ levels significantly. These oligo-isoprenylated GSMs are characterized by a high *clogP* (Table 4) and amphiphilic behavior, but they do resemble terpenes with essential biological activity in humans. Based on the GSM activity of the terpene-derived compounds **5a–b**, we aimed at tocopherol-derived GSMs with the *R*,*R*,*R*-α-tocopherol **10a** and the all-rac-α-tocopherol **10b** and the structurally related 6-hydroxy-2,5,7,8-tetramethylchroman-2-carboxylic acid **11** as starting materials (Fig. 2).

Referring to our previous studies we added a carboxylic acid to the tocopherol scaffolds **10a–b** and lipophilic chains to the chroman derivative **11**. The syntheses are outlined in Schemes 2–4[34] We synthesized two tocopherol derivatives **13a–b** in order to compare the influence of the different centers of chirality of the lipophilic side chain on γ-secretase activity. Additionally we generated two classes of chroman derivatives **16a–e** and **18a–e** to explore the impact of the acidic moiety's location on the putative GSM activity. We further compared the influence of several lipophilic chains of various lengths like octyl-, undecyl, tetradecyl and the terpene-related farnesyl- and phytyl moieties.

The experimental data confirmed our initial hypothesis: all synthesized tocopherol derivatives with an acidic moiety (see Table 3, entries 3–14) exhibit GSM activity and increased the generation of $A\beta_{38}$ and reduced the generation of $A\beta_{42}$; no other modes of action like inverse modulation or inhibition of γ-secretase activity were observed. The tocopherol **10b** itself displayed no GSM activity (IC_{50} ($A\beta_{42}$) > 100 μM). The tocopherol ester **12b** (IC_{50} ($A\beta_{42}$) > 100 μM) was also inactive while the corresponding tocopherol acid **13a** (IC_{50} ($A\beta_{42}$) = 11 μM) had strong GSM activity. This confirms the crucial role of the acidic functionality in these GSMs. The stereoisomers **13a** (IC_{50} ($A\beta_{42}$) = 11 μM) and **13b** (IC_{50} ($A\beta_{42}$) = 12 μM) displayed equipotent activities; thus the configuration of the chiral carbon atoms did not seem to influence GSM activity. All chroman derivatives (Table 3, entries 5–14) show

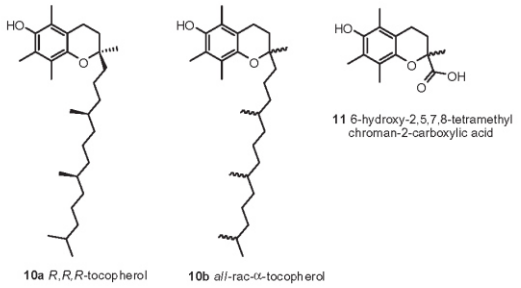

Figure 2. Starting materials of the tocopherol-derived compounds as GSMs.

Table 1
Activity of *trans*,*trans*-farnesyl-(**5a**) and phytyl (**5b**) derivatized carprofens

Compd	R^1	EC_{50} $A\beta_{38}$[a] (μM)	IC_{50} $A\beta_{40}$[a] (μM)	IC_{50} $A\beta_{42}$[a] (μM)
5a	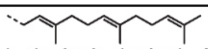	2 ± 1.1	26 ± 0.2	4 ± 0.4
5b	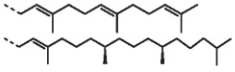	>50	>50	23 ± 0.1

[a] Enzyme-linked immunosorbent assay, CHO cells, for the increase of $A\beta_{38}$ see Supplementary data .

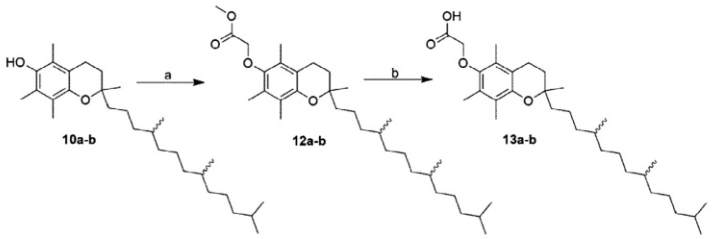

Scheme 2. Synthesis of tocopherol derivatives. Reagents and conditions: (a) NaH, methyl 2-bromoacetate, DMF, rt; (b) KOH, dioxane/water (5:1), 75 °C.[35]

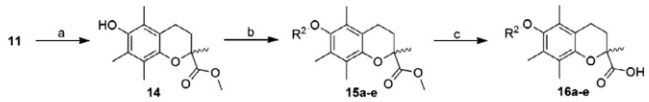

Scheme 3. Synthesis of chroman derivatives. Reagents and conditions: (a) K_2CO_3, MeI, DMF, rt; (b) Cs_2CO_3, R^2-X, DMF, 100 °C; (c) KOH, dioxane/water (5:1), 75 °C.[35]

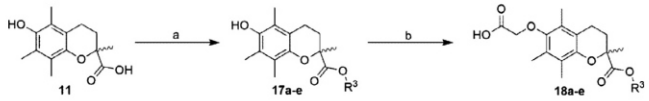

Scheme 4. Synthesis of chroman derivatives. Reagents and conditions: (a) K_2CO_3, R^3-X, DMF, rt; (b) NaH, 2-bromoacetic acid, DMF, rt.

GSM activity except for compound **16a** (IC_{50} ($A\beta_{42}$) = 57 μM) and compound **18a** (IC_{50} ($A\beta_{42}$) = 35 μM), which displayed only very low GSM activity. These derivatives (**16a/18a**) contain lipophilic chains with eight carbon atoms only, which are too short to provide stable anchoring in the membrane. Extending the lipophilic side chains (eight (**16a**) to fourteen carbon atoms (**16c**)) improves GSM activity (IC_{50} ($A\beta_{42}$) = 57 μM (**16a**) up to an IC_{50} ($A\beta_{42}$) = 14 μM (**16c**)). The branching of the lipophilic side chain, which is present in the farnesyl- (**16e**) and phytyl (**16d**) moieties, slightly lowered GSM activity (IC_{50} ($A\beta_{42}$) = 28 μM (**16e**), IC_{50} ($A\beta_{42}$) = 26 μM (**16d**)). The chroman derivatives (**18a–e**) with switched attachment of the acidic and the lipophilic moieties show nearly the same activities compared to the derivatives **16a–e** (see Table 3), which carry the same lipophilic side chains. The switch between the acidic and lipophilic substituents did not change the GSM activity. As a consequence of the higher molecular weights of the derivatives **18a–e**, compared to the compounds **16a–e**, the undecyl-substituted derivative **18b** (IC_{50} ($A\beta_{42}$) = 12 μM) was the most potent GSM, while compound **18c** with a lipophilic chain of fourteen carbon atoms exerted reduced GSM activity (IC_{50} ($A\beta_{42}$) = 22 μM). All synthesized compounds (**5a**–**18e**) carry a long lipophilic side chain and additionally an acidic moiety and thus resemble amphiphiles, which may form micelles at the concentrations employed for the in vitro assays. Dynamic light scattering experiments were conducted to exclude the formation of micelles or aggregates within the relevant concentration range of 5–100 μM (see Supplementary data). The critical micelle concentration of Pluronic F68 was determined as control and found to match the literature (40 μM).[36] Micelle formation or aggregation was neither observed below nor within the concentration range for the compounds **5a**–**18e**. Compound **16b** started to form micelles at a concentration of 100 μm, which is factor 10× above the EC_{50} observed for $A\beta_{38}$ production. Thus micelle formation is very unlikely to contribute to observed effects.

In conclusion we have developed a new series of GSMs with terpene moieties (Table 2). The compounds are not drug-like molecules, which is due to their high *c*log*P* values (Table 4) caused by the extended lipophilic side chains, however the evaluation of these lipophilic compounds suggests an anchoring in the membrane (for calculations of the lipophilic efficiency indices (LE, LLE, LELP) see Supplementary data). The less active GSMs **16a**, **16b** and **18a** display the highest ligand efficiency of 0.25, 0.21 and 0.22, respectively. Our results indicate a biphasic correlation between the modulation of γ-secretase activity and the length of the lipophilic side chains and the corresponding calculated *c*log*P* values (Table 3, **16a**: IC_{50} ($A\beta_{42}$) = 57 μM, **16b**: IC_{50} ($A\beta_{42}$) = 28 μM, **16c**: IC_{50} ($A\beta_{42}$) = 14 μM). A maximum of potency of the carprofen- and tocopherol derivatives was observed within a range of 450–490 g/mol both for the compounds with the branched lipophilic side chains and the compounds with linear lipophilic chains (**5a**: IC_{50} ($A\beta_{42}$) = 4 μM; **13a**: IC_{50} ($A\beta_{42}$) = 11 μM, Table 4, Fig. 3). This result is consistent with the correlation of the calculated *c*log*P* values and the GSM activity (Table 3, Fig. 4). With respect to the

Table 2
Structural variation of the tocopherol- and chroman derivatives

Entry	Compd	R	Substituent
1	**13a**		
2	**13b**		
3	**16a**	R^2	
4	**16b**	R^2	
5	**16c**	R^2	
6	**16d**	R^2	
7	**16e**	R^2	
8	**18a**	R^3	
9	**18b**	R^3	
10	**18c**	R^3	
11	**18d**	R^3	
12	**18e**	R^3	

Table 3
Activity of the tocopherol- and chroman derivatives

Entry	Compd	EC_{50} $A\beta_{38}$[a] (μM)	IC_{50} $A\beta_{40}$[a] (μM)	IC_{50} $A\beta_{42}$[a] (μM)
1	**10b**	>100	>100	>100
2	**12b**	>100	>100	>100
3	**13a**	6 ± 0.3	24 ± 0.1	11 ± 0.6
4	**13b**	4 ± 1.2	26 ± 2.4	12 ± 0.7
5	**16a**	>50	>50	57 ± 5.8
6	**16b**	10 ± 2.0	>50	28 ± 6.6
7	**16c**	9 ± 2.5	29 ± 1.7	14 ± 3.3
8	**16d**	10 ± 2.1	42 ± 5.1	26 ± 2.5
9	**16e**	8 ± 2.0	39 ± 14.5	28 ± 6.6
10	**18a**	11 ± 10.4	42 ± 5.1	35 ± 3.0
11	**18b**	5 ± 1.4	23 ± 0.6	12 ± 0.7
12	**18c**	6 ± 0.8	34 ± 3.5	22 ± 2.8
13	**18d**	13 ± 0.3	36 ± 8.6	24 ± 4.9
14	**18e**	1 ± 1.3	25 ± 1.1	27 ± 3.5

± Standard deviation.
[a] Enzyme-linked immunosorbent assay, CHO cells, for the increase of $A\beta_{38}$ see Supplementary data .

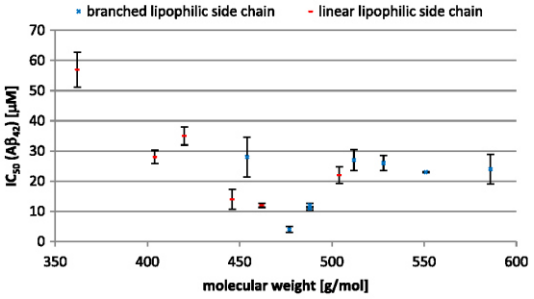

Figure 3. Correlation plot of IC_{50} ($A\beta_{42}$) of compounds **5a–b**, **13a–b**, **16a–e**, **18a–e** and molecular weight (see Table 4).

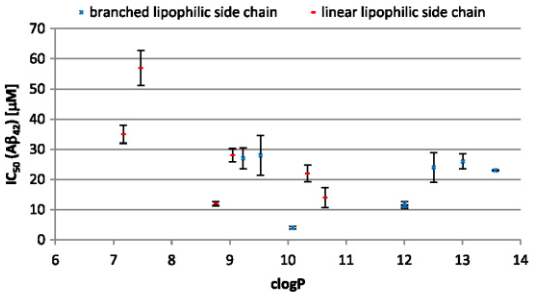

Figure 4. Correlation plot of IC_{50} ($A\beta_{42}$) of compounds **5a–b**, **13a–b**, **16a–e**, **18a–e** and *c*log*P* (see Table 4).

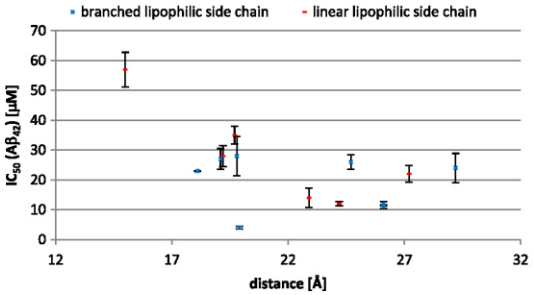

Figure 5. Correlation plot of IC_{50} ($A\beta_{42}$) of compounds **5a–b**, **13a–b**, **16a–e**, **18a–e** and distance (Å) of carbonyl oxygen of the acid functionality to the hydrogen atom at the end of lipophilic chain (see Table 4).

extension of the lipophilic side chain and the greater distance between the carbonyl-oxygen of the acid functionality and the terminal hydrogen atom of the branched or linear lipophilic side chain, a biphasic correlation is indicated (Table 3, Fig. 5). The maximum of potency is observed within the range of 20–27 Å for the compounds (**5a**: IC_{50} ($A\beta_{42}$) = 4 μM, **13a**: IC_{50} ($A\beta_{42}$) = 11 μM, **13b**: IC_{50} ($A\beta_{42}$) = 12 μM, **16c**: IC_{50} ($A\beta_{42}$) = 12 μM, **18b**: IC_{50} ($A\beta_{42}$) = 14 μM). In case of the chroman derivatives (**16a–e**, **18a–e**) both the branching of the lipophilic side chains and the presence of double bonds reduced the GSM activity considerably. We hypothesize that the rigidity, caused by the double bonds, disturbed the desired interaction of the lipophilic side chain in the membrane. Derivatives with evidently too long lipophilic chains cannot be anchored in the necessary orientation and thus result in weak GSM activity.

Table 4
Comparison of activity of γ-secretase modulators (IC_{50} ($A\beta_{42}$) (μM)), molecular weight (g/mol), *c*log*P* and distance of carbonyl-oxygen of the acid functionality and the terminal hydrogen atom of the lipophilic chain (Å)

Entry	Compd	Molar mass (g/mol)	IC_{50}[a] ($A\beta_{42}$) (μM)	*c*log*P*[b]	Distance[c] (Å)
1	**5a**	477	4 ± 0.4	10.08	19.9
2	**5b**	551	23 ± 0.1	13.57	18.1
3	**13a**	488	11 ± 0.6	12.02	26.1
4	**13b**	488	12 ± 0.7	12.02	26.1
5	**16a**	362	57 ± 5.8	7.47	15.0
6	**16b**	404	28 ± 2.2	9.05	19.2
7	**16c**	446	14 ± 3.3	10.64	22.9
8	**16d**	528	26 ± 2.5	13.01	24.7
9	**16e**	454	28 ± 6.6	9.53	19.8
10	**18a**	420	35 ± 3.0	7.17	19.7
11	**18b**	462	12 ± 0.7	8.76	24.2
12	**18c**	504	22 ± 2.8	10.34	27.2
13	**18d**	586	24 ± 4.9	12.51	29.2
14	**18e**	512	27 ± 3.5	9.23	19.1

[a] Enzyme-linked immunosorbent assay, CHO-cells.
[b] Calculated by ChemDraw Ultra 11.0.
[c] Distance of carbonyl-oxygen of the acid functionality and the terminal hydrogen atom of the lipophilic chain (Å), calculated by Chem3D Ultra 11.0.

Supplementary data

Supplementary data associated with this article can be found, in the online version, at http://dx.doi.org/10.1016/j.bmcl.2013.04.070.

References and notes

1. Alzheimer's Association. Alzheimer's Disease and Facts and Figures, Vol. 8, pp 131–168 http://www.alz.org/downloads/facts_figures_2012.pdf.
2. Glenner, G. G.; Wong, C. W. *Biochem. Biophys. Res. Commun.* **1984**, *120*, 885.
3. Gorevic, P. D.; Goni, F.; Pons-Estel, B.; Alvarez, F.; Peress, N. S.; Frangione, B. *J. Neuropathol. Exp. Neurol.* **1986**, *45*, 647.
4. Masters, C. L.; Simms, G.; Weinman, N. A.; Multhaup, G.; McDonald, B. L.; Beyreuther, K. *Proc. Natl. Acad. Sci. U.S.A.* **1985**, *82*, 4245.
5. Hardy, J.; Higgins, G. *Science* **1992**, *256*, 184.
6. Selkoe, D. J. *Neuron* **1991**, *6*, 487.
7. Haass, C.; Koo, E. H.; Mellon, A.; Hung, A. Y.; Selkoe, D. J. *Nature* **1992**, *357*, 500.
8. Sastre, M.; Steiner, H.; Fuchs, K.; Capell, A.; Multhaup, G.; Condron, M. M.; Teplow, D. B.; Haass, C. *EMBO Rep.* **2001**, *2*, 835.
9. Shoji, M.; Golde, T.; Ghiso, J.; Cheung, T.; Estus, S.; Shaffer, L.; Cai, X.; McKay, D.; Tintner, R.; Frangione, B., et al *Science* **1992**, *258*, 126.
10. Bitan, G.; Kirkitadze, M. D.; Lomakin, A.; Vollers, S. S.; Benedek, G. B.; Teplow, D. B. *Proc. Natl. Acad. Sci. U.S.A.* **2003**, *100*, 330.
11. Bitan, G.; Vollers, S. S.; Teplow, D. B. *J. Biol. Chem.* **2003**, *278*, 34882.
12. Walsh, D. M.; Klyubin, I.; Fadeeva, J. V.; Cullen, W. K.; Anwyl, R.; Wolfe, M. S.; Rowan, M. J.; Selkoe, D. J. *Nature* **2002**, *416*, 535.
13. Walsh, D. M.; Selkoe, D. J. *Neuron* **2004**, *44*, 181.
14. De Strooper, B.; Annaert, W.; Cupers, P.; Saftig, P.; Craessaerts, K.; Mumm, J. S.; Schroeter, E. H.; Schrijvers, V.; Wolfe, M. S.; Ray, W. J.; Goate, A.; Kopan, R. *Nature* **1999**, *398*, 518.
15. Struhl, G.; Greenwald, I. *Nature* **1999**, *398*, 522.
16. Ye, Y.; Lukinova, N.; Fortini, M. E. *Nature* **1999**, *398*, 525.
17. Wolfe, M. S. *Biochemistry* **2006**, *45*, 7931.
18. Avramovich, Y.; Amit, T.; Youdim, M. B. H. *J. Biol. Chem.* **2002**, *277*, 31466.
19. Eriksen, J. L.; Sagi, S. A.; Smith, T. E.; Weggen, S.; Das, P.; McLendon, D. C.; Ozols, V. V.; Jessing, K. W.; Zavitz, K. H.; Koo, E. H.; Golde, T. E. *J. Clin. Invest.* **2003**, *112*, 440.
20. Weggen, S.; Eriksen, J. L.; Das, P.; Sagi, S. A.; Wang, R.; Pietrzik, C. U.; Findlay, K. A.; Smith, T. E.; Murphy, M. P.; Bulter, T.; Kang, D. E.; Marquez-Sterling, N.; Golde, T. E.; Koo, E. H. *Nature* **2001**, *414*, 212.
21. Green Rc, S. L. S. A. D. A. et al *J. Am. Med. Assoc.* **2009**, *302*, 2557.
22. Baumann, S.; Höttecke, N.; Schubenel, R.; Baumann, K.; Schmidt, B. *Bioorg. Med. Chem. Lett.* **2009**, *19*, 6986.
23. Zall, A.; Kieser, D.; Höttecke, N.; Naumann, E. C.; Thomaszewski, B.; Schneider, K.; Steinbacher, D. T.; Schubenel, R.; Masur, S.; Baumann, K.; Schmidt, B. *Bioorg. Med. Chem. Lett.* **2011**, *19*, 4903.
24. Kukar, T. L.; Ladd, T. B.; Robertson, P.; Pintchovski, S. A.; Moore, B.; Bann, M. A.; Ren, Z.; Jansen-West, K.; Malphrus, K.; Eggert, S.; Maruyama, H.; Cottrell, B. A.; Das, P.; Basi, G. S.; Koo, E. H.; Golde, T. E. *J. Biol. Chem.* **2011**, *286*, 39804.
25. Narlawar, R.; Baumann, K.; Czech, C.; Schmidt, B. *Bioorg. Med. Chem. Lett.* **2007**, *17*, 5428.
26. Berman, K.; Brodaty, H. *CNS Drugs* **2004**, *18*, 807.
27. Sano, M.; Ernesto, C.; Thomas, R. G.; Klauber, M. R.; Schafer, K.; Grundman, M.; Woodbury, P.; Growdon, J.; Cotman, C. W.; Pfeiffer, E.; Schneider, L. S.; Thal, L. J. *N. Eng. J. Med.* **1997**, *336*, 1216.
28. Adams, J.; Klaidman, L.; Odunze, I.; Shen, H.; Miller, C. *Mol. Chem. Neuropathol.* **1991**, *14*, 213.
29. Jiménez-Jiménez, F. J.; Bustos, F.; Molina, J. A.; Benito-León, J.; Tallón-Barranco, A.; Gasalla, T.; Ortí-Pareja, M.; Guillamón, F.; Rubio, J. C.; Arenas, J.; Enríquez-de-Salamanca, R. *J. Neural Transm.* **1997**, *104*, 703.
30. Vatassery, G. T.; Lam, C.; Smith, W. E.; Quach, H. T. *J. Neurosci. Res.* **2006**, *84*, 1335.
31. Corder, E.; Saunders, A.; Strittmatter, W.; Schmechel, D.; Gaskell, P.; Small, G.; Roses, A.; Haines, J.; Pericak-Vance, M. *Science* **1993**, *261*, 921.
32. Proteggente, A. R.; Rota, C.; Majewicz, J.; Rimbach, G.; Minihane, A. M.; Kraemer, K.; Lodge, J. K. *Free Radic. Biol. Med.* **2006**, *40*, 2080.
33. Meier, R.; Tomizaki, T.; Schulze-Briese, C.; Baumann, U.; Stocker, A. *J. Mol. Biol.* **2003**, *331*, 725.
34. See Supplementary data for further details.
35. Bob G. Sanders, (A.T.X.); Kimberly Kline, (A.T.X.); Laurence Hurley, (A.T.X.); Robb Gardner, (A.T.X.); Marla Menchaca, (A.T.X.); Weiping Yu, (A.T.X.); Puthucode N. Ramanan, (A.T.X.); Shenquan Liu, (A.T.X.); Karen Israel, (A.T.X.). U.S. Patent 6,770,672, 2004.
36. http://www.sigmaaldrich.com/img/assets/15402/Detergent_Selection_Table.pdf.

Supplementary Material (ESI) for Bioorganic & Medical Chemistry Letters

Supporting Information

Membrane anchoring γ-secretase modulators with terpene-derived moieties

Eva Christine Naumann[*,a], Stefan Göring[*,a], Isabella Ogorek[b], Sascha Weggen[b] and Boris Schmidt[†,a]

[a] *Clemens Schöpf - Institute of Organic Chemistry and Biochemistry, Technische Universität Darmstadt, 64287 Darmstadt, Germany, Fax: +496151-163278; Tel: +496151-164531*

[b] *Department of Neuropathology, Heinrich-Heine-University, 40225 Düsseldorf, Germany*

† *E-mail: schmidt_boris@t-online.de*

[*]These authors contributed equally to this work.

Table of Content:

I. General comments

II. Experimental methods and chemical data

III. Determination of γ-secretase modulator (GSM) activity

IV. Calculations of LE and LLE

V. Dynamic light scattering experiments

VI. References

I. General comments

The ^{1}H-NMR spectra were recorded on a Bruker AC 300 spectrometer at 300 MHz and Bruker AC 500 spectrometer at 500 MHz. The ^{13}C-NMR spectra were recorded on a Bruker AC 300 spectrometer at 75 MHz and Bruker AC 500 spectrometer at 125 MHz. Chemical shifts are reported as ppm downfield from Me_4Si. Mass spectrometry was performed on a Bruker-Franzen Esquire LC mass spectrometer and a MAT 95 double focussing sector field MS. Microwave experiments were carried out using a Biotage® Initiator™ microwave apparatus. All microwave experiments were carried out in sealed microwave process vials utilizing the standard absorbance level (300 W maximum power). High performance liquid chromatographies were carried out in an Agilent 1100 (column: reversed phase, Zorbax Eclipse XDB-C8, 4.6 x 150 mm; 254 nm). The eluent is composed of: a) H_2O (1% TFA) (A) and acetonitrile (B) with a gradient: 30 to 90% B within 12 min. All reagents and solvents were purchased at ABCR, Acros, Sigma Aldrich or VWR.

II. Experimental methods and chemical data

1. Synthesis of (7*R*,11*R*,*E*)-1-bromo-3,7,11,15-tetramethylhexadec-2-ene 6[1]

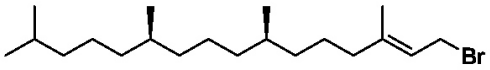

To a well stirred solution of phytol (350 mg, 1.18 mmol), pyridine (48 µL) and hexane (0.70 mL) under Argon atmosphere at 0° were added dropwise a solution of PBr_3 (640 mg, 2.26 mmol) in hexane (0.24 mL). After stirring for 3 hours at room temperature the mixture was quenched with ice water (10 mL) and extracted with DCM (3 x 15 mL). The combined organic layers were washed with 1N HCl (10 mL), saturated $NaHCO_3$ solution, dried over $MgSO_4$ and concentrated *in vacuo* to give the desired product **6** as a colorless oil, which was used for the next step without further purification and without structure determination. **HPLC**: R_t = 12.09 min.

2. (2E,6E)-1-bromo-3,7,11-trimethyldodeca-2,6,10-triene 7[2]

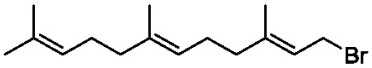

To a well stirred solution of farnesol (350 mg, 1.57 mmol), pyridine (48 µL) and hexane (0.70 mL) under Argon atmosphere at 0° was added dropwise a solution of PBr_3 (803 mg, 2.97 mmol) in hexane (0.24 mL). After stirring for 3 hours at room temperature the mixture was quenched with ice water (10 mL) and extracted with DCM (3 x 15 mL). The combined organic layers were washed with 1N HCl (10 mL), saturated $NaHCO_3$ solution, dried over $MgSO_4$ and concentrated *in vacuo* to give the desired product **7** as a brown oil, which was used for the next step without further purification and without structure determination.

3. General procedure for the synthesis of Carprofen derivatives

To a 0°C cooled solution of NaH (5 eq., 0.91 mmol) in THF (1.5 mL) under Argon atmosphere was slowly added carprofen (1.0 eq, 0.18 mmol). The mixture was stirred for 30 minutes at this temperature followed by the addition of phytyl- and farnesyl bromide **6** and **7** (5 eq, 0.91 mmol). After stirring for 24 hours the mixture was quenched with water and extracted with DCM (3 x 10 mL). The combined organic layers were dried over $MgSO_4$ and concentrated *in vacuo* to give the desired product.

2-(6-chloro-9-((2*E*,6*E*)-3,7,11-trimethyldodeca-2,6,10-trienyl)-9*H*-carbazol-2-yl)propanoic acid 5a

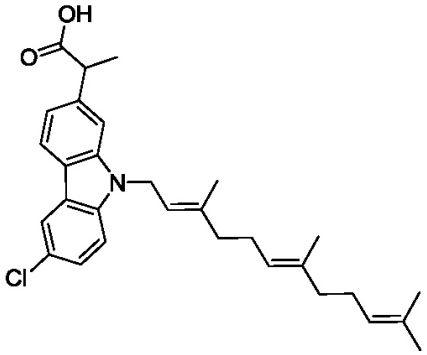

According to general procedure 3: Carprofen (50 mg, 0.18 mmol), NaH (36 mg, 0.91 mmol), (2*E*,6*E*)-1-bromo-3,7,11-trimethyldodeca-2,6,10-triene **7** (274 mg, 0.91 mmol). Yield after purification by silica gel chromatography (DCM/MeOH (10:1): 45 mg (52%) as a yellow solid. **HPLC**: R_t = 10.41 min. **^{1}H-NMR** ($CDCl_3$, 500 MHz, 300 K): δ = 8.00 (d, *J* = 1.8 Hz, 1H), 7.97 (d, *J* = 8.1 Hz, 1H), 7.37 (dd, *J* = 8.7 Hz, *J* = 2.0 Hz, 1H), 7.32 (d, *J* = 1.2 Hz, 1H), 7.26 (d, *J* = 8.7 Hz, 1H), 7.19 (dd, *J* = 8.1 Hz, *J* = 1.5 Hz, 1H), 5.23 (t, *J* = 6.4 Hz, 1H), 5.05-5.00 (m, 2H), 4.86 (d, *J* = 6.4 Hz, 2H), 3.93 (q, *J* = 7.1 Hz, 1H), 2.02-1.87 (m, 8H), 1.65 (s, 3H), 1.61 (d, *J* = 7.1 Hz, 3H), 1.56 (s, 3H), 1.52 (s, 3H), 1.26 (s, 3H) ppm. **^{13}C-NMR** ($CDCl_3$, 125 MHz, 300K): δ = 179.4, 141.0, 139.2, 139.0, 138.2, 135.5, 131.3, 125.6, 124.5, 124.3, 123.8, 123.4, 121.4, 120.7, 120.0, 119.3, 118.9, 109.9, 107.8, 45.8, 41.3, 39.6, 39.4, 26.7, 26.2, 25.7, 18.6, 17.6, 16.6, 16.0 ppm. **EI-MS**: *m/z* = 477 $[M]^+$.

2-(6-chloro-9-((7*R*,11*R*,*E*)-3,7,11,15-tetramethylhexadec-2-enyl)-9*H*-carbazol-2-yl)propanoic acid 5b

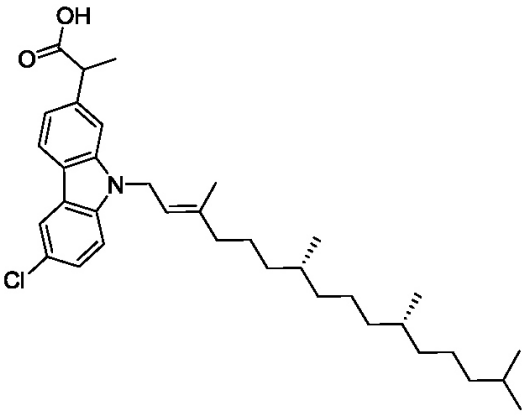

According to general procedure 3: Carprofen (50 mg, 0.18 mmol), NaH (36 mg, 0.91 mmol),

(7*R*,11*R*,*E*)-1-bromo-3,7,11,15-tetramethylhexadec-2-ene **6** (263 mg, 0.73 mmol). Yield after purification by silica gel chromatography (DCM/MeOH (20:1): 36 mg (36%) as a yellow solid. **HPLC**: R_t = 12.17 min. **^{1}H-NMR** ($CDCl_3$, 500 MHz, 300 K): δ = 8.00 (d, *J* = 1.8 Hz, 1H), 7.97 (d, *J* = 8.1 Hz, 1H), 7.37 (dd, *J* = 8.4 Hz, *J* = 2.1 Hz, 1H), 7.33 (d, *J* = 1.2 Hz, 1H), 7.26 (d, *J* = 8.7 Hz, 1H), 7.20 (dd, *J* = 8.1 Hz, *J* = 1.4 Hz, 1H), 5.22 (t, *J* = 6.3 Hz, 1H), 4.85 (d, *J* = 6.3 Hz, 2H), 3.93 (q, *J* = 7.1 Hz, 1H), 2.02-1.92 (m, 2H), 1.90 (s, 3H), 1.62 (d, *J* = 7.1 Hz, 3H), 1.56-1.55 (m, 1H), 1.35-1.00 (m, 18H), 0.88-0.86 (m, 6H), 0.83 (d, *J* = 6.6 Hz, 3H), 0.80 (d, *J* = 6.6 Hz, 3H) ppm. **^{13}C-NMR** ($CDCl_3$, 125 MHz, 300K): δ = 180.3, 141.0, 139.7, 139.0, 138.2, 125.6, 124.4, 123.8, 121.4, 120.7, 120.0, 119.0, 118.9, 109.9, 108.0, 45.9, 41.3, 39.7, 39.4, 37.4, 37.4, 37.7, 37.3, 32.8, 32.6, 28.0, 25.1, 24.8, 24.4, 22.7, 22.6, 19.7, 19.7, 18.6, 16.5 ppm. **EI-MS**: *m/z* = 551 $[M]^+$.

4. Synthesis of methyl 2-(2,5,7,8-tetramethyl-2-((4R,8R)-4,8,12-trimethyltridecyl)chroman-6-yloxy)acetate 12a[3]

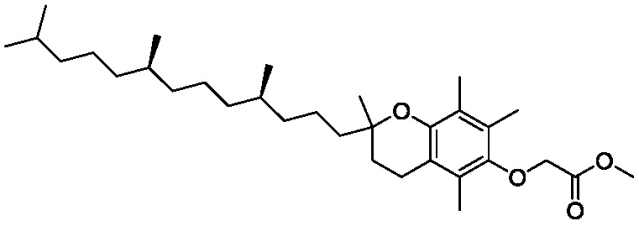

To a suspension of NaH (2.2 eq, 37 mg, 1.52 mmol) in dry DMF (2 mL) was added a solution of +-tocopherol **10a** (1eq, 298 mg, 0.69 mmol) in dry DMF (5 mL). The suspension was stirred at rt for 30 minutes. To the suspension was added a solution of methyl-2-bromoacetate (1.0 eq, 127 mg, 0.83 mmol) in dry DMF (1mL). The reaction mixture was stirred 8 h, quenched by sequential addition of H_2O, extracted with DCM (3 x 20 mL), the combined organic layers were dried over $MgSO_4$ and concentrated *in vacuo*. Compound **12a** was isolated as a yellow oil (285 mg, 82%). The compound was directly used for the next step without structure determination.

5. Synthesis of methyl 2-(2,5,7,8-tetramethyl-2-(4,8,12-trimethyltridecyl)chroman-6-yloxy)acetate 12b[3]

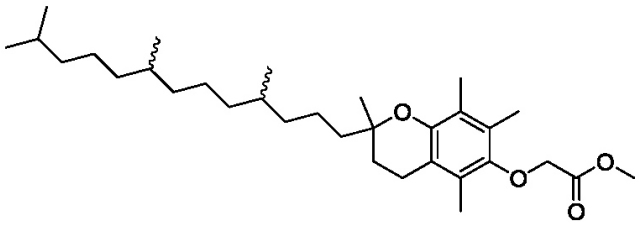

To a suspension of NaH (2.2 eq, 43 mg, 1.79 mmol) in dry DMF (2 mL) was added a solution of all-rac-a-tocopherol **10b** (1eq, 350 mg, 0.81 mmol) in dry DMF (5 mL). The suspension was stirred at rt for 30 minutes. To the suspension was added a solution of methyl-2-bromoacetate (1.2 eq, 149 mg, 0.98 mmol) in dry DMF (1mL). The reaction mixture was stirred 15 h, quenched by sequential addition of H_2O, extracted with DCM (3 x 20 mL), the combined organic layers were dried over $MgSO_4$ and concentrated *in vacuo*. Purification by silica gel chromatography (DCM) gave compound **12b** as a yellow oil (380 mg, 93%). **^{1}H-NMR** ($CDCl_3$, 500 MHz, 300 K): δ= 4.33 (s, 2H), 3.86 (s, 3H), 2.60 (t, *J* = 6.9 Hz, 2H), 2.21 (s, 3H), 2.17 (s, 3H), 2.11 (s, 3H), 1.87-1.75 (m, 2H), 1.61-1.52 (m, 3H), 1.48-1.22 (m, 12H), 1.19-1.06 (m, 7H), 0.92-0.86 (m, 14H) ppm. **^{13}C-NMR** ($CDCl_3$, 125 MHz, 300 K): δ= 170.2, 148.3, 147.7, 127.5, 125.6, 123.0, 117.7, 75.0, 69.9, 52.0, 40.1, 39.4, 37.5, 37.5, 37.4, 37.3, 32.8, 32.7, 31.3, 28.0, 24.8, 24.4, 23.9, 22.7, 22.6, 21.0, 20.6, 19.8, 19.7, 12.7, 11.9, 11.8 ppm. **EI-MS**: *m/z* = 502 $[M]^+$.

6. Synthesis of 2-(2,5,7,8-tetramethyl-2-((4R,8R)-4,8,12-trimethyltridecyl)chroman-6-yloxy)acetic acid 13a[3]

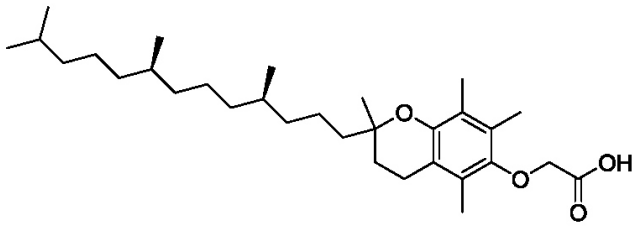

To a solution of **12a** (1 eq, 50 mg, 0.01 mmol) in dioxane/water (3 mL/1 mL) was added KOH (10 eq, 56 mg, 0.99 mmol). The reaction mixture was stirred at 75°C for two hours, acidified with 2N HCl and extracted with DCM (3 x 20 mL). The organic layer was dried over $MgSO_4$ and concentrated *in vacuo* to give **13a** as a colorless oil (45 mg, 94%). **^{1}H-NMR** ($CDCl_3$, 500 MHz, 300 K): δ= 4.38 (s, 2H), 2.61 (t, *J* = 6.9 Hz, 2H), 2.21 (s, 3H), 2.17 (s, 3H), 2.12 (s, 3H), 1.88-1.75 (m, 2H), 1.60-1.52 (m, 3H), 1.47-1.24 (m, 12H), 1.20-1.06 (m, 7H), 0.92-0.86 (m, 14H) ppm. **^{13}C-NMR** ($CDCl_3$, 125 MHz, 300 K): δ= 172.8, 148.6, 147.0, 127.3, 125.5, 123.4, 117.8, 75.0, 69.2, 40.1, 39.4, 37.5, 37.5, 37.4, 37.3, 32.8, 32.7, 31.2, 28.0,

24.8, 24.4, 23.8, 22.7, 22.6, 21.0, 20.7, 19.8, 19.7, 12.7, 11.9, 11.8 ppm. **EI-MS**: *m/z* = 488 $[M]^+$.

7. Synthesis of 2-(2,5,7,8-tetramethyl-2-(4,8,12-trimethyltridecyl)chroman-6-yloxy)acetic acid 13b[3]

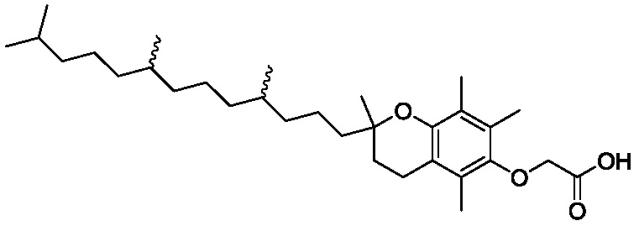

To a solution of **12b** (1 eq, 380 mg, 0.76 mmol) in dioxane/water (5 mL/1 mL) was added KOH (10 eq, 424 mg, 7.57 mmol). The reaction mixture was stirred at 75°C over night, acidified with 2N HCl and extracted with DCM (3 x 20 mL). The organic layer was dried over $MgSO_4$ and concentrated *in vacuo* to give **13b** as a colorless oil (350 mg, 95%). **^{1}H-NMR** ($CDCl_3$, 500 MHz, 300 K): δ = 4.38 (s, 2H), 2.61 (t, *J* = 6.9 Hz, 2H), 2.20 (s, 3H), 2.16 (s, 3H), 2.11 (s, 3H), 1.88-1.76 (m, 2H), 1.63-1.50 (m, 3H), 1.45-1.23 (m, 12H), 1.19-1.07 (m, 7H), 0.93-0.86 (m, 14H) ppm. **^{13}C-NMR** ($CDCl_3$, 125 MHz, 300 K): δ = 172.5, 148.5, 146.9, 127.4, 125.4, 123.4, 117.9, 75.1, 69.2, 40.0, 39.4, 37.5, 37.3, 32.8, 31.2, 28.1, 24.8, 24.4, 23.9, 22.7, 22.6, 21.0, 20.6, 19.8, 19.7, 19.6, 19.6, 19.6, 12.7, 11.9, 11.8 ppm. **EI-MS**: *m/z* = 488 $[M]^+$.

8. Synthesis of methyl 6-hydroxy-2,5,7,8-tetramethylchroman-2-carboxylate 14[3]

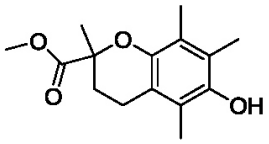

To a solution of methyl 6-hydroxy-2,5,7,8-tetramethylchroman-2-carboxylic acid **11** (1 eq, 300 mg, 1.20 mmol) in DMF (3 mL) was added K_2CO_3 (2 eq, 330 mg, 2.40 mmol). The suspension was stirred at rt for 30 minutes, MeI (1 eq, 170 mg, 1.20 mmol) was added dropwise. The reaction mixture was stirred for two hours, quenched and extracted with DCM (3 x 20 mL), the organic layer was dried over $MgSO_4$, concentrated *in vacuo* to give compound **14** as a colorless solid (301 mg, 95%). The compound was directly used for the next step without structure determination.

9. General procedure for phenol derivatisation to their corresponding ethers 15a-e

To a suspension of Cs_2CO_3 in DMF was added **14**. After 30 minutes the corresponding alkyl halogenide was added, the reaction mixture was stirred at 100°C for 6-10 h, quenched and extracted with DCM. The organic layer was dried over $MgSO_4$, evaporated *in vacuo* and purified by silica gel chromatography to give the corresponding ether. The compounds were directly used for the next step without structure determination.

methyl 2,5,7,8-tetramethyl-6-(octyloxy)chroman-2-carboxylate 15a

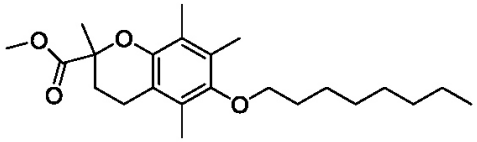

According to general procedure 9: **14** (1 eq, 100 mg, 0.38 mmol), Cs_2CO_3 (2 eq, 247 mg, 0.76 mmol), octylbromid (1 eq, 73 mg, 0.38 mmol), DMF (4 mL). Yield: 105 mg (74%) as a yellow oil.

methyl 2,5,7,8-tetramethyl-6-(undecyloxy)chroman-2-carboxylate 15b

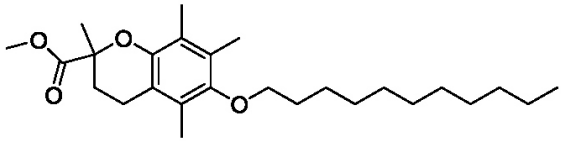

According to general procedure 9: **14** (1 eq, 100 mg, 0.38 mmol), Cs_2CO_3 (1.1 eq, 136 mg, 0.42 mmol), 1-bromundecan (1 eq, 89 mg, 0.38 mmol), DMF (4 mL). Yield: 150 mg (94%) as a colorless oil.

methyl 2,5,7,8-tetramethyl-6-(tetradecyloxy)chroman-2-carboxylate 15c

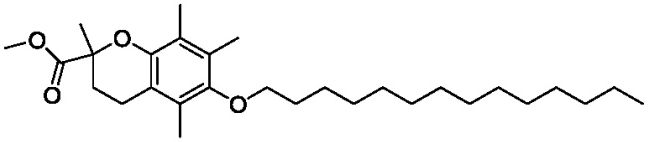

According to general procedure 9: **14** (1 eq, 50 mg, 0.19 mmol), Cs_2CO_3 (2 eq, 123 mg, 0.38 mmol), 1-Bromtetradecan (1 eq, 52 mg, 0.19 mmol), DMF (3 mL). Yield: 40 mg (46%) after purification by silica gel chromatography (CH/EE (10:1) as a colorless solid.

methyl 2,5,7,8-tetramethyl-6-((7*R*,11*R*,*E*)-3,7,11,15-tetramethylhexadec-2-enyloxy)chroman-2-carboxylate 15d

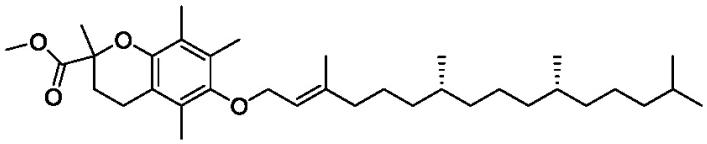

According to general procedure 9: **14** (1 eq, 50 mg, 0.19 mmol), Cs_2CO_3 (1.1 eq, 68 mg, 0.21 mmol), phytyl bromide **6** (1 eq, 59 mg, 0.19 mmol), DMF (3 mL). Yield: 38 mg (37%) after purification by silica gel chromatography (CH/EE (10:1) as a colorless solid.

methyl 2,5,7,8-tetramethyl-6-((2E,6E)-3,7,11-trimethyldodeca-2,6,10-trienyloxy)chroman-2-carboxylate 15e

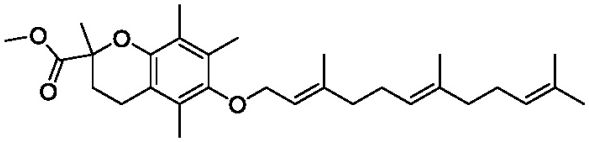

According to general procedure 9: **14** (1 eq, 50 mg, 0.19 mmol), Cs_2CO_3 (1.1 eq, 68 mg, 0.21 mmol), farnesylbromide **7** (1 eq, 54 mg, 0.19 mmol), DMF (3 mL). Yield: 45 mg (51%) after purification by silica gel chromatography (CH/EE (10:1) as a colorless solid.

10. General procedure for ester hydrolysis to their corresponding acids 16a-e

To a solution of the corresponding esters **15a-e** in dioxane/water (5:1) was added KOH. The reaction mixture was stirred at 75°C for four hours, quenched and extracted with DCM, dried over $MgSO_4$ and evaporated *in vacuo* to give the corresponding acid.

2,5,7,8-tetramethyl-6-(octyloxy)chroman-2-carboxylic acid 16a

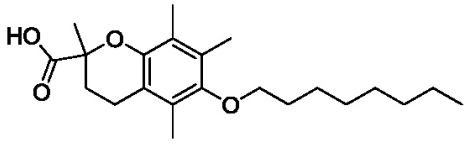

According to general procedure 10: **15a** (1 eq, 23 mg, 0.06 mmol), KOH (20 eq, 69 mg, 1.22 mmol), dioxane/water (5 mL/1 mL). Yield: 17 mg (77%) after purification by silica gel chromatography (CH/EE (2:1) as a colorless oil. **^{1}H-NMR** ($CDCl_3$, 500 MHz, 300 K): δ = 3.65 (t, *J* = 6.8 Hz, 2H), 2.70-2.56 (m, 2H), 2.44-2.38 (m, 1H), 2.20 (s, 3H), 2.17 (s, 3H), 2.13 (s, 3H), 1.97-1.90 (m, 1H), 1.81 (p, *J* = 6.7 Hz, 2H), 1.65 (s, 3H), 1.51 (p, *J* = 7.3 Hz, 2H), 1.41-1.26 (m, 8H), 0.93 (t, *J* = 6.8 Hz, 3H) ppm. **^{13}C-NMR** ($CDCl_3$, 125 MHz, 300 K): δ = 178.5, 149.5, 146.9, 128.5, 126.1, 122.7, 117.1, 76.9, 73.1, 31.9, 30.3, 30.0, 29.4, 29.3, 26.2, 24.9, 22.7, 20.6, 14.1, 12.8, 11.9, 11.8 ppm. **EI-MS**: *m/z* = 362 $[M]^+$.

2,5,7,8-tetramethyl-6-(undecyloxy)chroman-2-carboxylic acid 16b

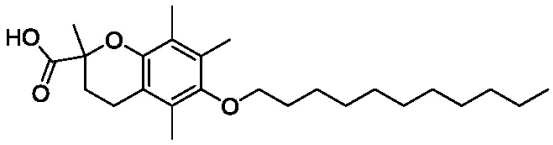

According to general procedure 10: **15b** (1 eq, 150 mg, 0.34 mmol), KOH (20 eq, 402 mg, 7.17 mmol), dioxane/water (5 mL/1 mL). Yield: 85 mg (62%) after purification by silica gel chromatography (CH/EE (2:1) as a colorless solid. **^{1}H-NMR** ($CDCl_3$, 500 MHz, 300 K): δ = 3.54 (t, *J* = 6.7 Hz, 2H), 2.58-2.45 (m, 2H), 2.32-2.27 (m, 1H), 2.09 (s, 3H), 2.06 (s, 3H), 2.02 (s, 3H), 1.87-1.81 (m, 1H), 1.73-1.68 (m, 2H), 1.54 (s, 3H), 1.43-1.39 (m, 2H), 1.30-1.15 (m, 14H), 0.80 (t, *J* = 6.8 Hz, 3H) ppm. **^{13}C-NMR** ($CDCl_3$, 125 MHz, 300 K): δ = 178.2, 149.6, 146.8, 128.5, 126.1, 122.7, 117.2, 77.0, 73.1, 31.9, 30.3, 30.0, 29.8, 29.7, 29.6, 29.6, 29.4, 26.2, 24.7, 22.7, 20.5, 14.2, 12.8, 11.9, 11.8 ppm. **EI-MS**: *m/z* = 404 $[M]^+$.

2,5,7,8-tetramethyl-6-(tetradecyloxy)chroman-2-carboxylic acid 16c

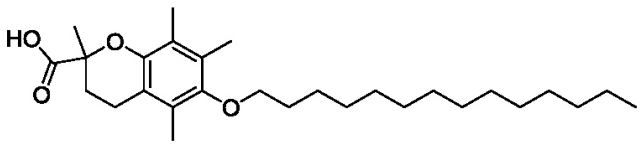

According to general procedure 10: **15c** (1 eq, 38 mg, 0.08 mmol), KOH (20 eq, 92 mg, 1.65 mmol), dioxane/water (5 mL/1 mL). Yield: 30 mg (83%) as a colorless solid. **^{1}H-NMR** ($CDCl_3$, 500 MHz, 300 K): δ = 3.56 (m, 2H), 2.56-2.49 (m, 2H), 2.32-2.27 (m, 1H), 2.09 (s, 3H), 2.06 (s, 3H), 2.02 (s, 3H), 1.87-1.81 (m, 1H), 1.73-1.68 (m, 2H), 1.54 (s, 3H), 1.41-1.39 (2H), 1.30-1.10 (m, 20H), 0.80 (t, *J* = 6.8 Hz, 3H) ppm. **^{13}C-NMR** ($CDCl_3$, 125 MHz, 300 K): δ = 178.0. 149.6, 146.8, 128.5, 126.1, 122.7, 117.2, 77.0, 73.1, 32.7, 31.9, 30.3, 30.0, 29.8,

29.7, 29.7, 29.5, 29.5, 29.4, 26.2, 26.7, 24.7, 22.7, 20.5, 14.2, 12.8, 11.9, 11.8 ppm. **EI-MS**: m/z = 446 $[M]^+$.

2,5,7,8-tetramethyl-6-((7*R*,11*R*,*E*)-3,7,11,15-tetramethylhexadec-2-enyloxy)chroman-2-carboxylic acid 16d

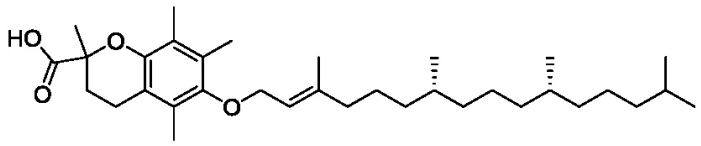

According to general procedure 10: **15d** (1 eq, 38 mg, 0.07 mmol), KOH (20 eq, 79 mg, 1.40 mmol), dioxane/water (5 mL/1 mL). Yield: 13 mg (33%) as a colorless solid. **^{1}H-NMR** ($CDCl_3$, 500 MHz, 300 K): δ= 8.05 (s, 1H), 5.50 (t, J= 6.8 Hz, 1H), 4.11 (d, J= 6.8 Hz, 1H), 4.09 (d, J= 6.8 Hz, 1H), 2.57-2.47 (m, 2H), 2.31-2.28 (m, 1H), 2.13 (s, 3H), 2.08 (s, 3H), 2.06 (s, 3H), 2.11 (m, 3H), 1.62 (s, 3H), 1.60-1.51 (m, 2H), 1.48-1.23 (m, 14H), 1.20-1.07 (m, 6H), 0.94-0.78 (m, 12H) ppm. **^{13}C-NMR** ($CDCl_3$, 125 MHz, 300 K): δ= 176.7, 149.7, 146.4, 141.3, 140.9, 128.8, 126.5, 122.6, 121.0, 120.1, 117.4, 77.2, 69.8, 69.5, 39.9, 39.4, 37.4, 37.3, 37.1, 37.0, 36.9, 36.8, 32.8, 32.7, 32.5, 29.8, 29.7, 28.0, 25.7, 25.1, 24.8, 24.5, 24.4, 23.5, 22.8, 22.7, 20.4, 19.7, 19.6, 16.4, 13.0, 12.1, 11.9 ppm. **EI-MS**: m/z = 528 $[M]^+$.

2,5,7,8-tetramethyl-6-((2*E*,6*E*)-3,7,11-trimethyldodeca-2,6,10-trienyloxy)chroman-2-carboxylic acid 16e

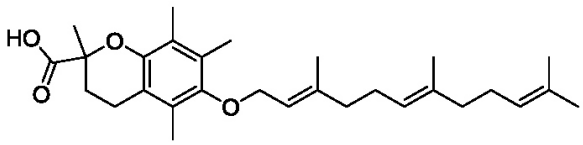

According to general procedure 10: **15e** (1 eq, 45 mg, 0.10 mmol), KOH (20 eq, 101 mg, 1.80 mmol), dioxane/water (5 mL/1 mL). Yield: 35 mg (77%) after purification by silica gel chromatography (CH/EE (2:1) as a colorless oil. **^{1}H-NMR** ($CDCl_3$, 500 MHz, 300 K): δ = 5.52 (t, J = 6.9 Hz, 1H), 5.08-5.01 (m, 2H), 4.10 (d, J = 6.9 Hz, 2H), 2.53-2.45 (m, 2H), 2.25-2.23 (m, 1H), 2.24-2.21 (s, broad, 3H), 2.20-2.17 (m, 2H), 2.17-2.13 (m, 8H), 2.13-2.09 (m, 3H), 2.05-2.01 (m, 2H), 1.72 (s, 6H), 1.66-1.63 (m, 6H), 1.61-1.55 (m, 3H) ppm. **^{13}C-NMR** ($CDCl_3$, 125 MHz, 300 K): δ= 179.0, 149.4, 147.1, 140.3, 135.4, 131.3, 128.5, 126.1, 124.4, 123.9, 122.8, 120.5, 117.2, 77.0, 69.8, 39.7, 39.7, 34.3, 30.0, 26.8, 25.7, 24.8, 20.6, 17.7, 16.5, 16.0, 12.9, 12.0, 11.9 ppm. **ESI-MS**: m/z = 477 $[M+Na]^+$.

11. General procedure for ester formation to their corresponding esters 17a-e

To a solution of 6-hydroxy-2,5,7,8-tetramethylchroman-2-carboxylic acid **11** in DMF K_2CO_3 was added. The suspension was stirred for 30 minutes, a solution of the corresponding alkyl halogenide in DMF was added dropwise, the reaction mixture was stirred at rt for 8-10 h. The reaction mixture was quenched, extracted with DCM, the organic layer was dried over $MgSO_4$ and evaporated *in vacuo* to give the corresponding ester. The compounds were directly used for the next step without structure determination.

octyl 6-hydroxy-2,5,7,8-tetramethylchroman-2-carboxylate 17a

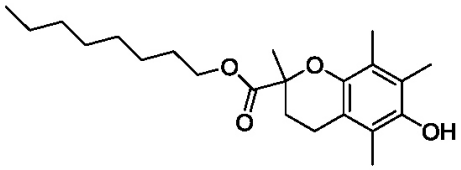

According to general procedure 11: 6-hydroxy-2,5,7,8-tetramethylchroman-2-carboxylic acid **11** (1 eq, 50 mg, 0.20 mmol), Octylbromid (1 eq, 39 mg, 0.20 mmol), K_2CO_3 (2 eq, 55 mg, 0.40 mmol), DMF (2 mL). Yield: 68 mg (94%) as a colorless solid.

undecyl 6-hydroxy-2,5,7,8-tetramethylchroman-2-carboxylate 17b

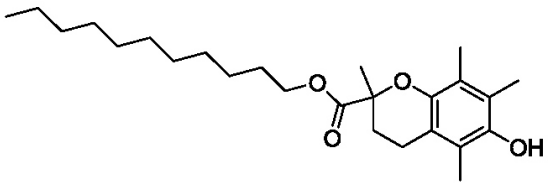

According to general procedure 11: 6-hydroxy-2,5,7,8-tetramethylchroman-2-carboxylic acid **11** (1 eq, 100 mg, 0.40 mmol), Bromundecan (1 eq, 94 mg, 0.40 mmol), K_2CO_3 (2 eq, 110 mg, 0.80 mmol), DMF (3 mL). Yield: 147 mg (91%) as a colorless solid.

tetradecyl 6-hydroxy-2,5,7,8-tetramethylchroman-2-carboxylate 17c

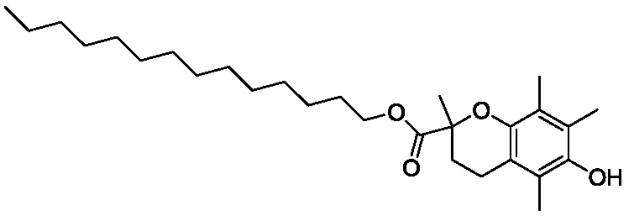

According to general procedure 11: 6-hydroxy-2,5,7,8-tetramethylchroman-2-carboxylic acid **11** (1 eq, 68 mg, 0.27 mmol), Bromtetradecan (1 eq, 75 mg, 0.27 mmol), K_2CO_3 (2 eq, 75 mg, 0.54 mmol), DMF (2 mL). Yield: 116 mg (97%) as a colorless solid.

(7*R*,11*R*,*E*)-3,7,11,15-tetramethylhexadec-2-enyl 6-hydroxy-2,5,7,8-tetramethylchroman-2-carboxylate 17d

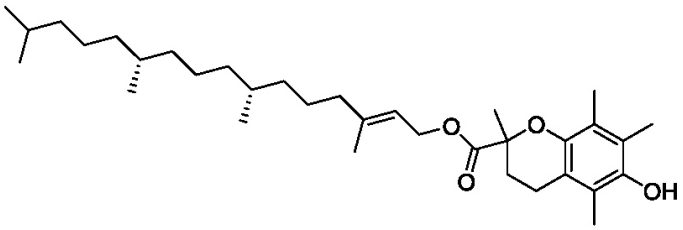

According to general procedure 11: 6-hydroxy-2,5,7,8-tetramethylchroman-2-carboxylic acid **11** (1 eq, 100 mg, 0.40 mmol), phytyl bromide **6** (1 eq, 119 mg, 0.40 mmol), K_2CO_3 (2 eq, 110 mg, 0.80 mmol), DMF (3 mL). Yield after purification by silica gel chromatography (CH/EE (10:1): 62 mg (30%) as a yellow oil.

(2*E*,6*E*)-3,7,11-trimethyldodeca-2,6,10-trienyl 6-hydroxy-2,5,7,8-tetramethylchroman-2-carboxylate 17e

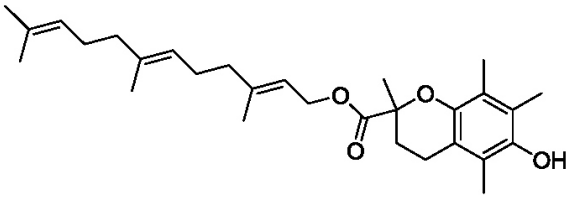

According to general procedure 11: 6-hydroxy-2,5,7,8-tetramethylchroman-2-carboxylic acid **11** (1 eq, 100 mg, 0.40 mmol), farnesyl bromide **7** (1 eq, 114 mg, 0.40 mmol), K_2CO_3 (2 eq, 110 mg, 0.80 mmol), DMF (3 mL). Yield: 172 mg (95%) as a yellow oil.

12. General procedure for derivatisation of phenols with 2-bromoacetic acid to their corresponding acids 18a-e

To a suspension of NaH in THF was added a solution of the corresponding ester **17a-e** in THF. The suspension was stirred for 30 minutes, a solution of 2-bromoacetic acid in THF was

added and the reaction mixture was stirred at rt over night. The reaction mixture was quenched, acidified with 2N HCl and extracted with DCM. The organic layer was dried over $MgSO_4$ and concentrated *in vacuo* to give the corresponding acid.

2-(2,5,7,8-tetramethyl-2-(octyloxycarbonyl)chroman-6-yloxy)acetic acid 18a

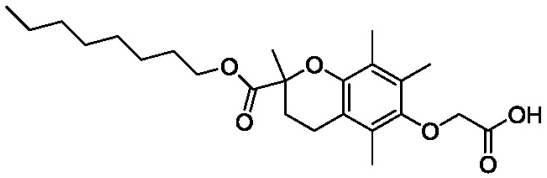

According to general procedure 12: Ester **17a** (1 eq, 61 mg, 0.17 mmol), NaH (2.2 eq, 9 mg, 0.37 mmol), 2-bromoacetic acid (1 eq, 23 mg, 0.17 mmol), THF (4 mL). Yield after purification by silica gel chromatography (CH/EE (1:1): 46 mg (65%) as a colorless oil. **^{1}H-NMR** ($CDCl_3$, 500 MHz, 300 K): δ = 4.26 (s, 2H), 4.03-3.93 (m, 2H), 2.57-2.51 (m, 1H), 2.44-2.35 (m, 2H), 2.11 (s, 3H), 2.09 (s, 3H), 2.02 (s, 3H), 1.82-1.75 (m, 1H), 1.54 (s, 3H), 1.48-1.41 (m, 2H), 1.26-1.09 (m, 10 H), 0.81 (t, *J* = 6.9 Hz, 3H) ppm. **^{13}C-NMR** ($CDCl_3$, 125 MHz, 300 K): δ = 172.8, 171.4, 147.7, 146.6, 126.6, 124.4, 122.3, 116.5, 68.1, 64.2, 30.8, 29.4, 28.7, 28.2, 28.1, 27.5, 24.6, 24.4, 21.6, 19.9, 13.1, 11.7, 10.8 ppm. **EI-MS**: *m/z* = 420 $[M]^+$.

2-(2,5,7,8-tetramethyl-2-(undecyloxycarbonyl)chroman-6-yloxy)acetic acid 18b

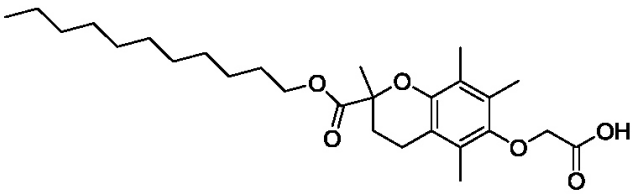

According to general procedure 12: Ester **17b** (1 eq, 193 mg, 0.48 mmol), NaH (2.2 eq, 25 mg, 1.05 mmol), 2-bromoacetic acid (1 eq, 67 mg, 0.48 mmol), THF (5 mL). Yield after purification by silica gel chromatography ($CHCl_3$/MeOH (10:1): 118 mg (53%) as a colorless oil. **^{1}H-NMR** ($CDCl_3$, 500 MHz, 300 K): δ = 3.95 (s (broad), 2H), 2.94-2.65 (m, 2H), 2.61-2.20 (m, 3H), 2.18-1.75 (m, 8H), 1.72-1.42 (m, 5H), 1.42-1.04 (m, 18H), 0.89 (t, *J* = 6 Hz, 3H) ppm.

^{13}C-NMR ($CDCl_3$, 125 MHz, 300 K): δ = 173.7, 162.7, 147.9, 147.8, 127.9, 125.7, 122.6, 116.9, 77.0, 65.1, 36.5, 31.9, 29.6, 29.5, 29.4, 29.3, 29.2, 29.1, 28.5, 25.7, 25.2, 22.7, 20.7, 14.1, 12.6, 11.7 ppm. **EI-MS**: *m/z* = 462 $[M]^+$.

2-(2,5,7,8-tetramethyl-2-(tetradecyloxycarbonyl)chroman-6-yloxy)acetic acid 18c

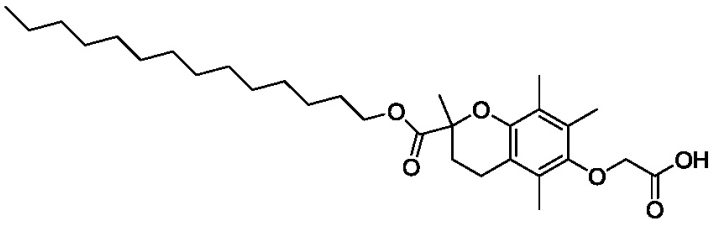

According to general procedure 12: Ester **17c** (1 eq, 188 mg, 0.42 mmol), NaH (2.2 eq, 22 mg, 0.92 mmol), 2-bromoacetic acid (1 eq, 59 mg, 0.42 mmol), THF (5 mL). Yield after purification by silica gel chromatography ($CHCl_3$/MeOH (10:1): 126 mg (60%) as a colorless oil. **^{1}H-NMR** ($CDCl_3$, 500 MHz, 300 K): δ = 3.95 (s (broad), 2H), 2.69-2.25 (m, 3H), 2.22-1.78 (m, 8H), 1.70-1.42 (m, 5H), 1.38-1.11 (m, 26H), 0.95-0.86 (t, *J* = 6.8 Hz, 3H) ppm. **^{13}C-NMR** ($CDCl_3$, 125 MHz, 300 K): δ = 174.7, 173,7, 148.2, 147.9, 127.9, 125.6, 122.7, 116.9, 77.0, 65.1, 63.0, 32.7, 31.9, 30.3, 29.7, 29.7, 29.6, 29.5, 29.4, 19.2, 28.5, 28.2, 25.7, 25.2, 22.7, 20.7, 14.1, 12.6, 11.8, 11.7 ppm. **EI-MS**: *m/z* = 504 $[M]^+$.

2-(2,5,7,8-tetramethyl-2-(((7*R*,11*R*,*E*)-3,7,11,15-tetramethylhexadec-2-enyloxy)carbonyl)chroman-6-yloxy)acetic acid 18d

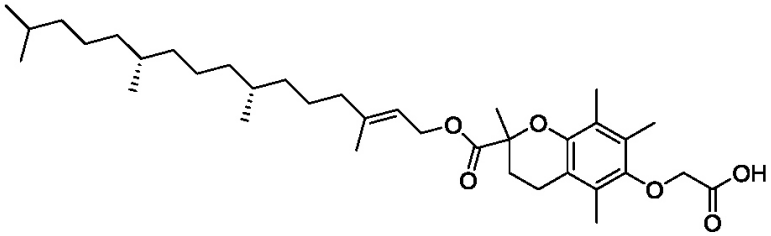

According to general procedure 12: Ester **17d** (1 eq, 188 mg, 0.42 mmol), NaH (2.2 eq, 22 mg, 0.92 mmol), 2-bromoacetic acid (1 eq, 59 mg, 0.42 mmol), THF (5 mL). Yield after purification by silica gel chromatography ($CHCl_3$/MeOH (10:1): 126 mg (60%) as a colorless oil. **^{1}H-NMR** ($CDCl_3$, 500 MHz, 300 K): δ = 5.20-5.16 (m, 1H), 4.48 (m, 2H), 4.02 (s,

(broad), 2H), 2.67-2.37 (m, 3H), 2.19-1.93 (m, 12H), 1.65-1.57 (m, 5H), 1.34-1.21 (m, 12H), 1.18-1.05 (m, 4H), 0.94-0.84 (m, 16H) ppm. **^{13}C-NMR** ($CDCl_3$, 125 MHz, 300 K): δ = 173.7, 173.5, 148.2, 148.0, 143.4, 127.7, 125.5, 123.0, 118.5, 117.7, 117.3, 77.1, 69.8, 61.9, 61.6, 39.9, 39.5, 37.4, 37.3, 36.9, 36.7, 36.6, 32.8, 32.7, 32.3, 30.3, 29.7, 28.0, 25.6, 25.1, 24.8, 24.5, 23.4, 22.7, 22.6, 20.8, 19.7, 19.6, 16.3, 12.7, 11.8, 11.7 ppm. **EI-MS**: *m/z* = 586 $[M]^+$.

2-(2,5,7,8-tetramethyl-2-(((2*E*,6*E*)-3,7,11-trimethyldodeca-2,6,10-trienyloxy)carbonyl)chroman-6-yloxy)acetic acid 18e

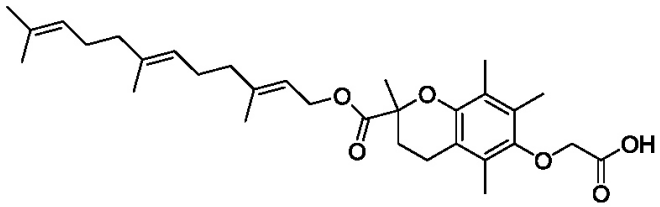

According to general procedure 12: Ester **18e** (1 eq, 170 mg, 0.37 mmol), NaH (2.2 eq, 20 mg, 0.82 mmol), 2-bromoacetic acid (1 eq, 51 mg, 0.37 mmol), THF (5 mL). Yield after purification by silica gel chromatography ($CHCl_3$/MeOH (15:1): 126 mg (87%) as a yellow oil. **^{1}H-NMR** ($CDCl_3$, 500 MHz, 300 K): δ = 5.21 (t, *J* = 7.0 Hz, 1H), 5.02 (m, 2H), 4.47 (d, *J* = 6.0 Hz, 2H), 3.94 (s, (broad), 2H), 2.62-2.35 (m, 2H), 2.20-1.95 (m, 16H), 1.88-1.76 (m, 1H), 1.72-1.67 (m, 3H), 1.66-1.54 (m, 12H), 1.34-1.24 (m, 2H) ppm. **^{13}C-NMR** ($CDCl_3$, 125 MHz, 300 K): δ = 174.2, 173.5, 148.2, 142.9, 135.4, 131.3, 127.8, 125.5, 125.4, 124.3, 123.6, 123.0, 118.0, 117.2, 77.1, 69.7, 61.8, 39.7, 39.5, 30.4, 26.7, 26.3, 25.7, 25.1, 20.8, 17.7, 16.4, 16.0, 12.6, 11.8, 11.7 ppm. **ESI-MS**: *m/z* = 535 $[M+Na]^+$. **EI-MS**: *m/z* = 512 $[M]^+$.

III. Determination of γ-secretase modulator (GSM) activity

The GSM activity of novel compounds was determined using a cell-based sandwich ELISA assay as described.[4] In brief, CHO cells stably overexpressing wild type human amyloid precursor protein and wild type human presenilin-1 were maintained in DMEM supplemented with 10% FBS. Cells were seeded in 96-well plates and treated with increasing concentrations of respective compounds or DMSO vehicle in triplicates. After 24 h of incubation, the cell culture supernatants were collected and analyzed by ELISA. Monoclonal antibody IC16 (1:250 in PBS, pH 7.2) raised against amino acids 1-15 of the Aß sequence was used as a

capture antibody. To generate standard curves, synthetic Aß$_{40}$, Aß$_{42}$, and Aß$_{38}$ peptides (JPT Peptide Technologies) were used. These Aß peptides were solubilized in DMSO at 1 mg/mL and aliquots were stored at –80°C. 96-well high-binding microtiter plates were incubated overnight at 4°C with the capture antibody. After excess capture antibody was removed, conditioned media samples (20 µl for detection of Aß40, 120 µl for Aß42, 70 µl for Aß38) and freshly diluted Aß peptide standards (125-6000 pg/mL in PBS containing 0.05 % Tween-20, 1 % BSA) were added.

Subsequently, C-terminal detection antibodies specific for Aß$_{40}$, Aß$_{42}$ and Aß$_{38}$ labeled with horseradish peroxidase (HRP) using the Pierce EZ-Link™ Plus Activated Peroxidase kit (Thermo Fisher Scientific) were diluted in PBS containing 0.05 % Tween-20, 1 % BSA, added to each well, and incubated overnight at 4°C. Plates were washed 3 times with PBS containing 0.05 % Tween-20 and once with PBS. Then 50 µl of TMB ultrasubstrate (Thermo Fisher Scientific) was added and incubated for 1-10 min at RT in the dark. The reaction was stopped by adding 50 µl of 2 M H_2SO_4 and the absorbance was measured using a Paradigm microplate reader (Beckman Coulter) at 450 nm. The average of triplicate measurements from each drug concentration was normalized to DMSO control condition. To calculate IC_{50} values, cells were treated with six to eight increasing concentrations of each compound and a nonlinear curve fit with variable slope model was applied to the results from two to three independent experiments. Statistical analysis was performed using GraphPad Prism (GraphPad Software).

Table 2. Activity of the synthesized compounds 5a-18e, including the increase of $A\beta_{38}$ at EC_{50}.

Compd.	EC_{50}(Aß$_{38}$) (µM)	increase of Aß$_{38}$ at EC_{50}	IC_{50}(Aß$_{40}$) (µM)	IC_{50}(Aß$_{42}$) (µM)
5a	2	80%	26	4
5b	>50		>50	23
13a	6	55%	24	11
13b	4	55%	26	12
16a	>50		>50	57
16b	10	65%	>50	28
16c	9	40%	29	14
16d	10	35%	42	26
16e	8	35%	39	28
18a	11	60%	42	35
18b	5	100%	23	12
18c	6	95%	34	22
18d	13	135%	36	24
18e	1	35%	25	27

IV. Calculations of LE, LLE and LELP [5]

Ligand effiency:

The ligand effiency is defined by the following formula:

$LE = \Delta G/n$

$\Delta G = -RT\ln(K_d) \approx -RT(\ln IC_{50})$

$LE = 1.4pIC_{50}/n$

Ligand lipophilicity effiency:

The ligand lipophilicity effiency is defined by the following formula:

$LLE = pIC_{50} - clogP$

Ligand efficiency-dependent lipophilicity:

The ligand efficiency-dependent lipophilicity is defined by the following formula:

$LELP = clogP/LE$

n	number of heavy atoms
R	universal gas constant (8.314 J/Kmol)
T	temperature
clogP	partition coefficient
IC_{50}	half maximal inhibitory concentration

The calculated values of LE, LLE and LELP of the synthesized γ-secretase modulators are shown in the following table:

Table 2. Calculations of the lipophilic efficiency indices LE, LLE and LELP.

Compd.	clogP	IC_{50} (*10^{-6})	n	pIC_{50}	LE	LLE	LELP
5a	10,1	4	34	4,5	0,18	-5,6	55
5b	13,6	23	39	4,4	0,16	-9,2	86
13a	12,0	11	35	4,5	0,18	-7,6	67
13b	12,0	12	35	4,5	0,18	-7,6	67
16a	7,5	57	26	4,6	0,25	-2,9	30
16b	9,1	28	29	4,5	0,22	-4,5	41

16c	10,6	14	32	4,5	0,20	-6,1	54
16d	13,0	26	38	4,4	0,16	-8,6	80
16e	9,5	28	33	4,5	0,19	-5,0	50
18a	7,2	35	30	4,5	0,21	-2,6	34
18b	8,8	12	33	4,5	0,19	-4,3	46
18c	10,3	22	36	4,4	0,17	-5,9	60
18d	12,5	24	42	4,4	0,15	-8,1	86
18e	9,2	27	37	4,4	0,17	-4,8	55

V. Dynamic light scattering experiments [6]

In order to check if the synthesized compounds **5a-18e** form micelles at the relevant assay concentrations, dynamic light scattering experiments were carried out on a Zetaziser Nano ZS (Malvern) using a laser wavelength of 514 nm.

Dilution series (from 50 mM DMSO stock solutions) of the compounds **5a-18e** were produced within the concentration range of 5-100 µM. Related to the assay conditions (compare section **III**) all diluted samples contain 2% DMSO and an aqueous salt solution consisting of: 1.8 mM $CaCl_2$, 0.8 mM $MgSO_4$, 5.3 mM KCl, 44.1 mM $NaHCO_3$, 110.3 mM NaCl, 0.9 mM NaH_2PO_4 (also contained in the assay buffer solution). All measurements were conducted in triplicates at 20 °C, ten acquisitions were performed for each concentration point with a fixed measurement point (4.65 mm). Data evaluation was done using the Malvern Zetasizer Software which directly converts the laser light scattering in particle size of possibly present aggregates. To evaluate the methodology, Pluronic F68 was used as a positive control. The critical micelle concentration of Pluronic F68 in the literature is consistent with the measured concentration (40 µM, figure 1).[7]

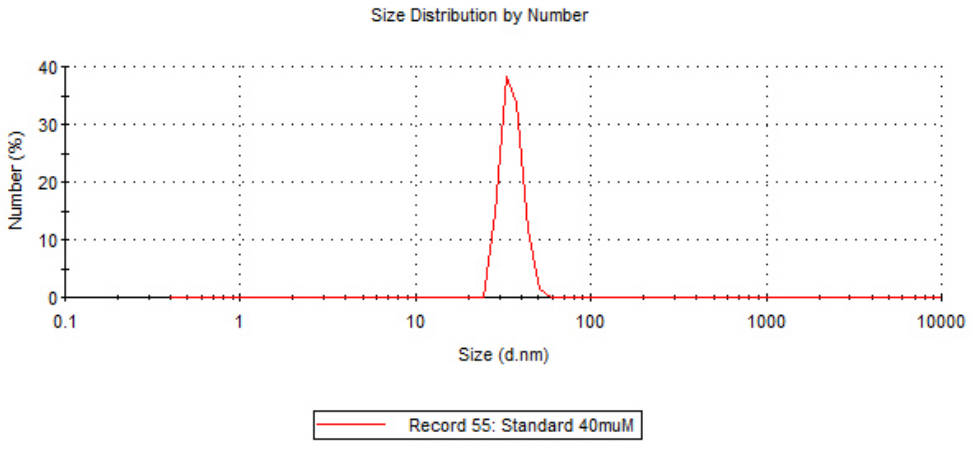

Figure 1. Micelle formation of Pluricon F68 at 40 µM.

All samples **5a-18e** were measured using the described methodology. No formation of aggregates or micelles could be observed within the relevant concentration range of 5-100 µM with the exception of compound **16b** at 100 µM (figure 2).

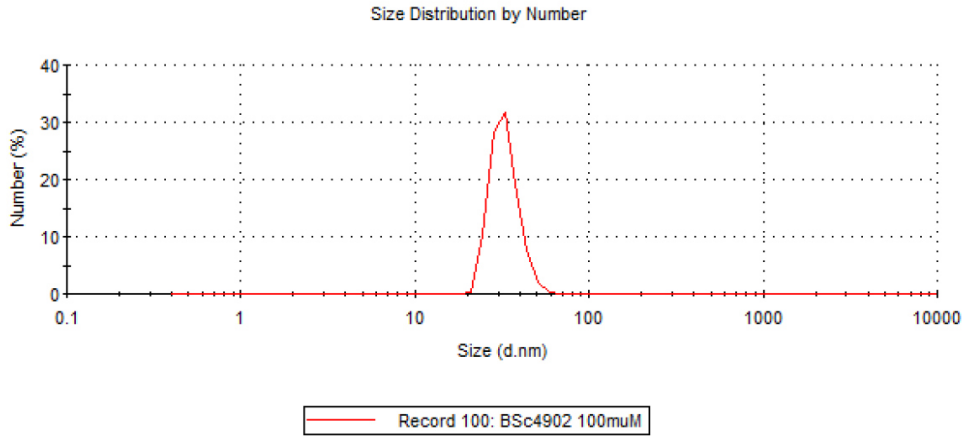

Figure 2. Micelle or aggregate formation of **16b** at 100 µM.

VI. References

1. Yamauchi, K.; Yamada, K.; Kinoshita, M.; Kamikawa, T. *The Chemical Society of Japan* **1991,** *64*, 2088.
2. Griffiths-Jones, C. M.; Knight, D. W. *Tetrahedron* **2010,** *66*, 4150.
3. Sanders, B. G.; Klein, K.; Hurley, L.; Gardener, R.; Menchaca, M.; Yu, W.; Ramanan, P. N.; Liu, S.; Israel, K. **U.S. 6770672, 2004.**
4. Hahn, S.; Bruning, T.; Ness, J.; Czirr, E.; Baches, S.; Gijsen, H.; Korth, C.; Pietrzik, C. U.; Bulic, C.; Weggen, S. *J. Neurochem* **2011,** *116*, 385.
5. Gijsen, H. J. M.; Mercken, M. *International Journal of Alzheimer's Disease* **2012,** 10.
6. Barrett, P. J.; Sanders, C. R.; Kaufman, S. A.; Michelsen, K.; Jordan, J. B. *Biochemistry* **2011,** *50*, 10328.
7. http://www.sigmaaldrich.com/img/assets/15402/Detergent_Selection_Table.pdf.

5 Zusammenfassung und Ausblick

5.1 Zusammenfassung

Die vorliegende Arbeit beschreibt die erfolgreiche Entwicklung hochaktiver sowie selektiver Wirkstoffe der *fms-like tyrosine kinase 3* und der *leucin-rich repeat kinase 2* zur Behandlung der akuten myelischen Leukämie bzw. der Parkinson-Krankheit.

Durch die etablierte Knoevenagel-Kondensation konnten ausgehend von der Leitstruktur **38** schnell und effizient eine Reihe von Indolinon-Derivaten als FLT3-Inhibitoren synthetisiert und optimiert werden. Der Großteil dieser Verbindungen zeigte eine Aktivität gegenüber FLT3 im niedriegen nanomolarem Bereich (Abbildung 25). Der potenteste Inhibitor **39** wies einen IC_{50}-Wert von 4,1 nM auf. Seine Selektivität wurde in einem Kinase-*screening* Anhand

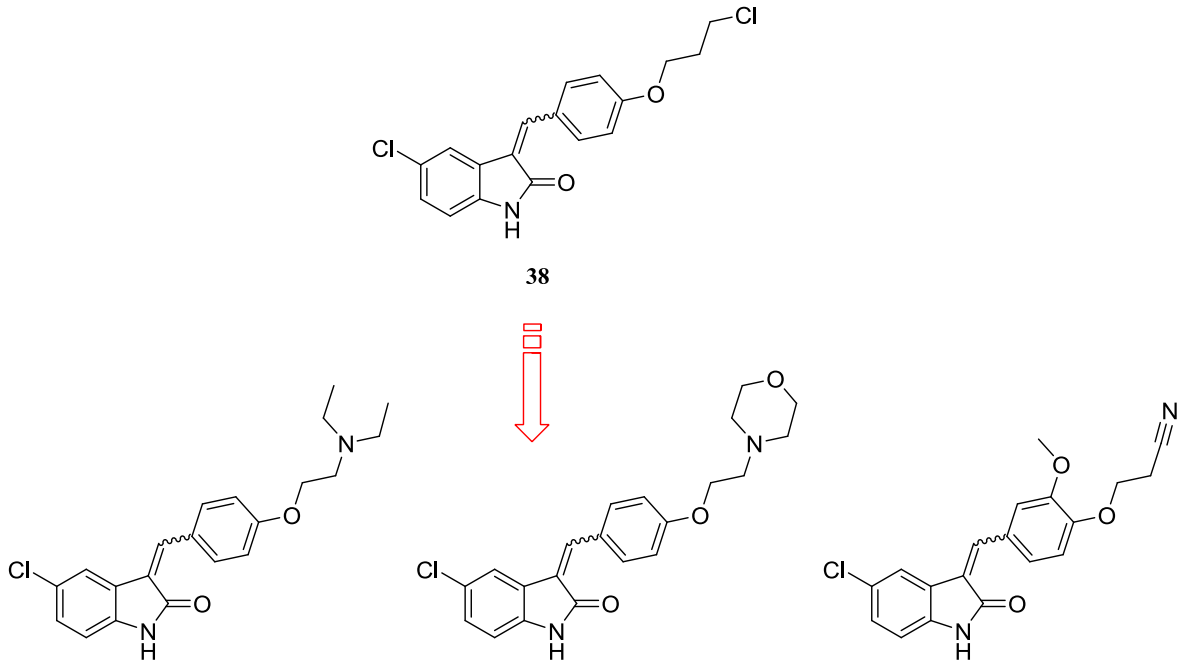

Abbildung 25: Aus der Leitstruktur **38** wurden verschiedene Indolinon-basierender FLT3-Inhibitoren synthetisiert.

von 50 humanen Kinasen untersucht. Verbindung **39** wies eine gute Selektivität bei einer Konzentration von 1 µM gegenüber FLT3 auf, lediglich zwei weitere Kinasen wurden

signifikant inhibiert. Der Zebrafisch-Toxizitäts-Assay wies keinerlei Sterblichkeit noch phänotypische Veränderungen bei 5 µM auf.

Die durch die Indolinonderivatisierung gewonnenen Erkenntnisse der Wechselwirkungen in der ATP-Bindungstasche von FLT3 stellten einen neuen Ansatzpunkt für die Entwicklung von Chinoxalinbisarylharnstoffen als FLT3-Inhibitoren dar.

Basierend auf den ersten publizierten FLT3-Chinoxalininhibitor AG1295 wurde ein Pharmakophormodell entwickelt, welches als Templat für den Zugang neuer FLT3-Inhibitoren dienen sollte. Diese Strategie diente im Folgenden der Synthese neuer Verbindungen, welche das Chinoxalin-Grundgerüst aufwiesen. Es gelang die Herstellung unterschiedlicher Derivate, welche Aktivitäten im nanomolarem Bereich aufweisen konnten (Abbildung 26).

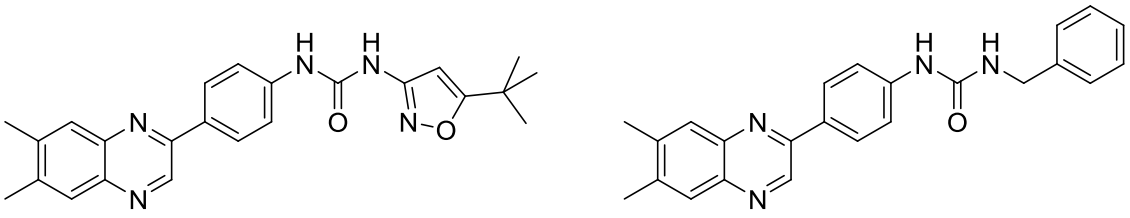

41
IC_{50} = 71 nM

42
IC_{50} = 42 nM

Abbildung 26: Übersicht ausgewählter FLT3-Inhibitorn basierend auf dem Chinoxalin-Grundgerüst.

In einem zweiten Teilprojekt zur Inhibition von LRRK2 wurden zunächst zurückliegende Daten aufgearbeitet und zusammengefasst. So konnte ein Überblick über die bislang publizierten *in vitro* und *in vivo* Daten bezüglich LRRK2 gewonnen werden. Mit Hilfe eines Homologie-Modells der Kinase-Domäne konnten erste Einblicke über Liganden und deren Wechselwirkungen visualisiert werden.

Das Grundgerüst der Indolinone wurde auch für die Inhibition von LRRK2 aufgegriffen. Aufgrund struktureller Ähnlichkeit zu literaturbekannten LRRK2-Inhibitoren konnten durch Struktur-Aktivitäts-Beziehungen potente und selektive Inhibitoren hergestellt werden. Die *in vitro* Daten haben belegt, dass es sich hierbei um hochaffine Inhibitoren mit Aktivitäten im zweistelligen nanomolarem Bereich handelt. Bei zwei der aussichtreichsten Verbindungen, **43** und **44**, wurde zusätzlich zum wild-Typ auch die Aktivität gegenüber der G2019S-Mutante bestimmt, da diese Mutante die häufigste krankheitsverursachende Mutation darstellt (Abbildung 27).

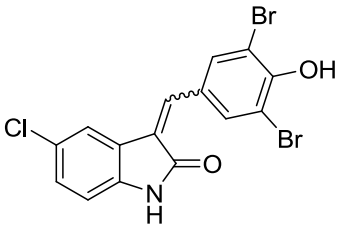

43
IC_{50} (wild-Typ) = 15 nM
IC_{50} (LRRK2-G2019S) = 10 nM

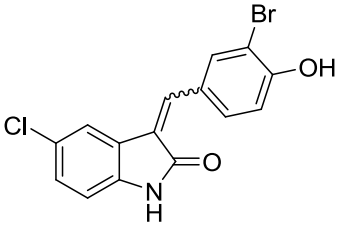

44
IC_{50} (wild-Typ) = 46 nM
IC_{50} (LRRK2-G2019S) = 64 nM

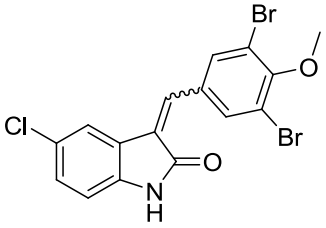

45
IC_{50} (wild-Typ) > 10000 nM

Abbildung 27: Erzieltes Ergebnis bezüglich der Inhibition von LRRK2.

Zusätzlich konnte durch Docking-Simulationen in der ATP-Bindungstasche von Verbindung **43** eine wichtige Wasserstoffbrücke nachgewiesen werden, welche für die Aktivität ausschlaggebend ist (Vergleich Verbindung **43** und **45** in Abbildung 27). Die Bestimmung der Selektivität von **43** wurde gegenüber 46 humanen Kinasen untersucht. Nur zwei weitere Kinasen wurden bei einer Konzentration von 1 µM inhibiert. Die LRRK2-Inhibitoren **43** und **44** wurden ebenfalls in einem Zebrafisch-Toxizitäts-Assay evaluiert und zeigten keine toxischen Effekte unterhalb von 10 µM.

Im Rahmen eines weiteren Projektes konnten Modulatoren der γ-Sekretase für die Behandlung der Alzheimer-Demenz hergestellt werden. Es konnten verschiedene Substanzen erhalten werden, welche Aktivitäten zwischen 4 µM und 57 µM aufwiesen.

5.2 Ausblick

Die erhaltenen und vorgestellten Ergebnisse bieten Ansatzpunkte für neue Arbeitshypothesen, welche in der Zukunft als Grundlage dienen können.
Im Bereich der Wirkstoffforschung ist die Überwindung der Blut-Hirn-Schranke ein Problem vieler Substanzen. Aufgrund dessen sollte der Focus auf die Verbesserung der pharmakologischen Eigenschaften gelegt werden. Ein Parameter ist dabei der clogP-Wert, welcher nach der „*rule of five*“ kleiner als 5 sein sollte.
Erste Versuche die Löslichkeit des Indolinon-basierten FLT3-Inhibitors **39** durch Einführung von Stickstoffatomen im Indol- bzw. in dem Phenylring zu erhöhen, wurden mit Einbußen

bezüglich der Aktivität beobachtet. Deshalb sollte im Folgenden von der Synthese weitere Indolderivate als FLT3-Inhibitoren abgesehen werden.

Die Synthese der Harnstoffderivate mit dem enthaltenen Chinoxalin-Motiv hingegen ist sehr vielversprechend. Eine Vielzahl der hergestellten Chinoxalin-Derivate weisen eine clogP um den Bereich von 5 auf und sind somit grenzwertig. Möglichkeiten zur Erhöhung der Löslichkeit bestehen durch Einführung von Stickstoffgruppen in den Phenylring bzw. durch Substitution einer Methylgruppe (Abbildung 28).

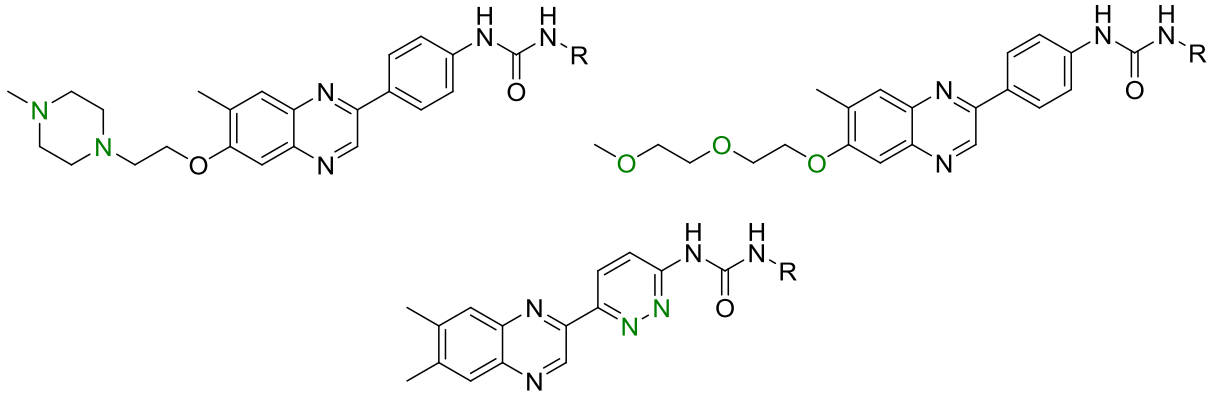

Abbildung 28: Optionen zur Erhöhung der Löslichkeit aktueller Verbindungen.

Um jedoch ein genaueres Verständnis für die Lage bzw. über die Wechselwirkungen der Inhibitoren in der ATP-Bindungstasche von FLT3 zu erhalten, wird in Kollaboration mit der Universität Frankfurt der FLT3-Inhibitor **39** mit der Kinase-Domäne von FLT3 co-kristalliert. Nach Erhalt dieser Daten können anschließend gezielte Änderung bzw. eine gezielte Struktur-Aktivitäts-Beziehungen vorgenommen werden.

Im Falle der LRRK2-Inhibition ist es sehr aussichtsreich Stickstoffgruppen in den Indolring einzufügen, um so die Löslichkeit zu erhöhen (Abbildung 29). Die so erhaltenen Azaindole sind wesentlich hydrophiler. Des Weiteren könnten auch Substitutionen an der 4ten Position des Indolrings durchgeführt werden. Durch Untersuchung der Struktur-Aktivitäts-Beziehung der Indolinone als LRRK2-Inhibitoren wurde gezeigt, dass das Proton an der Hydroxylgruppe essentiell für die Aktivität ist. Durch Variation der Hydroxylgruppe kann der Einfluss unterschiedlicher Reste auf die LRRK2-Aktivität untersucht werden.

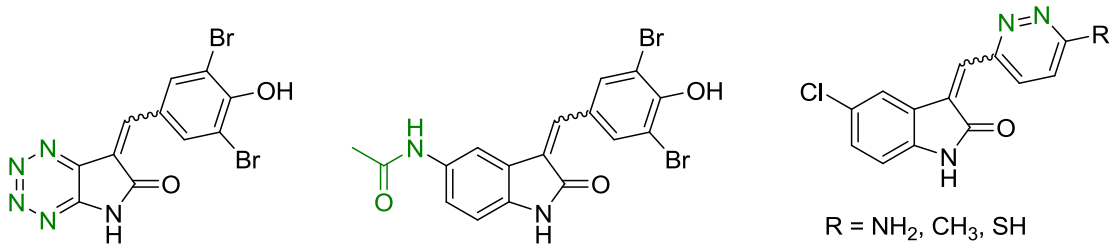

Abbildung 29: Möglichkeit der Erhöhung der Löslichkeit durch die Einführung von Stickstoffatomen.

6 Literaturverzeichnis

[1] G. Klebe, *Wirkstoffdesign, Vol. 2. Auflage*, 2. ed., Spektrum Akademischer Verlag Heidelberg, **2009**.

[2] D. A. Roberts, W. H. J. Ward, *Enzyme inhibition*, 2. ed., Royal Society of Chemistry, **2002**.

[3] J. Martin, K. Anamika, N. Srinivasan, *PloS one* **2010**, *5*, e12460.

[4] G. Manning, D. B. Whyte, R. Martinez, T. Hunter, S. Sudarsanam, *Science* **2002**, *298*, 1912-1934.

[5] P. Cohen, *Nature reviews. Drug discovery* **2002**, *1*, 309-315.

[6] P. Kaatsch, C. Spix, S. Hentschel, A. Katalinic, S. Luttmann, C. Stegmaier, S. Caspritz, J. Cernaj, A. Ernst, J. Folkerts, J. Hansmann, K. Kranzhöfer, E. Krieghoff-Henning, B. Kunz, A. Penzkofer, K. Treml, K. Wittenberg, *(Eds.: R. Koch-Institut, N. 20, Berlin). Robert Koch-Institut (Hrsg) und die Gesellschaft der epidemiologischen Krebsregister in Deutschland e.V. (Hrsg). Berlin,* **2013**, *8. Ausgabe*.

[7] Deutsche Krebshilfe e. V.

[8] M. Osawa, K. Hanada, H. Hamada, H. Nakauchi, *Science* **1996**, *273*, 242-245.

[9] E. Passegue, C. H. Jamieson, L. E. Ailles, I. L. Weissman, *Proceedings of the National Academy of Sciences of the United States of America* **2003**, *100 Suppl 1*, 11842-11849.

[10] E. Elert, *Nature* **2013**, *498*, S2-3.

[11] R. Virchow, *Weisses Blut, Froriep's Notizen aus dem Gebiete der Natur- und Heilkunde* **1845**, *36*, 1151-1846.

[12] A. Cagnetta, S. Adamia, C. Acharya, F. Patrone, M. Miglino, A. Nencioni, M. Gobbi, M. Cea, *Leukemia research* **2014**, *38*, 649-659.

[13] T. Grafone, M. Palmisano, C. Nicci, S. Storti, *Oncology Reviews* **2012**, *6*, 64-74.

[14] R. M. Stone, M. R. O'Donnell, M. A. Sekeres, *Hematology / the Education Program of the American Society of Hematology. American Society of Hematology. Education Program* **2004**, 98-117.

[15] B. Deschler, M. Lubbert, *Cancer* **2006**, *107*, 2099-2107.

[16] E. B. Lewis, *Science* **1957**, *125*, 965-972.

[17] D. A. Savitz, K. W. Andrews, *American journal of industrial medicine* **1997**, *31*, 287-295.

[18] www.apotheken-umschau.de.

[19] H. D. Preisler, Y. Rustum, E. S. Henderson, S. Bjornsson, P. J. Creaven, D. J. Higby, A. Freeman, S. Gailani, C. Naeher, *Blood* **1979**, *53*, 455-464.

[20] J. Cools, *Haematologica* **2012**, *97*, 1775.

[21] J. E. Lancet, J. E. Cortes, D. E. Hogge, M. S. Tallman, T. J. Kovacsovics, L. E. Damon, R. Komrokji, S. R. Solomon, J. E. Kolitz, M. Cooper, A. M. Yeager, A. C. Louie, E. J. Feldman, *Blood* **2014**, *123*, 3239-3246.

[22] J. W. Vardiman, N. L. Harris, R. D. Brunning, *Blood* **2002**, *100*, 2292-2302.

[23] L. Bullinger, K. Dohner, E. Bair, S. Frohling, R. F. Schlenk, R. Tibshirani, H. Dohner, J. R. Pollack, *The New England journal of medicine* **2004**, *350*, 1605-1616.

[24] R. F. Schlenk, K. Döhner, J. Krauter, S. Frohling, A. Corbacioglu, L. Bullinger, M. Habdank, D. Spath, M. Morgan, A. Benner, B. Schlegelberger, G. Heil, A. Ganser, H. Döhner, G. German-Austrian Acute Myeloid Leukemia Study, *The New England journal of medicine* **2008**, *358*, 1909-1918.

[25] U. Creutzig, M. M. van den Heuvel-Eibrink, B. Gibson, M. N. Dworzak, S. Adachi, E. de Bont, J. Harbott, H. Hasle, D. Johnston, A. Kinoshita, T. Lehrnbecher, G. Leverger, E. Mejstrikova, S. Meshinchi, A. Pession, S. C. Raimondi, L. Sung, J. Stary, C. M.

Zwaan, G. J. Kaspers, D. Reinhardt, A. M. L. C. o. t. I. B. S. Group, *Blood* **2012**, *120*, 3187-3205.
[26] H. Döhner, E. H. Estey, S. Amadori, F. R. Appelbaum, T. Buchner, A. K. Burnett, H. Dombret, P. Fenaux, D. Grimwade, R. A. Larson, F. Lo-Coco, T. Naoe, D. Niederwieser, G. J. Ossenkoppele, M. A. Sanz, J. Sierra, M. S. Tallman, B. Lowenberg, C. D. Bloomfield, L. European, *Blood* **2010**, *115*, 453-474.
[27] J. W. Vardiman, J. Thiele, D. A. Arber, R. D. Brunning, M. J. Borowitz, A. Porwit, N. L. Harris, M. M. Le Beau, E. Hellstrom-Lindberg, A. Tefferi, C. D. Bloomfield, *Blood* **2009**, *114*, 937-951.
[28] D. G. Gilliland, J. D. Griffin, *Blood* **2002**, *100*, 1532-1542.
[29] S. Scholl, R. Müller, J. H. Clement, I. F. Loncarevic, F. D. Böhmer, K. Höffken, *Leukemia research* **2006**, *30*, 633-642.
[30] D. Bossemeyer, *FEBS letters* **1995**, *369*, 57-61.
[31] S. K. Grant, *Cellular and molecular life sciences : CMLS* **2009**, *66*, 1163-1177.
[32] J. A. Ubersax, J. E. Ferrell, Jr., *Nature reviews. Molecular cell biology* **2007**, *8*, 530-541.
[33] A. K. Ghose, T. Herbertz, D. A. Pippin, J. M. Salvino, J. P. Mallamo, *Journal of medicinal chemistry* **2008**, *51*, 5149-5171.
[34] J. T. Reilly, *British journal of haematology* **2002**, *116*, 744-757.
[35] P. Blume-Jensen, T. Hunter, *Nature* **2001**, *411*, 355-365.
[36] J. T. Reilly, *Blood reviews* **2003**, *17*, 241-248.
[37] R. Gupta, C. L. Knight, B. J. Bain, *British journal of haematology* **2002**, *117*, 489-508.
[38] W. Matthews, C. T. Jordan, G. W. Wiegand, D. Pardoll, I. R. Lemischka, *Cell* **1991**, *65*, 1143-1152.
[39] O. Rosnet, S. Marchetto, O. deLapeyriere, D. Birnbaum, *Oncogene* **1991**, *6*, 1641-1650.
[40] O. Rosnet, M. G. Mattei, S. Marchetto, D. Birnbaum, *Genomics* **1991**, *9*, 380-385.
[41] A. Al-Mawali, D. Gillis, I. Lewis, *Oman medical journal* **2013**, *28*, 432-440.
[42] P. Brown, D. Small, *European journal of cancer* **2004**, *40*, 707-721, discussion 722-704.
[43] N. Pemmaraju, H. Kantarjian, F. Ravandi, J. Cortes, *Cancer* **2011**, *117*, 3293-3304.
[44] S. D. Lyman, S. E. Jacobsen, *Blood* **1998**, *91*, 1101-1134.
[45] J. Griffith, J. Black, C. Faerman, L. Swenson, M. Wynn, F. Lu, J. Lippke, K. Saxena, *Molecular cell* **2004**, *13*, 169-178.
[46] U. Testa, *Current Cancer Therapy Reviews* **2013**, *9*, 181-219.
[47] A. T. Fathi, Y. B. Chen, *American journal of blood research* **2011**, *1*, 175-189.
[48] D. L. Stirewalt, J. P. Radich, *Nature reviews. Cancer* **2003**, *3*, 650-665.
[49] J. S. Welch, T. J. Ley, D. C. Link, C. A. Miller, D. E. Larson, D. C. Koboldt, L. D. Wartman, T. L. Lamprecht, F. Liu, J. Xia, C. Kandoth, R. S. Fulton, M. D. McLellan, D. J. Dooling, J. W. Wallis, K. Chen, C. C. Harris, H. K. Schmidt, J. M. Kalicki-Veizer, C. Lu, Q. Zhang, L. Lin, M. D. O'Laughlin, J. F. McMichael, K. D. Delehaunty, L. A. Fulton, V. J. Magrini, S. D. McGrath, R. T. Demeter, T. L. Vickery, J. Hundal, L. L. Cook, G. W. Swift, J. P. Reed, P. A. Alldredge, T. N. Wylie, J. R. Walker, M. A. Watson, S. E. Heath, W. D. Shannon, N. Varghese, R. Nagarajan, J. E. Payton, J. D. Baty, S. Kulkarni, J. M. Klco, M. H. Tomasson, P. Westervelt, M. J. Walter, T. A. Graubert, J. F. DiPersio, L. Ding, E. R. Mardis, R. K. Wilson, *Cell* **2012**, *150*, 264-278.
[50] S. Knapper, *British journal of haematology* **2007**, *138*, 687-699.
[51] M. Levis, D. Small, *Leukemia* **2003**, *17*, 1738-1752.

[52] M. Nakao, S. Yokota, T. Iwai, H. Kaneko, S. Horiike, K. Kashima, Y. Sonoda, T. Fujimoto, S. Misawa, *Leukemia* **1996**, *10*, 1911-1918.
[53] S. Kayser, M. J. Levis, *Leukemia & lymphoma* **2014**, *55*, 243-255.
[54] C. Ustun, D. L. DeRemer, A. P. Jillella, K. N. Bhalla, *Expert opinion on investigational drugs* **2009**, *18*, 1445-1456.
[55] F. M. Abu-Duhier, A. C. Goodeve, G. A. Wilson, R. S. Care, I. R. Peake, J. T. Reilly, *British journal of haematology* **2001**, *113*, 983-988.
[56] Y. Yamamoto, H. Kiyoi, Y. Nakano, R. Suzuki, Y. Kodera, S. Miyawaki, N. Asou, K. Kuriyama, F. Yagasaki, C. Shimazaki, H. Akiyama, K. Saito, M. Nishimura, T. Motoji, K. Shinagawa, A. Takeshita, H. Saito, R. Ueda, R. Ohno, T. Naoe, *Blood* **2001**, *97*, 2434-2439.
[57] C. Reindl, K. Bagrintseva, S. Vempati, S. Schnittger, J. W. Ellwart, K. Wenig, K. P. Hopfner, W. Hiddemann, K. Spiekermann, *Blood* **2006**, *107*, 3700-3707.
[58] D. L. Stirewalt, S. Meshinchi, S. J. Kussick, K. M. Sheets, E. Pogosova-Agadjanyan, C. L. Willman, J. P. Radich, *British journal of haematology* **2004**, *124*, 481-484.
[59] S. Opatz, H. Polzer, T. Herold, N. P. Konstandin, B. Ksienzyk, E. Zellmeier, S. Vosberg, A. Graf, S. Krebs, H. Blum, K. P. Hopfner, P. M. Kakadia, S. Schneider, A. Dufour, J. Braess, M. C. Sauerland, W. E. Berdel, T. Buchner, B. J. Woermann, W. Hiddemann, K. Spiekermann, S. K. Bohlander, P. A. Greif, *Blood* **2013**, *122*, 1761-1769.
[60] M. R. Grunwald, M. J. Levis, *International journal of hematology* **2013**, *97*, 683-694.
[61] Y. Liu, N. S. Gray, *Nature chemical biology* **2006**, *2*, 358-364.
[62] F. Zuccotto, E. Ardini, E. Casale, M. Angiolini, *Journal of medicinal chemistry* **2010**, *53*, 2681-2694.
[63] R. Morphy, *Journal of medicinal chemistry* **2010**, *53*, 1413-1437.
[64] D. Rauh, *Nachrichten aus der Chemie* **2010**, *58*, 118-121.
[65] J. Zhang, P. L. Yang, N. S. Gray, *Nature reviews. Cancer* **2009**, *9*, 28-39.
[66] Z. Fang, C. Grutter, D. Rauh, *ACS chemical biology* **2013**, *8*, 58-70.
[67] M. Rabiller, M. Getlik, S. Kluter, A. Richters, S. Tuckmantel, J. R. Simard, D. Rauh, *Archiv der Pharmazie* **2010**, *343*, 193-206.
[68] T. Smith-Vikos, *Genetic Enggineering & Biotechnology News* **2013**, *33*.
[69] *Cancer discovery* **2014**, *4*, 753-754.
[70] Z. A. Knight, H. Lin, K. M. Shokat, *Nature reviews. Cancer* **2010**, *10*, 130-137.
[71] L. Sun, C. Liang, S. Shirazian, Y. Zhou, T. Miller, J. Cui, J. Y. Fukuda, J. Y. Chu, A. Nematalla, X. Wang, H. Chen, A. Sistla, T. C. Luu, F. Tang, J. Wei, C. Tang, *Journal of medicinal chemistry* **2003**, *46*, 1116-1119.
[72] C. Bissantz, B. Kuhn, M. Stahl, *J. Med. Chem.* **2010**, *53*, 5061-5084.
[73] L. M. Salonen, M. Ellermann, F. Diederich, *Angew. Chem. Int. Ed. Engl.* **2011**, *50*, 4808-4842.
[74] H. J. Böhm, G. Klebe, *Angew. Chem. Int. Ed. Engl.* **1996**, *35*, 2588-2614.
[75] E. A. Meyer, R. K. Castellano, F. Diederich, *Angew. Chem. Int. Ed. Engl.* **2003**, *42*, 1210-1250.
[76] L. A. Hardegger, B. Kuhn, B. Spinnler, L. Anselm, R. Ecabert, M. Stihle, B. Gsell, R. Thoma, J. Diez, J. Benz, J. M. Plancher, H. G., D. W. Banner, W. Haap, F. Diederich, *Angew. Chem.* **2011**, *123*, 329-334.
[77] R. Bhattacharyya, U. Samanta, P. Chakrabarti, *Protein engineering* **2002**, *15*, 91-100.
[78] N. Kannan, S. Vishveshwara, *Protein engineering* **2000**, *13*, 753-761.
[79] C. A. Lipinski, F. Lombardo, B. W. Dominy, P. J. Feeney, *Advanced drug delivery reviews* **2001**, *46*, 3-26.
[80] T. T. Wager, X. Hou, P. R. Verhoest, A. Villalobos, *ACS chemical neuroscience* **2010**, *1*, 435-449.

[81] T. Kindler, D. B. Lipka, T. Fischer, *Blood* **2010**, *116*, 5089-5102.
[82] M. Miano, C. Micalizzi, M. Calvillo, C. Dufour, *Immunology letters* **2013**, *155*, 47-50.
[83] E. Weisberg, R. Barrett, Q. Liu, R. Stone, N. Gray, J. D. Griffin, *Drug resistance updates : reviews and commentaries in antimicrobial and anticancer chemotherapy* **2009**, *12*, 81-89.
[84] K. Bagrintseva, S. Geisenhof, R. Kern, S. Eichenlaub, C. Reindl, J. W. Ellwart, W. Hiddemann, K. Spiekermann, *Blood* **2005**, *105*, 3679-3685.
[85] M. Levis, K. F. Tse, B. D. Smith, E. Garrett, D. Small, *Blood* **2001**, *98*, 885-887.
[86] K. F. Tse, E. Novelli, C. I. Civin, F. D. Bohmer, D. Small, *Leukemia* **2001**, *15*, 1001-1010.
[87] J. W. Tyner, W. F. Yang, A. Bankhead, 3rd, G. Fan, L. B. Fletcher, J. Bryant, J. M. Glover, B. H. Chang, S. E. Spurgeon, W. H. Fleming, T. Kovacsovics, J. R. Gotlib, S. T. Oh, M. W. Deininger, C. M. Zwaan, M. L. Den Boer, M. M. van den Heuvel-Eibrink, T. O'Hare, B. J. Druker, M. M. Loriaux, *Cancer research* **2013**, *73*, 285-296.
[88] E. Weisberg, C. Boulton, L. M. Kelly, P. Manley, D. Fabbro, T. Meyer, D. G. Gilliland, J. D. Griffin, *Cancer cell* **2002**, *1*, 433-443.
[89] T. Fischer, R. M. Stone, D. J. Deangelo, I. Galinsky, E. Estey, C. Lanza, E. Fox, G. Ehninger, E. J. Feldman, G. J. Schiller, V. M. Klimek, S. D. Nimer, D. G. Gilliland, C. Dutreix, A. Huntsman-Labed, J. Virkus, F. J. Giles, *Journal of clinical oncology : official journal of the American Society of Clinical Oncology* **2010**, *28*, 4339-4345.
[90] R. M. Stone, T. Fischer, R. Paquette, G. Schiller, C. A. Schiffer, G. Ehninger, J. Cortes, H. M. Kantarjian, D. J. DeAngelo, A. Huntsman-Labed, C. Dutreix, A. del Corral, F. Giles, *Leukemia* **2012**, *26*, 2061-2068.
[91] A. M. O'Farrell, J. M. Foran, W. Fiedler, H. Serve, R. L. Paquette, M. A. Cooper, H. A. Yuen, S. G. Louie, H. Kim, S. Nicholas, M. C. Heinrich, W. E. Berdel, C. Bello, M. Jacobs, P. Scigalla, W. C. Manning, S. Kelsey, J. M. Cherrington, *Clinical cancer research : an official journal of the American Association for Cancer Research* **2003**, *9*, 5465-5476.
[92] D. Auclair, D. Miller, V. Yatsula, W. Pickett, C. Carter, Y. Chang, X. Zhang, D. Wilkie, A. Burd, H. Shi, S. Rocks, R. Gedrich, L. Abriola, H. Vasavada, M. Lynch, J. Dumas, P. A. Trail, S. M. Wilhelm, *Leukemia* **2007**, *21*, 439-445.
[93] K. W. Pratz, E. Cho, M. J. Levis, J. E. Karp, S. D. Gore, M. McDevitt, A. Stine, M. Zhao, S. D. Baker, M. A. Carducci, J. J. Wright, M. A. Rudek, B. D. Smith, *Leukemia* **2010**, *24*, 1437-1444.
[94] F. Ravandi, J. E. Cortes, D. Jones, S. Faderl, G. Garcia-Manero, M. Y. Konopleva, S. O'Brien, Z. Estrov, G. Borthakur, D. Thomas, S. R. Pierce, M. Brandt, A. Byrd, B. N. Bekele, K. Pratz, R. Luthra, M. Levis, M. Andreeff, H. M. Kantarjian, *Journal of clinical oncology : official journal of the American Society of Clinical Oncology* **2010**, *28*, 1856-1862.
[95] S. Knapper, A. K. Burnett, T. Littlewood, W. J. Kell, S. Agrawal, R. Chopra, R. Clark, M. J. Levis, D. Small, *Blood* **2006**, *108*, 3262-3270.
[96] M. Levis, F. Ravandi, E. S. Wang, M. R. Baer, A. Perl, S. Coutre, H. Erba, R. K. Stuart, M. Baccarani, L. D. Cripe, M. S. Tallman, G. Meloni, L. A. Godley, A. A. Langston, S. Amadori, I. D. Lewis, A. Nagler, R. Stone, K. Yee, A. Advani, D. Douer, W. Wiktor-Jedrzejczak, G. Juliusson, M. R. Litzow, S. Petersdorf, M. Sanz, H. M. Kantarjian, T. Sato, L. Tremmel, D. M. Bensen-Kennedy, D. Small, B. D. Smith, *Blood* **2011**, *117*, 3294-3301.
[97] D. J. DeAngelo, R. M. Stone, M. L. Heaney, S. D. Nimer, R. L. Paquette, R. B. Klisovic, M. A. Caligiuri, M. R. Cooper, J. M. Lecerf, M. D. Karol, S. Sheng, N. Holford, P. T. Curtin, B. J. Druker, M. C. Heinrich, *Blood* **2006**, *108*, 3674-3681.

[98] S. Mahboobi, A. Uecker, A. Sellmer, C. Cenac, H. Hocher, H. Pongratz, E. Eichhorn, H. Hufsky, A. Trumpler, M. Sicker, F. Heidel, T. Fischer, C. Stocking, S. Elz, F. D. Bohmer, S. Dove, *Journal of medicinal chemistry* **2006**, *49*, 3101-3115.
[99] Y. Shiotsu, H. Kiyoi, Y. Ishikawa, R. Tanizaki, M. Shimizu, H. Umehara, K. Ishii, Y. Mori, K. Ozeki, Y. Minami, A. Abe, H. Maeda, T. Akiyama, Y. Kanda, Y. Sato, S. Akinaga, T. Naoe, *Blood* **2009**, *114*, 1607-1617.
[100] A. D. William, A. C. Lee, S. Blanchard, A. Poulsen, E. L. Teo, H. Nagaraj, E. Tan, D. Chen, M. Williams, E. T. Sun, K. C. Goh, W. C. Ong, S. K. Goh, S. Hart, R. Jayaraman, M. K. Pasha, K. Ethirajulu, J. M. Wood, B. W. Dymock, *Journal of medicinal chemistry* **2011**, *54*, 4638-4658.
[101] H. K. Lee, H. W. Kim, I. Y. Lee, J. Lee, J. Lee, D. S. Jung, S. Y. Lee, S. H. Park, H. Hwang, J. S. Choi, J. H. Kim, S. W. Kim, J. K. Kim, J. Cools, J. S. Koh, H. J. Song, *Blood* **2014**, *123*, 2209-2219.
[102] Q. Chao, K. G. Sprankle, R. M. Grotzfeld, A. G. Lai, T. A. Carter, A. M. Velasco, R. N. Gunawardane, M. D. Cramer, M. F. Gardner, J. James, P. P. Zarrinkar, H. K. Patel, S. S. Bhagwat, *Journal of medicinal chemistry* **2009**, *52*, 7808-7816.
[103] P. P. Zarrinkar, R. N. Gunawardane, M. D. Cramer, M. F. Gardner, D. Brigham, B. Belli, M. W. Karaman, K. W. Pratz, G. Pallares, Q. Chao, K. G. Sprankle, H. K. Patel, M. Levis, R. C. Armstrong, J. James, S. S. Bhagwat, *Blood* **2009**, *114*, 2984-2992.
[104] J. E. Cortes, D. Ghirdaladze, J. M. Foran, M. P. DeVetten, M. Zodelava, M. J. Levis, N. M. Padre, J. Joyce, P. P. Zarrinkar, R. Corringham, *Blood* **2008**, *112*, Abstract 767.
[105] J. E. Cortes, A. E. Perl, H. Dombret, S. Kayser, B. Steffen, P. Rousselot, G. Martinelli, E. H. Estey, A. K. Burnett, G. Gammon, D. Trone, E. Leo, M. J. Levis, *Blood* **2012**, *120*, Abstract 48.
[106] M. J. Levis, A. E. Perl, H. Dombret, H. Döhner, B. Steffen, P. Rousselot, G. Martinelli, E. H. Estey, A. Burnett, K., G. Gammon, D. Trone, E. Leo, J. E. Cortes, *Blood* **2012**, *120*, Abstract 673.
[107] C. C. Smith, Q. Wang, C. S. Chin, S. Salerno, L. E. Damon, M. J. Levis, A. E. Perl, K. J. Travers, S. Wang, J. P. Hunt, P. P. Zarrinkar, E. E. Schadt, A. Kasarskis, J. Kuriyan, N. P. Shah, *Nature* **2012**, *485*, 260-263.
[108] M. Kesarwani, E. Huber, M. Azam, *Blood cancer journal* **2013**, *3*, e138.
[109] G. Wernig, M. G. Kharas, R. Okabe, S. A. Moore, D. S. Leeman, D. E. Cullen, M. Gozo, E. P. McDowell, R. L. Levine, J. Doukas, C. C. Mak, G. Noronha, M. Martin, Y. D. Ko, B. H. Lee, R. M. Soll, A. Tefferi, J. D. Hood, D. G. Gilliland, *Cancer cell* **2008**, *13*, 311-320.
[110] J. M. Gozgit, M. J. Wong, S. Wardwell, J. W. Tyner, M. M. Loriaux, Q. K. Mohemmad, N. I. Narasimhan, W. C. Shakespeare, F. Wang, B. J. Druker, T. Clackson, V. M. Rivera, *Molecular cancer therapeutics* **2011**, *10*, 1028-1035.
[111] T. O'Hare, W. C. Shakespeare, X. Zhu, C. A. Eide, V. M. Rivera, F. Wang, L. T. Adrian, T. Zhou, W. S. Huang, Q. Xu, C. A. Metcalf, 3rd, J. W. Tyner, M. M. Loriaux, A. S. Corbin, S. Wardwell, Y. Ning, J. A. Keats, Y. Wang, R. Sundaramoorthi, M. Thomas, D. Zhou, J. Snodgrass, L. Commodore, T. K. Sawyer, D. C. Dalgarno, M. W. Deininger, B. J. Druker, T. Clackson, *Cancer cell* **2009**, *16*, 401-412.
[112] N. P. Shah, M. Talpaz, M. W. Deininger, M. J. Mauro, I. W. Flinn, D. Bixby, S. Lustgarten, J. M. Gozgit, T. Clackson, C. D. Turner, F. G. Haluska, H. Kantarjian, J. E. Cortes, *British journal of haematology* **2013**, *162*, 548-552.
[113] C. C. Smith, E. A. Lasater, X. Zhu, K. C. Lin, W. K. Stewart, L. E. Damon, S. Salerno, N. P. Shah, *Blood* **2013**, *121*, 3165-3171.
[114] A. Galanis, H. Ma, T. Rajkhowa, A. Ramachandran, D. Small, J. Cortes, M. Levis, *Blood* **2014**, *123*, 94-100.

[115] M. C. Heinrich, D. Griffith, A. McKinley, J. Patterson, A. Presnell, A. Ramachandran, M. Debiec-Rychter, *Clinical cancer research : an official journal of the American Association for Cancer Research* **2012**, *18*, 4375-4384.
[116] E. I. Zimmerman, D. C. Turner, J. Buaboonnam, S. Hu, S. Orwick, M. S. Roberts, L. J. Janke, A. Ramachandran, C. F. Stewart, H. Inaba, S. D. Baker, *Blood* **2013**, *122*, 3607-3615.
[117] E. Burton, B. Wong, J. Zhang, B. West, G. Bollag, G. Habets, A. Galanis, H. Nguyen, O. Arowojolu, T. Rajhowa, M. J. Levis, *ASH Annual Meeting Abstracts* **2011**, *118*, Abstract 615.
[118] C. C. Smith, A. E. Perl, E. Lasater, C. Zhang, G. R. Jeschke, L. E. Damon, M. Carroll, N. P. Shah, *ASH Annual Meeting Abstracts* **2011**, *118*, Abstract 615.
[119] M. Korte, *Jung im Kopf: Erstaunliche Einsichten der Gehirnforschung in das Älterwerden, Vol. Auflage 5*, Deutsche Verlags-Anstalt, **2012**.
[120] J. Parkinson, *London: Whittingham and Rowland for Sherwood, Neely and Jones* **1817**.
[121] C. G. Goetz, *Cold Spring Harbor Perspectives in Medicine* **2011**, 1.
[122] H. Braak, K. Del Tredici, *Neurology* **2008**, *70*, 1916-1925.
[123] C. M. Tanner, D. A. Aston, *Current opinion in neurology* **2000**, *13*, 427-430.
[124] H. Ehringer, O. Hornykiewicz, *Klinische Wochenschrift* **1960**, *38*, 1236-1239.
[125] T. L. Sourkes, L. Poirier, *Nature* **1965**, *207*, 202-203.
[126] K. E. Lyons, R. Pahwa, *The International journal of neuroscience* **2011**, *121 Suppl 2*, 27-36.
[127] A. E. Lang, A. M. Lozano, *The New England journal of medicine* **1998**, *339*, 1130-1143.
[128] R. Takahashi, Y. Imai, *Journal of neurology* **2003**, *250 Suppl 3*, III25-29.
[129] Deutsche Gesellschaft für Neurologie.
[130] L. M. de Lau, M. M. Breteler, *The Lancet. Neurology* **2006**, *5*, 525-535.
[131] R. Betarbet, T. B. Sherer, G. MacKenzie, M. Garcia-Osuna, A. V. Panov, J. T. Greenamyre, *Nature neuroscience* **2000**, *3*, 1301-1306.
[132] G. Bringmann, R. God, S. Fahr, D. Feineis, K. Fornadi, F. Fornadi, *Analytical biochemistry* **1999**, *270*, 167-175.
[133] B. I. Giasson, V. M. Lee, *Nature neuroscience* **2000**, *3*, 1227-1228.
[134] J. Lotharius, P. Brundin, *Nature reviews. Neuroscience* **2002**, *3*, 932-942.
[135] J. W. Langston, P. Ballard, J. W. Tetrud, I. Irwin, *Science* **1983**, *219*, 979-980.
[136] E. Andres-Mateos, R. Mejias, M. Sasaki, X. Li, B. M. Lin, S. Biskup, L. Zhang, R. Banerjee, B. Thomas, L. Yang, G. Liu, M. F. Beal, D. L. Huso, T. M. Dawson, V. L. Dawson, *The Journal of neuroscience : the official journal of the Society for Neuroscience* **2009**, *29*, 15846-15850.
[137] G. Muthian, V. Mackey, J. King, C. G. Charlton, *Neuroscience* **2010**, *169*, 1085-1093.
[138] S. Przedborski, V. Jackson-Lewis, A. B. Naini, M. Jakowec, G. Petzinger, R. Miller, M. Akram, *Journal of neurochemistry* **2001**, *76*, 1265-1274.
[139] L. S. Forno, *Journal of neuropathology and experimental neurology* **1996**, *55*, 259-272.
[140] F. Blandini, G. Nappi, C. Tassorelli, E. Martignoni, *Progress in neurobiology* **2000**, *62*, 63-88.
[141] O. Rascol, P. Payoux, F. Ory, J. J. Ferreira, C. Brefel-Courbon, J. L. Montastruc, *Annals of neurology* **2003**, *53 Suppl 3*, S3-12; discussion S12-15.
[142] Helmholtz Zentrum München - Deutsche Forschungszentrum für Gesundheit und Umwelt.
[143] J. M. Taymans, M. R. Cookson, *BioEssays : news and reviews in molecular, cellular and developmental biology* **2010**, *32*, 227-235.

[144] W. Marui, E. Iseki, M. Kato, H. Akatsu, K. Kosaka, *Acta neuropathologica* **2004**, *108*, 121-128.
[145] E. Greggio, M. Bisaglia, L. Civiero, L. Bubacco, *Molecular neurodegeneration* **2011**, *6*, 6.
[146] E. Forster, F. Lewy, *In Pathologische Anatomie. Handbuch der Neurologie (edited by M. Lewandowsky)* **1912**, Berlin: Springer Verlag, 920-933.
[147] R. A. Hauser, *The International journal of neuroscience* **2011**, *121 Suppl 2*, 53-62.
[148] S. H. Fox, *Drugs* **2013**, *73*, 1405-1415.
[149] www.parkinson-web.de.
[150] G. Ebersbach, K. Hahn, M. Lorrain, A. Storch, *Archives of gerontology and geriatrics* **2010**, *51*, e125-128.
[151] J. F. Rocha, A. Falcao, A. Santos, R. Pinto, N. Lopes, T. Nunes, L. C. Wright, M. Vaz-da-Silva, P. Soares-da-Silva, *European journal of clinical pharmacology* **2014**, *70*, 1059-1071.
[152] W. Seol, *BMB reports* **2010**, *43*, 233-244.
[153] C. Klein, A. Westenberger, *Cold Spring Harb Perspect Med* **2012**, *2*, a008888.
[154] C. Klein, M. G. Schlossmacher, *Nature clinical practice. Neurology* **2006**, *2*, 136-146.
[155] Z. Berger, K. A. Smith, M. J. Lavoie, *Biochemistry* **2010**, *49*, 5511-5523.
[156] M. H. Polymeropoulos, C. Lavedan, E. Leroy, S. E. Ide, A. Dehejia, A. Dutra, B. Pike, H. Root, J. Rubenstein, R. Boyer, E. S. Stenroos, S. Chandrasekharappa, A. Athanassiadou, T. Papapetropoulos, W. G. Johnson, A. M. Lazzarini, R. C. Duvoisin, G. Di Iorio, L. I. Golbe, R. L. Nussbaum, *Science* **1997**, *276*, 2045-2047.
[157] R. Krüger, W. Kuhn, T. Muller, D. Woitalla, M. Graeber, S. Kosel, H. Przuntek, J. T. Epplen, L. Schols, O. Riess, *Nature genetics* **1998**, *18*, 106-108.
[158] J. J. Zarranz, J. Alegre, J. C. Gomez-Esteban, E. Lezcano, R. Ros, I. Ampuero, L. Vidal, J. Hoenicka, O. Rodriguez, B. Atares, V. Llorens, E. Gomez Tortosa, T. del Ser, D. G. Munoz, J. G. de Yebenes, *Annals of neurology* **2004**, *55*, 164-173.
[159] M. Farrer, J. Kachergus, L. Forno, S. Lincoln, D. S. Wang, M. Hulihan, D. Maraganore, K. Gwinn-Hardy, Z. Wszolek, D. Dickson, J. W. Langston, *Annals of neurology* **2004**, *55*, 174-179.
[160] P. Ibanez, S. Lesage, S. Janin, E. Lohmann, F. Durif, A. Destee, A. M. Bonnet, C. Brefel-Courbon, S. Heath, D. Zelenika, Y. Agid, A. Durr, A. Brice, G. French Parkinson's Disease Genetics Study, *Archives of neurology* **2009**, *66*, 102-108.
[161] A. B. Singleton, M. Farrer, J. Johnson, A. Singleton, S. Hague, J. Kachergus, M. Hulihan, T. Peuralinna, A. Dutra, R. Nussbaum, S. Lincoln, A. Crawley, M. Hanson, D. Maraganore, C. Adler, M. R. Cookson, M. Muenter, M. Baptista, D. Miller, J. Blancato, J. Hardy, K. Gwinn-Hardy, *Science* **2003**, *302*, 841.
[162] A. Recchia, P. Debetto, A. Negro, D. Guidolin, S. D. Skaper, P. Giusti, *FASEB journal : official publication of the Federation of American Societies for Experimental Biology* **2004**, *18*, 617-626.
[163] B. I. Giasson, I. V. Murray, J. Q. Trojanowski, V. M. Lee, *The Journal of biological chemistry* **2001**, *276*, 2380-2386.
[164] D. J. Irwin, V. M. Lee, J. Q. Trojanowski, *Nature reviews. Neuroscience* **2013**, *14*, 626-636.
[165] M. Funayama, K. Hasegawa, H. Kowa, M. Saito, S. Tsuji, F. Obata, *Annals of neurology* **2002**, *51*, 296-301.
[166] C. Paisan-Ruiz, S. Jain, E. W. Evans, W. P. Gilks, J. Simon, M. van der Brug, A. Lopez de Munain, S. Aparicio, A. M. Gil, N. Khan, J. Johnson, J. R. Martinez, D. Nicholl, I. M. Carrera, A. S. Pena, R. de Silva, A. Lees, J. F. Marti-Masso, J. Perez-Tur, N. W. Wood, A. B. Singleton, *Neuron* **2004**, *44*, 595-600.

[167] A. Zimprich, S. Biskup, P. Leitner, P. Lichtner, M. Farrer, S. Lincoln, J. Kachergus, M. Hulihan, R. J. Uitti, D. B. Calne, A. J. Stoessl, R. F. Pfeiffer, N. Patenge, I. C. Carbajal, P. Vieregge, F. Asmus, B. Muller-Myhsok, D. W. Dickson, T. Meitinger, T. M. Strom, Z. K. Wszolek, T. Gasser, *Neuron* **2004**, *44*, 601-607.
[168] C. Paisan-Ruiz, P. A. Lewis, A. B. Singleton, *Journal of Parkinson's disease* **2013**, *3*, 85-103.
[169] E. Greggio, M. R. Cookson, *ASN neuro* **2009**, *1*.
[170] I. F. Mata, W. J. Wedemeyer, M. J. Farrer, J. P. Taylor, K. A. Gallo, *Trends in neurosciences* **2006**, *29*, 286-293.
[171] L. Bosgraaf, P. J. Van Haastert, *Biochimica et biophysica acta* **2003**, *1643*, 5-10.
[172] G. Y. Liou, K. A. Gallo, *The Biochemical journal* **2009**, *424*, e1-3.
[173] M. R. Cookson, *Nature reviews. Neuroscience* **2010**, *11*, 791-797.
[174] U. Kumari, E. K. Tan, *The FEBS journal* **2009**, *276*, 6455-6463.
[175] L. Guo, P. N. Gandhi, W. Wang, R. B. Petersen, A. L. Wilson-Delfosse, S. G. Chen, *Experimental cell research* **2007**, *313*, 3658-3670.
[176] P. A. Lewis, E. Greggio, A. Beilina, S. Jain, A. Baker, M. R. Cookson, *Biochemical and biophysical research communications* **2007**, *357*, 668-671.
[177] V. S. Anand, S. P. Braithwaite, *The FEBS journal* **2009**, *276*, 6428-6435.
[178] J. M. Taymans, *Expert opinion on therapeutic patents* **2014**, *24*, 727-730.
[179] X. Deng, H. G. Choi, S. J. Buhrlage, N. S. Gray, *Expert opinion on therapeutic patents* **2012**, *22*, 1415-1426.
[180] X. Deng, N. Dzamko, A. Prescott, P. Davies, Q. Liu, Q. Yang, J. D. Lee, M. P. Patricelli, T. K. Nomanbhoy, D. R. Alessi, N. S. Gray, *Nature chemical biology* **2011**, *7*, 203-205.
[181] H. G. Choi, J. Zhang, X. Deng, J. M. Hatcher, M. P. Patricelli, Z. Zhao, D. R. Alessi, N. S. Gray, *ACS medicinal chemistry letters* **2012**, *3*, 658-662.
[182] J. Zhang, X. Deng, H. G. Choi, D. R. Alessi, N. S. Gray, *Bioorganic & medicinal chemistry letters* **2012**, *22*, 1864-1869.
[183] A. D. Reith, P. Bamborough, K. Jandu, D. Andreotti, L. Mensah, P. Dossang, H. G. Choi, X. Deng, J. Zhang, D. R. Alessi, N. S. Gray, *Bioorganic & medicinal chemistry letters* **2012**, *22*, 5625-5629.
[184] A. W. Garofalo, M. Adler, D. L. Aubele, E. F. Brigham, D. Chian, M. Franzini, E. Goldbach, G. T. Kwong, R. Motter, G. D. Probst, K. P. Quinn, L. Ruslim, H. L. Sham, D. Tam, P. Tanaka, A. P. Truong, X. M. Ye, Z. Ren, *Bioorganic & medicinal chemistry letters* **2013**, *23*, 1974-1977.
[185] G. M. Amombo, T. Kramer, F. Lo Monte, S. Göring, M. Fach, S. Smith, S. Kolb, R. Schubenel, K. Baumann, B. Schmidt, *Bioorganic & medicinal chemistry letters* **2012**, *22*, 7634-7640.
[186] T. Kramer, F. Lo Monte, S. Göring, G. M. Okala Amombo, B. Schmidt, *ACS chemical neuroscience* **2012**, *3*, 151-160.
[187] S. Schulz, S. Göring, B. Schmidt, C. Hopf, *RSC Drug Discovery Series* **2013**, *34 (Emerging Drugs and Targets for Parkinson's Disease)*, 266-293.
[188] E. C. Naumann, S. Göring, I. Ogorek, S. Weggen, B. Schmidt, *Bioorganic & medicinal chemistry letters* **2013**, *23*, 3852-3856.

7 Anhang

7.1 Abbildungsverzeichnis

Abbildung 1: Schematische Darstellung des menschlichen Kinoms, sowie deren wichtige Hauptgruppen. AGC: *protein kinases A, G and C group* (beinhaltet PKA, PKG und PKC Familien); CAMK: *calcium/calmodulin-dependent protein kinase*; CK1: *casein kinase 1*; CMCG: beinhaltet CDK, MAPK, GSK3, CLK Familien; STE: *homologs of yeast sterile 7, sterile 11, sterile 20 kinases*; TK: *tyrosine kinase*; TKL: *tyrosine kinase-like*. In Anlehnung an Manning *et al*.[4] 2

Abbildung 2: Prozentualer Anteil der Tumorlokalisationen bei Krebsneuerkrankungen in Deutschland 2010.[6] 3

Abbildung 3: Prozentualer Anteil der Krebsneuerkrankungen bei Kinder in Deutschland aus den Jahren 2003-2012.[6] 3

Abbildung 4: Entstehung der Leukämien ausgehend von den LT-HSC (*long term hematopoietic stem cells*) über den myeloischen und lymphatischen Differenzierungsweges. In Anlehnung an E. Elert.[10] 5

Abbildung 5: Strukturen der Zytostatika von Cytarabin **1** und Daunorubicin **2** für die Behandlung der AML.[19, 20] 9

Abbildung 6: Das „2-Klassen-Modell“ der akuten myeloischen Leukämie. Nach diesem Modell fördert das Auftreten zweier Mutationen aus den Klasse-I und Klasse-II die Entwicklung der AML. ATRA (Vitamin-A-Säure bzw. all-*tans*-Retinsäure, *all-trans-retinoic acid*).[28, 29] 11

Abbildung 7: Schematische Darstellung der Übertragung einer γ-Phosphatgruppe des ATPs auf ein Substrat. In Anlehnung an Ubersax *et al*.[32] 12

Abbildung 8: Allgemeine Struktur einer Kinase dargestellt anhand von FLT3 (PDB: 1RJB). Dargestellt mit *Discovery Studio 4 Visualizer*. 13

Abbildung 9: Schematische Darstellung der RTKs aus den Klassen I-V. In Anlehnung an Blume-Jensen *et al*.[35] 15

Abbildung 10: Links: Schematische Darstellung des FLT3-Rezeptors. TM: Transmembran-Domäne; JM: Juxtamembran-Domäne; TK1 und TK2: Tyrosinkinase-Domäne 1 und 2; KI: Kinase-Insert, AS: Aktivierungsschleife. Rechts: Kristallstruktur von FLT3 (PDB: 1RJB). Dargestellt mit *Discovery Studio 4 Visualizer*. 16

Abbildung 11: Bindung des FLT3-Liganden (FL) mit anschließender Homodimerisierung des Rezeptors. Durch die Aktivierung von FLT3 wird ein intrazelluläres Signalnetzwerk gestartet.[13, 46] 18

Abbildung 12: Auswahl der von der FDA zugelassenen Medikamente für die Krebsbehandlung.[68-70] 22

Abbildung 13: Häufig auftretende molekulare Interaktionen in biologischen Systemen.[73, 75] 25

Abbildung 14: FLT3-Inhibitoren der ersten Generation. Diese wurden nicht speziell für FLT3 entwickelt, sondern gegenüber anderen Kinasen.[46, 53] 27

Abbildung 15: FLT3-Inhibitoren der zweiten Generation, welche speziell für FLT3 entwickelt worden sind. 29

Abbildung 16: Die vier unterschiedlichen Arten des Parkinson-Syndroms. Das IPS, auch Morbus-Parkinson genannt, ist mit ca. 90 % das häufigste aller Parkinson-Syndrome.[127] 32

Abbildung 17: Vereinigungen von MPTP **23** in synthetisch hergestelltem Heroin lösten 1983 Symptome der Parkinson-Krankheit aus.[135] 33

Abbildung 18: Immunhistologische Färbung von α-Synuclein. Links: intrazytoplasmatische *Lewy-bodies* in der immunhistologischen Färbung mit Fuchsinrot. Rechts: *Lewy neurites* im Mittelhirn in der immunhistologischen Färbung mit Fuchsinrot. Mit freundlicher Genehmigung von Dr. med. Roland Heyny-von Haussen (Klinikum Darmstadt). 34

Abbildung 19: Auswahl der zurzeit angewendeten Medikamente zur Behandlung der Parkinson-Krankheit.[126, 147, 148, 150, 151] 36

Abbildung 20: Häufigkeit des familiären Parkinson-Syndroms im Vergleich zum idiopathischen Parkinson-Syndrom. In Anlehnung an Klein *et al*.[154] 38

Abbildung 21: Schematische Darstellung der α-Synuclein Aggregation nach Recchia *et al*. und Irwin *et al*.[162, 164] 39

Abbildung 22: Schematische Illustration von LRRK2. Domänen: ANK (*ankyrin-repeat-domain*), LRR (*leucine-rich repeat domain*), ROC (*Ras of complex,* (GTPase)), COR (*C-terminal of Ras*), am C-terminalen Ende befindet sich eine WD40-Einheit. Die meist bekanntesten pathogenen Mutationen sind unterhalb der Struktur gezeigt. Mutationen von R1441 sowie Y1699 erniedrigen die GTPase-Aktivität, wohingegen G2019S die Kinase-Aktvität erhöht. Dies führt dazu, dass die Kinase-Domäne die ROC-Domäne phosphoyliert, obwohl dies *in vivo* noch nicht bestätigt wurde. In Anlehnung an M. Cookson.[173] 41

Abbildung 23: Selektive, hochpotente LRRK2-Aminopyrimidin-Inhibitoren.[180-182] 43

Abbildung 24: LRRK2-Inhibitoren der Stoffklassen der Arylbenzylamide **36** und der Cyancinnoline **37**.[183, 184] 45

Abbildung 25: Aus der Leitstruktur **38** wurden verschiedene Indolinon-basierender FLT3-Inhibitoren synthetisiert. 208

Abbildung 26: Übersicht ausgewählter FLT3-Inhibitorn basierend auf dem Chinoxalin-Grundgerüst. 209

Abbildung 27: Erzieltes Ergebnis bezüglich der Inhibition von LRRK2. 210

Abbildung 28: Optionen zur Erhöhung der Löslichkeit aktueller Verbindungen. 211

Abbildung 29: Möglichkeit der Erhöhung der Löslichkeit durch die Einführung von Stickstoffatomen..... 212

7.2 Erklärungen

Stefan Göring
Karl-Räder-Straße 3
67117 Limburgerhof

19.10.2014

Erklärung

Ich erkläre hiermit, dass ich meine Dissertation selbständig und nur mit den angegebenen Hilfsmitteln angefertigt habe.

[Stefan Göring]

Stefan Göring
Karl-Räder-Straße 3
67117 Limburgerhof

19.10.2014

Erklärung

Ich erkläre hiermit, noch keinen Promotionsversuch unternommen zu haben.

[Stefan Göring]

7.3 Lebenslauf

Persönliche Daten

Name	Stefan Göring
Adresse	Karl-Räder-Straße 3, 67117 Limburgerhof
Geburtsdatum und -ort	18. August 1983 in Gera
Familienstand	verheiratet
Staatsangehörigkeit	Deutsch

Hochschulausbildung

01/2012	**Promotionsstudent im Arbeitskreis von Prof. Dr. B. Schmidt** an der Technischen Universität Darmstadt, mit dem Schwerpunkt Medizinalchemie und organische Chemie
05/2011 - 11/2011	**Master-Thesis im Arbeitskreis von Prof. Dr. B. Schmidt** an der Technischen Universität Darmstadt, mit dem Thema „*ATP-kompetitive Kinaseinhibitoren – Docking, Synthese, SAR –*“
10/2009 - 11/2011	**Studium *Master of Science* in Chemie** an der Technischen Universität Darmstadt
05/2009 - 08/2009	**Bachelor-Thesis im Arbeitskreis von Prof. Dr. B. Schmidt** an der Technischen Universität Darmstadt, mit dem Thema „*Polyetherderivate substratbindender γ-Sekretase-Modulatoren*“
10/2006 – 09/2009	**Studium *Bachelor of Science* in Chemie** an der Technischen Universität Darmstadt

Berufserfahrung

02/2006 – 09/2006	**BASF SE, Ludwigshafen** Abteilung GVP – Forschung/Veredelungschemikalien

Berufsausbildung

09/2003 – 01/2006 **Ausbildung zum Chemielaborant**

BASF SE, Ludwigshafen

Wehrdienst / Zivildienst

07/2002 – 07/2003 **Grundwehrdienst mit anschließendem freiwilligem Wehrdienst im 3. Jägerlehrbataillon**

in Hammelburg (Bayern)

Schulausbildung

09/1994 – 06/2002 **Friedrich-Schiller-Gymnasium, Gera**
Mit dem Abschluss: Allgemeine Hochschulreife

09/1990 – 08/1994 **6. Grundschule, Gera**

[Stefan Göring]